Flexible, Wearable and Reconfigurable Antennas Based on Novel Conductive Materials: Graphene, Polymers and Textiles

by

Shengjian Jammy Chen

B. Eng. (Information Engineering),
Guangdong University of Technology, China, 2003
M. Eng. (Electrical and Electronic Engineering),
The University of Adelaide, Australia, 2013

Thesis submitted for the degree of

Doctor of Philosophy

in

School of Electrical & Electronic Engineering
Faculty of Engineering, Computer & Mathematical Sciences
The University of Adelaide

2017

Supervisors:
Prof. Christophe Fumeaux, School of Electrical & Electronic Engineering
Dr. Damith Chinthana Ranasinghe, School of Computer Science
Dr. Thomas Kaufmann, School of Electrical & Electronic Engineering

To my dearest parents,
my stunning wife, Deyan
my two gorgeous daughters Bojin and Boyi
and my parents-in-law
with all my love.

Contents

Abstract

DUE to high demand and ubiquity of novel wireless communication systems, numerous new technical challenges have risen in modern antenna design to satisfy emerging unconventional system requirements. Typical examples include radio frequency identification (RFID) systems and wearable electronic systems. RFID systems usually consist of a reader and a tag integrated with an antenna which is attached to the item(s) to be tracked. Therefore, for the commercial viability of the system, it is desired to have flexible, light-weight, highly integratable and low-cost antennas for the tags. These characteristics are also desired for the antennas used in wearable electronic systems, with an additional critical requirement, namely electrical and mechanical robustness to the loading effect from the human body when worn. Hence traditional metallic conductors and dielectric materials such as ceramics are usually not suitable, as these materials lack mechanical flexibility and resilience while having a high intrinsic cost.

In this context, flexible, wearable and reconfigurable antennas based on novel conductive and dielectric materials are of significant interest. This is in line with the goals of this thesis which comprise four main different objectives. Firstly, the dissertation presents the development of non-metallic, highly efficient and flexible antennas based on conductive polymers and graphene thin films as conductors. Through efficiency-driven and material-oriented engineering methods, it is shown that these antennas can overcome the process-related inherent limitations of the non-metallic conductors, demonstrating the excellent potential of these novel materials. Secondly, the thesis also focuses on the investigation of appropriate shorting strategies and connection solutions for textile antennas, in terms of ease of fabrication, connection reliability and antenna efficiency. This work aims to provide reliable and efficient solutions to the critical connection requirement between flexible textile antennas and rigid electronic components. Thirdly, modular and reconfigurable wearable textile antennas which provide passive and/or active system reconfigurability are proposed, based on commercial snap-on buttons operating as shorting vias and connectors. The modular wearable antenna concept utilizes different modules which are designed to achieve specific antenna characteristics and fulfill various functionalities. The reconfigurable antenna is based on a reconfigurable module which integrates varactors and a dedicated bias circuit board inside snap-on buttons. This button module can solve the main challenge in realizing reliable connections between bias circuit, lump components and textiles, which arises because of the very different physical properties of rigid and flexible components. Fourthly, the last part of the thesis presents a compact and high efficiency series-fed microstrip patch array and a flexible dielectric resonator antenna, as examples of novel designs suitable for wearable applications.

All the results and findings in this thesis illustrate that, antennas realized in novel conductive and dielectric materials including conductive polymers, graphene, conductive textiles and polydimethylsiloxane (PDMS), can potentially satisfy the unconventional characteristics desired for future wearable electronic systems. Furthermore, the interdisciplinary combination of antenna technology and material science paves a promising path for advanced antenna developments, towards next generations of mobile wireless communication systems.

Originality Declaration

I certify that this work contains no material which has been accepted for the award of any other degree or diploma in my name, in any university or other tertiary institution and, to the best of my knowledge and belief, contains no material previously published or written by another person, except where due reference has been made in the text. In addition, I certify that no part of this work will, in the future, be used in a submission in my name, for any other degree or diploma in any university or other tertiary institution without the prior approval of the University of Adelaide and where applicable, any partner institution responsible for the joint-award of this degree.

I give consent to this copy of the thesis, when deposited in the University Library, being available for loan, photocopying, and dissemination through the library digital thesis collection, subject to the provisions of the Copyright Act 1968.

I also give permission for the digital version of my thesis to be made available on the web, via the University's digital research repository, the Library Search and also through web search engines, unless permission has been granted by the University to restrict access for a period of time.

	05/25/2017
Signed	Date

Acknowledgments

I would like to express my deep gratitude to my supervisors Prof. Christophe Fumeaux, Dr. Damith Chinthana Ranasinghe and Dr. Thomas Kaufmann. Prof. Fumeaux and Dr. Kaufmann accepted me as a Ph.D student in the early 2013. Since then, they have been patiently guiding me into the research in antenna technology, always encouraging me to explore more. Prof. Fumeaux has been a very supportive, approachable and responsible supervisor for my Ph.D study. He has always patiently guided and encouraged me to explore and research more. His profound and comprehensive knowledge of electromagnetics, antennas, and optics has always inspired me. Extremely high standard and rigorous attitudes towards research is one of his iconic images. He is always happy and open for any discussions regarding research and I really enjoy exploring new research ideas on his little whiteboard. Dear ***Prof. Christophe Fumeaux***, I would like to, from the bottom of my heart, acknowledge your enthusiastic supervision, encouraging and patient guidance, technical and financial support and being a role model for me as a scholar. Dr. Kaufmann is an outstanding scholar with broad and profound knowledge in electromagnetics and antennas. He has always pointed out critical points in our discussions and encouraged me solve problems from the fundamentals. Dr. Ranasinghe has very comprehensive knowledge about computer science and RFID-based systems and their applications. Therefore, a very strong linkage between wearable antennas and RFID-based wearable applications has been established, which has made my research more project-oriented. These three respectful supervisors have always patiently and critically corrected my manuscripts, with emphasis on writing with critical and rigorous arguments. The responsible care and guidance from my supervisors have transformed me from a science curious student into a researcher. They have been making my Ph.D journey marvellous and invaluable. I highly appreciate all their time, ideas, generous experience sharing, high standard requirements and contributions.

I also wish to express my appreciation for Prof. Dusan Losic and Dr. Tran Thanh Tung from the School of Chemical Engineering for their provision of exceptional novel materials including graphene inks and thin films, as well as their critical contributions to our publications. I am indebted to Dr. Roderick Shepherd and Mr. Benjamin Chivers from the University of Sydney, for providing the outstanding conductive polymers and the critical comments to our manuscripts. Dr. Pejman Talemi from the School of Chemical Engineering is another key person whom I highly appreciate, because he has provided professional advices for materials-related matters, performed critical treatments for our conductive polymers, offered novel materials such as carbon textiles, and trained me how to fabricate components using some of these materials. I am so grateful to the provision of materials, as well as the support and the training from Dr. Rick Fabretto and Dr. Drew Evans from the University of South Australia.

I am so grateful for the support and advices from my friends and colleagues in our Applied Electromagnetics Group at the University of Adelaide, Dr. Withawat Withayachumnankul, Dr. Zhi Xu, Dr. Pouria Yaghmaee, Dr. Ali Karami Horestani, Dr. Zahra Shaterian, Dr. Tiaoming Niu, Dr. Amir Ebrahimi, Dr. Fengxue Liu, Dr. Chengjun Zou, Dr. Nghia Nguyen, Mr. Sree Pinapati, Ms. Wendy Suk Ling Lee, Mr. Andrew Udina and Mr. Deshan Govender. I enjoyed very much the time of our group meetings and discussions. In particular, I am indebted to Dr. Withawat Withayachumnankul who always welcomed scientific discussions and ready to give critical feedback. His deep knowledge in the field of electromagnetics, microwave and terahertz engineering has strongly supported our projects. I also would like to acknowledge the kindness and assistances from my colleagues and friends in the School of Electrical and Electronic Engineering: Mr. Brandon Pullen, Mr. Alban O'Brien, Mr. Pavel Simcik, Mr. Henry Ho, Mr. Stephen Guest, Mr. Mark Innes, Mr. David Bowler, Mr. Danny Di Giacomo, Dr. Brian W-H Ng, Ms. Rose-Marie Descalzi, Ms. Ivana Rebellato, Ms. Deborah Koch, Mr. Matthew Trinkle, and Ms. Jodie Schluter.

I gratefully acknowledge the generous financial support from the Australian Government, Australian Postgraduate Award (APA), without which I would not have been able to carry on the research. Additionally, I would like to express my gratitude to the School of Electrical & Electronic Engineering for the annual travel grants (2014-2017), and to the Australia's Defence Science and Technology Group (DSTG) for Simon Rockliff Supplementary Scholarship (2015), with which I could attend several international conferences to explore new ideas and knowledge.

Now to my lovely family, the most important part of my life, above all, my deepest gratefulness and love go to my parents who have always unconditionally loved (spoiled), supported and offered me the best they can. I love you so much! I also wish to express my sincere appreciation to my parents-in-law who treat me as their biological son with infinite love and support. My two gorgeous daughters, **Bojin** and **Boyi**,

are the apples of my eye and endow me with endless power and spirit to fight for them and for my dreams.

Last but not least, I would like to express my heartfelt and warmest appreciation to my stunning, tender and considerate wife, **Deyan (Yanice)**, my spiritual pillar, who always stands by me in ups and downs, supports and believes in me unconditionally. Darling, you are the one I love most!

Shengjian Jammy Chen
May 2017
Adelaide, Australia

Thesis Conventions

The following conventions have been adopted in this Thesis:

Typesetting

This document was compiled using LaTeX2e. TeXstudio is used as text editor interfaced to LaTeX2e. Inkscape was used to produce schematic diagrams and other drawings.

Referencing

The referencing and citation style adopted in this thesis are based on the Institute of Electrical and Electronics Engineers (IEEE) Transaction style.

System of units

The units comply with the international system of units recommended in an Australian Standard: AS ISO 1000–1998 (Standards Australia Committee ME/71, Quantities, Units and Conversions 1998).

Spelling

American English spelling is adopted in this thesis.

Abbreviation

AR	Axial Ratio
CNT	Carbon Nanotubes
CPW	Coplanar Waveguide
DR	Dielectric Resonator
DRA	Dielectric Resonator Antenna
EMI	Electromagnetic Interference
G/PANI/PSS	Graphene/Polyaniline/Poly(4-styrenesulfonate)
GO	Graphene Oxide
HMSIW	Half-Mode Substrate-Integrated Waveguide
ISM	Industrial, Scientific and Medical
LHCP	Left-hand Circular Polarization
LP	Linear Polarization
PANI	Polyaniline
PCB	Printed Circuit Board
PDMS	Polydimethylsiloxane
PEC	Perfect Electrical Conductor
PEDOT	Poly(3,4-ethylenedioxythiophene)
PEDOT:PSS	Poly(3,4-ethylenedioxythiophene):poly(styrenesulfonate)
PIFA	Planar Inverted-F Antenna
PPV	Polyphenylenevinylene
PPy	Polypyrrole
RCS	Radar Cross Section
RF	Radio Frequency
RFID	Radio Frequency Identification
RGO	Reduced Graphene Oxide
RHCP	Right-hand Circular Polarization
SEM	Scanning Electron Microscopy
SIW	Substrate-Integrated Waveguide
SMA	SubMiniature Version A
SPP	Surface Plasmon Polariton

TeM	Transmission Electron Microscopy
TEM	Transverse Electromagnetic
THz	Terahertz
TM	Transverse Magnetic
UWB	Ultra-Wideband
VSWR	Voltage Standing Wave Ratio
WBAN	Wireless Body Area Network

Awards and Scholarships

2017

- Honorable Mention, IEEE AP-S Symposium on Antennas and Propagation and USNC-URSI Radio Science Meeting (APS/URSI 2017)

2016

- Young Scientist Best Paper Award, International Conference on Electromagnetics in Advanced Applications (ICEAA 2016)
- Travel Bursary Award, International Conference on Electromagnetics in Advanced Applications (ICEAA 2016)

2015

- Young Scientist Best Paper Award, International Conference on Electromagnetics in Advanced Applications (ICEAA 2015)
- Simon Rockliff Scholarship, Australia's Defence Science and Technology Group (DSTG)

2013

- Australian Postgraduate Award (APA), The Australian Government

Publications

Journal Articles

S. J. Chen, T. Kaufmann, R. Shepherd, B. Chivers, B. Weng, A. Minett, and C. Fumeaux, "A compact, highly efficient and flexible polymer ultra-wideband antenna," *IEEE Antennas Wirel. Propag. Lett.*, vol. 14, pp. 1207 – 1210, 2015.

S. J. Chen, C. Fumeaux, D. C. Ranasinghe, and T. Kaufmann, "Paired snap-on buttons connections for balanced antennas in wearable systems," *IEEE Antennas Wirel. Propag. Lett.*, vol. 14, no. X, pp. 1498–1501, 2015. **(Invited paper)**

S. J. Chen, T. Kaufmann, D. C. Ranasinghe, and C. Fumeaux, "A modular textile antenna design using snap-on buttons for wearable applications," *IEEE Trans. Antennas Propag.*, vol. 64, no. 3, pp. 894–903, 2016.

T. T. Tung and **S. J. Chen**, C. Fumeaux and D. Losic,"Scalable realization of conductive graphene films for high-efficiency microwave antennas," *J. Mater. Chem. C*, vol. 4, no. 45, pp. 10620–10624, 2016. **(Two first authors)**

S. J. Chen, C. Fumeaux, Y. Monnai and W. Withayachumnankul, "Dual circularly polarized series-fed microstrip patch array with coplanar proximity coupling," *IEEE Antennas Wirel. Propag. Lett.*, vol. 16, no. X, pp. 1500–1503, 2017.

Conference Articles

S. J. Chen, T. Kaufmann, and C. Fumeaux, "Shorting strategies for a wearable L-slot planar inverted-F antenna," in *Int. Work. Antenna Technol. (iWAT)*, 2014, pp. 18–21.

S. J. Chen, T. Kaufmann, and C. Fumeaux, "Snap-on buttons connections for transmission lines and antennas," in *14th Australian Symposium on Antennas*, Feb 2015.

S. J. Chen, B. Chivers, R. Shepherd, and C. Fumeaux, "Bending impact on a flexible ultra-wideband conductive polymer antenna," *2015 Int. Conf. Electromagn. Adv. Appl.*, pp. 422–425, 2015. **(Invited paper) [The Young Scientist Best Paper Award of ICEAA2015]**

S. J. Chen, P. Talemi, B. Chivers, R. Shepherd, and C. Fumeaux, "A highly flexible and efficient dipole antenna realized in methanol-treated conductive polymers," *Proc. 2015 Int. Symp. on Antennas and Propagation (ISAP2015)*, pp. 422–425, 2015.

S. J. Chen, P. Talemi, B. Chivers, R. Shepherd, and C. Fumeaux, "Purely polymeric antennas with exceptional flexibility and high efficiency," in *2nd Australian Microwave Symposium*, Feb 2016.

S. J. Chen, P. Talemi, B. Chivers, R. Shepherd, and C. Fumeaux, "Progress in conductive polymer antennas based on free-standing polypyrrole and PEDOT:PSS," in *2016 17th Int. Symp. Antenna Technol. Appl. Electromagn.* IEEE, Jul 2016, pp. 1–4. **(Invited paper)**

S. J. Chen, C. Fumeaux, B. Chivers, and R. Shepherd, "A 5.8-GHz flexible microstrip-fed slot antenna realized in PEDOT:PSS conductive polymer," in *2016 IEEE Int. Symp. Antennas Propag.*, vol. 2015. IEEE, Jun 2016, pp. 1317–1318.

S. J. Chen, D. C. Ranasinghe, and C. Fumeaux, "A Foldable Textile Patch for Modular Snap-On-Button-Based Wearable Antennas," in *2016 URSI Int. Symp. Electromagn. Theory*, 2016, pp. 842–845. **(Invited paper)**

S. J. Chen, D. C. Ranasinghe, and C. Fumeaux, "Snap-on buttons as detachable shorting vias for wearable textile antennas," in *2016 Int. Conf. Electromagn. Adv. Appl.* IEEE, Sep 2016, pp. 521–524. **[The Young Scientist Best Paper Award and Travel Bursary Award of ICEAA2016]**

S. J. Chen, D. C. Ranasinghe, and C. Fumeaux, "A reconfigurable wearable antenna based on snap-on buttons," in *15th Australian Symposium on Antennas*, Feb 2017.

S. J. Chen, D. C. Ranasinghe, and C. Fumeaux, "A polarization/frequency interchangeable patch for a modular wearable textile antenna," in *11th European Conference on Antennas and Propagation*, Mar 2017.

S. J. Chen, T. T. Tung, D. Losic, and C. Fumeaux, "High-efficiency microwave graphene antenna," in *IEEE AP-S Symposium on Antennas and Propagation and USNC-URSI Radio Science Meeting*, Jul 2017. **[Honorable Mention in APS/URSI 2017]**

List of Figures

List of Tables

Chapter 1

Introduction

THIS introductory chapter presents a short overview on flexible, wearable and reconfigurable antennas based on novel conductive materials and discusses the importance and challenges associated with these material-oriented antenna design. The chapter also includes an overview of the objectives and motivations of the thesis which highlights the original contributions of this research work. At the end of the chapter, the structural organization of the thesis is outlined.

1.1 Introduction and motivation

As an indispensable branch of wireless communication system design, planar antenna technology has been intensively and broadly advanced in the last five decades. In recent times, however, due to the very high demand of novel mobile communication systems, numerous new technical challenges have arisen for the antenna designers because of additional unconventional performance requirements. Typical examples of applications of relevance to this thesis include radio frequency identification (RFID) systems [1] and wearable electronics [2]. RFID systems usually consist of an RFID reader and a tag integrated with an antenna attached to the item(s) to be tracked. Therefore, it is preferable to have flexible, light-weight, highly integratable and low-cost antennas for the tags. These characteristics are also desired for the antennas used in wearable electronic systems, with additional critical requirements, namely electrical robustness to the loading by the human body, as well as mechanical robustness to deformation when worn by people. The combination of antenna technology and material sciences can provide new paths to satisfy these requirements.

To design antennas exhibiting the aforementioned characteristics, traditional conductors and dielectric materials such as metals and ceramics are not necessarily suitable, since these materials are usually costly and lack flexibility and mechanical resilience. As a result, various novel conducting and dielectric materials with suitable properties have been emerging in antenna technology. On the side of the conducting materials, typical examples of alternative materials to metals as antenna conductors include conductive polymers [3–5], graphene films [6, 7], conductive inks, conductive treads [8] and conductive textiles [9–22]. One the side of the dielectrics, polyimide films [23, 24], liquid crystal polymers [25–27], polydimethylsiloxane (PDMS) [28–31] and closed-cell polyethylene foams [21, 32] have been explored in the literature. Due to the unconventional different physical and (or) electrical characteristics of these materials, dedicated design strategies as well as appropriate technologies for the fabrication, connections and integration into the systems are extremely critical to achieve well-performing antennas. Consequently, research on these particular aspects is of significant interest for antenna designs based on novel conductors and dielectrics.

In this context, this dissertation investigates the design, fabrication and system interconnection, for flexible, wearable and reconfigurable antennas based on conductive polymers, graphene/graphite films and conductive textiles, with emphasis placed on material side of antenna engineering principles.

1.2 Objectives of the thesis

There are four main objectives of the thesis which are described in details in the following.

1. **Efficient and flexible non-metallic antennas based on conductive polymers and graphene composites**

   As mentioned earlier, compared to metallic materials, non-metallic conductive materials can be more mechanically resilient, environmentally friendly and economical and thus more suitable for flexible and wearable antennas. Among non-metallic materials which have high electrical conductivity, conductive polymers and graphene stand out as materials which have been widely investigated in engineering research, due to their attractive physical and electrical properties. Since electrical conductivity in polymer materials was first reported in 1977 [33, 34], conductive polymers have been developed as a class of attractive conductor materials for antenna designs, with steadily increasing electrical conductivity and improving mechanical resilience. Several antenna designs realized in various conductive polymers including Pani [35], Polypyrrole (PPy) [36, 37] and poly 3, 4- ethylenedioxthiophene (PEDOT) [4, 38] have been reported in the literature. The majority of these antennas however showed a relatively low efficiency since the conductive polymers typically exhibit a process-limited thickness and a relatively low electrical conductivity compared to metals. Very similar situation can be observed in the antennas realized in graphene, especially for the microwave region, since graphene has inherent limitations due to the fabrication process in terms of material thickness, size and shape [39, 40]. Additionally, flexible antenna designs taking advantages of the mechanical flexibility of these materials in a free-standing form are very limited in the literature. In this context, one of the main objects in this dissertation is to overcome these inherent process and material limitations to develop efficient and flexible antennas with different engineering methods. These approaches include efficiency-driven antenna design for efficiency improvement, simple and robust chemical treatment for material conductivity enhancement and exploitation of multilayer laminated structure for effective material thickness increase.

2. **Practical shorting and connection strategies for wearable textile antennas**

   Conductive textile are metallized textiles which can attain a sheet resistance close to that of metal layers. These so-called e-fibers generally are comprised of a non-conductive textile substrate such as cotton or nylon combined with electrically conductive elements such as copper and silver which can be coated as layer on or embedded as wires into the substrate. Since conductive textiles have highly desirable properties such as reversible physical flexibility and robustness, biocompatibility, washability and high electrical performance, they are one of the most promising conductors for flexible and wearable antennas. A variety of antennas based on conductive textiles have been developed for wearable applications [9, 11, 13, 14, 17, 19–22, 31]. One very important design aspect for these wearable textile antennas is the connection between the flexible antenna textile components and the rigid electronic system, since the textiles have very different physical properties from the electronics [41]. A similar connection challenges between flexible layer arises for wearable textile antennas that require shorting point(s) and/or shorting wall(s). This leads to the challenging task of providing reliable antenna shorting strategies where ease of fabrication, connection robustness and antenna efficiency are especially taken into account. In both cases mentioned above, the requirements for reliable, efficient and detachable connections between flexible textile layers and a ground or an electronic system are challenging to fulfil. To this end, as the second objective of this thesis, a solution based on commercial snap-on buttons is investigated and developed to address connection strategies in conductive textiles technologies.

3. **Modular and reconfigurable wearable antennas based on conductive textiles**

   An extremely important consideration in wearable antennas design is the impacts of the human body in the immediate vicinity of the devices, as well as the bending associated with movement of the body. This requires that high-performance antenna design should minimize the coupling to the human body in proximity and should be electromagnetically resilient due to bending [2]. However, those requirements are very challenging to fulfil for all possible cases, and therefore, it would be very beneficial if the antennas could include reconfigurability to compensate detuning due to these impacts and uphold performance. In addition, reconfigurability could be exploited to achieve different desired antenna characteristics to fulfil various functionalities. However, because of the difficulties in realizing reliable connection between lumped components and textiles as mentioned previously, very limited reports of reconfigurable wearable antenna designs based on conductive textiles can be found in the literature. Aiming to resolve the issue, the third objective of this dissertation is to design some novel wearable textile antennas having passive and active system reconfigurability.

4. **Novel antenna structures for wearable applications**

   The fourth objective of this thesis has two parts and they are discussed separately as follows:

   (i) Microstrip patch antennas [13–15] and arrays [16, 42] have been widely exploited for wearable applications, since they are light-weight, low-profile, compact and more importantly isolated electromagnetically from the human body due to their ground plane. For wearable applications requiring antenna array(s), the size of the array should be kept as compact as possible due the limited real estate of human body. As a result, it will be advantageous to design arrays with compact size and simple feed network while maintaining high efficiency for wearable applications. The first part of the fourth objective is to design, a compact and efficient patch array which is serially fed by one single microstrip line with dual polarization, for wearable applications.

   (ii) Dielectric resonator antenna (DRA) [43–45] is another type of antennas suitable for wearable applications. This is because they can be made compact with various shapes and aspect ratios while maintaining high radiation efficiency, wide impedance bandwidth and broad beamwidth. However, only very limited reports on wearable DRAs can be found in the literature. It is believed that one of the main reasons is their inherent physical rigidity which significantly decreases their wearability. To address this problem, as the second part of the fourth objective of this thesis, a non-metallic flexible DRA realized in PDMS mixed with ceramic powder, and graphite paper as a conductor, is proposed for wearable applications.

1.3 Summary of original contributions

This dissertation includes several original contributions to the field of flexible, wearable and reconfigurable microwave antennas based on novel conductive and dielectric materials. The contributions can be generally categorized into four major parts. The first part of the thesis presents flexible and high-efficiency non-metallic antenna designs based on conductive polymers and graphene thin films. The second part of the thesis focuses on the solutions of connection and shorting for textile transmission lines and antennas. The third part regards wearable modular and reconfigurable antenna designs based on conductive textiles and commercial snap-on buttons. And finally, the last part of the thesis investigates novel antenna structure including series-fed microstrip patch antenna arrays and flexible DRAs for wearable applications.

1.3.1 Non-metallic antennas realized in conductive polymers and graphene composites

This section lists the original contributions for high-efficiency and flexible antennas realized in non-metallic conductors including conductive polymers and graphene thin films.

- A compact, highly efficient and flexible ultra-wideband (UWB) antenna operating from 3 to 20 GHz is proposed. The antenna is completely made from polymer comprising a patterned conductive polymer (PEDOT) thin film attached to a transparent sticky tape substrate. The overall dimension is less than a quarter-wavelength at the lowest frequency of operation and the device reaches a radiation efficiency of over 85% averaged throughout the frequency band. The realized antenna offers great mechanical flexibility and robustness which indicates its promising potential for possible seamless integration in flexible electronics. This design has been published in *IEEE Antennas and Wireless Propagation Letters* under the title of “A Compact, Highly Efficient and Flexible Polymer Ultra-Wideband Antenna ” [5].

- A numerical and experimental study of the impact of bending on the characteristics of a conductive polymer UWB antenna reported in [5] is conducted. Since the antenna under investigation is highly flexible, it is very important to investigate possible performance degradations in various bending conditions, including variations in matching and radiation characteristics. The results indicate that the antenna still performs well in terms of impedance matching even with considerable bending angles whereas degradation due to bending has to be taken into account for polarization. The study results were presented at *International Conference on Electromagnetics in Advanced Applications (ICEAA), 2015* under the title of "Bending impact on a flexible ultra-wideband conductive polymer antenna " [46]. This was an invited paper and was awarded The Young Scientist Best Paper Award of ICEAA2015.

- A highly flexible and efficient 2.45-GHz dipole antenna realized in methanol-treated conductive polymers PEDOT:PSS (PEDOT) is proposed. The originally highly conductive PEDOT thin films have been further treated by immersion in a methanol solution, to realize a five-times conductivity improvement from approximately 3500 S/m to 18500 S/m. As a result, a more than 25% antenna efficiency enhancement is attained, which brings the averaged efficiency up to 91.4% of the efficiency of a copper reference antenna with identical geometry. The results of this work were presented at *International Symposium on Antennas and Propagation (ISAP), 2015* under the tile of "A highly flexible and efficient dipole antenna realized in methanol-treated conductive polymers " [47]. A summary of the antenna designs reported in [5, 47] was also presented at *2nd Australian Microwave Symposium, 2016* under the tile of "Purely polymeric antennas with exceptional flexibility and high efficiency " [48].

- A flexible 5.8-GHz microstrip-fed slot antenna realized in thin films of conductive polymer PEDOT:PSS is designed, fabricated and tested. Due to the utilization of a highly conductive and flexible polymeric film, the antenna has a high efficiency of 82% and fully reversible conformability. The outcomes of this design were presented at *IEEE International Symposium on Antennas and Propagation (APSURSI), 2016* under the tile of "A 5.8-GHz flexible microstrip-fed slot antenna realized in PEDOT:PSS conductive polymer " [49].

- A review of various realizations of microwave antennas based on free-standing conductive polymers including polypyrrole (PPy) and PEDOT:PSS (PEDOT) is done in regard to two significant aspects: improvement of their efficiency and exploitation of their mechanical flexibility for antenna designs. This points out design strategies able to achieve high antenna efficiencies and reproducible mechanical conformability. This review was presented at *17th International Symposium on Antenna Technology and Applied Electromagnetics (ANTEM), 2016* under the tile of "Progress in conductive polymer antennas based on free-standing polypyrrole and PEDOT: PSS " [50]. This was an invited paper.

- A three-layer laminated thin film structure based on two layers of conductors of PEDOT and one layer laminae of SiO_2 in between has been tested in a dedicated microstrip line test jig, showing a 5 to 15 dB higher $|S_{21}|$ parameter compared to the single layer PEDOT. These results indicate the laminated structure is promising to overcome the insufficient film thickness problem for some conductive polymers.

- A highly efficient UWB antenna based on graphene films made of binder-free and surfactant-free graphene inks is proposed. The fabricated antenna exhibits an efficiency averaging 79% over the bandwidth from 3.1 to 10.6 GHz, which is, to the authors' best knowledge, the highest reported value for graphene antennas for the microwave region. This outstanding performance is attributed to the combination of high-quality graphene films, efficiency-driven antenna design strategy and appropriate fabrication technique. This work has been published in *Journal of Materials Chemistry C* under the tile of "Scalable realization of conductive graphene films for high-efficiency microwave antennas " [51]. The details of the antenna design has been accepted to *IEEE AP-S Symposium on Antennas and Propagation and USNC-URSI Radio Science Meeting, 2017* under the tile of "High-efficiency microwave graphene antenna " [52]. This conference paper was awarded an 'Honorable Mention'.

1.3.2 Shorting and connection strategies for wearable textiles antennas

In this section, a summary of the original contributions in relation to connection and shorting strategies for wearable antennas and transmission lines realized in conductive textiles.

- Various shorting strategies including a folded strip of silver fabric, embroidered vias and eyelets are investigated for wearable textile antennas, based on a test bed, namely an L-slot planar inverted-F antenna (PIFA). The performance of the antenna under test with these three shorting methods is compared through simulations with realistic shorting models. The results indicate that the embroidered vias shorting method, which is the simplest and cheapest method to implement, has slightly lower efficiency and gain than the silver fabric folded strip and eyelet shorting methods due to its higher resistance. This investigation results was presented at *International Workshop on Antenna Technology (iWAT), 2014* under the tile of "Shorting strategies for a wearable L-slot planar inverted-F antenna " [53].

- Commercial snap-on buttons are proposed to be used as detachable shorting vias for wearable textile antennas. A patch antenna prototype using these button shorting vias is designed and experimentally characterized. By engaging selected male buttons from the ground plane with female buttons to form shorting vias, various antenna patterns can be selected. This illustrates that commercial snap-on buttons can be utilized as detachable shorting vias for wearable textile antennas. This design was presented at *International Conference on Electromagnetics in Advanced Applications (ICEAA), 2016* under the tile of "Snap-on buttons as detachable shorting vias for wearable textile antennas " [54]. This paper was awarded The Travel Bursary Award and The Young Scientist Best Paper Award of ICEAA2016.

- A pair of commercial snap-on buttons is demonstrated as a detachable radio-frequency (RF) balanced connection between a garment-integrated textile dipole antenna and a passive sensor-enabled RFID tag in a wearable wireless system. This arrangement offers reliable, low-cost and easily detachable RF coupling and feeding connections for balanced antennas, as conceptualized in simulations and validated through measurements. In addition, a back-to-back balanced transmission line structure has been designed and measured to characterize the RF performance of the proposed snap-on button connection. The resulting S-parameters indicate the good performance of the snap-on buttons as RF connectors for balanced antennas/transmission lines at least up to 5 GHz with insertion loss better than 0.8 dB. This research work has been published at *IEEE Antennas and Wireless Propagation Letters* under the tile of "Paired snap-on buttons connections for balanced antennas in wearable systems " [55]. This was an invited paper. In addition, an overall review of connections based on snap-on buttons was presented at *14th Australian Symposium on Antennas, 2015* under the tile of "Snap-on buttons connections for transmission lines and antennas " [56].

1.3.3 Modular and reconfigurable antennas based on conductive textiles

The following list provides the details of the original contributions on wearable textile antenna designs with modularity and reconfigurability.

- An antenna design concept with detachable radiation elements offering modular geometry reconfigurabilities for wearable applications is presented. By utilizing snap-on buttons, both as the radio-frequency RF connection and mechanical holding mechanism, different modularly interchangeable microstrip patches are employed to demonstrate geometry reconfigurabilities in terms of polarization and resonance frequency. Three patches offering interchangeability in circular polarization at 5 GHz, interchangeability in resonance frequencies of 2.4- and 5.3-GHz and operation at 8-GHz are proposed as typical designs, respectively. Experimental results of the fabricated antennas in free space, worn by a torso phantom and in bending conditions, validate the concept and prove that this type of modular design offers convenient, passive, low-cost, and versatile system reconfigurabilities, which can benefit wearable applications. This unique and versatile design has been published at *IEEE Transactions on Antennas and Propagation* under the tile of "A modular textile antenna design using snap-on buttons for wearable applications " [57].

- A foldable patch module for the modular wearable textile antenna concept in [57] is presented, demonstrating passive discrete resonance frequency modularity at 8, 9 and 10 GHz. Through a simple folding of the textile radiating element at predetermined lengths denoted by position markers, particular resonance frequencies can be manually interchanged. Prototype-based experimental characterization shows a good agreement with simulations, which indicates that the foldable module performs as expected. This design emphasizes that the reported modular antenna design promotes a practical, low-manufacture-cost, low-maintenance-cost, passive and versatile solution to reconfigure system characteristics for multi-functional wearable systems. The results of this design were presented at *URSI International Symposium on Electromagnetic Theory (EMTS), 2016* under the tile of "A foldable textile patch for modular snap-on-button-based wearable antennas " [58]. This was an invited paper.

- A further illustration of the versatility of the modular concept, a circular patch module with a rectangular flap cut in the middle is proposed. This module can provide interchangeability between right-handed circular polarization (RHCP), left-handed circular polarization (LHCP) and linear polarization (LP), as well as passive reconfigurability in resonance frequency for LP, through simple module rotation and different flap configurations (opened or closed). The design and the measurement results have been presented at *11th European Conference on Antennas and Propagation, 2017* under the tile of "A polarization/frequency interchangeable patch for a modular wearable textile antenna " [59].
- A reconfigurable module based on snap-on buttons with integrated varactors and a dedicated bias circuit board is proposed for reconfigurable wearable textile antennas. This varactor-loaded module can solve the main challenge in realization of reliable connection between bias circuit, lumped components and conductive textiles. The very different physical properties of those flexible and rigid components have been the main obstacle to truly reconfigurable wearable designs. A reconfigurable PIFA antenna utilizing this button module is designed to validate the concept. The preliminary results of this antenna were presented at *15th Australian Symposium on Antennas, 2017* under the tile of "A reconfigurable wearable antenna based on snap-on buttons " [60].

1.3.4 Novel antenna structures for wearable applications

The following list shows the detailed information for the last main part of the thesis' original contributions dedicated to exploration of novel wearable antenna structures, namely a microstrip patch array and a DRA for wearable applications.

- A compact and highly efficient circular travelling wave series-fed microstrip patch array for wearable applications is proposed. The patch elements are excited by a microstrip line through coplanar proximity coupling. A dual-port feeding allows to select the direction of the travelling waves, and consequently the sense of circular polarization of the patches. Simultaneous feeding to both ports with proper amplitude and phase difference can result in radiated waves of arbitrary polarization. Since the antenna array exhibits a simple feeding structure, a relatively compact size and a very good isolation from the human wearer owing to the ground plane, it is suitable for wearable applications. The outcomes of this design have been published at *IEEE Antennas and Wireless Propagation Letters* under the tile of "Dual circularly polarized series-fed microstrip patch array with coplanar proximity coupling " [61].

- A non-metallic DRA whose dielectric resonator and substrate are both made mechanically flexible for wearable applications is designed and subjected to experimentally characterization. This microstrip-patch-fed antenna is realized in a mixture of PDMS and ceramic powder, as well as carbon paper as a conductor. Since this non-metallic antenna has decent mechanical flexibility, a ground plane and thus electromagnetic isolation to the human body, a measured wide impedance bandwidth of 53% and a measured broad beamwidth of nearly 100°, it is promising for wearable applications.

1.4 Thesis structure

As illustrated in Fig. 1.1, this thesis starts with introduction and literature review in the first two chapters and ends up with conclusion and future work discussion in the last chapter. The main chapters in between focus on the original contributions of the thesis, as described in detail in the following.

I **Introduction (Chapters 1 & 2)**

The initial part of the thesis encompasses the current introductory chapter and Chapter 2 where the context and the background information required for the rest of the thesis are provided. The second chapter contains two major topics: i) a general literature review on flexible, wearable and reconfigurable antennas with emphasis on antenna design and materials; ii) a survey of the novel conductive and electric materials used in the different parts of this thesis, focusing on the challenges in utilizing these materials for antenna designs as well as the possible solutions.

II **Non-metallic antennas (Chapters 3 & 4)**

The second part of the thesis focuses on non-metallic antenna designs based on conductive polymers and graphene thin films. Chapter 3 demonstrates various highly flexible and efficient polymeric antennas including both narrow-band and ultra-wideband UWB designs. The application of different engineering methods has helped to successfully overcome the process-limited inherent problems

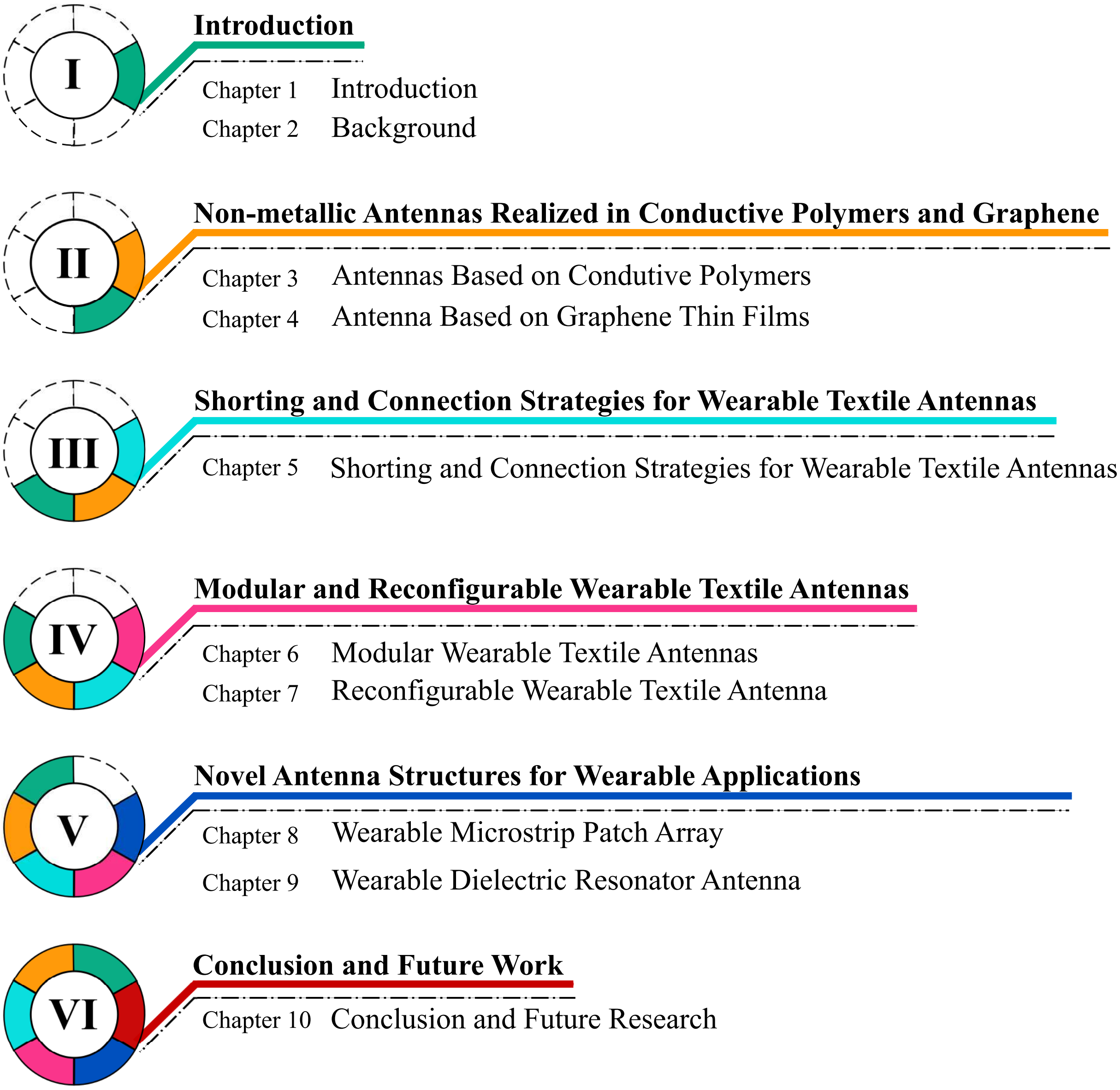

Figure 1.1. Thesis outline. The thesis comprises 10 chapters where the first two chapters include introduction and literature review while the last chapter concludes the dissertation. The chapters in between discuss the four main original contributions of the thesis: i) non-metallic antennas; ii) textile antenna connection and shorting strategies; iii) modular and reconfigurable wearable textile antennas and iv) novel antenna structures for wearable applications.

of the conductive polymers. Additionally, a study investigating the antenna performance degradation attributed to various state of bending is conducted, aiming to illustrate the necessary considerations while using the antenna in conformal configurations. Chapter 4 provides the design details of an UWB antenna possessing a very high efficiency of nearly 80% realized in graphene thin films, which suggests the excellent potential of graphene as environmentally-friendly, low-cost and non-metallic conductor for antennas operating in the microwave region.

III **Textile antenna connection and shorting Strategies (Chapter 5)**

Chapter 5 proposes some appropriate, convenient and efficient shorting and connection strategies for textile antennas and transmission lines. The aim of the investigation is to solve the difficulty in textile-to-electronics connection. Various shorting methods for textile antennas are compared, laying emphasis on implementation cost, antenna efficiency and gain, as well as fabrication complexity. This study sheds light on the important factors to be considered when deciding shorting strategies for textile antennas. Following that, it describes a detachable and reliable connection for a wearable RFID-based elderly monitoring system and its textile dipole antenna, using commercials snap-on buttons. Through this inexpensive solution, very solid mechanical connection with a satisfactory RF performance can be achieved for the system. The approach which also enables detachable connections and thus allows separating the sensitive electronic parts to wash the garment-integrated textile antenna.

IV **Modular and reconfigurable wearable antennas (Chapters 6 & 7)]**

This part of the thesis presents two types of wearable textile antennas in which one can passively and the other can actively change their characteristics such as their resonance frequency or polarization. Chapter 6 depicts a modular wearable textile antenna concept based on snap-on buttons, which can fulfil different system requirements by interchanging tailor-made patch modules. A variety of patch modules which share one common feed base are also proposed for diverse functionalities, extending the patch module library. Chapter 7 shows a reconfigurable wearable textile antenna based on a reconfigurable module in which snap-on button, lumped components and bias circuit are integrated together. This reconfigurable module gets over the connection reliability problem between textiles and electronic components and circuit, by utilizing snap-on buttons in the integration design.

V **Novel antenna structures for wearable applications (Chapters 8 & 9)**

The next part of the thesis describes the exploration of novel designs, namely a microstrip patch array and a DRA for wearable applications. The design, fabrication and measurement of a series-fed microstrip patch array in free space and worn by a torso phantom are discussed in Chapter 8, exhibiting a compact and high efficiency array design concept with excellent electromagnetic isolation to the human body. In Chapter 9, a non-metallic conformal DRA design composed of flexible dielectric resonator, substrate and ground plane is demonstrated, for the sake of improving the comfortability when wearing these antennas. The measurement results indicate that the DRA has decent mechanical flexibility, a wide bandwidth and a broad beamwidth which make it promising for wearable applications.

VI **Conclusion and future work (Chapter 10)**

The last chapter provides a conclusive summary of all the projects included in this thesis, as well as a prospective view about the further work.

Chapter 2

Background

ANTENNA designs based on unconventional or novel conductive materials have gained intensive research attention in recent years. This is motivated by desirable antenna characteristics such as mechanical resilience, light weight, affordability and environmental friendliness, which are required for new generations of wireless electronic systems, for example wireless body area network (WBAN) or RFID technology. This chapter reviews typical antenna designs based on conductive polymers, graphene/graphene composites and conductive textiles, laying emphasis on the design and fabrication challenges associated with these novel non-ideal material properties, and outlining the corresponding possible solutions.

2.1 Introduction

Antenna are essential components of every wireless communication system. Compared to bulky and rigid fixed antennas commonly seen on rooftops such as Yagi antenna and parabolic antennas, antennas for new generation of wireless mobile systems such as WBAN are required to be low in profile, light in weight, small in size, resilient in deformation and robust to exterior electromagnetic impacts. Therefore, one important aspect of current antenna developments is exploiting novel materials to realize superior designs, since conventional antenna materials such as metals and ceramics cannot perfectly fulfil the aforementioned characteristics. As a result, many types of novel materials have been emerging in antenna technology. Among these materials, conductive polymers, graphene/graphene composites and conductive textiles are very promising due to their unique properties. For instance, conductive polymers and conductive textiles have excellent mechanical resilience whereas graphene are potentially economical and can be produced in environmentally-friendly ways. However, due to their special physical and electrical properties, extra considerations in material preparation, antenna design and fabrication are required to maximize achievable antenna performance. For conductive polymers, due the relatively low conductivity compared to metals, efficiency-driven antenna design strategies are necessary to overcome this issue and achieve high antenna efficiency.

In this chapter, a brief literature review of conductive polymers, graphene/graphene composites and conductive textiles will be presented from the perspective of antenna technology, with special focus on the challenges of using these materials for antenna designs while retaining appreciable performance. In particular, Section 2.2 and 2.3 will discuss typical antenna designs based on conductive polymers and graphene respectively, while the use of conductive textiles will be reviewed in Section 2.4.

2.2 Antenna designs based on conductive polymers

Conductive polymers combine high electrical conductivity (simply referred to as 'conductivity' for the rest of this thesis unless otherwise stated) and mechanical elasticity. They also exhibit low density, ease of processability and corrosion resistance. These properties make them very attractive for a very wide range of applications such as chemical sensors [62–64], biosensors [65], printed electronics [66], supercapacitors [67, 68] and electromagnetic devices [3, 36, 69, 70]. Since the initial report on their electrical conductivity in 1977 [33, 34], conductive polymers have attracted significant attention from the research world. Three scientists mainly contributed to this breakthrough, Hideki Shirakawa, Alan J. Heeger and Alan G. MacDiarmid, who jointly received the Nobel Prize in Chemistry in 2000 for the discovery and development of electrically conductive polymers. With steadily growing resources and efforts invested into the research on conductive polymers, increasingly higher electrical conductivity, better mechanical resilience and tunability in resistance have been gradually reported in the literature. Of particular interest in this thesis, due to their steadily improving electrical conductivity and mechanical elasticity, conductive polymers have become very promising as antenna conductors, especially in the view of achieving flexible and purely non-metallic flexible designs. In addition, since the conductivity can be to some extent controllable in some polymers, the realization of reconfigurable antenna becomes another potential development, as proposed in [71]. As a result, many antennas based on various conductive polymers have been emerging recently. The following section will give a descriptive introduction about conductive polymers and their electromagnetic properties.

2.2.1 Conductive polymers

Polymers consist in large molecules or macromolecules which are formed by chains of many repeated carbon-based sub-units. They can be found in our body as fundamental building blocks, including for example in DNA, and are present in nearly everything around us such as plastics and rubber. Generally, most natural and synthetic polymers are highly insulating. In contrast, polymers with electrical conductivity are referred to as conducting/conductive polymers, or more precisely, as intrinsically conducting polymers. The chemical structures of some typical conductive polymers, including polyacetylene ($(CH)_x$), polyphenylene vinylene (PPV) and polyaniline (PANI) are shown in Fig. 2.1, all demonstrating a conjugated molecular structure in the main chain with π-electrons delocalized. The unique electrical and optical properties are a result of this conjugated π system [72].

One of the earliest conductive polymer references described the preparation of polyaniline by the anodic oxidation of aniline was published by Henry Letheby, as early as 1862 [73]. The polymer reported in this reference was conductive and exhibited an electrochromic characteristic. Around 100 years later, description of polymers with much higher conductivity appeared in the literature. For example, in 1963, Australian

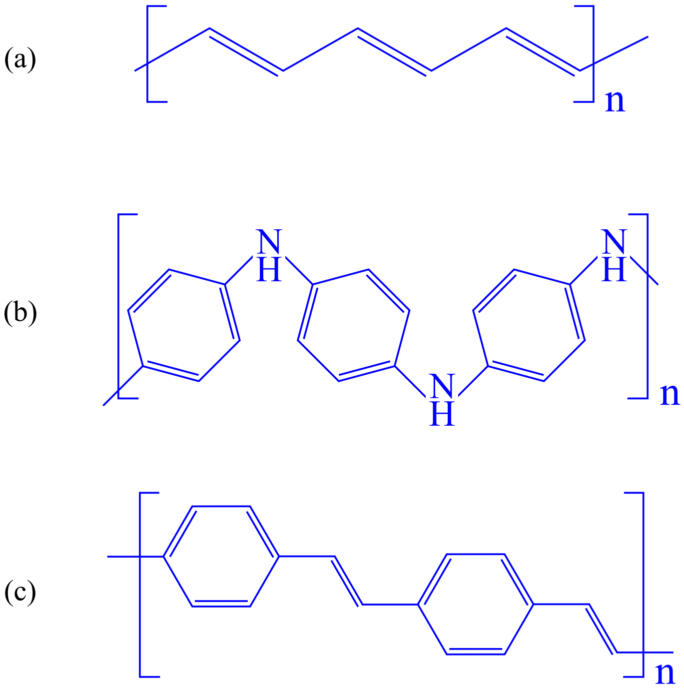

Figure 2.1. Chemical structure of some typical conductive polymers. The chemical structure of three typical conductive polymers: (a) polyacetylene ($(CH)_x$); (b) polyphenylene vinylene (PPV); (c) polyaniline (PANI).

scientists reported a series of highly conductive PPys, which had a measured conductivity as high as 1×10^{-2} S/m. In 1968, R. De Surville and co-workers showed a PANI which possessed a similar conductivity of $1.3 \times 10^{-2} S/m$ [74]. Even thought these experimental values of polymer conductivity were much greater than the ones reported before, they were still not high enough for practical applications.

In late 1970s, the interest in conductive polymers started to grow significantly following the demonstration by researchers at IBM Research Laboratory that polythiazyl ($(SN)_x$) can be superconductive [75]. In 1977, the attention on these materials became even intense, when MacDiarmid's team showed that the doping of polyacetylene films could achieve an unprecedented of conductivity of 3800 S/m [33]. Since then, expectations in polymer conductivity have been raising continuously. As depicted in Fig. 2.2, the DC conductivity of conductive polymers can range from 10^{-10} S/m to 10^{7} S/m which can be very close to that of silver, the most conductive metal.

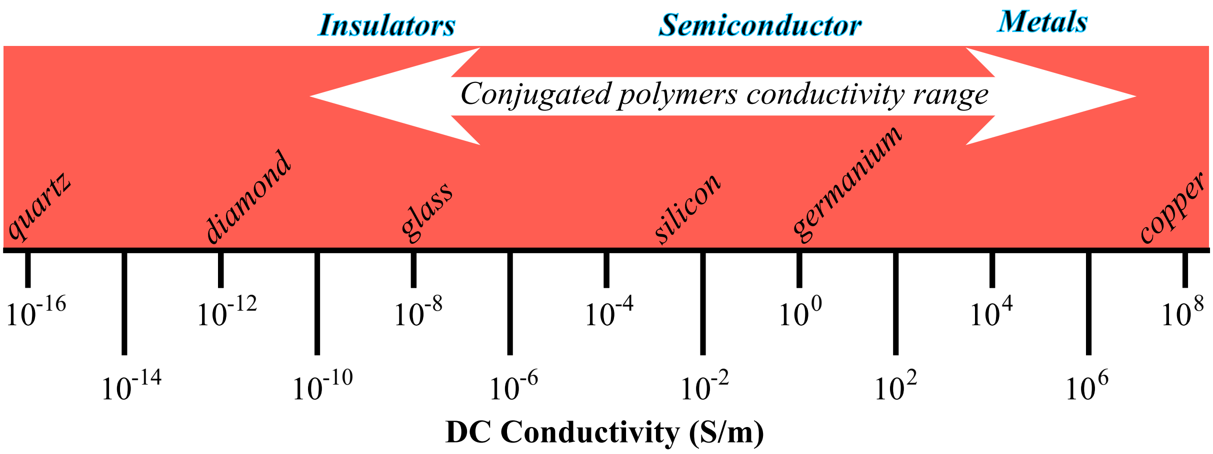

Figure 2.2. DC electrical conductivity range of conductive polymers. The DC electrical conductivity of conductive polymers can range from 10^{-10} to 10^{7} S/m.

During the last four decades, many conductive polymers have been studied in details and these include polyacetylene, PPV, PANI, polypyrrole (PPy) and Poly(3,4-ethylenedioxythiophene) (PEDOT). Although polyacetylene is probably the most conductive polymers investigated so far, the potential applications using this material are quite limited due to the difficulty in processing and its inherent chemical instability. In contrast, PPy can have reasonably high conductivity and environmental stability due to its heteroaromatic and extended p-conjugated backbone structure [76]. The chemical structure and a scanning electron microscope (SEM) image of PPy are shown in Fig 2.3. By means of doping, which permits partial charge extraction from the chain, the conductivity of neutral PPy can be dramatically increased from an insulating level to a metallic level. PPy has been intensively studied for many applications such as for electrodes in capacitors and rechargeable batteries, sensors, actuator and electromagnetic devices [76].

Another type of polymer, namely Poly(3,4-ethylenedioxythiophene) usually referred to as PEDOT, has drawn much attention recently, since it has excellent environmental and chemical stability combined with high conductivity under doping [77]. These advantages have made it as promising material for broad applications in solid state capacitors, electrode materials and antistatic painting. Doping with poly(styrenesulfonate) (PSS), PEDOT becomes PEDOT:PSS which exhibits high mechanical flexibility and excellent thermal stability, not to mention high conductivity [78,79]. The chemical structure and an SEM image of PEDOT:PSS are displayed in Fig. 2.4.

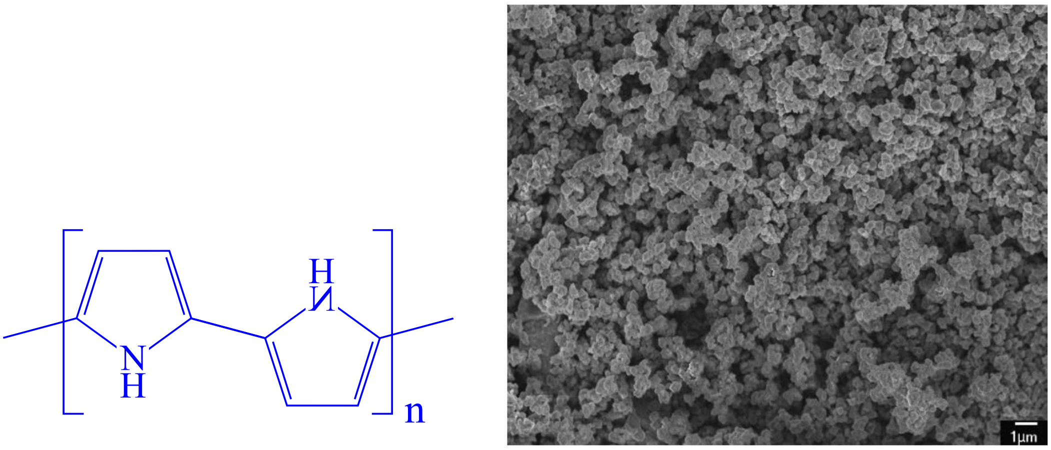

(a) (b)

Figure 2.3. Chemical structure and an SEM image of PPy. (a) Chemical structure and (2) an SEM image of PPy. The SEM image was adapted from [63].

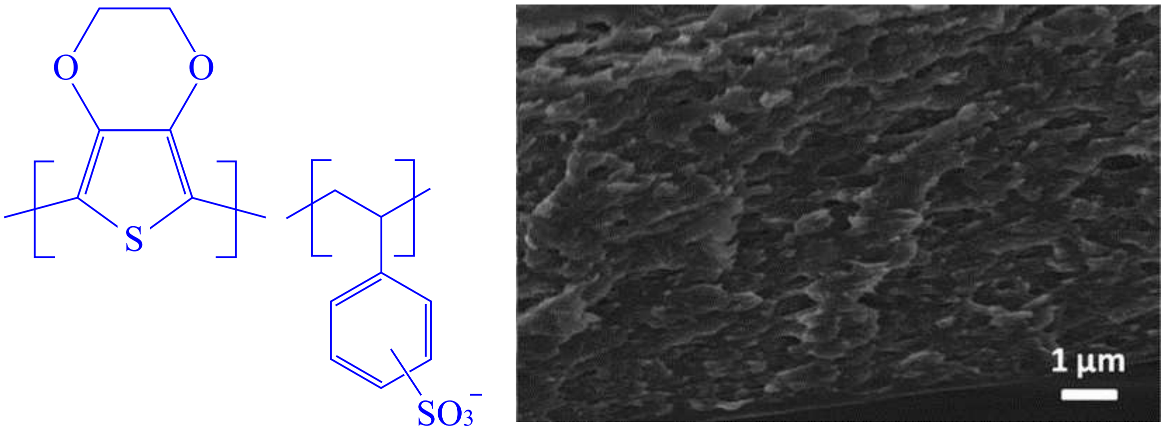

(a) (b)

Figure 2.4. Chemical structure and an SEM image of PEDOT:PSS. (a) Chemical structure and (2) an SEM image of PEDOT:PSS. The SEM image was adapted from [68].

In regard to electromagnetic applications of conductive polymers, electromagnetic interference (EMI) shielding and antenna designs in the microwave region have generally been the two key aims. This is because conductive polymers have desired feature, namely a high conductivity that can be easily controlled in the fabrication process. For instance, metals or metal-coated materials are suitable for EMI shielding by wave reflection. However, they can not be adopted for EMI shielding that is based on absorption due to their very shallow skin depth which is a direct consequence of their extremely high conductivity. In contrast, because of the comparatively low conductivity, conductive polymers not only can reflect but also absorb electromagnetic waves, and thus they hold a critical advantage over metallic materials.

In a different context, namely for antenna design, high conductivity is obviously one of the major criteria for judging the suitability of polymeric materials, since high conductivity is one of the two most crucial conditions guaranteeing high antenna efficiency. The other crucial condition is the thickness of the conductive polymers, because it has been proven to be very challenging to simultaneously synthesize conductive polymers with high conductivity and sufficient thickness, due to the extraordinary challenge in achieving conductive nanostructured grains vertically in the materials. As a result, highly conductive polymers usually exhibit a very small thickness in the order of less than one skin depth for RF and microwave applications. Therefore, the process-limited thickness of conductive polymers determines the cross section area in the material where RF current is flowing which is inversely proportional to the effective resistance. If the polymer thickness is too small, for example much less a skin depth, this will lead to a significant increase in the effective surface resistance by confining the RF currents in an insufficient cross-sectional area.

A good understanding of the concept of skin depth is fundamental here. We assume that a harmonic plane wave with an angular frequency of ω is propagating in a conductive medium with permittivity, permeability and conductivity of ε, μ and σ, respectively. The governing Maxwell's equations in phasor form are:

$$\nabla \times \underline{\mathbf{E}} = -j\omega\mu\underline{\mathbf{H}} \tag{2.1}$$

$$\nabla \times \underline{\mathbf{H}} = \sigma\underline{\mathbf{E}} + j\omega\varepsilon\underline{\mathbf{E}}. \tag{2.2}$$

Then the corresponding wave equation for the electric field vector $\underline{\mathbf{E}}$ is

$$\nabla^2\underline{\mathbf{E}} + \omega^2\mu\varepsilon(1 \; - \; j\frac{\sigma}{\omega\varepsilon})\underline{\mathbf{E}} = 0, \tag{2.3}$$

where the propagation constant γ for the plane wave in the medium is defined as

$$\gamma^2 = \omega^2\mu\varepsilon(1 - j\frac{\sigma}{\omega\varepsilon}). \tag{2.4}$$

Then the complex γ can be seen as a combination of the attenuation constant α and the phase constant β which are its real and imaginary parts respectively:

$$\gamma = \alpha + j\beta = \sqrt{\omega^2\mu\varepsilon(1 - j\frac{\sigma}{\omega\varepsilon})} = j\omega\sqrt{\mu\varepsilon}\sqrt{1 - j\frac{\sigma}{\omega\varepsilon}}. \tag{2.5}$$

A non-zero attenuation constant α indicates that the field amplitude has an exponential decay in the medium along the propagation direction. Since the conductive polymers suitable for use in antenna technology are chosen with a high conductivity, meaning that $\sigma >> \omega\varepsilon$, Formula 2.2.1 the can simplified to:

$$\gamma = \alpha + j\beta \approx (1 + j)\sqrt{\frac{\omega\mu\sigma}{2}}). \tag{2.6}$$

The skin depth δ for good conductors then can be defined as

$$\delta = \frac{1}{\alpha} = \sqrt{\frac{2}{\omega\mu\sigma}}, \tag{2.7}$$

describing the depth for which the field amplitude in the conductor will decay by a factor of e^{-1} (36.8%).

Based on the skin depth concept discussed above, it is noted that when electromagnetic waves at microwave frequency flow in a good conductor, the skin depth is very small. Nevertheless, it is very challenging to achieve sufficient thickness in the range of dozens of micrometers with high conductivity for conductive polymers as mentioned before. For instance, in [79], a five-layer spin-coated PEDOT:PSS thin film had one of the highest conductivity reported, namely $2.35 \times 10^5 S/m$, however with a thickness only of 109 nm, which is approximately a one hundredth of the skin depth at 10 GHz. As a result, even with a very high conductivity, this PEDOT:PSS thin film is not appropriate for microwave antenna designs due to the very limited thickness.

Consequently, to justify whether a sub-skin-depth-thick thin film material is suitable or not for microwave antenna designs, a quantity called sheet resistance which is dependent on conductivity and thickness can be conveniently adopted. Sheet resistance R_s, in $\Omega/square$, is defined through the following relationship:

$$R_s = \frac{1}{\sigma d}, \tag{2.8}$$

where σ and d is the thin film conductivity and thickness, respectively. To quantitatively illustrate this measure, a copper thin film ($5.8 \times 10^7 S/m$) with one 10-GHz skin depth (661 nm) is calculated to be 0.026 $\Omega/square$ whereas the PEDOT:PSS film in [79] mentioned before had a value of 39 $\Omega/square$. It is noted that generally the highest achievable thickness for polymers with satisfactory conductivity is under the order of 100 μm. This places challenges in realizing high efficiency antenna designs in the microwave region. The next section will go through some typical polymeric antenna designs for which the described trade-off between conductivity and layer thickness is of concern.

2.2.2 Conductive polymer antenna designs

A variety of antennas based on different types of conductive polymers have been reported in the literature, from optically transparent to opaque, rigid to flexible, and narrow-band to UWB. In this context, it is worth mentioning the very first antenna designs based on conductive polymers, as introduced by the pioneers who could sense these materials' great potential. The earliest reported transparent polymeric antennas were presented by National Aeronautics and Space Agency (NASA) in 1997 [80], namely including two antennas working at 2.3 and 19.5 GHz based on a transparent conductive dioxide polymer AgHT-8. This work has showed the feasibility of transparent and conformal antenna design based on polymeric materials, although the antennas were not flexible.

The following research work can be considered as a classical specialized antenna example that does require to be made of conductors with relatively low conductivity - a requirement that conductive polymers can fit very well. In this case, a four-element crossed dipole direction-finding antenna assembly based on a fabric realized in S2 glass fibers with PPy coating layer(s) was reported in 1999 [36]. This design used PPy rather than metal to reduce the antenna radar cross section (RCS), to gain corrosion resistance and to exploit adjustable electromagnetic properties, by smartly taking advantage of the relative low conductivity (from 10 to 100 S/m) in the PPy coating. The rationale for avoiding metals in this design is two-fold: i) metals are heavy and have very high metallic conductivity leading to a large RCS due to the strong incident wave reflection, and ii) low antenna efficiency is acceptable or can be compensated. However, this concerned a very special application, and more generally highly conductive conductors are naturally a common requirement for the majority of antenna designs, so as to achieve high antenna efficiency.

Because of the relatively low conductivity and the process-limited thickness, antennas based on conductive polymers usually have a low efficiency. For instance, S. Cichos and co-workers presented a performance study of polymer-based RFID antennas working at 13.56 MHz for short range communication in 2002 [69]. The experimental results from this study demonstrated that antennas realized with conductive polymer pastes achieved approximately only an half of the read range of a corresponding copper antenna. This can be straightforwardly attributed to the higher ohmic losses, and it was also demonstrated that the read range can be improved by increasing the paste thickness and using lamination. Making the paste thickness larger or laminating them are two ways to improve the paste conductivity and thus lower its ohmic losses. Although the achieved read range is shorter for the polymeric antennas, they do offer the advantages of low cost and light weight. Another two dipole antennas based on PEDOT:PSS also for RFID applications were proposed by N. J. Kirsch et al [38], as shown in Fig 2.5. These antennas were realized on a polyethylene terephthalate (PET) substrate using modified PEDOT:PSS ink patterned with screen printing and inject printing technologies. Hence, the antennas exhibited a light weight and excellent mechanical flexibility, as demonstrated in Fig. 2.5. In spite of the impressively high conductivity of the polymer ink ($5 \times 10^5 S/m$), the polymeric antenna prototypes have a much lower gain (2 to 6 dB lower) than the copper ones, due to the very limited achievable printed polymer thickness and low film quality. Having said that, the best antenna reported in this study can still be practically used in an RFID system [81]. The authors also have conducted a performance study of a similar polymeric dipole antenna in a multiple-input multiple-output (MIMO) system, which concluded that the antenna yields approximately half of the copper antenna efficiency due to the relatively low conductivity [82].

Through theoretical and experimental analysis, researchers quantified that, besides high conductivity, sufficient thin film thickness is another critical condition for achieving high antenna efficiency. In 2010, Verma et al. investigated the effect of film thickness on the radiation efficiency of a 4.5 GHz PPy patch antenna [83]. Four PPy thin films with identical conductivity but different thicknesses (all below one skin depth) were utilized to manufacture four patch antennas of identical geometry. The results of

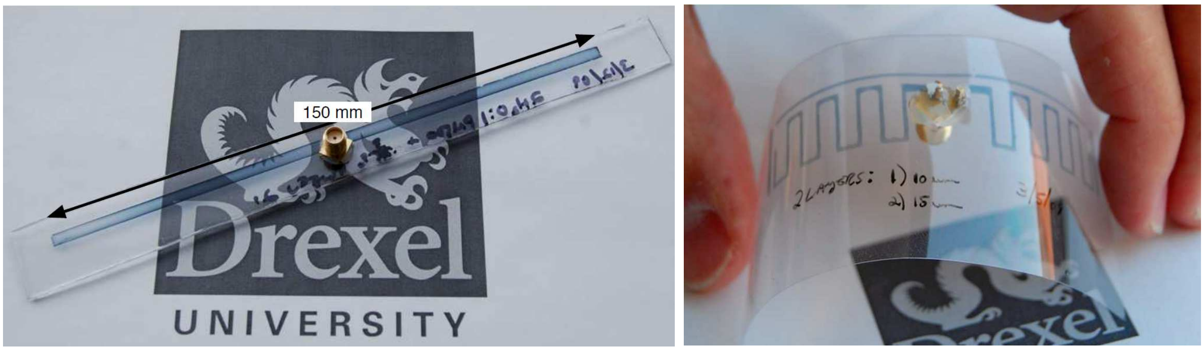

(a) (b)

Figure 2.5. Two dipole antennas realized in PEDOT:PSS for RFID applications. (a) a half-wave dipole and (2) a meandering dipole, all adapted from [38]. These antennas exhibit excellent mechanical flexibility.

Table 2.1. Film thickness effect on antenna efficiency. PPy thin film thickness and DC sheet resistance, and the corresponding antenna radiation efficiency, with respect to a copper reference antenna, reported in [83]

	Thickness (μm)	DC sheet resistance ($\Omega/square$)	Radiation efficiency (%)
PPy	40	12.5	38.5
PPy	50	10	47.8
PPy	90	5.56	52.3
PPy	140	3.57	64.8
Copper	17	N/A	99.6

this experimental are shown in Table 2.1 where a larger film thickness translated to a higher antenna efficiency. Another similar study for an UWB antenna realized in two PPy films with different thickness was accomplished by Kaufmann et al., which also confirmed that sufficient film thickness is crucial for antenna efficiency. The conduction efficiencies of both PPy UWB antennas are shown in Fig. 2.6 where the thicker PPy film offers a higher antenna efficiency.

The efficiency of antennas based on lossy conductors like conductive polymers can be strongly dependent on the antenna radiation characteristics. For example, a resonant antenna such as slot antenna will have a lower antenna efficiency compared to a non-resonant antenna such as a leaky-wave antenna, since the resonance process will typically build up a higher current density and thus cause higher ohmic losses

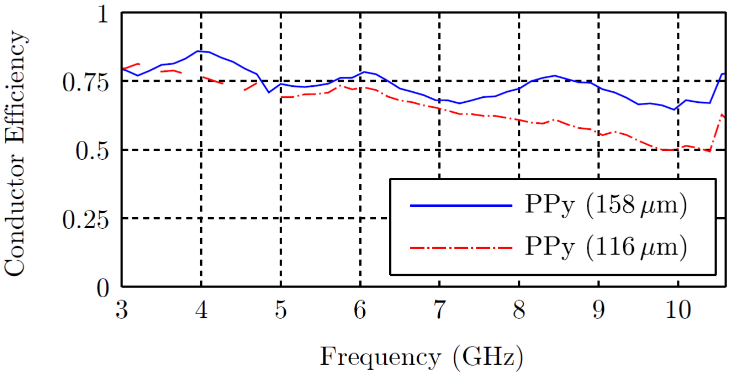

Figure 2.6. Conductor efficiencies of two PPy UWB antennas. The conductor efficiencies of two identical UWB antennas realized in a 116-μm- and a 158-μm-thick PPy thin film, adapted from [84].

in the conductor. Especially when the conductor has a thickness well below a skin depth and a relatively low conductivity, the discrepancy between antenna types can be significant. As a good example to show this phenomena, an UWB antenna realized using PPy film was reported by Kaufmann et al, with a remarkable antenna efficiency of nearly 80% [4]. As shown in Fig. 2, the UWB antenna is of a three-layer structure which consist of a Rogers Ultralam 2000 dielectric substrate between two patterned layers of 158-μm-thick and highly conductive (2700 S/m) PPy films. The DC sheet resistance of the PPy film is 2.3 $\Omega/square$. In contrast, a proximity patch antenna made from a sufficiently thick and conductive PANI films only has an efficiency of 56% [35]. The PANI film features a higher conductivity of 6000 S/m and a sufficient thickness of 100 μm, equalling to a DC sheet resistance of 1.66 $\Omega/square$. The main reason why this patch yields a much lower efficiency compared to the UWB antenna in [4] even if using a better polymer film (i.e. with lower DC sheet resistance) , is that the UWB antenna is not a resonant antenna while the patch antenna is.

One potentially groundbreaking application of conductive polymers in antenna design is for reconfigurable devices in which the polymer adjustable conductivity can used as the antenna turning mechanism. A published article has proposed this concept using a patch antenna with two strips loaded on the patch edges [71], as shown in Fig 2.8. These two strips can be made from conductive polymers with tunable conductivity and therefore, the patch resonant frequency can be reconfigured by ’electrically turning on or off’ these strips. However, this design was only experimentally verified by physically removing the two edges, raising doubts on the feasibility of a practical realization.

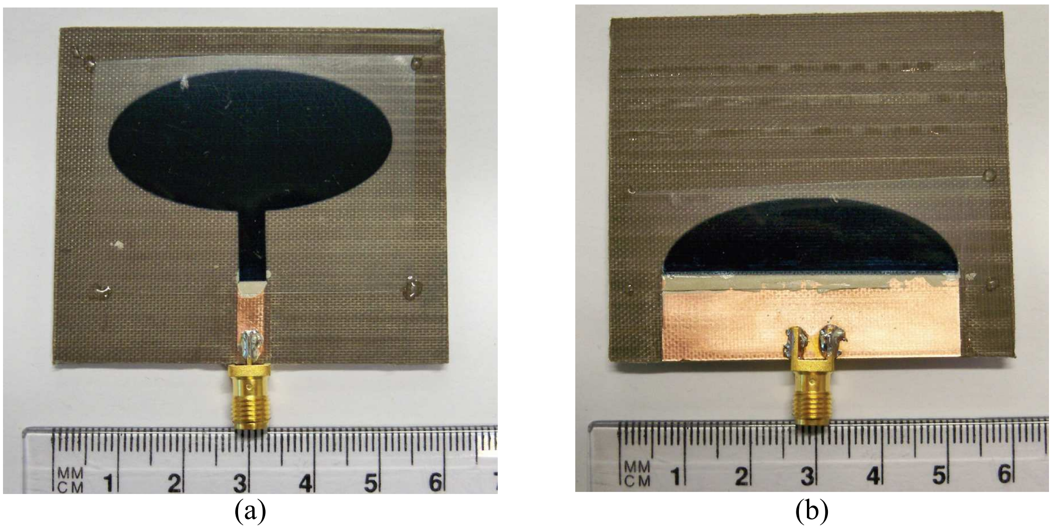

Figure 2.7. High efficiency PPy UWB antennas. The UWB antenna has one layer substrate in the middle, two patterned layers of 158-μm-thick PPy on top and bottom, exhibiting a very satisfactory efficiency of nearly 80%. (a) Antenna top view and (b) bottom view, adapted from [4].

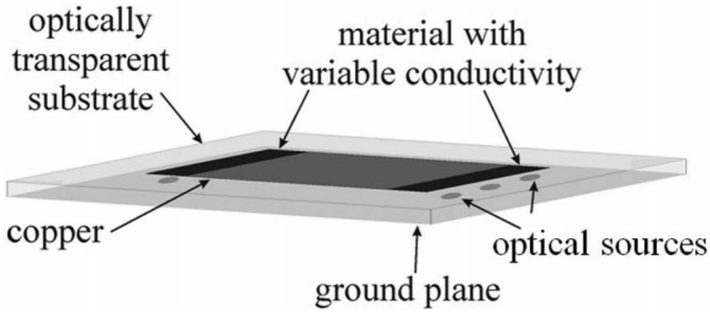

Figure 2.8. A reconfigurable patch antenna concept. A reconfigurable patch antenna concept with two patch edges realized in conductivity-adjustable materials such as conductive polymers, adapted from [71].

Another important aspect in polymeric antenna design is the mechanical flexibility. A dual-band elliptical planar conductive polymer antenna with reversible mechanical flexibility was reported in [85], as illustrated in Fig. 2.9. By incorporating carbon nanotubes (CNT) to a PANI film, a high conductivity of 4500 S/m was achieved, together with an appreciable thickness of 75 μm. In this design, a 130 μm- thick flexible kapton substrate was used to attain a decent conformability. However, the antenna flexibility and thickness can be improved if a thinner and more flexible substrate is used.

Table 2.2 summarizes the state of the art for antennas based on conductive polymers found in the literature, and highlights their key parameters and features. The significant parameters and performance measures include thickness, conductivity and DC

Figure 2.9. A flexible dual-band planar elliptical antenna. The crumpled dual-band antenna, adapted from [85].

Table 2.2. The state of the art of conductive polymer antennas. The key parameters and features of typical antennas based on conductive polymers

Materials	σ (S/m)	d (μm)	R_s ($\Omega/square$)	Efficiency	Flexibility	Year
PANI	6000	100	1.6	56.0%	None	2006 [35]
PEDOT:PSS	500000	Unknown	Unknown	~56.2%	Excellent	2009 [38]
PEDOT:PSS	10000	7	14.3	33.6%	None	2010 [3]
PPy	2000	140	3.6	64.8%	None	2010 [83]
PEDOT:PSS	2720	158	2.3	79.2%	None	2012 [4]
PANI/CNT	4500	75	2.9	Unknown	Excellent	2015 [85]

sheet resistance of the conductive polymer films, as well as the efficiency and mechanical flexibility of the antennas.

In summary, a brief review on the development, the features and the state of art of conductive polymers and their application to antenna technology has been given in this section. Based on this review, one can identify the desired performance/functionalities and the corresponding main challenges in conductive polymer antenna designs as follows:

- Achieving high antenna efficiency, which requires overcoming the inherent limitations in conductive polymers synthesis, namely the relative low conductivity and process-limited thickness;

- Designing antennas with mechanical flexibility and reconfigurability, which requires, taking advantage of the properties of conductive polymers such as mechanical resilience and conductivity tunability.

2.3 Antenna designs based on graphene composites

Graphene has high mechanical strength and exceptionally high thermal and electrical conductivities [86]. In 2004, A. Geim and K. Novoselov rediscovered, isolated and characterized graphene. For this groundbreaking work they were awarded the Nobel Prize in Physics in 2010. Since then graphene development has become a 'gold rush' in the global research community, with developments targeting the production, the synthesis with other materials and the applications of graphene/graphene composites. Graphene can be applied for a variety of advanced applications including optoelectronic devices [87, 88], energy storage [89], sensors [90], EMI shielding [91] and antenna design [6,7,92–94]. More specifically for this last mentioned application, antennas based on a piece of graphene which is a monolayer of carbon atoms were proposed for application in terahertz (THz) communications [95–98]. This appears more appropriate in that frequency range than at microwave, due to graphene's high loss of monolayer graphene in the microwave region [39]. However, to date, due to the difficulties in fabrication and measurement, a practical THz antenna realization is yet to become available in the literature, even if intensively researched in theoretical and numerical works. In contrast to monolayer concepts, various antennas based on graphene composites including graphene inks have been realized and experimentally demonstrated recently for applications in the microwave range [6, 7, 93]. This section presents a brief overview on graphene/graphene composites and their application to antenna designs, with focus on microwave realization and their challenges in terms of efficiency and fabrication.

2.3.1 Graphene and graphene composites

Graphene is a two-dimensional carbon atom layer that take the form of a honeycomb lattice. An atomic force microscopy (AFM) image of graphene is shown in Fig. 2.10, where graphene layer thickness can be found in the region of 9 $\AA$ (0.9 nm). It is a basic building structure of other allotropes such as graphite, fullerenes and carbon nanotubes, as depicted in Fig. 2.11 [86]. This famous material has been proven to possess unique properties such as high mechanical strength and exceptionally high electrical and thermal conductivities for a non-metallic material. Particularly, it has interesting electronic properties allowing ballistic transport with a high ambipolar charge carrier mobility of 2.5×10^5 $cm^2V^{-1}s^{-1}$ and carrier density of 1013 cm^{-2} [86, 99]. Besides, with increasing bias voltage, the graphene resistivity will quickly decrease and hence the graphene conductivity can be controlled. As a result, graphene can be very promising for electromagnetic applications such as EMI shielding [91], RF electronic [100] and antennas [6,7,93,95–98].

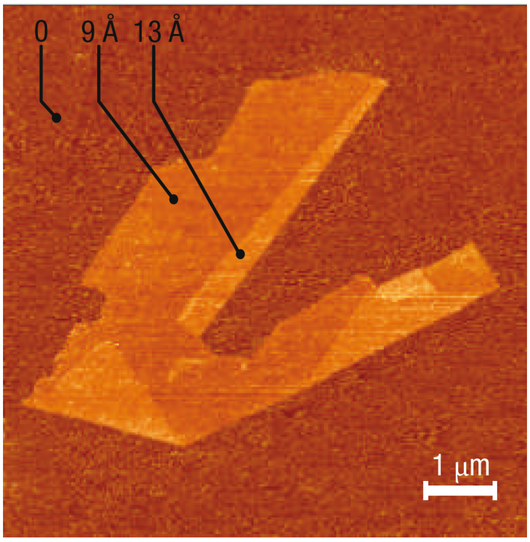

Figure 2.10. An atomic force microscopy image of a flack of graphene. An atomic force microscopy image of a flack of graphene adapted from [86], where the single layer region has a thickness of 9 $\AA$ (0.9 nm).

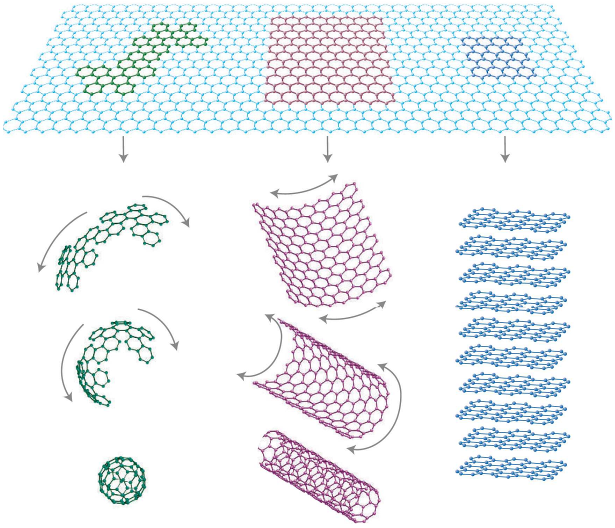

Figure 2.11. Mother of all graphitic forms. Graphene is a 2D layer of carbon atom which can be made to different forms such as fullerenes, nanotubes or stacks, adapted from [86].

In particular, graphene can especially find prospective application in the antenna design dedicated for the THz band. A typical application is for nanoscale wireless communications such as on-chip optical communication where classical metallic antennas in the required nanometer scale are not fitting any more. This is because, metallic antennas in this scale will have very high operating frequency thus low antenna efficiency which will be fatal for the system [95]. The main reason is that, at very high frequency, the low electron mobility in a metallic nanoscale structure will cause high power consumption. In contrast, when compared to a metallic counterpart, graphene-based nanoscale antennas of a few microns, can theoretically radiate electromagnetic waves with a remarkably lower operating frequency (in THz band) and a higher radiation efficiency, by exciting transverse magnetic (TM) surface plasmon polaritons (SPPs) in graphene [95, 97]. Also as aforementioned, with higher bias voltage the graphene resistivity will quickly drop and therefore the graphene-based antennas status has the potential to be dynamically controlled. In addition, graphene exhibits impressive characteristics such massless Dirac electronic structure and extremely high electrical and thermal conductivity, which are desired for the THz region [97]. All these outstanding properties open promising perspective for graphene in antenna applications for the THz band. However, these antennas are yet to be experimentally demonstrated, since the challenges for producing graphene sheet with a thickness of a few micrometers and accurate patterns suitable for realizing antennas remain.

Monolayer graphene is not a good candidate as conductor materials for antenna designs in the microwave range, because of the very high sheet resistance caused by the extremely thin 2D atomic structure. In addition, one can mention the significant difficulty in realizing large size graphene sheets [39, 40]. Fortunately, other form of graphene-related materials such as exfoliated graphite, graphene oxide (GO) and reduced graphene oxide (RGO) can be reliably produced in large scale and thus can be used for synthesising graphene-based materials [101]. This actually opens numerous opportunities to create more graphene-based products specifically dedicated to various new applications.

One of the most critical steps is, in a affordable and time-effective way, creating large quantities of quality graphene ingredients, namely defect-free and oxide-free graphene sheets. This is the reason why significant efforts have been placed into the method development for graphene mass production [101–103]. One of the most inexpensive and environmentally-friendly method for large-scale single and few-layer graphene production is liquid-phase exfoliation of graphite in aqueous solution [90, 104, 105]. A graphene product based on this method reported in [105] is shown in Fig. 2.12, with a size of approximately 3 $\mu m \times 10 \mu m$.

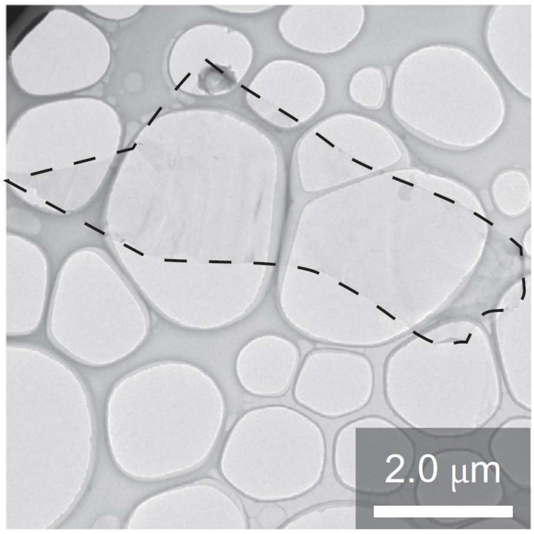

Figure 2.12. A TeM image of a flack of graphene. A TeM image of a flack of graphene adapted from [105], this graphene was fabricated using liquid-phase exfoliation of graphite in aqueous solution.

Once a great amount of high quality graphene sheets are available, the next step is material synthesis using these products. They can be either included in graphene inks with dispersants, solvents and binders, or mixed with other elements such polymers and metal nanoparticles to form graphene-based composites. The main graphene-based composites can classified into three main types: graphene-polymer, graphene-metal nanoparticles and graphene-semiconductor nanomaterials [101]. The graphene-polymer composites are widely used in different applications including microwave antenna technology due to their high electrical conductivity, mechanical strength, thermal stability and high thermal conductivity [101]. Graphene inks, particularly those available commercially, can also find their roles as conductors in antenna designs. Figure 2.13 shows one commercial graphene ink containing graphene nano-flakes well-dispersed in aqueous solution, which can be deployed to generate electrical and thermal conductive films. The advantage of these inks is their binder-free feature, which implies high conductivity since binder material builds a barrier that deteriorates the electrical connection between graphene platelets.

Figure 2.13. Graphene ink: Grat-ink 102E, from BGT Materials Limited. Illustration of a commercial graphene ink from BGT Materials Limited, consisting of well-dispersed graphene nanoflakes in aqueous solution.

2.3.2 Antenna designs

As mentioned previously, nanoantennas based on graphene monolayers are theoretically one of the most suitable materials for THz micro- and nano-antenna, potentially enabling reconfigurability in antennas. Consequently, many theoretical studies on THz graphene antenna designs [95, 106] and especially reconfigurable ones [94, 96–98, 107], have been reported in the literature. Nevertheless, these THz nanoantennas concepts will not be described here in details since they are beyond the scope of this thesis.

As discussed before, graphene according to its strict definition, namely as single-atom sheet with a thickness of less than 1 nm, is not suitable for antennas working at microwave frequency due to the skin depth effect, even if assuming its size and shape is controllable. The DC sheet resistance of a monolayer graphene sheet without any DC bias can be as high as 3500 $\Omega/square$ according to the literature [108]. However, microwave antennas can benefit from using graphene composites by which chemical stability, mechanical flexibility and low-cost synthesis can be achieved. These properties are highly desired for antennas dedicated to RFID and WBAN systems. As a consequence, various antennas realized in graphene composites including commercial graphene inks for RFID applications have been presented in the literature, suggesting an excellent potential of this concept.

In 2013, Shin et al. realized a conductive thin film based on a graphene/polyaniline/-poly(4-styrenesulfonate) (G/PANI/PSS)-based conducting paste, with a conductivity of 1.4×10^3 S/m and a thickness of 70 μm [93] which lead to a DC sheet resistance of 10 $\Omega/square$. Then a 910-MHz flexible loop antenna for RFID application, as shown in Fig. 2.14, was fabricated using this thin film, showing a satisfactory reflection coefficient. In this work the antenna efficiency was not reported and it is to expect that the actual efficiency should be not high due to the relative high surface resistance. Nevertheless, the system test results indicate that the antenna worked and achieved a read range of 0.42 m. In contrast to graphene-based materials synthesized in research laboratories, commercially available graphene inks are more convenient and economical to use. The same group has presented the first fabrication of patterned graphene sheets by injet printing and used these materials for a 500-MHz dipole antenna realization [109]. The patterned graphene sheets exhibited a DC sheet resistance of $65\ \Omega/square$ which suggests a very low antenna efficiency, even if no efficiency data are presented in the paper. However, this paper indicates the promising feasibility of printing-technology-based graphene antenna realization.

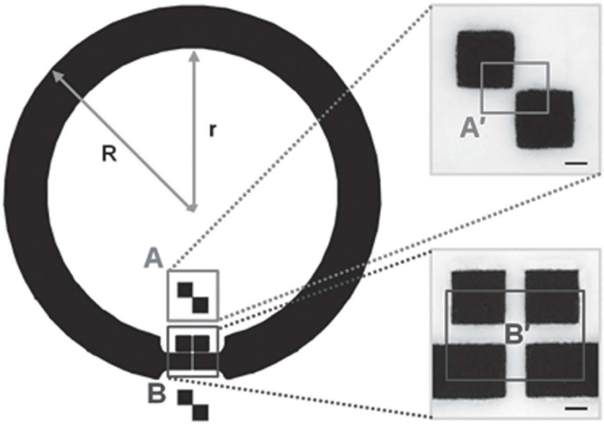

Figure 2.14. A graphene-based loop antenna. A flexible loop antenna based on G/PANI/PSS-based film, adapted from [93].

Very recently, a few RFID antennas based on commercial graphene inks were reported. An RFID dipole antenna for the industrial, scientific and medical (ISM) 915-MHz band realized in the graphene ink shown in Fig. 2.13 was reported in [6]. The antenna was printed using graphene inks on a thin foam substrate, following the printing process by a rolling compression process, which enhanced the conductivity by 5 time to $4.3 \times 10^4\ S/m$. The antenna and its fabrication process are depicted in Fig 2.15. The final graphene laminate had a thickness of $6\ \mu m$ which is only 0.075 times one skin depth, yielding a DC sheet resistance of $3.8\ \Omega/square$. As a result of the limited film thickness, the antenna holds a relatively low efficiency of 50% approximately, estimated based on the measurement results presented in [6]. Nevertheless, the proposed antenna offers a very cost-effective and environmentally-friendly solution for high-volume low-cost RFID applications, while retaining a practically viable antenna performance.

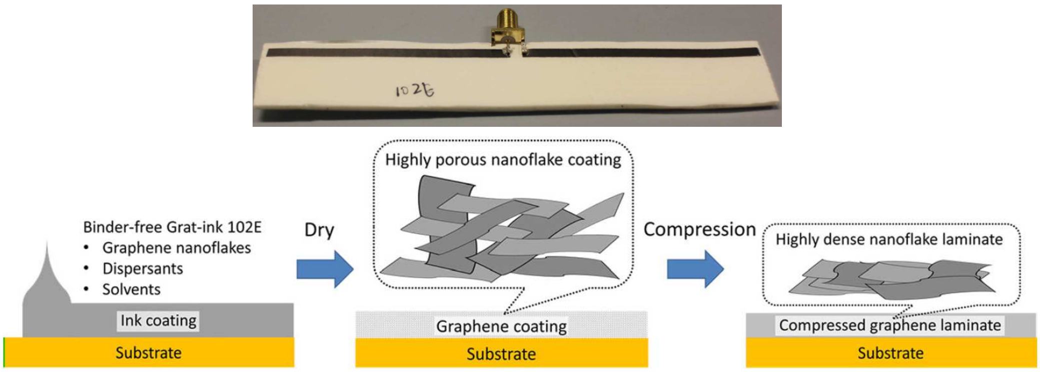

Figure 2.15. A graphene-based dipole antenna. The dipole antenna was printed on a thin foam substrate using commercial graphene ink, followed by a drying and a rolling compression process. These figures are adapted from [6].

Another very similar RFID dipole antenna design fabricated based on commercial graphene ink using a doctor-blading technique was reported in [7], as shown in Fig 2.16. The antenna was realized by evenly spreading graphene ink on the substrate with a mechanical mask where a doctor blade was used to flatten and control the ink thickness. This dried graphene-based film achieved a conductivity of $1.25 \times 10^4\ S/m$ and a thickness of 42 μm, leading to a DC sheet resistance of 1.9 $\Omega/square$. The antenna was measured to have an efficiency of 40% and this modest performance is mainly attributed to the fact that the film thickness is only approximately one third of the skin depth. However, this low-cost and environmentally-friendly antenna can still be practically used in RFID applications. An analysis of the performance of RFID antennas realized in graphene inks have been conducted and the results are discussed in [110], where a relative low antenna efficiency was also observed.

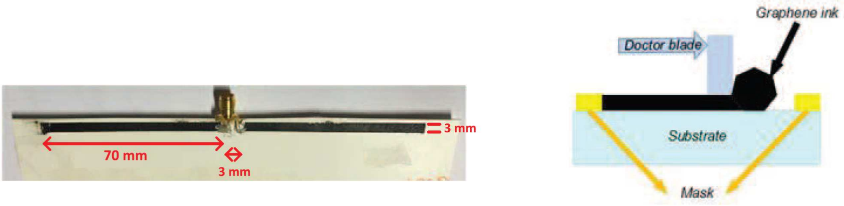

Figure 2.16. A graphene-based dipole antenna. The dipole antenna was fabricated on a cardboard using commercial graphene inks, with a doctor-blading technique. These figures are adapted from [7].

Table 2.3. The state of the art of antenna realizations based on graphene composites. The key parameters of typical antennas realizations based on graphene composites

Materials	σ (S/m)	d (μm)	R_s ($\Omega/square$)	Efficiency	Year
Graphene	50000	0.3	65	Unknown	2011 [109]
Graphene/PANI/PSS	1400	70	10	Unknown	2013 [93]
Graphene	43000	6	3.8	∼50%	2015 [6]
Graphene	12500	42	1.9	∼40%	2016 [7]

Table 2.3 summarizes the key parameters of typical antenna realizations based on graphene thin film, which include the thickness, conductivity and DC sheet resistance of the graphene films, as well as the antenna efficiency. In summary, these aforementioned graphene-based antenna realizations have demonstrated that graphene-based composites can be very beneficial for microwave antenna development, since they can offer high electrical and thermal conductivity, mechanical flexibility, chemical stability, low cost and environmental friendliness. However, a common problem can still be observed in the available designs in the form of a relatively low antenna efficiency. Therefore, the improvement of graphene-based antenna efficiency is a significant requirement, which can be achieved by adapting the design and increasing the graphene film conductivity and thickness, as demonstrated later in Chapter 4.

2.4 Antenna designs based on conductive textiles

Conductive textiles are fabrics that have electrical conductivity. These fabrics can be made highly conductive, flexible and lightweight, and they are generally extremely robust [111]. These textiles can perfectly serve as conductors for the main components of wearable systems such as antennas, transmission lines and electric components, since they are able to offer outstanding mechanical conformability and resilience, highly comfortable wearability and excellent bio-compatibility [112]. A large number of conformal and wearable antennas realized in conductive textiles have been reported in the literature in the last decade, with a trend of rapid growth [113]. Nevertheless, since textile antennas have very different physical properties compared to rigid antennas, challenges in antenna feeding, ground-shorting and interconnection with electronics are encountered by antenna researchers and engineers [112]. This section briefly reviews firstly conductive textile materials and secondly wearable textile antenna designs, with particular attention placed on the feeding, shorting and interconnection challenges associated with these antennas.

2.4.1 Conductive textiles

Conductive textiles have an unbelievably long history and the earliest realizations are believed to have been developed for aesthetical purpose, for example taking the form of gold-coated threads produced in ancient times. In recent times however, these fabrics have been given more meanings in their functionality. Nowadays, development of conductive textiles have accelerated because of the intensive demands in e-textiles which are also widely known as smart textiles or electronic textiles. As a consequence, the available fabrics are now subjected to increasingly strict criteria in their electrical and physical properties [112]. More specifically in regard to conductive textiles typically employed in the wearable antenna domain, satisfactory antenna performance is required while maintaining comfort and wearability. Thus, the conductive textiles are generally required to have homogeneous conductivity with value close to that of metals, while exhibiting a very thin thickness with mechanical resilience, light weight and bio-compatibility [114].

There are different methods to fabricate conductive textile and the most commonly employed ones include coating, embroidery, weaving, knitting and printing, as illustrated in Fig. 2.17. Thanks to these mature and continuously improving fabrication technologies, conductive textiles with premium quality can now be very cost-effectively manufactured at large scale, providing essential and affordable constituent building materials for wearable antennas with outstanding physical and electrical characteristics. As a consequence, since the last decade or so, antenna researchers and engineers have conveniently exploited commercial conductive fabrics for textile antenna designs [17, 116, 117].

Some popular commercial conductive textiles are shown in Fig. 2.18. Some of the available products can have a very small thickness of 80 μm and extremely low DC sheet resistance of 0.01 $\Omega/square$ [118]. This corresponds to the same order of magnitude as a pure copper thin film. As a result, antennas realized based on these materials operating in the microwave region will have an extremely low ohmic loss, and therefore

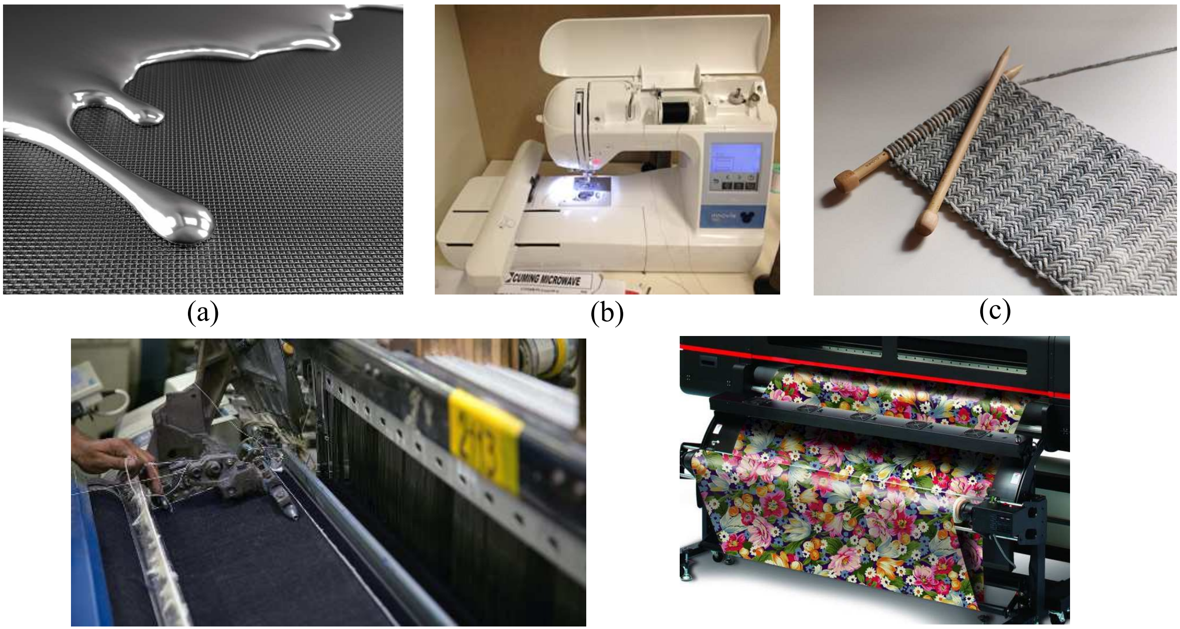

(a) (b) (c)

(d) (e)

Figure 2.17. Main fabrication methods for conductive textiles. The most commonly utilized fabrication methods for conductive textiles: (a) coating (adapted from [115]) (b) embroidery (c) knitting (d) weaving and (e) printing.

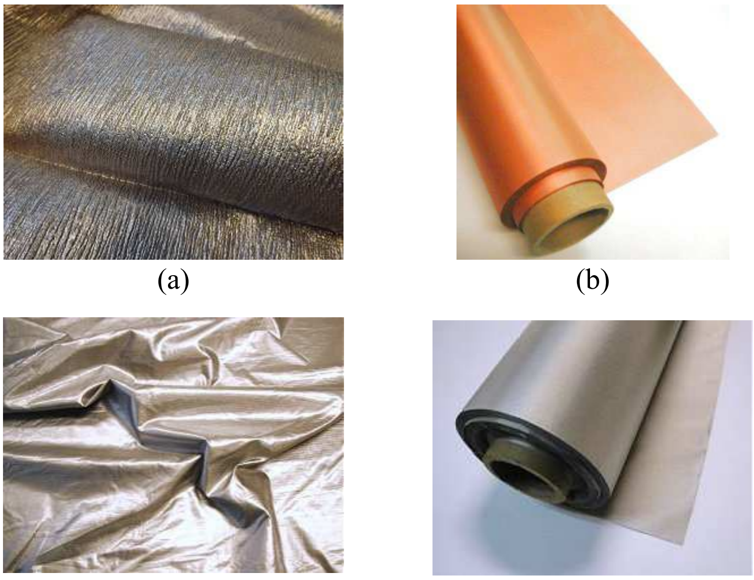

(a) (b)

(c) (d)

Figure 2.18. Some commercially available conductive textiles from LessEMF. Some commercially available conductive textiles from LessEMF: (a) textured silver shielding fabric (b) pure copper polyester taffeta fabric (c) ripstop silver fabric and (d) nickel/copper ripstop fabric, all adapted from [118].

antennas made of such fabrics are very likely to achieve a high total efficiency provided other losses such as dielectric and mismatch losses are small. Indeed, such high performance can be observed in the relevant antenna review in the next section. However, new scientific and technical challenges in antenna design, for example concerning shorting and connection strategies, are encountered by researchers and engineers. More specifically, due to the very unique physical features of textile materials, dedicated shorting and connection arrangements based on textile-compatible components such as embroidery vias and metallic shorting vias are critically required to realize reliable and performing textile antennas.

2.4.2 Wearable antenna designs

Wearable antennas are an essential component towards garment-integrated wearability for wireless applications. They are required to have reversible mechanical flexibility, deformation-insensitive electrical performance, high wearability implying light weight, low profile, and they should be amenable to garment integration. Not surprisingly conductive textiles are one of the most appropriate classes of conductors for wearable antenna designs [112]. As a result, a wide range of conventional wearable textile antennas, including dipoles [41], slots [119], microstrip patches [10, 11, 13, 31, 120–123], PIFA [124], substrate-integrated-waveguide- (SIW) [20] and half-mode-substrate-integrated-waveguide- (HMSIW) based cavities [21, 22], and UWB [17, 18] antennas, have been reported in the literature.

Standing out amongst wearable textile antenna designs, microstrip patch antennas are the most reported garment-integrated antenna type since they are best suited for garment integration due to their low profile, compactness and electromagnetic isolation from the human object arising from their ground plane. For instance, Hertleer et al. have presented a textile patch antenna operating at 2.4 GHz integrated into a protective clothing for fire-fighters [14]. Thanks for the superior mechanical flexibility and low DC sheet resistance (0.1 $\Omega/square$) of the textile materials, the proposed antenna was shown to be very easily integrated into the garment with a satisfactory antenna efficiency of 62%. The antenna geometry and the integration configuration are displayed in Fig 2.19, which indicates that the antenna was covered by two protective layers. Similarly, Vallozzi et al. have reported another garment-integrated patch antenna with dual polarization in 2010 [125]. The antenna electrical connections are shown in

Fig. 2.20, where the antenna was connected through two SMA connectors and coaxial cables.

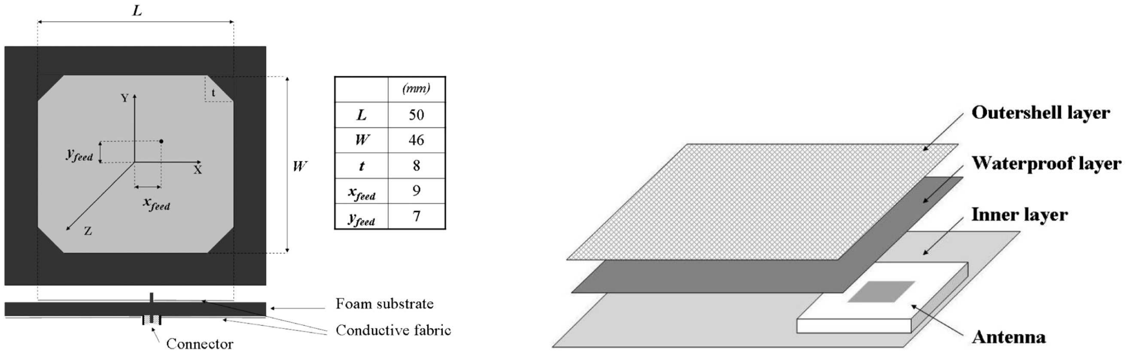

(a) (b)

Figure 2.19. A patch antenna geometry and its garment integration configuration. (a) Antenna geometry and (b) garment integration configuration, all adapted from [14].

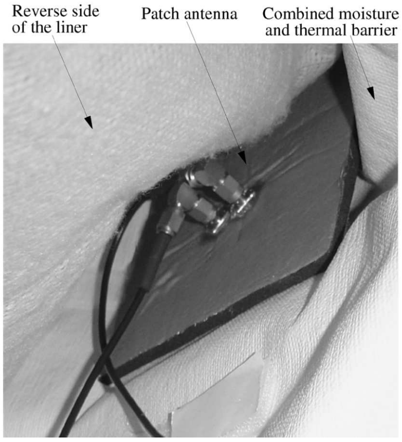

Figure 2.20. A patch antenna inside the hosting garment. The antenna electrical connection through SMA connectors and coaxial cables inside the garment, adapted from [125].

Another aspect of importance for garments with integrated textile antenna is the reliable connection to electronics. Since the antennas are usually not removable from the garment, they will remain on the garment when it needs washing for hygiene or maintenance purpose. However, the electronics connected to the antenna have to be taken away, as they would be damaged by the washing process. Therefore, a reliably detachable electrical connection between the antenna and the electronics is highly desired to form a convenient and repeatable reconnection. An investigation of a removable feeding arrangement for wearable textile patch antenna was performed in [126]. As shown in Fig 2.21, the removable electrical connection between the antenna and the coaxial

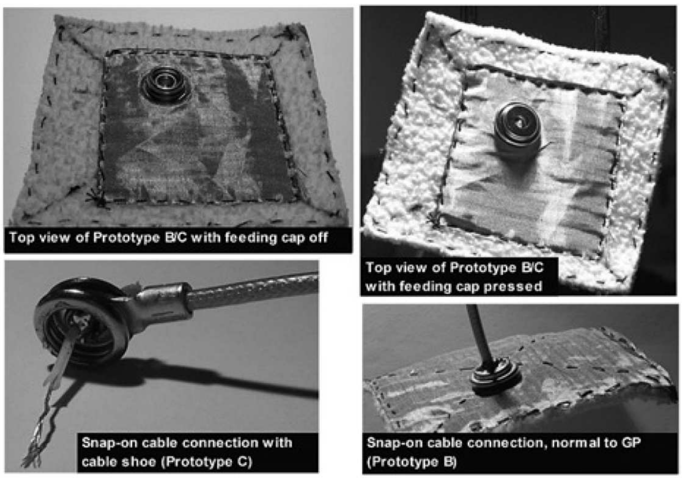

Figure 2.21. A removable feeding for a textile patch antenna. A removable electrical connection for wearable garment-integrated textile antenna based on a snap-on connector, adapted from [126].

cable is realized based on a purpose-made snap-on connector. Through this connection arrangement, the clothes with integrated antenna can be safely washed while the electronics can be disconnected by simply detaching the snap-on connector.

A further relevant aspect in textile wearable antenna technology is the realization of vias. Cavity-based antennas or antennas with ground-shorting(s) may require vias to form the cavity wall(s) or the shorting(s). When these devices are made from textiles, textile-compatible vias are critical to ensure high-quality vias connections, which is a difficult task because of the special physical properties of textiles. Specific metallic shorting vias are required, taking the form of conductive textiles strips, embroidered conductive threads or metallic eyelets.

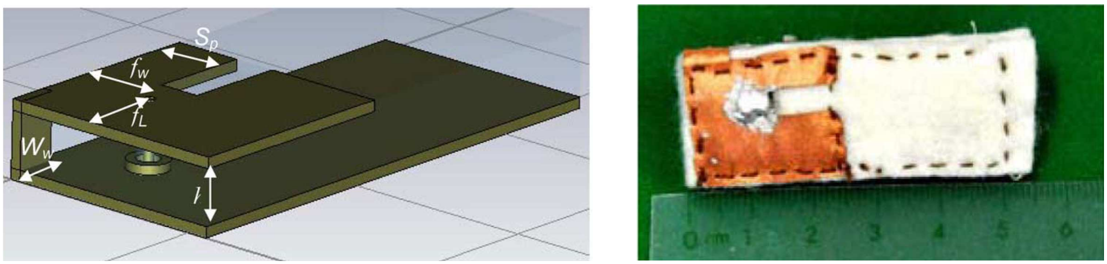

(a) (b)

Figure 2.22. Textile PIFA using textile shorting vias. A textile PIFA antenna whose ground shorting is realized in the same conductive textiles: (a) antenna geometry and (b) a realization, adapted from [124].

One of the most convenient method to realize a short is shown in Fig. 2.22. If the antenna short can be accommodated outside of the substrate, the short, the patch and

(a) (b)

Figure 2.23. Textile antennas using metallic eyelet vias. (a) A textile cavity-backed slot antenna (adapted from [20]) and (b) a textile HMSIW-based antenna using metallic vias to form a shorting wall (adapted from [22]).

the ground plane can be just simply realized using a single piece of conductive textile. However, for other cases where the shorting or the cavity wall is located inside the substrate, more complex methods are needed. For example, as shown in Fig 2.23, a textile cavity-backed slot antenna [20] and a textile HMSIW-based antenna [22] use metallic eyelet vias to realize a shorting wall. Using a different approach, figure 2.24 shows a textile HMSIW-based antenna using embroidery vias based on conductive threads to form a shorting wall [21]. Similarly, a textile patch antenna with two ground shortings based on the same technique was reported in [123]. The two embroidered shortings are there to form the boundary conditions for achieving higher-order mode in the antenna. The metallic vias method generally provides better electrical performance but this is counterbalanced by higher manufacturing cost when compared to the embroidery method. Based on these observations, shorting and connection strategies for textile antennas should be carefully considered during antenna design process, since they can significantly affect for the antenna performance.

Finally, reconfigurable or active antennas can be very useful for wearable applications, since they are capable of providing adaptive antenna characteristics and thus better reliability in changing environmental conditions. However, a very limited number of wearable reconfigurable designs have been reported in the literature. This is attributed to the difficulty of creating reliable connections between the textiles and the solid electronic components and/or printed circuit boards (PCB), which is caused by their very different physical properties. An active microstrip patch with a circuit for amplifying the antenna gain was reported in [127]. The antenna with its electronic circuit board is shown in Fig. 2.25. The circuit board and the surface-mount components are not realized on textiles, because doing that would lead to very unreliable connections between

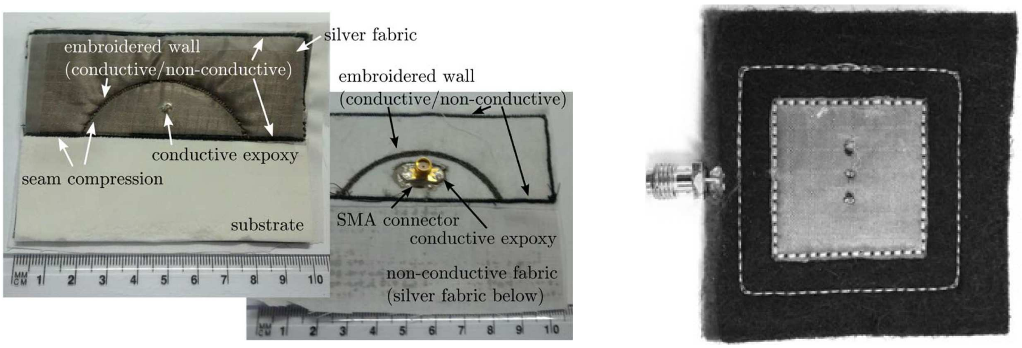

(a)

(b)

Figure 2.24. Textile antennas using embroidery conductive threads as shorting vias. (a) A textile HMSIW-based antenna using embroidery conductive vias to from the shorting wall (adapted from [21]) and (b) a textile patch antenna using embroidery conductive vias to form a ground shorting (adapted from [123]).

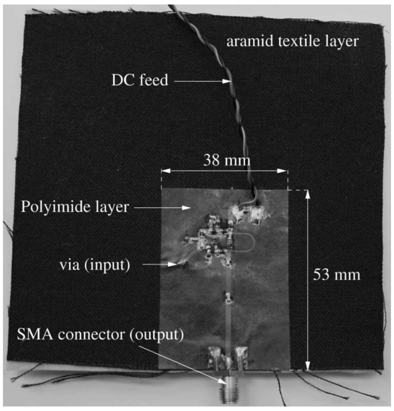

Figure 2.25. An active textile antenna with its circuit board. An active textile antenna with its circuit board loaded with surface-mount components. adapted from [127]).

the components and textiles, when worn by a human object. Hence, reliable connection between textiles and rigid electronic components is a significant requirement to achieve advanced textiles antenna designs like reconfigurable devices.

In summary, on the one hand, conductive textiles have been shown to offer the desired electrical and mechanical features for wearable antenna designs. However, on the other hand, significant efforts are crucially necessary for enhancing their practical applicability. This includes designing appropriate antenna feeding, as well as shorting and interconnection with other electronics.

2.5 Summary

This chapter has presented a descriptive review on three promising antenna conductors including conductive polymers, graphene/graphene composites and conductive textiles, in the perspective of their application in antenna technology. The analysis of the advantages and disadvantages of each of these three materials for antenna technology has revealed the specificities for each approach. This builds the fundamental knowledge for the following chapters of this thesis.

Chapter 3

Conductive Polymer Antennas

ANTENNAS based on conductive polymer thin films can have very attractive characteristics such as reversible mechanical flexibility, light weight, ease of processability, corrosion resistance and low cost. However, due to the relatively low conductivity and the process-limited thickness, achieving high antenna efficiency becomes the highest priority for designing this type of antennas. Additionally, exploiting the reversible mechanical conformability of the materials to realize highly flexible antennas is another significant aspect.

This chapter proposes three different engineering methods to improve the efficiency of conductive polymer antennas. Firstly, a non-resonant antenna design strategy is adapted, for the aim of minimizing RF current density and therefore the ohmic losses in the antenna. Secondly, a very simple but effective chemical treatment using methanol is utilized to dramatically improve the polymeric film conductivity. Following that, a multilayer laminated structure which can effectively reduce the skin effect losses in lossy conductors through increasing the wave penetration, is proposed as the third strategy. Finally, a multilayer conductive polymer microstrip-fed slot antenna is demonstrated, with focus on considerations for a robust design, both in terms of mechanical flexibility and radiation properties.

3.1 Introduction

Conductive polymers have become a significant research thrust since the very first report of very high electrical conductivity in polyacetylene was published in 1977 [33,34]. Since then, the combined efforts from chemists, physicists and engineers has broadly accelerated the research progress. Nowadays, conductive polymers are utilized for a wide range of applications including chemical sensors [62–64], biosensors [65], printed electronics [66], supercapacitors [67, 68] and electromagnetic devices [3, 36, 69, 70]. In particular, these materials are very promising for antenna design, especially for devices dedicated to flexible and wearable applications, since these materials can possess sufficiently high electrical conductivity, outstanding mechanical flexibility and resilience, light weight, bio-compatibility, and convenient processability [72]. Amongst the dominant conductive polymers such as polyacetylene, PPV, PEDOT, PEDOT:PSS, PANI and PPy, the last three have been frequently used as antenna conductors, as they can be excellent electrical conductors with outstanding chemical stability. As such, they can provide an environmental friendly alternative to metals [76, 77].

However, it has been proven that simultaneously synthesizing conductive polymers with high conductivity and sufficient thickness is very challenging. This is because forming stable conductive nanostructure grains vertically in the material is extraordinarily difficult. As a result, the majority of conductive-polymer-based antennas exhibit a relatively low efficiency. For instance, a proximity-coupled microstrip antenna whose ground plane and feed line were realized in copper whereas the radiating patch was made of PANI, has been reported to have a 56% efficiency [35]. Similarly, two microstrip antennas using copper for their ground plane and PPy for their patch, have also been demonstrated with efficiencies of 62% [128] and 65% [83] respectively. If all conductors in these three antennas were polymers, the efficiency would be even lower. Additionally, these antennas were not realized on flexible substrate, meaning that the polymers' advantage of mechanical resilience was not exploited. These situations suggest that improving antenna efficiency and implementing truly flexible devices are two major necessary steps to express the potential of conductive polymer antennas. Several avenues can lead to an improvement of the antenna efficiency: one can utilize an efficiency-driven antenna design, enhance the film conductivity or increase the film thickness while maintaining the conductivity.

The first part of the present chapter is focused on all these three strategies and provide detailed analysis and experimental validation. First, a non-resonant antenna design strategy is adapted, with the aim of minimizing RF current density and therefore the ohmic losses in the antenna. Second, a very simple but effective chemical treatment using methanol is utilized to dramatically improve the polymeric film conductivity. Third, a multilayer laminated structure which increases the effective film thickness by reducing the skin effect losses is proposed. Another important aspect for polymer antennas is their mechanical conformability. Therefore, in the second part of the chapter, as illustration, a polymeric microstrip-fed slot antenna is discussed with emphasis on dedicated antenna engineering considerations to maximize mechanical flexibility.

3.2 Non-resonant antenna strategy

This strategy is based on the fact that, compared to non-resonant antennas, resonant antennas generally have relatively high ohmic loss due to the higher current densities built up through the resonance process [129]. By utilizing a non-resonant design, the impact from the limited conductivity on the antenna efficiency can be significantly reduced. To demonstrate that, a non-resonant new coplanar waveguide (CPW) fed UWB antenna realized in PEDOT:PSS thin film has been designed and measured. According to the measurement results, the antenna exhibits an averaged radiation efficiency above 85% and a nearly 90% averaged conduction efficiency over the operating frequency range from 3 to 20 GHz. This is, to the best of our knowledge, the highest reported efficiency to date for a non-metallic antenna of this type. All these findings indicate that this type of antenna has successfully overcome the limitations in conductivity and thickness of conductive polymers. Furthermore, by using a CPW feeding structure and a sticky tape as the substrate, the antenna features exceptional reversible mechanical flexibility and robustness, which shows its promising potential for possible seamless integration in flexible electronics.

3.2.1 Antenna materials

PEDOT:PSS is a stable conductive polymer and can be produced using commercial formulations with low-cost manufacturing techniques such as spin or spray coating and screen or inkjet printing [130]. Therefore, a PEDOT:PSS thin film has been chosen as the conductors for the antenna. To maximize the flexibility and minimize the weight of the antenna, a sticky tape has been selected as the substrate. The tape not only offers flexible and robust mechanical support, but also provides fabrication convenience for

Table 3.1. Copper and PEDOT:PSS thin films skin depth comparison. DC conductivity and skin depths of copper foils and PEDOT at the antennna's lowest and highest operating frequencies

	Conductivity	Skin depth (3 GHz)	Skin depth (20 GHz)
PEDOT	9532 S/m	94.12 μm	36.45 μm
Copper	5.80×10^7 S/m	1.20 μm	0.46 μm

laser cutting technology due to its transparency which will be discussed in detail in Section 3.2.3.

While DC conductivities exceeding 3×10^5 S/m have been reported in the literature [79] for sub-micron thick PEDOT films, it has been proven very challenging to simultaneously achieve sufficient thickness and satisfactory conductivity to satisfy the requirements for microwave antenna applications. The PEDOT:PSS thin film used in this project presents a unique combination of substantial thickness of 70 μm while retaining a relatively high measured DC conductivity of 9532 S/m. Free-standing PEDOT:PSS films were fabricated by a solvent casting method using Clevios PH1000 (Heraeus) with ethylene glycol. Films were annealed at 130°C to ensure all residual solvent was removed.

A piece of copper foil with thickness of 60 μm is used to fabricate a reference antenna, for conduction efficiency evaluation. In Table 3.1, the conductivity and skin depth of the PEDOT film and the chosen copper foil at the lowest and highest frequencies are shown. The thickness of the PEDOT thin film corresponds approximately to three quarters of a skin depth at the lowest frequency and to slightly more than two skin depths at the highest frequency of operation. In contrast, the copper foil offers a skin depth roughly two orders of magnitude lower than PEDOT, which promises better performance. The substrate material is a commonly used transparent sticky tape with thickness of only 150 μm, and as such permittivity and loss tangent are not critical parameters for the antenna design. Hence, a relative permittivity $\varepsilon_r = 3$ and loss tangent $\tan\delta = 0.01$ are assumed as the values for the sticky tape. An uncut PEDOT:PSS thin film, the copper foil, and the sticky tape are displayed in Fig. 3.1.

3.2.2 Antenna design

The layout and dimensions of the antenna are shown in Fig. 3.2 and Table 3.2, respectively. The antenna consists of a coplanar waveguide (CPW) feeding section and two trapezoidal radiating elements on a thin substrate. A CPW feeding is adopted in order to achieve a single layer design for ease of fabrication and high flexibility. Generally antennas with single-layer structure have less stability and isolation to electromagnetically changing environments compared to antennas with a ground plane, but this drawback can be eliminated by appropriate isolation techniques such as spacer, or artificial magnetic wall.

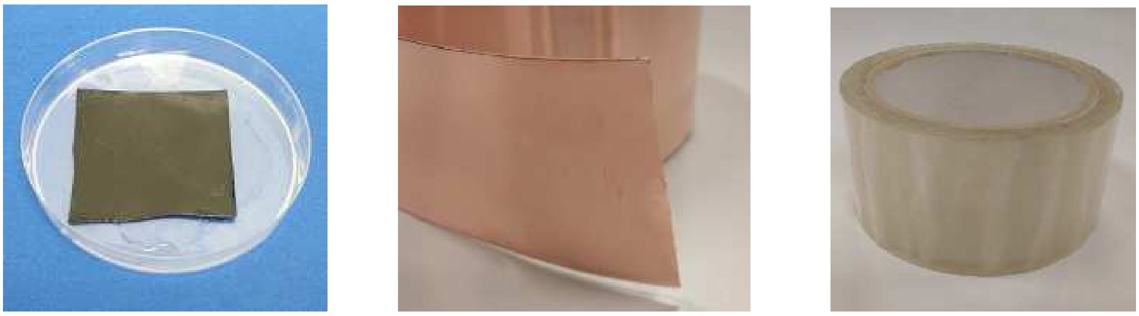

(a) (b) (c)

Figure 3.1. UWB antenna materials. UWB antenna materials: (a) PEDOT:PSS thin film, (b) copper foil (for reference antenna) and (c) sticky tape.

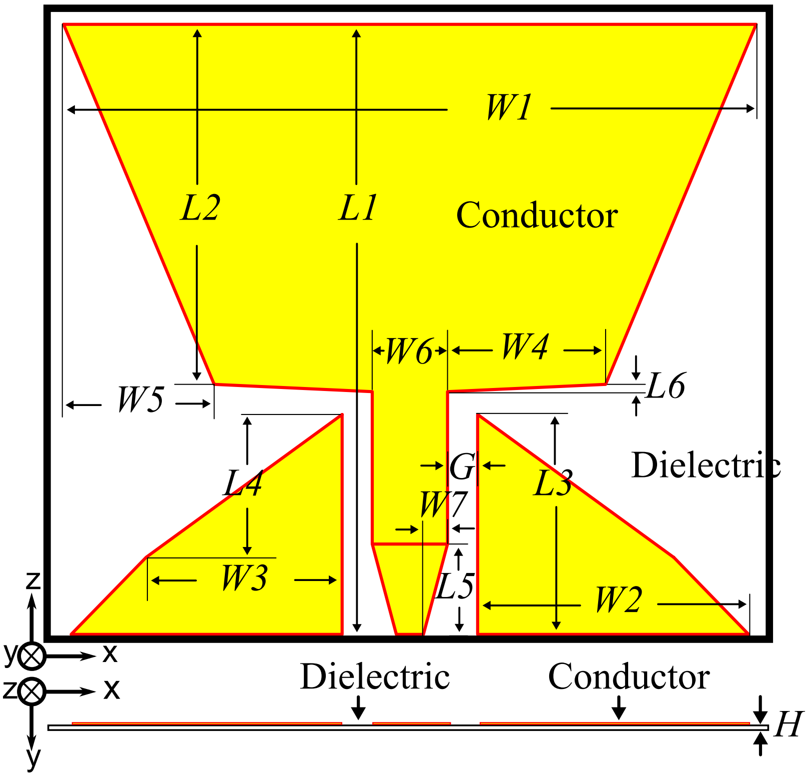

Figure 3.2. UWB antenna geometry. Layout of the proposed antenna. The substrate thickness $H = 150$ μm.

Table 3.2. UWB antenna dimensions. Dimensions of the proposed antenna in (mm)

L_1	L_2	L_3	L_4	L_5	L_6	G
20.25	11.95	7.30	5.00	3.05	0.24	0.85

W_1	W_2	W_3	W_4	W_5	W_6	W_7
23.00	9.00	6.30	5.25	5.00	2.50	0.80

The tapered slots between the trapezoidal elements and CPW ground planes operate as radiating structures with a predominately vertical linear polarization. The tapered slots yield a smooth and continuous characteristic impedance transition between the feeding SMA connector and free space, which ensures the broadband performance. The substrate size is roughly a square with 1 mm margin to the antenna outline. The two largest dimensions of the antenna L_1 and W_1 are inversely proportional to the lower frequency limit. The combination of dimension parameters such as L_2/W_5, L_3/W_2, L_4/W_3 and L_6/W_4 determine the tapering rate between the trapezoidal elements and CPW ground planes which significantly influences the input impedance. The final geometry of the antenna was obtained through full-wave simulations based on CST.

The slots between the two ground planes and the center conductor of the CPW play a key role in the optimization of the antenna. On one hand, they determine the characteristic impedance of the CPW which impacts the antenna matching. On the other hand, and more importantly in this case, their dimension significantly affects the losses in the transmission line. As the gap increases, the density of the coupled currents running along the edges of the CPW slots decreases, which results in lower conduction losses. This can be explained using the CPW circuit model. The circuit model of a CPW is shown in Fig. 3.3, where R, L, C and G' are the distributed resistance, inductance, capacitance and conductance, respectively. The CPW characteristic impedance can be approximated as

$$Z_0 = \sqrt{\frac{R + j\omega L}{G' + j\omega C}} \approx \sqrt{\frac{L}{C}} \tag{3.1}$$

since the polymer is a good conductor [131]. When the slots of the CPW become narrower, Z_0 decreases since C raises due to the increased stored electric energy while L drops with the decreased stored magnetic energy. This will lead to a current increase as governed along the line by

$$\frac{V(x)}{I(x)} = \pm Z_0. \tag{3.2}$$

These phenomena can be observed in the simulated surface currents in the CPW for the cases when G = 0.1, 0.5 and 0.85 mm which correspond to a characteristic impedance Z_0 of approximately 42, 73 and 88 Ω, as shown in Fig 3.4. The narrower the slot width is, the lower the line impedance and thus higher the surface current is. Therefore, the requirements of good matching and maximized radiation efficiency set the trade-off for optimal width of the slot. A parametric study of the CPW slot width G in numerical simulations demonstrates that, as the gap increases from 0.1 mm to 1 mm, the average predicted radiation efficiency increases from 60% to 90%. An optimal value of the gap is obtained through iterative optimizations in CST Microwave Studio. The proposed antenna with an optimal gap of 0.85 mm shows a satisfactory matching from 3 to 20 GHz.

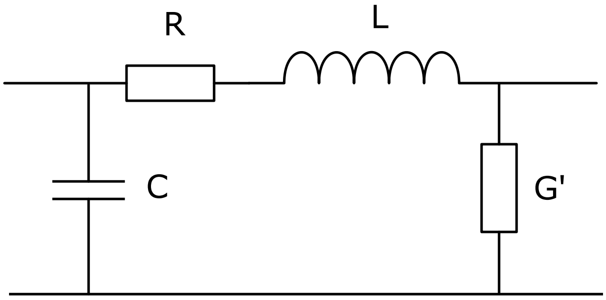

Figure 3.3. Circuit model of a CPW. Circuit model of a CPW, where R, L, C and G' are the distributed resistance, inductance, capacitance and conductance, respectively.

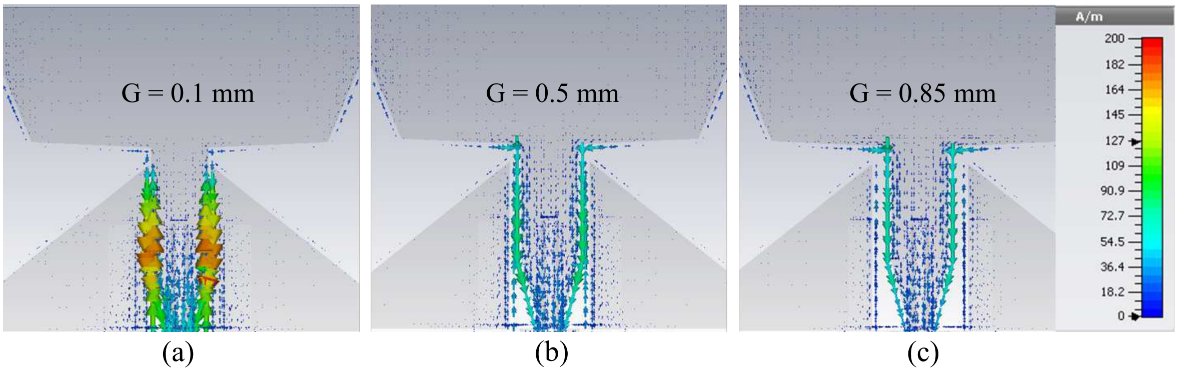

Figure 3.4. Simulated surface current on CPW. Simulated surface current on the CPW with the slot width G of (a) 0.1 mm, (b) 0.5 mm and (c) 0.85 mm.

3.2.3 Antenna fabrication

In order to validate the design and simulation results, the proposed PEDOT antenna has been fabricated and experimentally characterized. An identical design realized using copper has also been manufactured, to serve as a reference for the conduction efficiency measurement. The two antennas are shown in Fig. 3.5. To achieve accurate patterning of the structure, the PEDOT antenna has been fabricated using a laser milling machine (LPKF: Protolaser_S). In this process, a thin sheet of PEDOT is firstly attached to a piece of sticky tape, which is then fixed on the cutting platform of the laser machine. Secondly, the antenna is tailored from the sheet with the laser power and the focal position adjusted so that only the PEDOT is trimmed. The sticky tape substrate is transparent to the laser, that means, it can be kept intact from the laser which simplifies the fabrication. Besides, it is noted that common sticky tape can be a very appropriate substrate/superstrate and protection materials for polymeric antennas, since it can conveniently provide insulation as well as robust and flexible mechanical support while having negligible impacts on the antenna performance. Thirdly, the redundant PEDOT pieces are peeled off from the sheet and the excess substrate is removed. Finally, the antenna is mounted in a fixture for alignment and connection to an SMA connector. Conductive epoxy (CW2400 from CircuitWorks) is applied to form a solid mechanical and electrical connection to the connector.

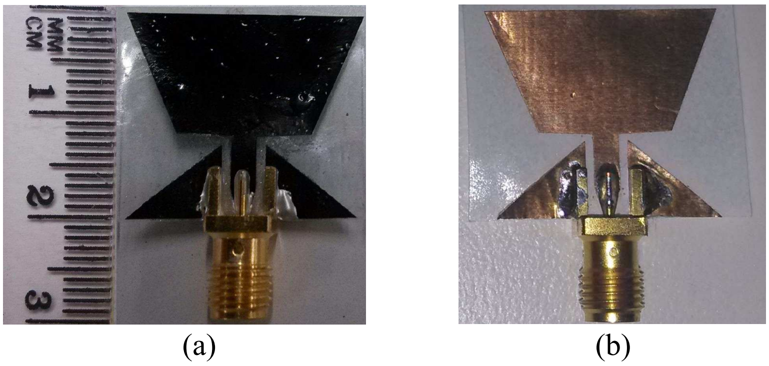

(a) (b)

Figure 3.5. Polymeric and copper UWB antenn realization. The realized antennas. a) The antenna made from PEDOT thin sheet. b) The antenna made from copper foil.

3.2.4 Experimental results

The next step after fabrication is the experimental characterization. As shown in Fig. 3.6, a reasonable agreement between the measured and simulated reflection coefficient is achieved, with a measured $|S_{11}|$ parameter below -10 dB over almost the whole frequency range from 2.2 to 20 GHz. Return RF currents on the outer conductor of the coaxial cable artificially increase the bandwidth at low frequency, but do not alter the response significantly in the UWB band. These currents could be in principle mitigated by a choke on the feeding cable, and are naturally suppressed in the efficiency measurement using the Wheeler cap method (as described later in this section).

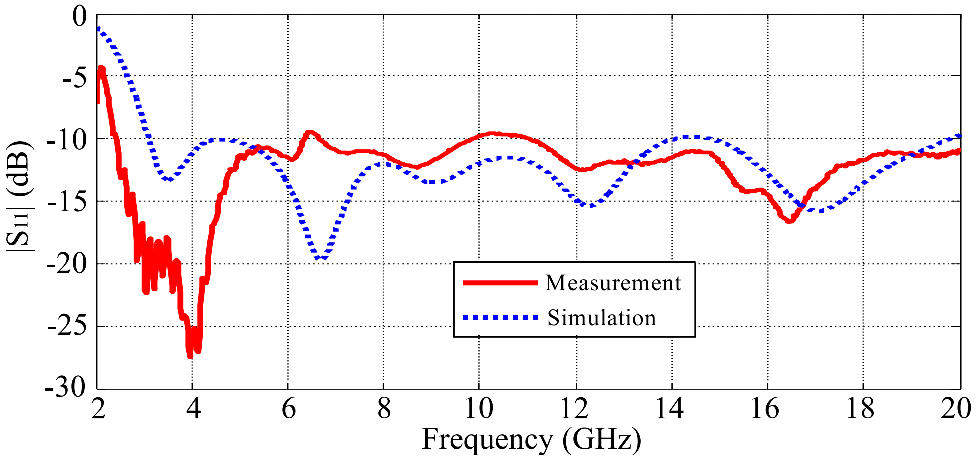

Figure 3.6. UWB antenna simulated and measured reflection coefficient. Simulated and measured reflection coefficient $|S_{11}|$ of the proposed antenna.

Group delay is defined as the rate of change of the frequency-dependent phase shift $d\phi(\omega)$ with respect to angular frequency ω of the radiated signal, namely:

$$T_g(\omega) = -\frac{d\phi(\omega)}{d\omega}. \tag{3.3}$$

This is an important parameter for UWB antennas which are expected to operate linearly in a very wide frequency range, as it quantifies pulse distortion and far-field phase linearity [132]. A radiating device with no signal distortion is characterized by a constant group delay, i.e., linear phase in the frequency range. The group delay of the proposed antenna has been measured with 100 mm distance between two manufactured UWB antennas, as illustrated in Fig. 3.7. As shown in Figure 3.8, the measured group delay variation is less than 1 ns over the operating frequency range which indicates a nearly linear phase in the far-field region and no sensible pulse distortion. Since the nonlinearities in group delay reflect the device resonant characteristic, the measured result also suggests that the antenna is not a resonant structure [133].

The most interesting parameter in our design is the antenna efficiency, as this factor verifies whether our strategy is successful. The antenna radiation and conductive efficiencies both are measured in this experiment. The antenna radiation efficiency e_{cd} has been directly measured by using the Wheeler Cap Method [134] whereas the conduction efficiency e_c has been indirectly computed by comparing the radiation gain

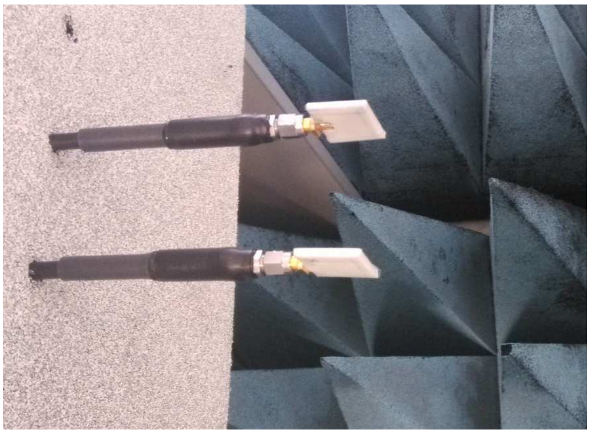

Figure 3.7. Group delay measurement configuration. Two identical antennas mounted on pieces of radome foam are separated by 100 mm in an anechoic environment. The group delay is measured using a network analyzer in a transmission scenario.

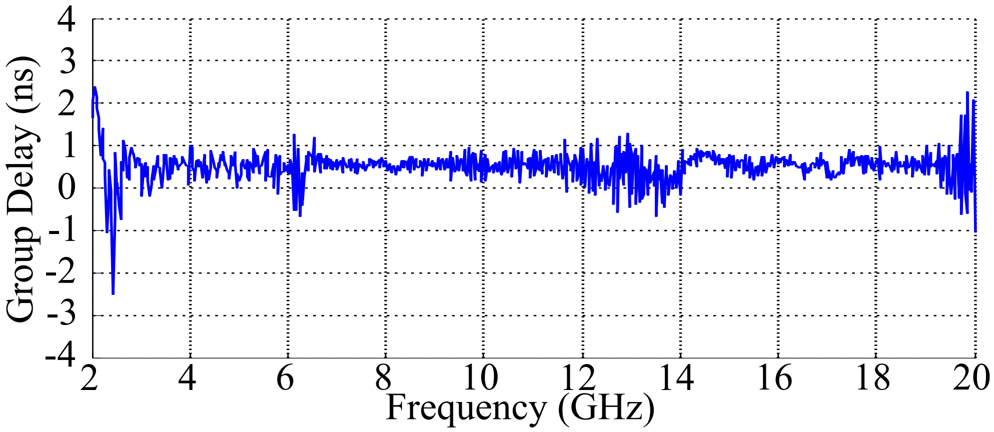

Figure 3.8. Measured group delay for the UWB antenna. Group delay measured for the UWB antenna with the configuration illustrated in Fig 3.7.

performance relative to the reference copper antenna. The dielectric loss is assumed insignificant as a result of the very small substrate thickness. Hence only the conduction losses due to the limited conductivity of PEDOT are estimated.

For the Wheeler Cap method measurement, the antenna has been placed into a rectangular closed metallic box (140 mm x 80 mm x 30 mm, copper coated) and the reflection coefficient parameter has been measured, as shown in Fig. 3.9. The reflection coefficient in this setup $S_{11-wheeler}$ and in free space $S_{11-free}$ have been used to estimate e_{cd} according to (7.11) in [134]:

$$e_{cd} = \sqrt{(1 - |S_{11-free}|^2)(|S_{11-wheeler}|^2 - |S_{11-free}|^2)}. \tag{3.4}$$

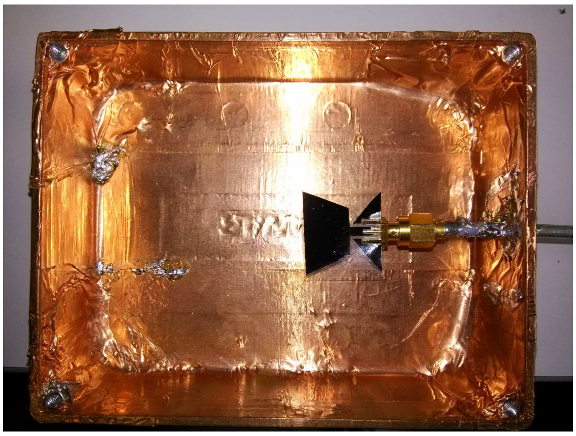

Figure 3.9. Wheeler cap measurement configuration. An antenna prototype under test in the metallic box for Wheeler cap measurement, with the box lid opened.

As shown in Fig. 3.10, the measured radiation efficiency is mainly in the range between 80% and 90% in the operation spectrum. This is in good agreement with the simulated efficiency which is between 85% to 90%.

For the conduction efficiency estimation, the radiation performance, namely the 2D radiation patterns in xz-, yz-plane as well as in two planes at angles in between have been measured for the PEDOT antenna and compared to the corresponding measurements for the copper antenna. The conduction efficiency of copper is assumed to be approximately 1. In this comparison, it is assumed that the directivity of both antennas are the same, which is confirmed by the nearly identical shapes of the radiation patterns. The dielectric losses are assumed to be the same as well, due to the very thin substrate. The radiated power is averaged over all measured angles (in standard spherical coordinates) and the conduction efficiency can then be estimated as follows [4]

$$e_c \approx \frac{\Sigma_\phi \Sigma_\theta G_{PEDOT}(\theta, \phi) \sin\theta \Delta\theta \Delta\phi}{\Sigma_\phi \Sigma_\theta G_{Copper}(\theta, \phi) \sin\theta \Delta\theta \Delta\phi}. \tag{3.5}$$

The resulting conductor efficiency of the PEDOT is included as a solid line in Fig. 3.10. As expected, the overall conduction efficiency is slightly higher than the radiation efficiency and remains between 85% to 90% over most of the operation band. A 89.9% averaged conduction efficiency is measured from 3 to 20 GHz which clearly demonstrates the high efficiency of the polymer antenna. Consequently, the gain of the PEDOT antenna is expected to be between 1.1 to 4.4 dB, only around 0.5 dB lower than copper over the operation spectrum.

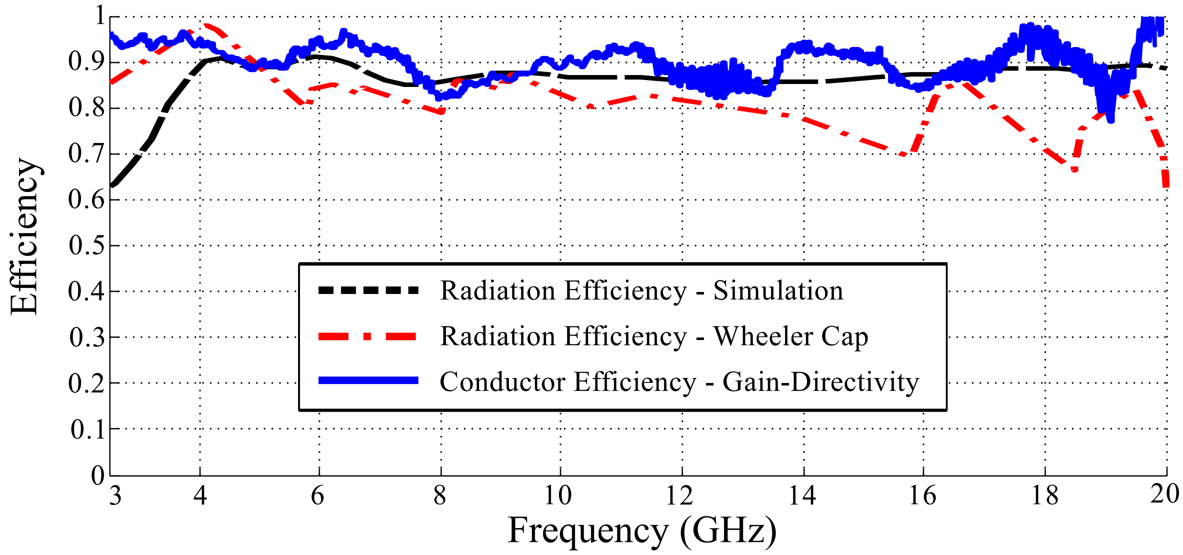

Figure 3.10. Simulated and measured antenna efficiencies. Simulated and measured radiation and conductor efficiency.

The measured radiation patterns at 5, 10 and 15 GHz are shown in Fig. 3.11, normalized to the maximum gain of both antennas. As anticipated, the patterns exhibit typical UWB dipole-like characteristics with an omnidirectional pattern in the xy-plane and zeros at $\theta = 0^\circ$, 180°. As the frequency approaches the higher end of the spectrum, this dipole behaviour starts to deteriorate which is typical for this type of antenna. The prominent similarity in the radiation patterns of the PEDOT and copper antennas demonstrates again the exceptional performance of the PEDOT antenna.

3.2.5 Antenna bending performance

In addition to the good electrical performance, the realized polymer antenna also proves to have excellent mechanical characteristics similar to plastic. The materials feature exceptional flexibility and robustness, hence the antenna can be bent dramatically without mechanical damage, as shown in Fig 3.12. The antenna has been measured under 90° and 180° upward and downward bending conditions, held in place by a piece of radome foam. This Cuming Microwave C-Foam PF-4 is chosen as fixture since it has very similar dielectric properties (relative permittivity $\varepsilon_r = 1.06$ and the loss tangent $\tan\delta = 0.0001$) to air. The measured S_{11} parameter shown in Fig. 3.13 indicates that the antenna bending at ±90° does not cause dramatic variations in the matching, while ultimate bending at ±180° has detrimental impact on the performance in the lower spectral region due to the significant reduction of the effective antenna length. It is

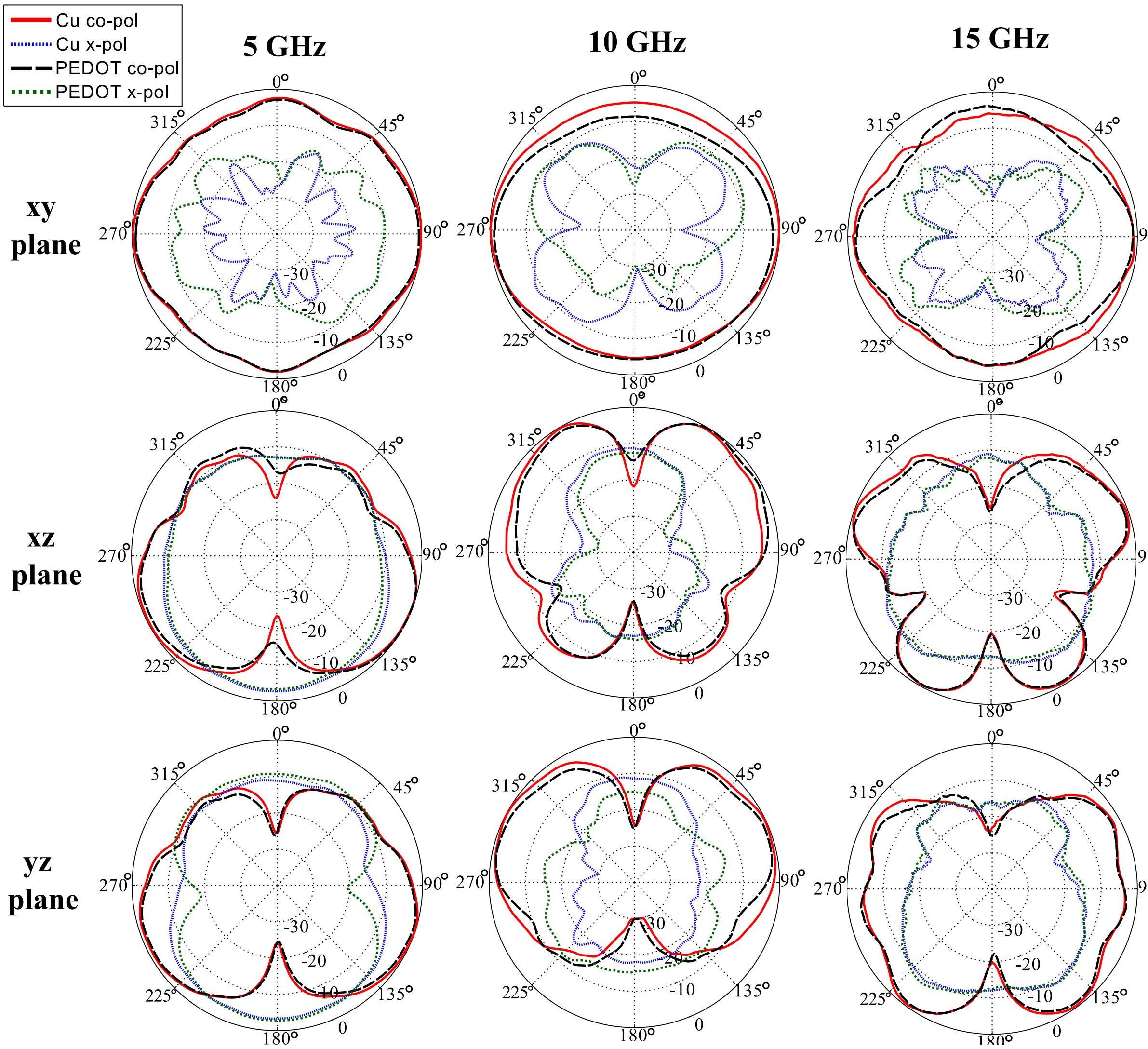

Figure 3.11. The measured radiation patterns. The radiation patterns of the copper and PEDOT antennas in *xy*-, *zx*- and *yz*-planes at 5, 10 and 15 GHz.

noted that such dramatic bending is of little practical interest, but it demonstrates the flexibility of the antenna.

Flexible antennas are supposed to be bent or even conformed to a specific surface during operation, and thus tests in various bending conditions are necessary to investigate bending-dependent characteristics variations including impedance matching [135] and radiation patterns [24, 27]. Therefore the influence of typical bending configurations on the antenna matching and radiation performance is investigated numerically with CST and validated experimentally. The 3D antenna representation and the considered bending setup in CST are depicted in Fig. 3.14. Antenna characteristics including

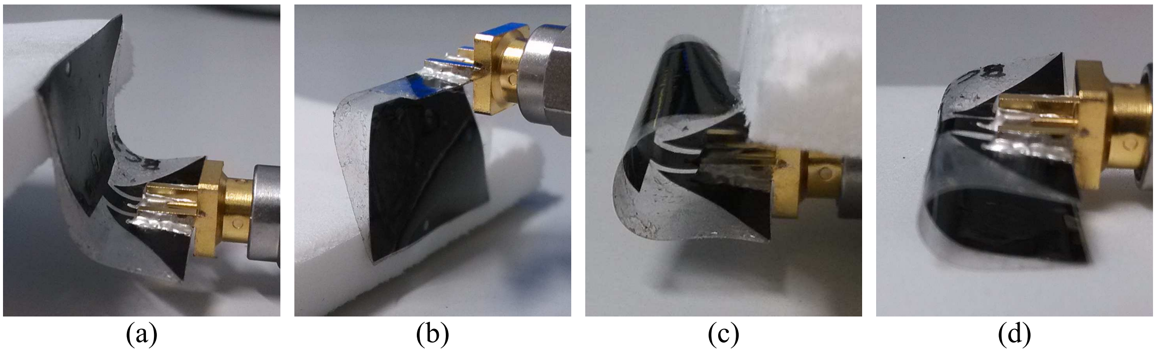
(a) (b) (c) (d)

Figure 3.12. Antenna under various bending conditions. Antenna in various bending conditions. a) 90° bending upward. b) 90° bending downward c) 180° bending upward. d) 180° bending downward.

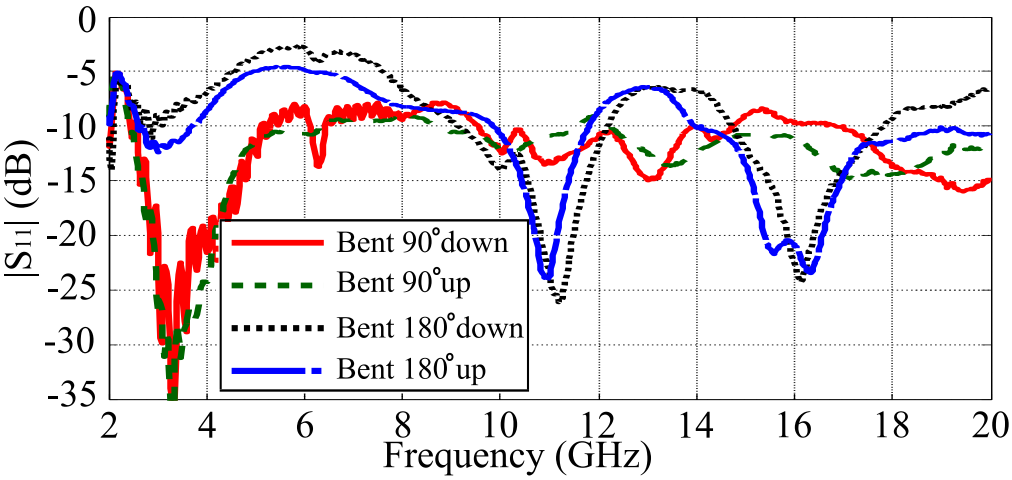

Figure 3.13. Measured reflection coefficient of bent antennas. Measured reflection coefficient $|S_{11}|$ of the proposed antenna under various bending conditions: 90°, 180° bending upward and backward.

S-parameters, polarization and radiation patterns are examined with regards to the bending angles from 0° to 180°, as defined in the inset of Fig. 3.14.

The simulated reflection coefficient under various bending angles from 0° to 180° (Fig. 3.14) with steps of 30° is shown in Fig. 3.15. For bending angles under 60°, the degradation of the $|S_{11}|$ is insignificant. However, for more pronounced bending above 60°, prominent differences are then observed. Generally the antenna operation band tends to shift to a higher frequency spectrum along with the increase in bending angle. This can be intuitively interpreted as follows: with increasing bending angle, the tapered slots between the trapezoidal elements and the CPW ground planes become

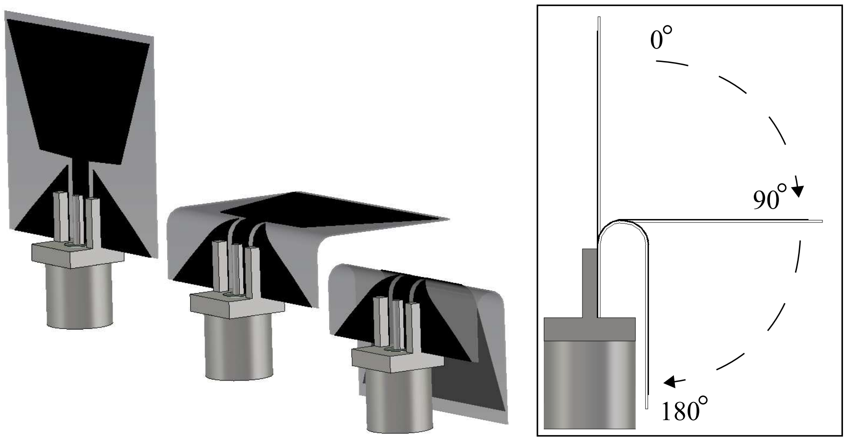

Figure 3.14. Bending simulation configurations in CST. The antenna and its 3D bending setup in CST. Inset: Definition of the bending angle (side-view).

narrower which shifts the operation range to higher frequencies. Strong coupling between the antenna and the SMA connector case which corresponds to resonances at some particular frequencies are observed in simulation. However, such SMA connector is unlikely to appear in practice, and the extreme bending conditions are not likely to occur as well. The results suggest that this antenna still performs nearly as well as the planar configuration in terms of impedance matching for bending angles up to around 60°, and might be usable with slight matching degradation up to at least 90° bending.

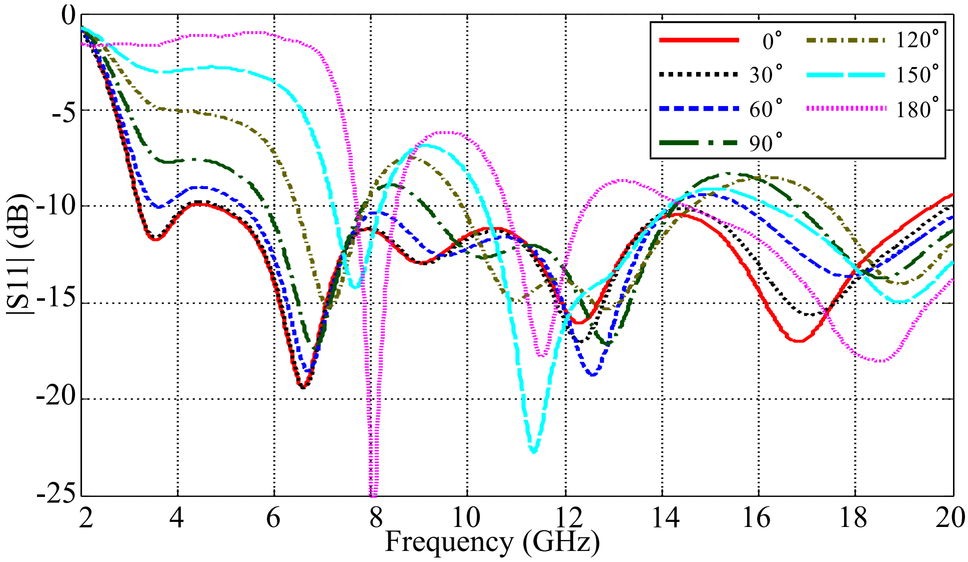

Figure 3.15. Simulated reflection coefficients under different bending conditions. Simulated $|S_{11}|$ for different bending angles (defined in Fig. 3.14).

The unbent antenna is vertically linearly polarized but this fact can be expected to change when the bending angle starts to increase. As illustrated in Fig. 3.16, a qualitative analysis suggests that the linear polarization direction should broadly rotate clockwise simultaneously with the bending angle and reach 45° and 90° for the antenna bent at 90° and 180° respectively. Therefore, this important aspect which will affect the polarization loss factor must be taken into account when considering the conditions of operation for those antennas in a wireless communication link influenced by various bending conditions.

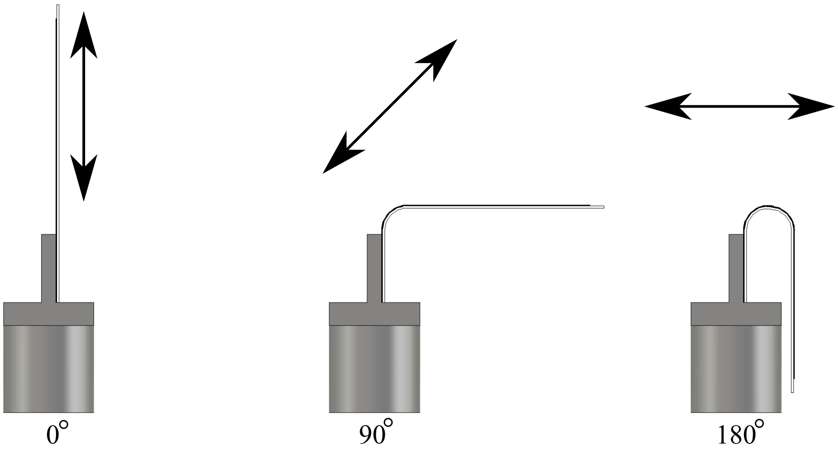

Figure 3.16. Antenna predominent polarization under different bending conditions. Antenna predominent polarization with bending angles of 0° (unbent), 90° and 180°.


(a) (b)

Figure 3.17. Antenna bending configuration for radiation pattern measurement. The 90°-bent antenna as prepared for radiation patterns measurement in an anechoic chamber. A piece of PF-4 radar foam (white) is used as holding material with a nearly unity relative permittivity. (a) Side view. (b) Top view.

The 90°-bent antenna, as illustrated in Fig. 3.17, has been chosen for experimental study of radiation patterns due to its nearly diagonal linear polarization. The xy-plane radiation patterns for both 90°-bent and planar (0°) configurations measured at 4, 7, 10, 13 and 16 GHz are normalized and plotted in Fig. 3.18. It is noted that the interpretation of the results can only be qualitative, as the exact location of the bending will influence the pattern and polarization. Therefore, only the patterns in xy-plane are discussed here, since they correspond to nearly omnidirectional patterns in unbent condition and are clearly illustrating the effect of bending.

As observed in the right-hand side column of Fig. 3.18, the bent co-polarized patterns (E_θ) in the xy-plane still largely retain an omnidirectional characteristic, similarly as the unbent ones, however with a marked reduction in gain, due to radiation in cross-polarization. This is confirmed by a dramatic increase of the cross-polarization (E_ϕ) by 10-20 dB. As a result, under bent condition, the component defined as cross-polarization reaches a similar or even higher level as the co-polarization, suggesting the 45° polarization tilt angle mentioned above. The cross-polarization patterns in bending condition show a dipole characteristic, with maximum gain at $\phi = 0°, 180°$, and minimum gain at $\phi = \pm 90°$. This is indicative of the alignment of the cross-polarized component with that of the linearly polarized reference horn antenna used in the measurement.

The results attained through simulation and experiments demonstrate that the antenna still performs well even with serious bending angles as regards impedance matching. In addition, extra attention needs to be dedicated to the polarization direction change when the antenna is bent or conformed to a curved surface, although this is usually not a problem in communication systems heavily affected by multi-path, e.g. for urban or indoor operation.

3.2.6 Summary on non-resonant design

The proposed antenna is completely fabricated from polymer, namely a thin PEDOT layer as the conductor and sticky tape as the substrate. As a result, the compact antenna exhibits features such as high flexibility and robustness, without sacrificing efficiency. By using laser cutting technology, the antenna has been precisely fabricated so that it performs as predicted by the simulations. Above 85% averaged radiation efficiency has been achieved over the operating frequency range from 3 to 20 GHz, which, to the best of our knowledge, is the highest reported to date for a non-metallic antenna of this type. The estimated average conduction efficiency of nearly 90% also

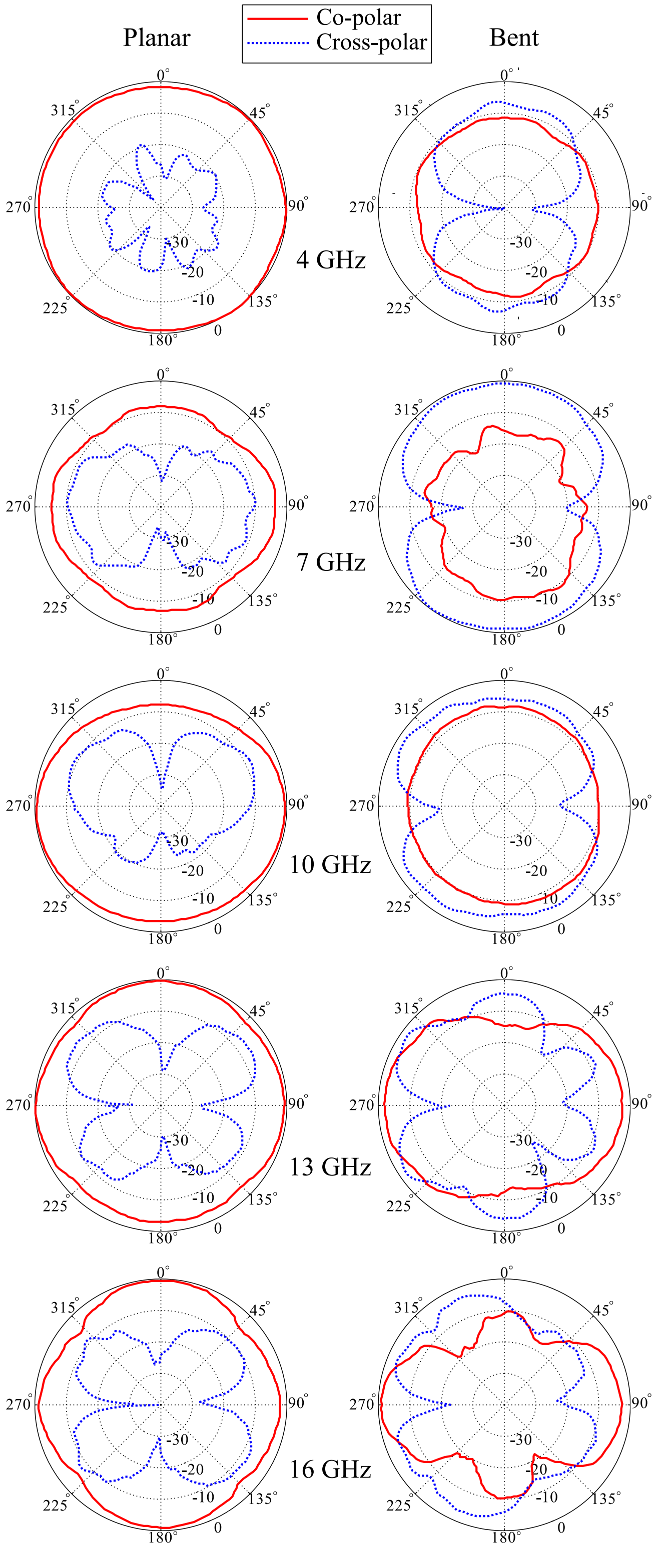

Figure 3.18. Measured radiation patterns under 90° bending condition. The measured xy-plane radiation patterns of the antenna in planar and 90°-bent conditions at 4, 7, 10, 13 and 16 GHz.

indicates that this type of non-resonant antenna has successfully overcome the limitations in conductivity and thickness of conductive polymers. The promising potential of the proposed antenna in flexible and wearable electronic systems is obvious. This UWB antenna exhibits plastic-like physical properties as well as metallic-like electrical properties, which illustrates a typical successful conductive polymer antenna design.

3.3 Chemical treatment strategy

A straightforward strategy is demonstrated here to increase the electrical conductivity of a PEDOT layer. This strategy utilizes a simple, inexpensive yet effective chemical treatment to improve the conductive polymer conductivity and consequently the antenna efficiency. There are increasingly intensive research works on chemical treatments for conductivity enhancement for conductive polymers. One of the simplest yet effective methods is methanol treatment proposed by [136] where the PEDOT:PSS film conductivity was enhanced from 30 S/m to 136200 S/m. Therefore, this treatment was adopted as a post-fabrication conductivity enhancement for our PEDOT:PSS samples. Then a 2.45-GHz dipole antenna realized in methanol-treated conductive polymers PEDOT:PSS is presented as a test bed, with exceptional reversible flexibility and high-efficiency. More specifically, the originally highly conductive PEDOT:PSS thin films have been further treated by immersion in a methanol solution, to realize a significant conductivity improvement from approximately 3500 S/m to 18500 S/m. As a result, a more than 25% antenna efficiency enhancement is attained, which brings the averaged efficiency up to 91.4% of the efficiency of a copper reference antenna with identical geometry.

3.3.1 Material and treatment

As mentioned previously, conductive polymers inherently hold a process-limited thickness and a relatively lower conductivity compared to metallic materials. The free-standing PEDOT:PSS thin film used in this work was quite challenging to produce since it has a relatively high estimated dc-conductivity of 3500 S/m and a substantial thickness of 113 μm. This unique combination of thickness and conductivity enables a sufficiently low sheet resistance of approximately 2.5 $\Omega/square$. Such competitive materials are prepared with Clevios PH1000 (Heraeus) solution and ethylene glycol using a solvent casting method. All residual solvent is eliminated completely from the films through a 130°C annealing process. The PEDOT:PSS film thickness is approximately two thirds of the skin depth at 2.45 GHz which is around 170 μm. This fact implies an increase in conductor ohmic loss and consequently a decrease in antenna efficiency. This loss in efficiency can be partially overcome by using well established techniques to enhance the conductivity [137].

To further increase the conductivity, a simple, stable and economic treatment with methanol solution immersion reported in [136] is deployed. Changes to morphology, improved alignment of the PEDOT particles and removal of excess insulating PSS from the PEDOT:PSS film are the mentioned main mechanisms for the high conductivity enhancement [136]. The mechanism of this methanol conductivity improvement method is investigated and a illustrative diagram is shown in Fig. 3.19 [136].

Figure 3.19 shows a schematic illustration of the morphology of PEDOR:PSS solid films which comprises grains based on a highly conductive and hydrophobic PEDOT-rich core and an insulating hydrophilic PSS-rich shell [78]. By using methanol which has a high permittivity and is highly hydrophilic, interactions with the hydrophilic PSS will induce a screening effect between the PEDOT and PSS chains. This will lead to the PSS dissolution in methanol due to the phase separation between the PEDOT and PSS chains induced by this screening effect. Consequently due to this process, reorientation of the PEDOT polymer chains from a coiled to linear or extended-coil configuration is facilitated which will then enhance the inter-chain interaction between the polymer layers. Eventually a much easier charge hopping and thus a much higher conductivity is achieved [136]. It is shown that this simple technique can enhance the conductivity of the samples by 3 orders of magnitude [136].

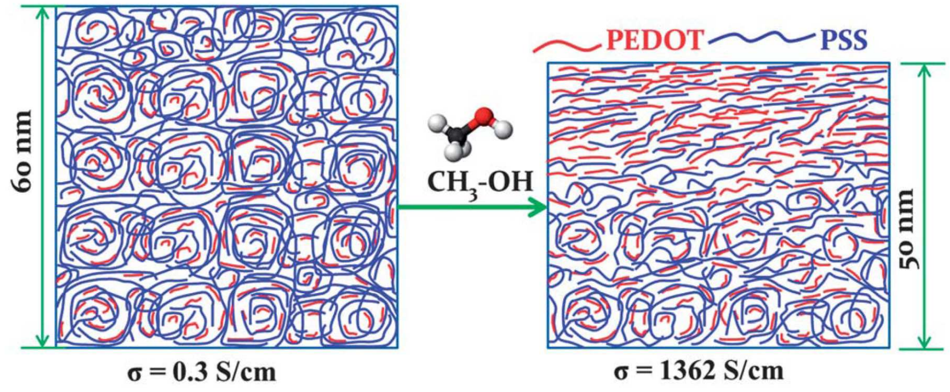

Figure 3.19. The methanol treatment mechanism. The conductivity enhancement mechanism of the methanol treatment method, adapted from [136]

For the details of our method, the PEDOT:PSS samples were immersed in methanol overnight and dried at room temperature. The original and the treated PEDOT:PSS thin films are shown in Fig. 3.20. Some sort of distortions in the treated PEDOT:PSS film are observed, which might become problematic for antenna designs requiring large areas. However, this could be solved by clipping or flattening during treatment with dedicated tools. Resistance measurement with a four-probe measuring system has been conducted and the resulting DC-conductivity of the original and the treated PEDOT:PSS has been determined to be around 3500 S/m and 18500 S/m respectively. Therefore, the sheet resistance of the treated PEDOT:PSS film is estimated to be approximately 0.5 $\Omega/square$, which is about one fifth of the untreated film.

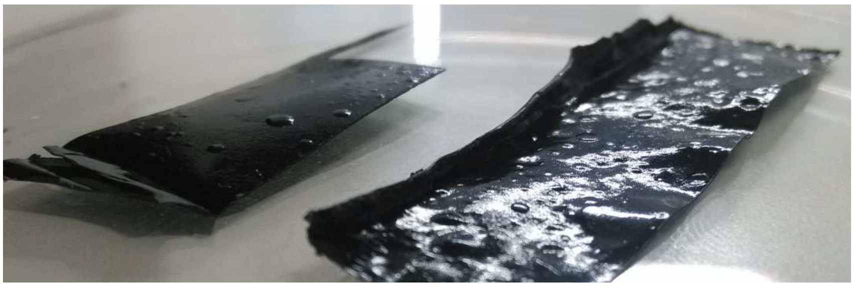

Figure 3.20. The untreated and treated PEDOT:PSS thin films. The original (left) and methanol-treated (right) PEDOT:PSS.

3.3.2 Antenna design

To test the performance of the treated film, a resonant antenna test bed is chosen, in the form of a 2.45-GHz dipole antenna. The realizations of the antenna in copper, untreated and treated PEDOT:PSS are shown in Fig. 3.21. The three prototypes are fed with a 50-Ω microstrip line to 78-Ω balanced coplanar strips impedance transition which is employed as a balun [138,139]. The antenna dimensions are also illustrated in Fig. 3.22. The dipole arm length L is inversely proportional to the resonance frequency while the width W is proportional to the impedance bandwidth. The gap G between the two arms determines the input impedance of the antenna. Therefore, L and W are determined to obtain resonance at 2.45 GHz and to ensure ease of fabrication respectively, while G is chosen such that the input impedance is 78 Ω. The copper antenna arms are soldered whereas the polymeric arms are glued with conductive epoxy for connection to the balun.

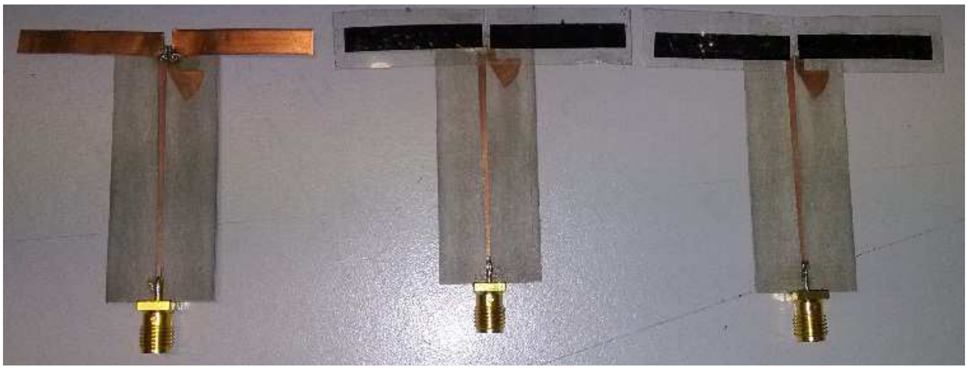

Figure 3.21. Three dipole antenna realizations. Antenna realizations in copper (left), original (middle) and treated (right) PEDOT:PSS. The three antennas are connected to a balun.

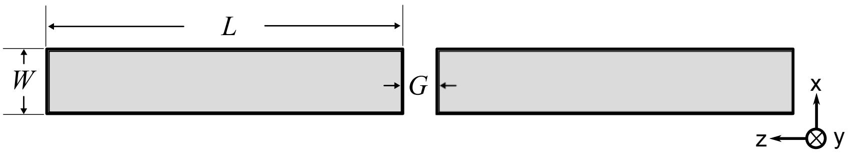

Figure 3.22. Antenna configuration. Antenna configuration and its dimensions: $L = 27.3$ mm, $W = 5$ mm, $G = 1.5$ mm.

In order to achieve high accuracy in fabrication, the antennas are trimmed with a laser milling machine (LPKF: Protolaser_S). Sticky tape is used as a protective layer for the PEDOT antennas which also provides a straightening support. The impact of this tape on the antenna performance is negligible owing to its very small thickness. Thanks to the plastic-like flexibility of the PEDOT:PSS film, the antennas feature an exceptional reproducible non-destructive mechanical conformability, as illustrated by the two bending configurations shown in Fig. 3.23. Therefore, seamless integration in flexible electronic systems is possible with this type of polymeric antennas.

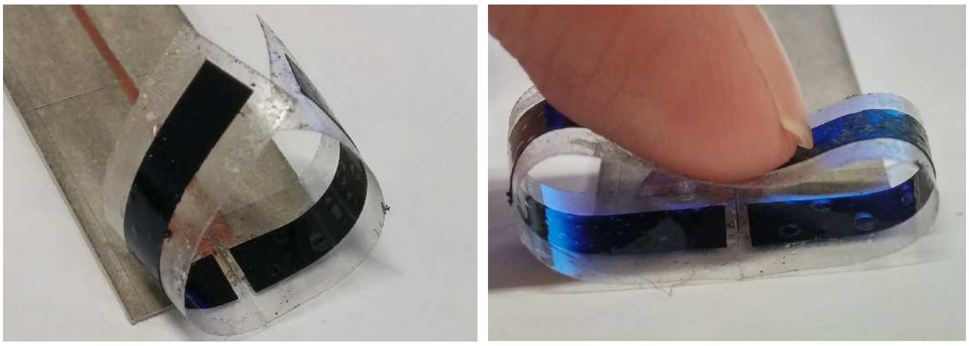

Figure 3.23. Bent dipole antenna. PEDOT antenna in two bending configurations.

3.3.3 Experimental results

The prototype PEDOT antennas have been experimentally characterized and compared with the reference copper antenna to investigate the performance improvement due to the material treatment. The results have been analyzed together with corresponding simulations performed using CST. They show encouraging improvements in antenna performance in terms of matching and antenna efficiency, as described in the following.

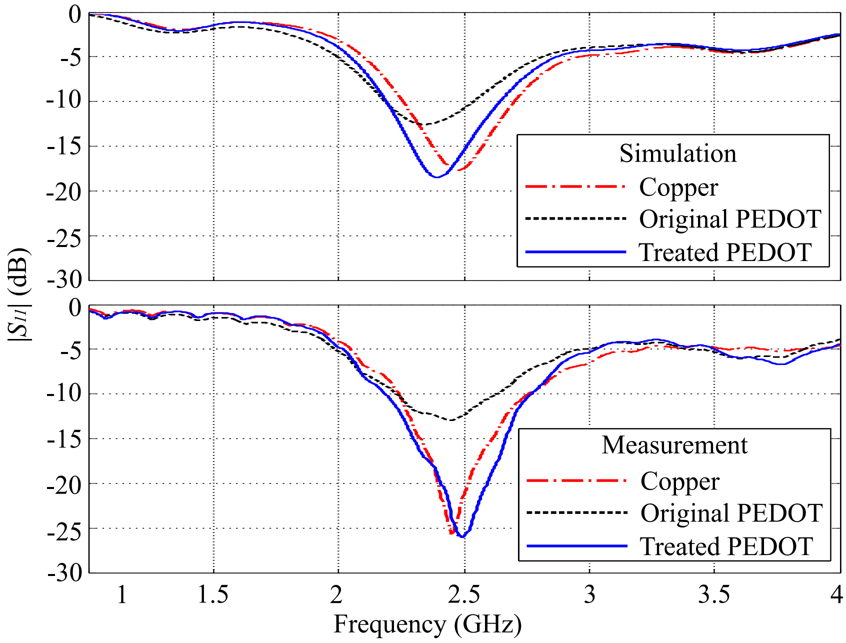

Figure 3.24. All dipole antennas simulated and measured $|S_{11}|$. Antenna reflection coefficient comparison. Top: simulations. Bottom: measurements.

The simulated and measured reflection coefficients are depicted in the top and bottom sub-figures in Fig. 3.24 respectively. The simulated and measured curves for corresponding devices are in good agreement. Slight resonances shifts are observed which can be attributed to fabrication tolerances. The similarity in the reflection coefficient of the copper and treated PEDOT antenna suggests that they should have comparable performance in terms of efficiency.

The measured radiation patterns at 2.45 GHz in *xy*-, *xz*- and *yz*-plane are shown in Fig. 3.25, normalized to the overall maximum gain of the copper reference antenna. The co-polarization and cross-polarization components are depicted in the left-hand side and the right-hand side columns, respectively. The striking similarity in the shape of the patterns for the copper and treated PEDOT antennas suggests a similar antenna

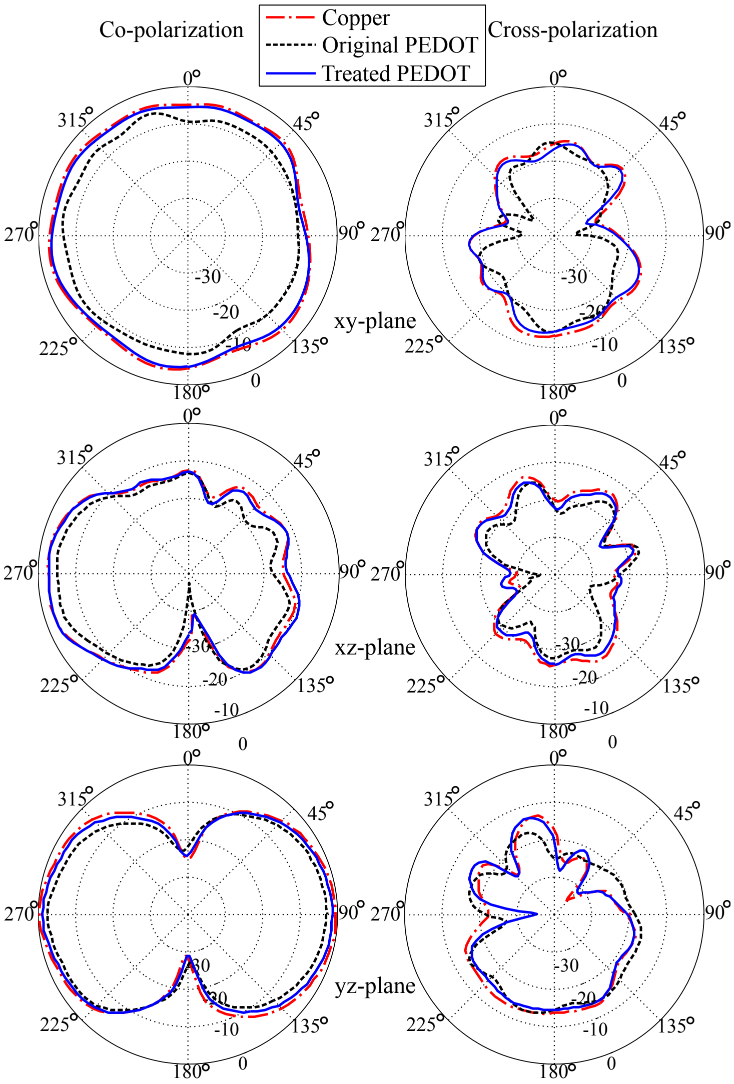

Figure 3.25. All dipole antennas measured radiation patterns. Measured radiation patterns at 2.45 GHz in principal planes. Left: co-polarization. Right: cross-polarization. All patterns are normalized to the overall maximum gain of the copper antenna.

efficiency. As expected for a dipole antenna, the patterns in xy-plane is omnidirectional and zeros are observed at $\theta = 0^\circ$, 180°, along the z axis. The asymmetry of the co-polar components in the xz-plane is introduced due to the presence of the SMA and a right angle connectors in the measurement path.

The antenna efficiency is estimated through an approximate gain-directivity measurement relative to the reference antenna. Comparisons of the radiation patterns in xz- and yz-plane, as shown in Fig. 3.25, indicate that the antennas have nearly identical directivity since the patterns are of the same shape. To compare the gains, the radiated power is averaged over all elevation angles, assuming 100% efficiency for the copper antenna. The PEDOT antenna efficiency is then evaluated as shown before through [4]

$$e_c \approx \frac{\Sigma_\phi \Sigma_\theta G_{PEDOT}(\theta,\phi)\sin\theta\Delta\theta\Delta\phi}{\Sigma_\phi \Sigma_\theta G_{Copper}(\theta,\phi)\sin\theta\Delta\theta\Delta\phi}. \tag{3.6}$$

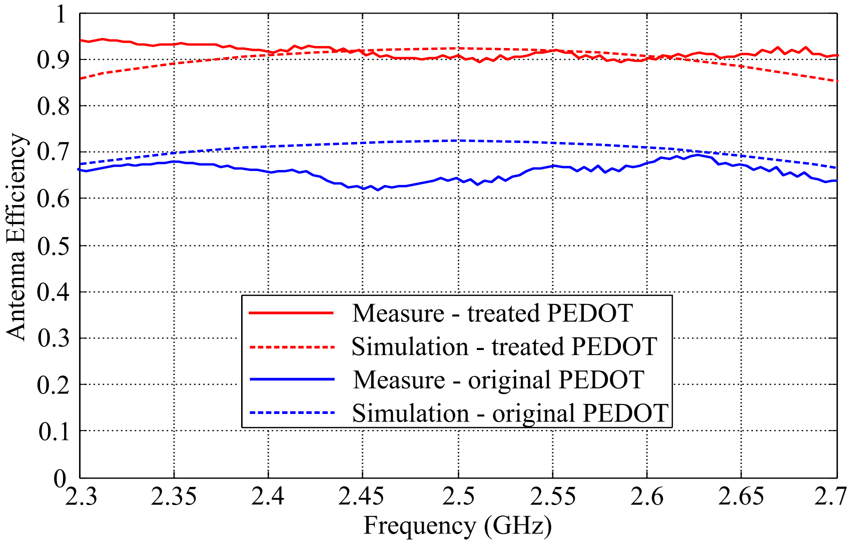

Figure 3.26. Simulated and measured antenna efficiencies. Simulated and measured antenna efficiency relatively to the copper reference antenna.

The simulated and estimated efficiencies are both illustrated in Fig. 3.26. A good correspondence between simulated efficiencies and pattern-based estimations is observed. Over the operation band, the antenna made from the original PEDOT:PSS yields an averaged 65% efficiency whereas the one realized with the treated polymer holds an averaged 91.4% efficiency. The last value is, to the best of our knowledge, the highest reported efficiency for this type of resonant polymeric antenna. An efficiency increase of more than 25% is achieved through the conductivity enhancement fulfilled with a simple methanol treatment.

3.3.4 Summary on chemical conductivity enhancement

A highly flexible and efficient 2.45-GHz dipole antenna realized with treated PEDOT has been presented, to demonstrate a simple yet effective chemical treatment based on methanol to significantly enhance conductivity in conductive polymers. Three identical antenna designs realized in copper, standard and treated PEDOT have been fabricated and experimentally characterized. The PEDOT antennas exhibit an exceptional plastic-like reversible mechanical flexibility, and the resulting reflection coefficient measurements and gain-directivity efficiency estimations are in a good agreement with CST simulations. The methanol-solution-based treatment of the PEDOT thin film boosts the antenna efficiency by 25% to an averaged value of 91.4% over the operation band. The result is remarkable in conjunction with a resonant design, and is, to the best of our knowledge, the highest value reported for this type of polymeric antennas. All these results emphasize that this cost-effective chemical treatment can significantly enhance the potential of conductive polymers as conductors for microwave applications such as antennas.

3.4 Laminated multilayer strategy

The third strategy is effectively increasing the thickness of the thin film materials by stacking multiple layers of materials with laminating dielectric layers in between. The method is based on the fact that the penetration depth of the electromagnetic waves in the conductor can be increased by this laminated sandwich structure. This section discusses the concept of this method and shows some preliminary measurement results of a microstrip line realized using a 1-layer PEDOT and a 3-layer SiO_2-laminated PEDOT thin film. A 15-dB improvement in the transmission coefficient is observed when using the laminated polymeric thin film, which validates this strategy.

3.4.1 Laminated conductor

In 1951, the concept of laminated conductor was firstly proposed and analyzed by A. M. Clogston [140], and it predicted that a thin (less than one skin depth) laminated conductor can be used to increase the electromagnetic wave penetration depth and thus lower ohmic loss compared to a single conductor. Recently this concept was used again by Shafai et al. to show that a multilayered laminated transmission line can have a dramatic reduction in ohmic loss [141]. With these laminated conductors, a square-ring antenna design was shown to achieve a 30% efficiency improvement in [142, 143]. It was also concluded that the improvement would be negligible if a near-perfect conductor was used. This laminated sandwich configuration can well fit applications of conductive polymers with a thickness much less than a skin depth. Thin layers are preferable, since it is very challenging to fabricate a pure conductive polymer multi-layer structures with high conductivity, as a good electrical connection and physical bonding between polymer layers are difficult to achieve.

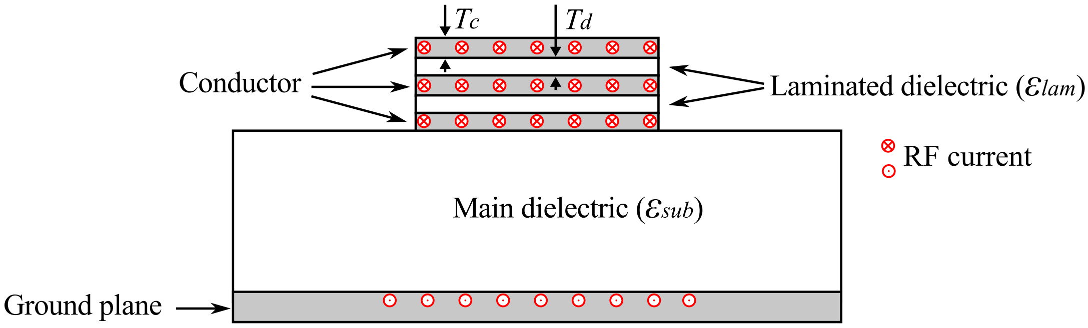

Figure 3.27. Cross section of a sandwich structure. A microstrip line model with a multilayer laminated conductor.

In our investigation of multilayer conductive polymers, we consider a microstrip line realized on a substrate with permittivity ε_{sub} using a laminated conductor, as shown in Fig 3.27. The stack has three conductor layers with a thickness of T_c and two laminating layers with permittivity of ε_{lam} and a thickness of T_d which is much less than a skin depth. The conductor layers in the stack are assumed with finite conductivity and a thickness much less than a skin depth. Then the time-varying electric field can penetrate this stack and induce RF currents in the conductor layers. When the phase velocity of the wave propagating inside the stack equals the one propagating in the substrate, the ohmic losses become minimum due to a higher current uniformity in all layers, which is referred to as the phase velocity matched condition [144]. The phase velocity V_p is governed by:

$$V_p = \frac{c}{\sqrt{\varepsilon_r}}, \tag{3.7}$$

where c is the speed of light and ε_r is the medium (or effective medium) relative permittivity. Since the laminating layers are very thin and therefore the fringing fields are negligible, one can assume that the waves propagate in the stack at the fundamental transverse electromagnetic (TEM) mode. As a result, the matched condition is fulfilled when

$$\varepsilon_{lam} = \varepsilon_{eff}, \tag{3.8}$$

where ε_{eff} is the effective permittivity of the microstrip line, which can be obtained using the well-known closed-form approximate expression developed by Wheeler [145].

If the microstrip line dimensions and substrate permittivity are known, then the laminating material which has appropriate permittivity and processability can be chosen for the laminated conductor to meet this condition. The measurement of the permittivity of SiO_2 laminae is a difficult matter, which could not be achieved during the time of this thesis. Therefore, an unequivocal verification of the exact matched condition is yet to be realized. Nevertheless preliminary tests were conducted and their results suggest a successful application of this lamination strategy using conductive polymers, as described in the next paragraph.

3.4.2 Preliminary experimental results

A single layer PEDOT with a thickness of 200 nm and a conductivity of 91000 S/m and a three-layered sandwich consisting of two layers of these PEDOT and a 100-nm-thick laminating layer of SiO_2 are used in this experiment, as shown in Fig. 3.28. Both are cut into a strip with identical dimension which are then put onto a test jig to form a microstrip transmission line, as shown in Fig 3.29.

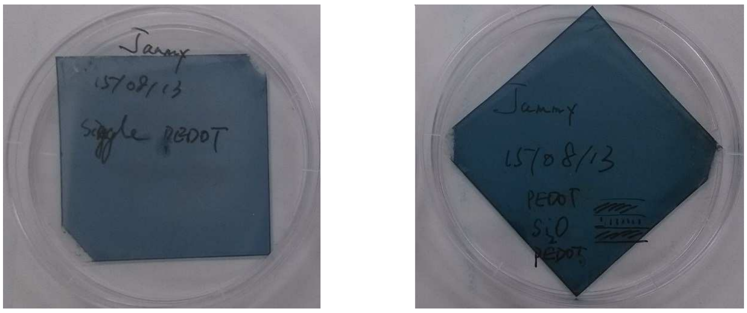

(a) (b)

Figure 3.28. 1-layer PEDOT and 3-layer PEDOT laminated films. (a) A single layer PEDOT thin film and (b) a three-layer laminated PEDOT with a laminae of SiO_2.

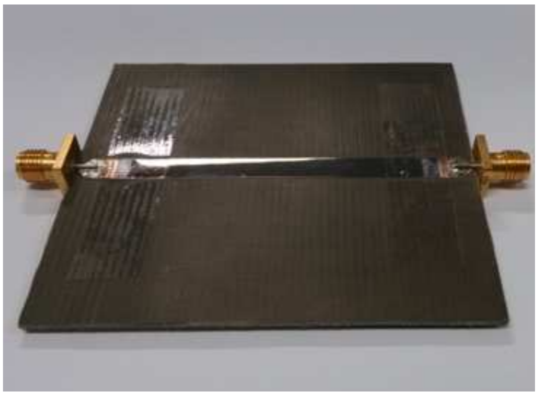

Figure 3.29. The microstrip line test jig. The test jig used to measure transmission coefficients of the microstrip lines with 1-layer and laminated PEDOT conductor.

The simulated and measured transmission coefficients of both cases are compared in Fig. 3.30. The strips are simulated based on the 'thin panel' material model in CST which is penetrable to electromagnetic field and does not require meshing inside the constituting layers, because they are well below one skin depth. A good agreement between the simulated and measured $|S_{21}|$ for the single layer transmission line is observed, indicating that this material model is appropriate. The larger discrepancy between simulation and measurement for the 3-layer strip might be because the simulated laminating layer properties such as permittivity are not accurately known. Nevertheless, as can be seen from the measurement, the laminated stack has a 5 to 15 dB higher $|S_{21}|$ parameter compared to the single layer PEDOT, indicating that this strategy is promising, even if associated with a potentially higher fabrication cost. We also note that further layers of lamination would be required to increase the transmission coefficient to a practically usable level.

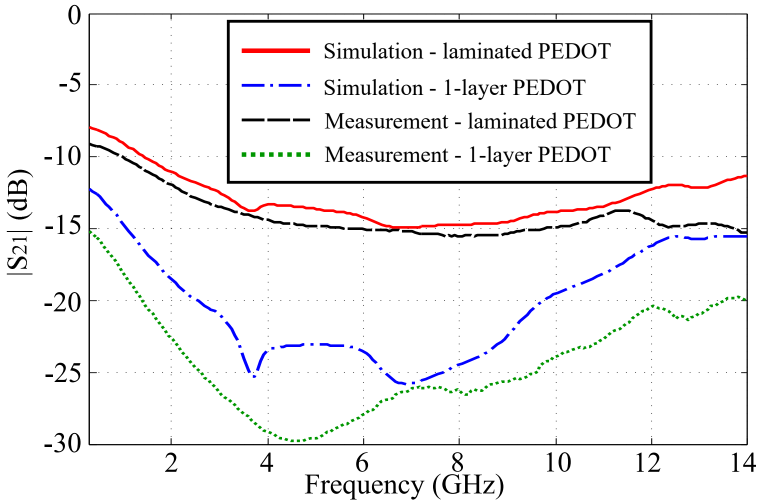

Figure 3.30. Simulated and measured $|S_{21}|$ parameters of the microstrip lines. Simulated and measured transmission coefficients of the microstrip lines with 1-layer and laminated PEDOT conductor.

3.4.3 Summary on laminated conductors

A multilayer laminated conductor structure is used as a strategy to effectively increase the thickness of conductive polymer thin film, since this structure is able to increase the wave penetration into the conductor. As a preliminary validation, a single layer PEDOT and a 3-layer PEDOT sandwich structure with a SiO_2 laminae are cut into a strip and tested using a microstrip line test fixture. The measured and simulated transmission coefficients have a good agreement and show a maximum 15-dB improvement with the sandwich configuration, which validates this strategy. Increasing the stacking layers quantity, up to a certain limit, will lead to even a lower DC sheet resistance [142]. Further experimental comparison to a pure multilayer PEDOT film will be naturally the next step. Nevertheless, this strategy is a promising engineering technology which can be exploited for conductive polymers to overcome their limitation in thickness.

3.5 Exploitation of polymeric antenna flexibility

The polymeric antennas discussed so far in this chapter comprise either a single layer or two layers, and thus they intuitively are expected to have outstanding flexibility. However, making multilayer antennas highly flexible requires extra efforts in the design, since the more layers involved the harder to attain flexibility. In this section, a microstrip-fed slot antenna realized in PEDOT:PSS which exhibits a high efficiency and decent flexibility is presented, to illustrate some engineering considerations in polymeric antenna designs in terms of flexibility and efficiency.

3.5.1 Antenna design

A flexible 5.8-GHz microstrip-fed slot antenna, made from a PEDOT:PSS thin film with a very low DC sheet resistance of 0.5 $\Omega/square$, is designed and experimentally characterized. The antenna configuration with all dimensions indicated, and a PEDOT:PSS realization are depicted in Fig 3.31. Both the 50-Ω open-end microstrip line feed and the ground plane with a slot are realized in PEDOT:PSS films. They are mounted on both sides of a substrate which is made of a highly flexible Cuming Microwave C-Foam PF-4 foam. The free-standing PEDOT:PSS films were made from Clevios PH1000 (Heraeus) with ethylene glycol using a solvent casting method, then all residual solvent was removed with annealing at 130°C. The 110-μm-thick polymeric film has a conductivity of 18000 S/m leading to a dc sheet resistance of 0.5 $\Omega/square$. Regarding the PF-4 foam, its relative permittivity ε_r, loss tangent tanδ and thickness are 1.06, 0.0001 and 1.6 mm, respectively.

The resonance frequency and the impedance bandwidth of the proposed antenna are determined main by the slot length and the slot width respectively. The slot length W_2 is 19.5 mm roughly half of the operational wavelength, and the slot width L_4 is chosen to be 2 mm for easy manufacture. The microstrip feed line length determines the matching and an optimal value was obtained through iterative parameter sweep with CST.

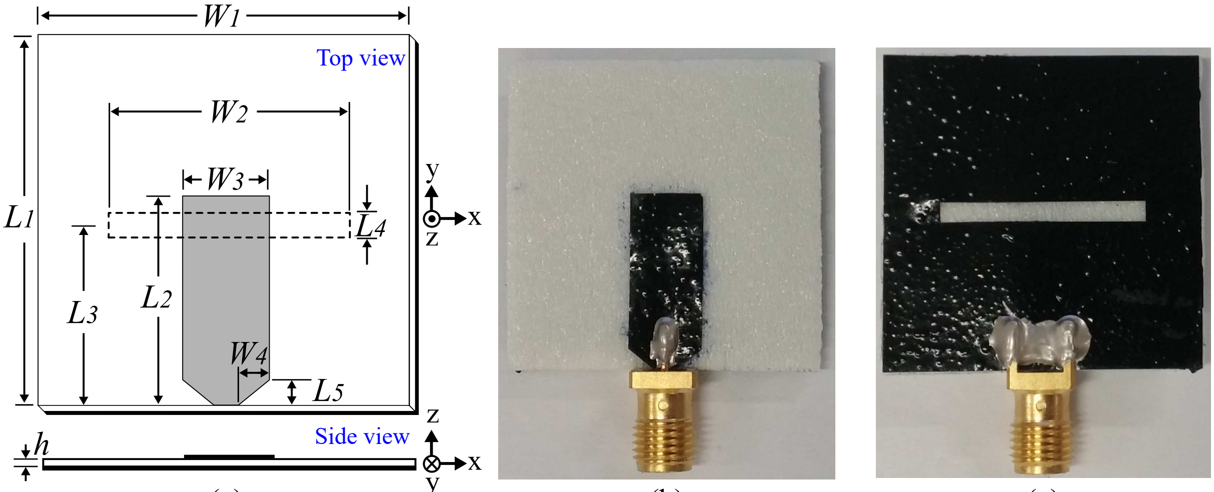

(a) (b) (c)

Figure 3.31. Microstrip-fed slot antenna configuration and realization. The antenna (a) configuration and a PEDOT realization: (b) top view and (c) back view. Dimensions (mm): $W_1 = 30$; $W_2 = 19.5$; $W_3 = 7$; $W_4 = 2.5$; $h = 1.6$; $L_1 = 30$; $L_2 = 17$; $L_3 = 15$; $L_4 = 2$; $L_5 = 2$.

3.5.2 Experimental results

To verify the design, a PEDOT and a copper reference prototypes were fabricated and experimentally characterized. The simulated and measured reflection coefficients are shown in Fig 3.32, and a good agreement between them is observed. The PEDOT antenna has a wider bandwidth than the copper one since it has slightly higher losses in the conductors. As expected, the antenna has an operational bandwidth extending from 5.3 to 6.3 GHz, centered at 5.8 GHz. Moreover, the simulated $|S_{11}|$ under bent condition with a radius R = 30 mm is included as well and it indicates that the bending configuration (Fig. 3.32 inset) does not introduce significant variations in the impedance bandwidth.

The measured radiation patterns of both antennas in *xz*- and *yz*-plane at 5.8 GHz are displayed in Fig. 3.33. Typical characteristics of slot antennas on a finite ground plane are observed in the patterns where maximum radiation is directed normal to the ground plane. More importantly, the similarity in both PEDOT and copper antennas radiation patterns is prominent which suggests that the polymeric antenna should have a very satisfactory efficiency.

An approximate gain-directivity comparison with the reference antenna is exploited to obtain an estimation of the polymeric antenna efficiency, as discussed in Section 3.2.4. It is assumed that the copper antenna is 100% efficient and that both antennas have identical directivity which is confirmed by the nearly identical angular distribution in

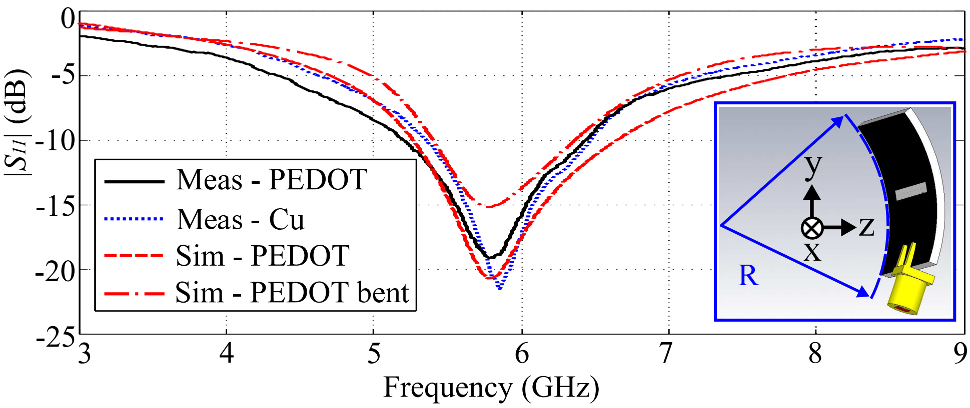

Figure 3.32. Microstrip-fed slot antenna simulated and measured $|S_{11}|$. The simulated and measured reflection coefficients. Inset: Bending configuration in CST to obtain the simulated $|S_{11}|$ when R = 30 mm.

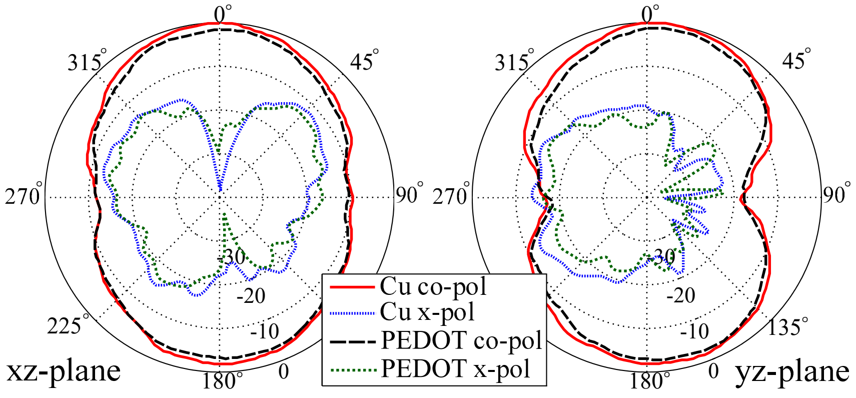

Figure 3.33. Microstrip-fed slot antenna measured radiation patterns. Radiation patterns of the copper and PEDOT antennas in xz- (H-plane) and yz-plane (E-plane) at 5.8 GHz.

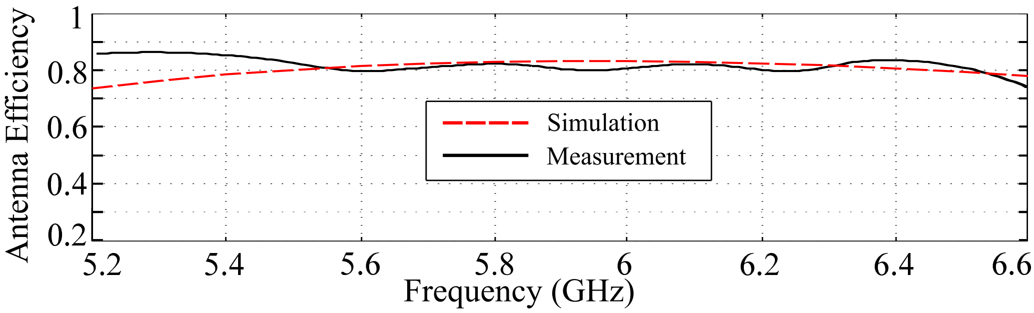

Figure 3.34. Microstrip-fed slot antenna simulated and measured efficiencies. Simulated and measured radiation efficiencies of the PEDOT antenna.

the pattern measurements (Fig. 3.33). This method evaluates the efficiency by comparing the average absolute gain of both antennas as computed through integrating the received power of all measured angles of the xz- and yz-patterns, namely based on equation (3.5). As demonstrated in Fig 3.34, the measured antenna efficiency remains approximately between 80% and 88% which agrees closely with predicted values obtained through simulations. The average antenna efficiency of 82% is very encouraging but slightly lower than that of a complementary 5.8-GHz dipole antenna simulated with the same PEDOT material in CST, namely 90.7%. The lower efficiency can be attributed to the extra ohmic losses introduced in the slot antenna microstrip line feed section which does not exist in the dipole antenna. This can be a consideration while designing antennas with conductive polymers which usually have relatively lower conductivity than metals.

3.5.3 Antenna mechanical flexibility

One of the important advantages of conductive polymers over metals for foreseen applications is their mechanical resilience and plastic-like texture. Therefore, making full use of this property for flexible designs is another significant requirement. In terms of the film form, free-standing conductive polymers generally offer more freedom in flexible antenna designs compared with non-free-standing ones, which require a supporting substrate. Moreover, appropriate substrate materials are critical to achieve conformability for antennas with substrate(s).

Owing to the excellent mechanical resilience of the free-standing conductive polymers, their inherent flexibility is particularly expressed in antennas which do not require a substrate. For instance, the single-layer dipole antenna with excellent mechanical flexibility has been discussed in Section 3.3.2 previously, as shown in Fig. 3.23. The antenna is made of free-standing PEDOT thin films which are inherently highly flexible and possess plastic-like features, as shown in Fig 3.23. It is worth mentioning that common sticky tape was used as a protection layer rather than a supporting substrate for the antenna experimental characterization process.

For antennas requiring a substrate to support multiple disconnected element of a planar design or from a cavity, flexible, robust and low-loss materials are needed to keep design integrity while maintaining flexibility. For instance, the UWB antenna discussed in Section 3.2.5, as shown in Fig 3.12, has been shown to have an exceptional mechanical flexibility through the utilization of sticky tape as substrate. Common sticky tape can conveniently provide mechanical support and insulation while having negligible impact on the antenna performance. Other flexible dielectric materials such as polyethylene foams and Polydimethylsiloxane (PDMS) can be used as substrate materials as well, as alternative the PF-4 foam used in the microstrip-fed slot antenna just discussed in this section.

3.6 Conclusion

This chapter has illustrated three strategies to overcome the inherent limitations in conductive polymers such as relatively low conductivity and insufficient material thickness. The first strategy is, to utilize non-resonant antenna designs, in order to minimize RF current density and therefore the ohmic losses in the antenna, eventually leading to a high antenna efficiency. The second one is a very simple but effective chemical treatment using methanol to dramatically improve the polymeric film conductivity. The third solution is based on a multilayer laminated structure which can increase the effective film thickness by reducing the skin effect losses. At the end, a multilayer polymeric microstrip-fed slot antenna has been discussed, with emphasis on design considerations for antenna mechanical flexibility in terms of antenna engineering and materials selection. All these facts emphasize that conductive polymers are a class of very promising conducting materials for flexible and wearable antenna designs, or in the view of seamless integration with polymer electronics.

Chapter 4

High Efficiency Microwave Graphene Antenna

GRAPHENE and its composites are promising materials in nearly every engineering field, and thus they are the subject of intense global research thrust. Graphene-based materials can also be very appropriate for microwave antenna designs, because besides high conductivity, chemical stability and mechanical flexibility, they have the potential of becoming affordable for large scale fabrication in the near future. Some microwave antennas realized in graphene film have been reported in the past, however with modest efficiency, due to limited conductivity and film thickness. To address this problem, this chapter initially presents a scalable production of graphene films dedicated to microwave antenna design. Subsequently a high-efficiency UWB antenna realized in graphene films is designed, fabricated and experimentally characterized. The antenna exhibits a very satisfactory efficiency of nearly 80% averaged over the UWB bandwidth, which is attributed to the non-resonant antenna design and the high-quality graphene films. The very encouraging antenna performance suggests that the proposed graphene films are promising as environmentally-friendly, inexpensive and efficient non-metallic conductors for high-volume applications in the microwave region.

4.1 Introduction

Graphene, a layered carbon material, is an outstanding representative of 2D crystals and has become the subject of intense global research towards the exploitation of its unique properties in various applications [86, 89, 99]. This material possesses many attractive properties including extremely high mechanical strength, as well as exceptionally high electrical and thermal conductivities for a non-metallic material. In particular, the interesting electronic properties allowing ballistic transport with a high ambipolar charge carrier mobility ($2.5 \times 10^5\ cm^2V^{-1}s^{-1}$) and carrier density ($1013\ cm^{-2}$) [89, 99] are highly desirable for applications such as optoelectronic devices [87], energy storage [89], sensors [90], EMI shielding [91] and antenna designs [6, 7, 93]. The last two listed application domains usually require substantial areas of conducting materials, and thus replacing metals by environmentally friendly and low cost non-metallic conductors would be highly appealing to industries. It is then conceivable that the use of conductive 2D carbon allotropes in antenna design would revolutionize high-volume applications such as wireless consumer electronics and RFID, provided the performance is maintained. Nevertheless, utilizing graphene as a conductor for antennas in the microwave region is still challenging and underexplored. This is because firstly its mono-atomic structure leads to a very high surface resistance and consequently high ohmic losses [39, 40], and secondly because controlling the graphene sheet size and shape is difficult and places limitations in terms of the required accurate device realization. In this context, it is expected that multilayer graphene films with a sufficiently large area can be a solution to overcome these two key issues.

Very recently, a few microwave antennas realized in graphene thin films which are based on commercial graphene inks were reported. An RFID dipole antenna for 915-MHz ISM band realized in graphene inks was reported in [6]. The antenna was printed using graphene inks on a thin foam substrate, following the printing process by a rolling compression, which enhanced the conductivity by 5 time to $4.3 \times 10^4\ S/m$. The final graphene laminate had a thickness of $6\ \mu m$ which is only 0.075 times one skin depth, yielding a DC sheet resistance of $3.8\ \Omega/square$. As a result of the limited film thickness, the antenna holds a relatively low efficiency of 50% approximately, estimated based on the measurement results presented in [6]. Another very similar RFID dipole antenna design fabricated based on commercial graphene inks using a doctor-blading technique was reported in [7]. The antenna was realized by evenly spreading graphene inks on the substrate with a mechanical mask where a doctor blade was used to flatten and control the ink thickness. This dried graphene-based film achieved a conductivity of $1.25 \times 10^4\ S/m$ and a thickness of 42 μm, leading to a DC sheet resistance of 1.9 $\Omega/square$. The antenna was measured to have an efficiency of 40% and this modest performance is mainly attributed to that the film thickness is only approximately one third of the skin depth. To improve the antenna efficiency, a graphene film with high conductivity and sufficient thickness is a must.

Therefore, in this chapter, we firstly report a scalable production of highly conductive graphene films made of binder-free and surfactant-free graphene inks via vacuum filtration. Secondly a non-resonant design, namely an UWB antenna, made of the produced graphene film, is designed, fabricated and experimentally characterized, as a typical demonstration of high-efficiency microwave antennas. It is emphasized that the material side of this project is not a contribution to this thesis, and was developed by the co-authors of [51] from the School of Chemical Engineering at the University o Adelaide. The graphene film preparation method is specifically tailored to satisfy the requirements of antenna technology in terms of film conductivity and thickness in the microwave frequency band. The experimentally validated excellent performance of the UWB antenna operating from 3.1 to 10.6 GHz suggests the tangible possibility of replacing existing metal-based antennas, by graphene-based antennas, which can be manufactured in a scalable, environmentally friendly and low-cost process.

4.2 Graphene film preparation and characterization

Numerous methods have been proposed for graphene production, either top-down from mined graphite or bottom-up by direct-templated chemical processing from carbon sources [102, 103]. The liquid-phase exfoliation of graphite in aqueous solution has been demonstrated as the most inexpensive large-scale production method for the exfoliation of single to few-layer graphene in an environmentally friendly process [90,104,105]. However, the direct aqueous exfoliation of graphene from hydrophobic graphite has been considered as extremely difficult or even not feasible. Whereas the use of amphiphilic surfactants to assist mechanical exfoliation leads to some negative effects on the graphene quality and limits its further processing and applications, especially in antenna technology [146]. For example, recently Hu et al. reported a graphene film laminate realized with graphene inks for the implementation of an RFID dipole antenna [6]. In this approach, the graphene inks, even if binder-free, contain dispersants which can be detrimental to the electrical conductivity and consequently can lower the antenna efficiency. Aiming to resolve these problems and produce more conductive graphene films, utilization of graphene oxide (GO) as a surfactant for cost-effective exfoliation of high-quality graphene [90] is adapted in this project.

4.2.1 Pristine graphene preparation

This method is based on the physical absorption (π-π and/or electrostatic interactions) of GO on destacking graphene surface under sonication. Subsequently, the desorption of GO from graphene by high-speed centrifugation leads to a graphene product containing a small amount of GO fragments (less than 5 wt%), which are possibly sandwiched between graphene sheets. The microstructure of graphene products from the initial graphite materials to the final products using our procedure has been investigated using scanning electron microscopy (SEM) and transmission electron microscopy (TeM) as presented in Fig. 4.1. Expanded graphite (EG) consists of intumescent graphite flakes with a worm and accordion-like structure, which results in multilayers of graphene with a typical thickness of 430 nm under direct aqueous exfoliation as shown in Fig. 4.1a and d. In contrast, GO sheets are adsorbed and intercalated between graphene layers when an energy-induced shear force is applied to separate graphene from EG in GO aqueous dispersion as evidenced in the SEM image (Fig. 4.1b). This structure exhibits a castle card conformation of a GO/graphene complex as in the corresponding TeM image (Fig. 4.1e). It is worth mentioning that distinguished graphene and GO in its complex could be observed since GO is easily desorbed and then damaged under electron beam energy radiation, whereas graphene sheets are quite stable. Figure. 4.2a illustrates the TeM image of GO-adsorbed onto graphene surface, this physical interaction however can be easily desorbed under radiation of electrons beam, as seen in Fig. 4.2b and c. Subsequently, the pristine graphene product, containing single to few-layer graphene (FLG), is obtained by the removal of GO from the GO/graphene complex showing a very thin layer with a high level of structural integrity.

As shown in Fig. 4.1c, the lateral size of these graphene sheets range from 5 to 10 mm and tend to fold into overlapped regions. The individual graphene sheet shows a high polycrystallinity and perfect lattice arrangement, which is observed in Fig. 4.1f, where the corresponding selected area electron diffraction pattern (SAED) (shown as inset) indicates a typical six-fold rotational symmetry of six-member carbon rings in the basal

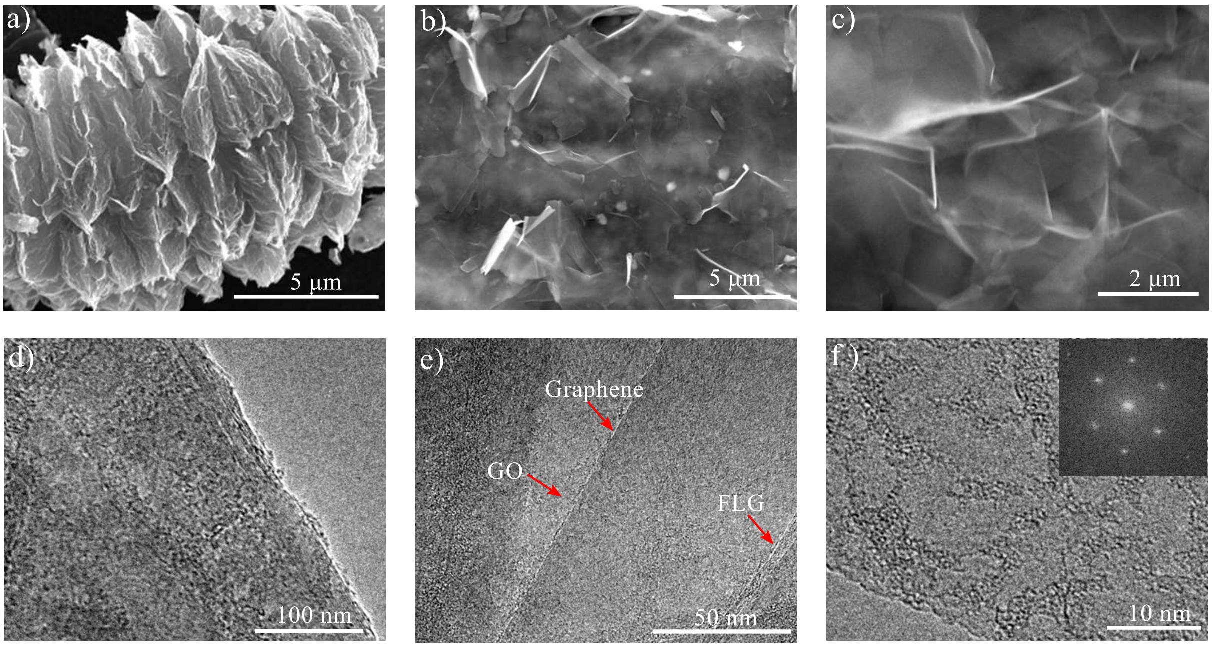

Figure 4.1. SEM and TeM images of the graphene products in process. SEM images of the (a) EG worm-like structure, (b) GO/graphene complex before, and (c) after GO sheet removal followed by thermal annealing, showing pristine graphene sheets. TeM images of (d) partially exfoliated EG revealing multilayered graphene sheets, (e) GO/graphene complex showing both GO adsorbed on the surface and/or sandwiched between graphene platelets, and (f) polycrystallinity of the monolayer graphene sheets.

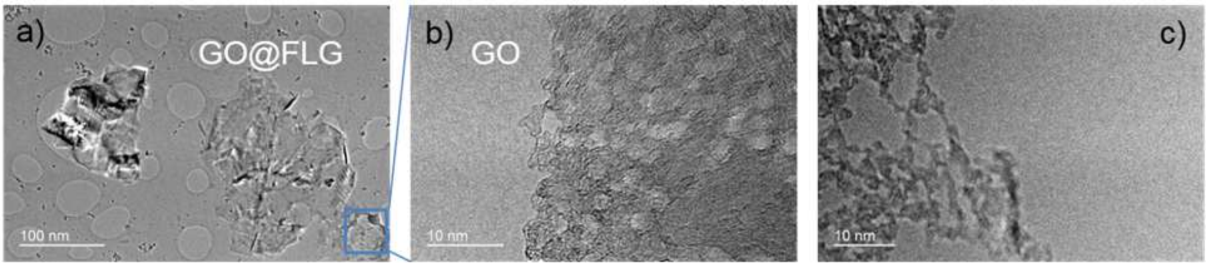

Figure 4.2. TeM images of GO-FLG complex. TeM images of (a) GO-FLG complex, (b and c) desorbed GO under radiation of electrons beam

plane. Furthermore, the number of graphene layers was confirmed by using atomic force microscopy (AFM). As depicted in Fig. 4.3, the average thickness of the graphene sheets is approximately 2 nm. This is a characteristic of a solvent-assisted exfoliation method, in which graphene production contains different configurations (from single to few-layer graphene), and is consistent with the Raman analysis results.

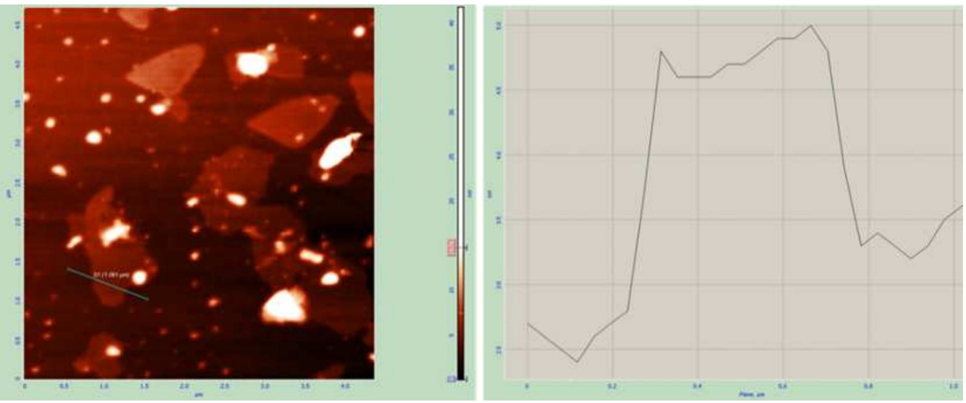

Figure 4.3. AFM image of the graphene product. AFM image of graphene production with average thickness of 2 nm

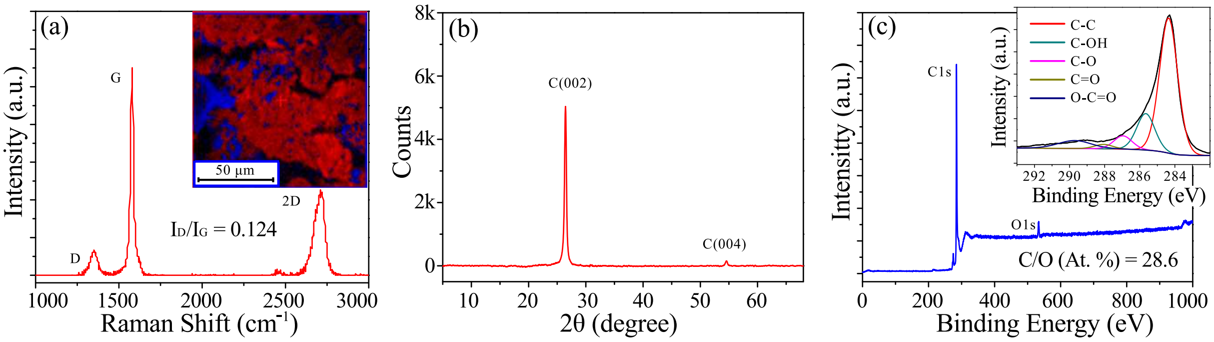

Figure 4.4. Spectra of the graphene product. Spectra of the graphene product: (a) Raman and its mapping image (inset), (b) XRD and (c) survey XPS and C1s (inset).

The prepared graphene product quality has been further characterized by Raman, X-ray diffraction (XRD) and X-ray photoelectron spectroscopy (XPS). The Raman spectrum of the graphene film shown in Fig. 4.4a indicates three typical graphene bands: D-band (1350 cm^{-1}), G-band (1580 cm^{-1}) and 2D-band (2688 cm^{-1}). The 2D peak position is shifted noticeably (24 cm^{-1}), and its intensity curve is more symmetric and higher than that of the precursor graphite, suggesting a graphene product with less than 6 layers [91]. The obtained I_D/I_G value of around 0.12 is slightly higher than the graphite one ($\approx$ 0.09) indicating low defects in this graphene. As shown in Fig. 4.4b, the XRD diffraction pattern demonstrates a high crystalline degree with characteristics of the (002) and (004) reflection of graphite originated from the interlayer distance between the sheets. The intensity of these peaks are four times decreased as compared to the values for their precursor due to structural disorder and/or high efficiency graphite exfoliation [104]. The XPS was used to study the nature and concentration of oxygen present in the graphene product. Based on the XPS survey spectra displayed in Fig. 4.4c, the composition of graphene is defined as C and O, and the atomic ratio between them was estimated as C/O (at%) = 28.6. This value is much higher than reduced GO ($C/O \sim 8$–14) [147,148] and closer to graphite ($C/O \sim 26$–33) [105]. This suggests that the present purified graphene contains less oxygen, high sp^2 carbon bonds and has a high graphitic structure level, which are crucially important for achieving high electrical conductivity. The C1s spectra is shown in the inset of Fig. 4.4c where a considerable degree of oxidation with five components that correspond to carbon atoms is observed.

4.2.2 Graphene film preparation

The successful preparation of high quality pristine graphene with low defects is the first and a very critical step for the realization of high-performing antennas. The modest performance of existing graphene-based antennas is mainly due to the use of unpurified graphene and the limited graphene film thickness. These two problems are both solved in this work.

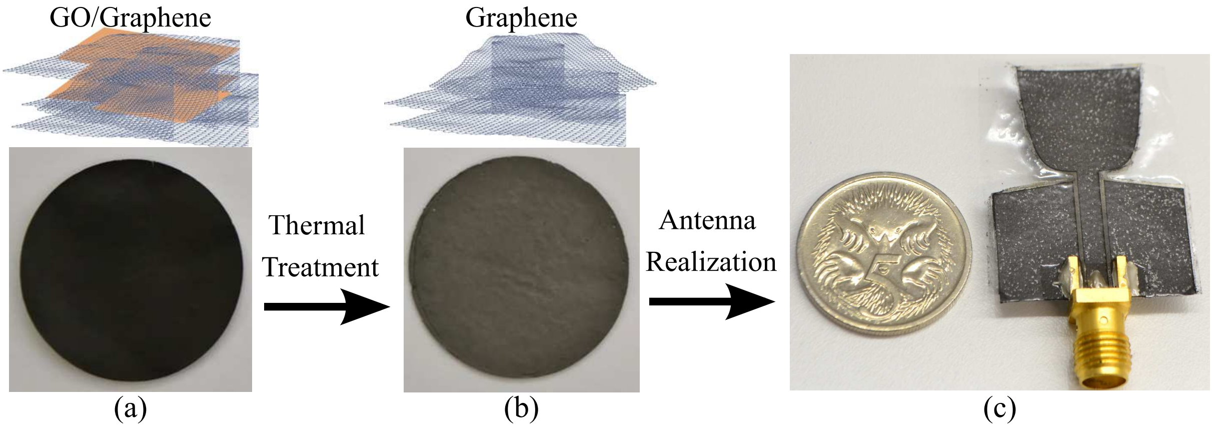

Figure 4.5. Graphene film preparation process. (a) Graphene film prepared by filtering a GO-mediated aqueous dispersion of graphene inks. (b) Purified graphene film after thermal treatment at 900 1C for 1 h under an Ar atmosphere. (c) The graphene-based UWB antenna design.

A three-step procedure is applied for the preparation of the proposed graphene film towards antenna realization as presented in Fig. 4.5. First step, the graphene film is made of the graphene ink by vacuum filtration. This is unlike the commercial graphene inks, in which the graphene flakes are separated by a binder or stabilized by a dispersant leading to better stacking but lower electrical conductivity. In contrast, the present graphene ink is binder-free and dispersant-free. However, the residual GO sheets not only serve as the dispersant for dispersing graphene but also act as glue for graphene platelet linkage, which makes the graphene film robust with better stacking via pressure driven graphene assembly.

We performed another step to improve the graphene film conductivity using thermal annealing at 900°C under a protective environment. This step is introduced for two reasons: (i) to transform interconnected residual GO into reduced GO for reducing the presence of inter-flake tunneling barriers, and (ii) to improve the graphitization level of the graphene film. As a result, the produced graphene film is suitable for microwave antenna designs, as it exhibits a very high conductivity of $3.3 \times 10^4\ S/m$ and a thickness of 100 μm, which leads to a very low DC sheet resistance of around $0.3\ \Omega/square$. The obtained film thickness is around twice to three times the corresponding skin depth δ_s from 3 GHz ($\delta_s = 50.6\ \mu$m) to 10 GHz ($\delta_s = 27.7\ \mu$m), as typically required for efficient antenna operation.

To confirm the thickness of graphene film is sufficient for our antenna design, an investigation based on CST is performed. The simulation results are shown in Fig. 4.6 where antenna radiation efficiencies are plotted against the corresponding graphene thin film thickness at 3.1, 6 and 10.6 GHz. As the graphene thin film thickness increases from 4 to 130 μm, the antenna radiation efficiency rises with a decreasing gradient. This means that it increases rapidly at the beginning, reaches its maximum around 100 μm and stays nearly unchanged afterwards. Therefore, the simulation results suggest that a sufficient graphene thin film thickness is very critical for achieving satisfactory antenna efficiency, and that our film has an optimal thickness.

One aspect worth mentioning is in relation with the CST model for these graphene films, which is very critical to attain accurate antenna efficiency simulation results. Due to the skin effect and the surface roughness of the graphene materials, the sheet resistance increases with higher frequency. The images showing thickness and surface roughness of the graphene film are plotted in Fig. 4.7, where the averaged surface roughness is estimated to be 10 μm. As the frequency increases, firstly, the AC currents will be confined in a thinner layer of the graphene materials (skin effect), the effective material thickness will decrease leading to a higher sheet resistance; and secondly, the graphene surface roughness becomes comparable to the wavelength which will increase the sheet resistance as well. Therefore, a tabulated surface impedance as a function of frequency considering these two main factors was generated using the built-in Macro in CST, which was used as the graphene thin film material model in our

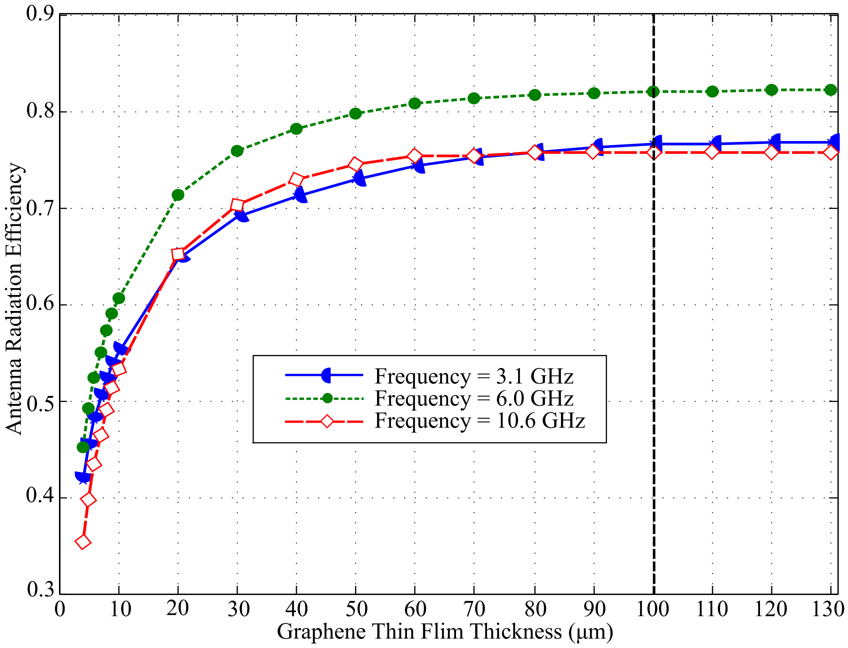

Figure 4.6. Simulated radiation efficiency versus film thickness. Simulated antenna radiation efficiency versus different film thickness.

simulation. The general agreement of simulations with measured data confirms that the dispersion of resistance is not dramatic in the frequency range we studied.

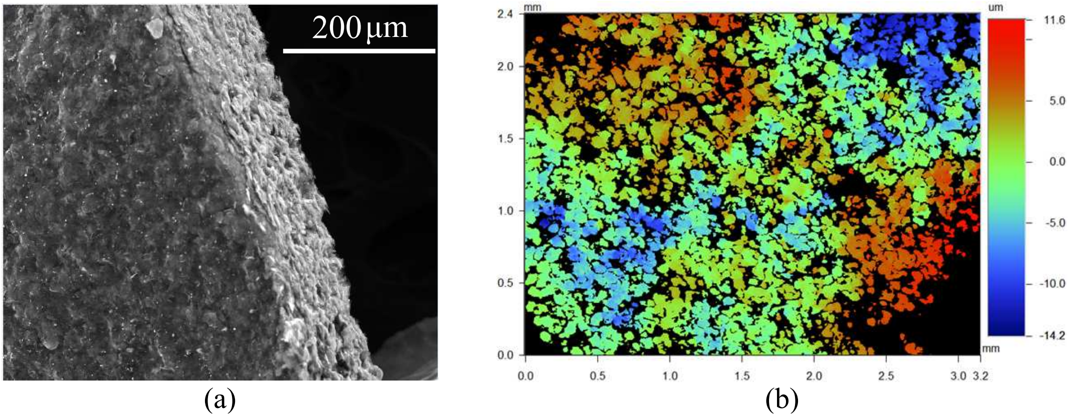

(a) (b)

Figure 4.7. Graphene film thickness and surface roughness. Graphene film (a) thickness and (b) surface roughness.

4.3 Graphene antenna design

UWB technology is very promising for wireless communication systems, since its wide frequency band signals offer high data rate while a very low power level is needed when compared with conventional narrowband technologies. Therefore, as a critical component of the technology, UWB antenna designs have been receiving considerable attention [133, 149, 150]. In this work, an UWB antenna based on the graphene film, with operational frequency from 3.1 to 10.6 GHz, is designed and experimentally characterized. More importantly, this non-resonant antenna design is expected to have a higher efficiency compared to resonant designs as it does not operate based on resonance, as discussed in Chapter 3. This efficiency-driven strategy in antenna design is a crucial step for achieving high antenna efficiency.

4.3.1 Antenna configuration

The graphene antenna is designed and optimized based on CST. The configuration and a prototype realization of the antenna are shown in Fig. 4.8 whereas the dimensions are listed in Table 4.1. This UWB antenna has one layer conductor and one layer dielectric substrate as mechanical support. The conductor layer consists of two main parts, namely an exponentially tapered patch as a typical UWB monopole and a coplanar waveguide (CPW) as feeding structure. These two components operate together as a radiator with a predominately vertical linear polarization. The broadband antenna performance is achieved through the smooth antenna intrinsic impedance transition from the feed to free space, which is formed by the two exponentially tapered edges and the two slanted top CPW edges. The CPW center conductor width W_3 and its slot width W_5 are two key parameters in the antenna design, since they dictate the CPW characteristic impedance which influences the antenna matching. The later parameter W_5 is more relevant in this case, because a small W_5 can lead to a strong induced current density along the CPW slot which will result in high ohmic losses and thus a low antenna efficiency. A detailed analysis can be found in Section 3.2.2. Therefore an optimal W_5 was obtained through parametric sweeps in CST to attain the achievable maximum antenna efficiency while maintaining a satisfactory antenna matching.

4.3.2 Antenna fabrication

In order to achieve accurate patterning, a laser milling machine was used. A transparent substrate based on adhesive tape was used, since it is unaffected by the laser beam and thus can be kept intact during milling. Moreover, it provides robust mechanical support and physical isolation for the antenna. The 100-μm-thick adhesive tape has a relative permittivity of $\varepsilon = 3$ and loss tangent $tan\delta = 0.01$ both estimated based on fitted

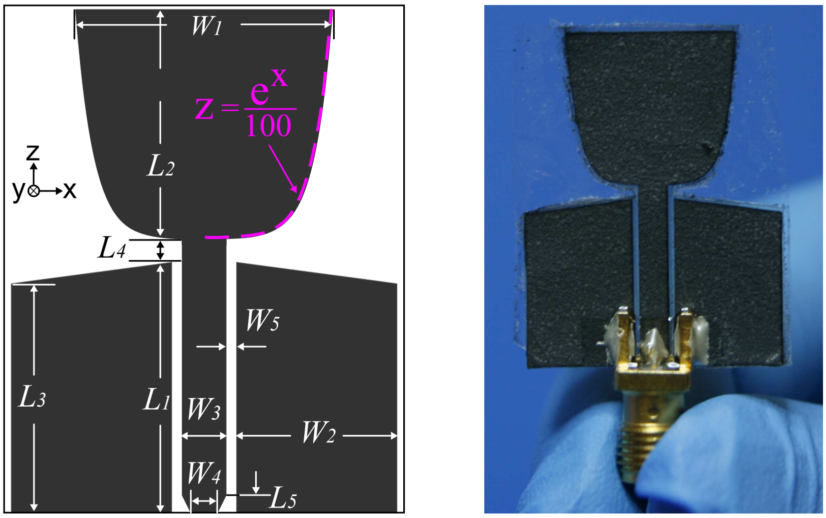

(a) (b)

Figure 4.8. Graphene UWB antenna geometry and realization. (a) Graphene antenna configuration and (b) a prototype realization.

Table 4.1. Graphene UWB antenna dimensions. Dimensions of the proposed antenna in (mm)

$L1$	$L2$	$L3$	$L4$	$L5$	$W1$	$W2$	$W3$	$W4$	$W5$
14.0	13.8	12.8	1.2	1.0	14.3	9.0	2.5	2.0	0.5

values in simulation. Firstly, the graphene film was attached to a piece of adhesive tape, and placed into the laser milling machine, then the laser cutting beam was swept on the film with a programmed path by which all redundant graphene film was vaporized to define the geometry of the antenna. Secondly, the antenna was adhered to another piece of adhesive tape, which has a rectangular notch trimmed at the bottom of the CPW to leave space for electrical connection of an SMA connector. Thirdly, conductive epoxy (Circuit works CW2400) was applied between the SMA connector and the antenna CPW to realize an excellent electrical connection. Finally, a very thin layer of nonconductive epoxy was coated on top of the conductive silver pain to provide a secure mechanical bond.

4.4 Experimental results

The fabricated antenna has been experimentally characterized to validate the graphene film and the design. An identical antenna made of copper has also been manufactured for direct comparison and evaluation of the antenna efficiency. As shown in Fig. 4.9,

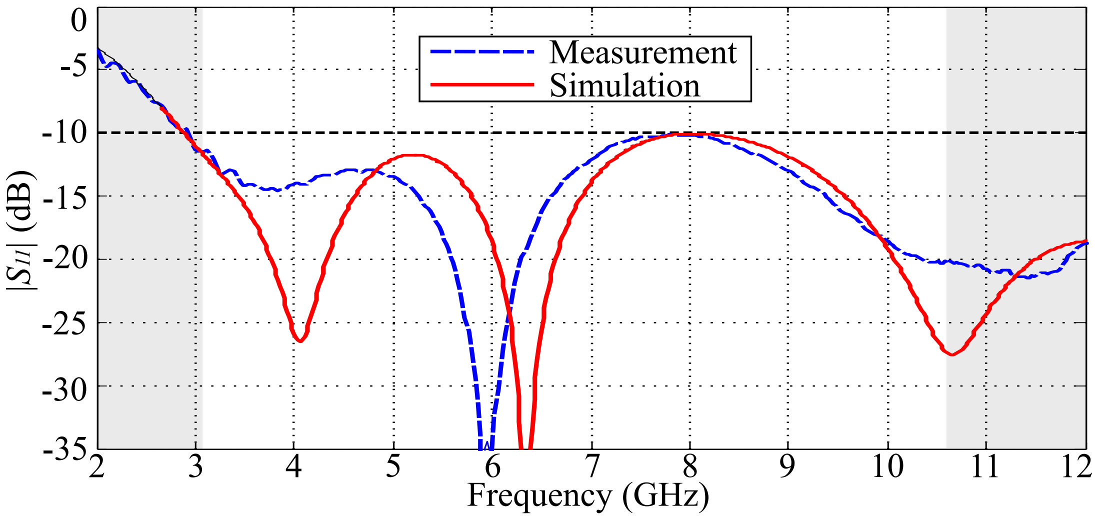

Figure 4.9. Graphene UWB antenna simulated and measured S_{11}. Simulated and measured reflection coefficients $|S_{11}|$, with the operation frequency from 3.1 to 10.6 GHz highlighted in white.

the simulated and measured reflection coefficients $|S_{11}|$ have a good agreement where a satisfactory matching ($|S_{11}| <$ -10 dB) is observed between 3.1 to 10.6 GHz.

The measured radiation pattens at 5 and 10 GHz in the xy-, xz- and yz-planes are depicted in Fig. 4.10, normalized to the maximum gain of the reference copper antenna. The radiation patterns demonstrate UWB dipole-like antenna characteristics as expected: (i) a nearly omnidirectional pattern in the xy-plane and (ii) zeros in the z-axis direction in the xz- and yz-planes. More importantly, the similarity in both antenna patterns implies that the graphene antenna has a very high conduction efficiency since it is very close to that of the reference copper antenna, as confirmed through dedicated experimental data in the following.

The antenna radiation efficiency e_{cd} is one of the most important parameters since it provides indication of the power losses due to the antenna materials. It includes conduction efficiency e_c and dielectric efficiency e_d, namely $e_{cd} = e_c e_d$. As the dielectric materials used in our graphene and copper antennas are very thin and low-loss, the dielectric efficiency e_d can be assumed to be very close to 100%. In contrast, the conduction efficiency is more significant and of primary interest in our study, since losses due to the lower conductivity of the graphene film compared to metallic materials will be the main source of performance degradation. The antenna radiation efficiency can be measured directly with the Wheeler cap method [134] which is based on the antenna reflection coefficient measurement in free space and in a rectangular closed

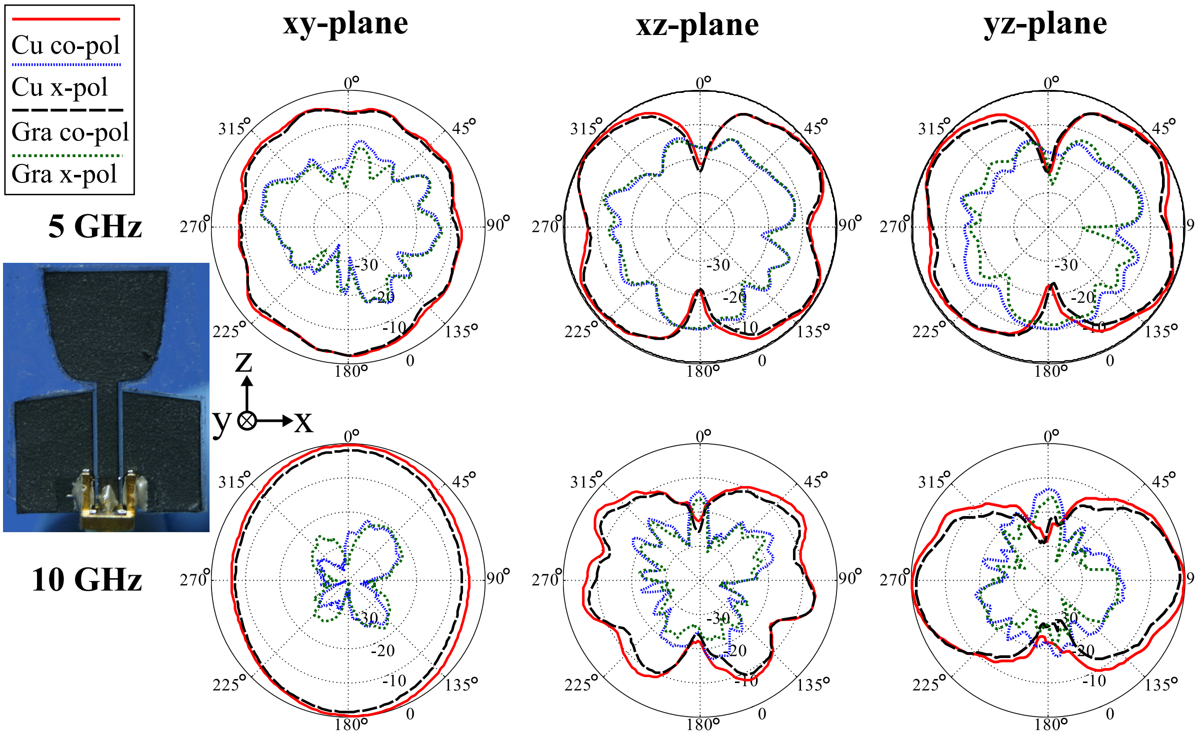

Figure 4.10. Graphene UWB antenna measured radiation patterns. Measured co- and cross-polarized radiation patterns for the graphene (Gra) and reference copper (Cu) antennas in the xy-, xz- and yz-planes at 5 and 10 GHz, normalized to the maximum gain of the copper antenna.

metallic cavity, as shown in Fig 4.11. For the details of this method, one can refer to Section 3.2.4.

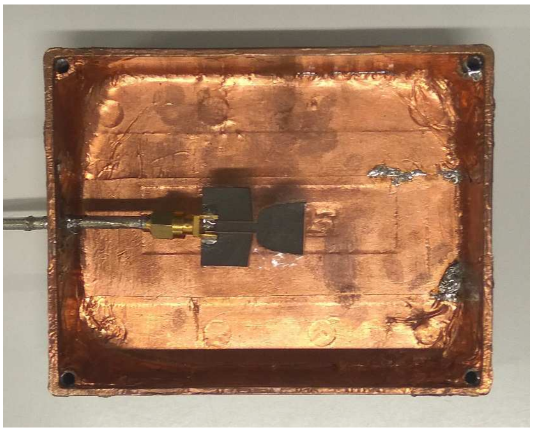

Figure 4.11. Wheeler cap measurement configuration. An antenna prototype under test in the metallic box for Wheeler cap measurement, with the box lid opened.

In parallel, the conduction efficiency was estimated based on a direct gain-directivity comparison between the graphene antenna and copper reference [4, 5]. This method assumes that the copper antenna has a nearly 100% conduction efficiency, and that both antennas possess identical directivity which is confirmed by their very similar radiation patterns. This measurement method for the efficiency has also been introduced previously in Section 3.2.4. As shown in Fig 4.12, a good agreement between the simulated and measured radiation efficiency is observed. The simulation and measurement results show efficiencies ranging from 65 to 96% and from 74 to 86% respectively. The averaged simulated and measured values are 76 and 77%, respectively. The conduction efficiency measurement results are within the range between 67 and 87%, with an averaged value of 79%. The consistency of these results is a definite indicator that the graphene antenna has a very satisfactory efficiency based on non-metallic conductors.

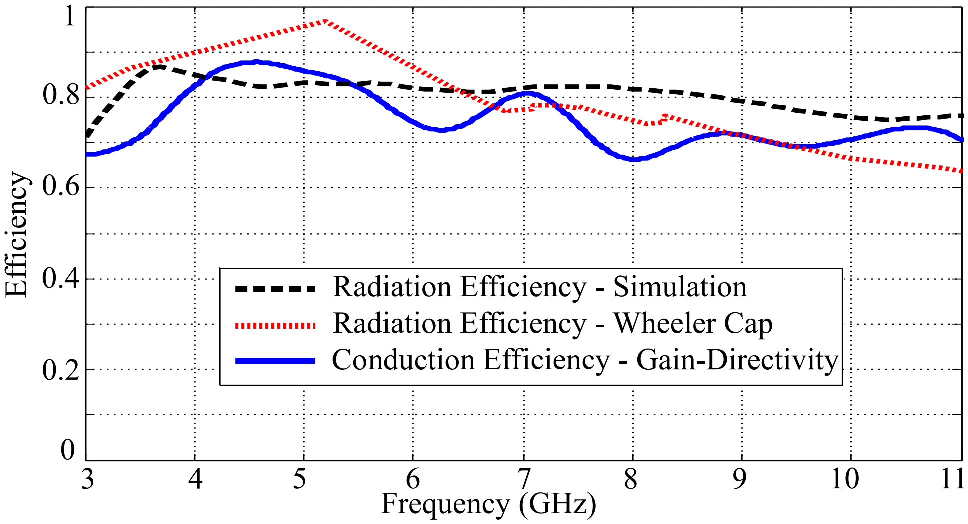

Figure 4.12. Graphene UWB antenna simulated and measured efficiencies. Simulated and measured radiation and conductor efficiency.

4.5 Conclusion

In conclusion, an UWB microwave antenna based on highly conductive graphene films has been demonstrated. The graphene films were fabricated through vacuum filtration of binder-free and surfactant-free graphene inks and a thermal treatment. The high electrical conductivity of $3.3 \times 10^4\ S/m$ with a substantial thickness of 100 μm makes these films suitable conductors for designing highly efficient microwave antennas. The simulation and measurement results indicate that the UWB antenna operates as expected, and more importantly, has a very satisfactory antenna efficiency of nearly 80% over the operation band. This is due to the high quality of the graphene films as well as the efficiency-driven antenna design strategy and accurate fabrication technology.

These measured antenna efficiencies are, to the best of our knowledge, the highest reported values for antennas in the microwave region based on graphene films, and even surpass realizations with silver nanowires [151]. The presented results suggest that the proposed graphene films are very promising as environmentally-friendly, inexpensive and efficient non-metallic conductors for high-volume applications in the microwave region.

Chapter 5

Shorting and Connection Strategies for Wearable Textile Antennas

---

WEARABLE antennas are essential components of any wearable wireless communication systems. Besides conventional antenna requirements, these antennas should be mechanically flexible, lightweight, low-cost, and garment-integratable. Since conductive textiles possess outstanding properties such as superior mechanical conformability and resilience, comfortable wearability and excellent bio-compatibility, they are increasingly utilized as conductors for wearable antennas. Nevertheless, challenges in feeding, ground shorting and interconnecting textile antennas with electronics is very challenging, due to the different mechanical properties of textiles compared to conventional rigid antenna materials.

This chapter focuses on shorting and connection strategies for wearable textile antennas based on textile-compatible components including textiles strips, embroidery vias, metallic eyelets and commercial snap-on buttons. The investigation includes considerations on system and antenna performance as well as realization complexity and cost.

5.1 Introduction

A dramatic growth in wearable antenna technology has been witnessed in the last couple of decades. One can expect that this technology is going to be an essential part of our daily life, since smart textiles or smart garments are anticipated to be integral part of the next generation of daily dress. Generally speaking, textile materials including conductive or non-conductive are inherently one of the best suited 'ingredients' for wearable antenna technology, as they offer outstanding mechanical flexibility and resilience, highly comfortable wearability and excellent bio-compatibility [112]. Textile-based antennas will lead to many new scientific and engineering challenges not only in antenna design but also in system integration, owing to the very unique characteristics of conducting fabrics compared to the conventional antenna materials like bulk metals or metallized substrates. This chapter has two major parts which investigate practical aspects of textile antennas technology: the first one mainly focuses on shorting strategies while the second one discusses connection methods for textile antennas.

The first part of this chapter will consider convenient, stable and low-loss shorting vias or shorting wall realizations for textile antennas. Efficient shorting components are essential building blocks of many well-developed antenna types such as patch, PIFA and cavity-based antennas. In the case of wearable realizations of such antennas, textile-compatible materials and components are needed to practically realize shorts or conductive walls. To this end, and conductive textiles, embroidery vias and metallic eyelets are three possible components as discussed in Chapter 2. Firstly, realizing a conducting wall using part of the conductive textile itself is a perfect choice if the specific antenna design permits. For instance in [124], a short was accommodated outside of the substrate for a PIFA textile antenna. Therefore, it was possible to fold a single piece of copper polyester taffeta fabric to include the short together with the patch and the ground plane. This arrangement leads to a convenient integration of a shorting wall, by avoiding additional interconnections involving conductive glues or epoxy. Secondly, realizing shorting vias through embroidery using conductive yarns has become a popular technology owing to its ease of implementation. As a typical illustration, a HMSIW-based textile antennas with a shorting wall fabricated based on embroidered vias was reported in 2013 [21], where a precise and easy arrangement of the shorting wall was achieved using computerized embroidery with conductive threads. The last shorting method makes use of metallic eyelets, as one traditional class of connectors employed in the cloth industry since more than hundred years. A textile cavity-backed slot antenna [20] and a textile HMSIW-based antenna [22] were reported using metallic eyelets to realize the shorting wall. This technology is mature and able to provide metallic electrical connection however with higher manufacturing cost and less wearing comfort. In the first part of this chapter, an L-slot PIFA with a short realized using a folded textile strip, embroidered vias and a metallic eyelet is selected as a test bed for simulations to systematically compare the performance of these shorting strategies.

The second part of the chapter will be dedicated to the connection between textile antennas and the electronics. This is usually not straightforward and requires dedicated engineering, owing to the very different physical properties of textiles and electronic components. Soldering is the main connection technique for electronics, however, it not compatible with textile materials because of the high temperature requirement. As a result, connection technology compatible with both textiles and electronics is highly desired. In addition, special connection features such as detachability, can be a significant advantage for wearable systems that have garment-integrated antennas. For example, two garment-integrated textile patch antennas were reported in [14,125], where a detachable connection between the antenna and the electronics can be very beneficial. This is because a detachable connection can enable washing of a garment, with the electronic parts disconnected, or maintenance of a wearable system through replacement of the electronic parts and/or electronics interchanging. In order to achieve this aim, a reliable, inexpensive and detachable connection based on a pair of commercial snap-on buttons is proposed for balanced textile antennas and transmission lines. This connection concept exhibits satisfactory performance, as validated in an RFID-based elderly monitoring system, as covered by the second part of this chapter.

5.2 Wearable textile antenna shorting strategies

Planar antenna structures such as microstrip patch antennas [10, 31, 120, 122, 123], and planar inverted-F antennas (PIFAs) [124,152] are widely used in wearable applications, due to their compactness, low profile and limited backward radiation towards the human body. Therefore, a representative design of a wearable multi-band silver-fabric-based L-slot PIFA is chosen as a test bed for the aforementioned shorting strategies - textiles strips, embroidery vias and metallic eyelets. The performance of the proposed antenna with these three shorting methods is compared through simulations with realistic shorting models. According to the obtained numerical results, the antenna has three resonances at 4.5 GHz, 5.0 GHz and 6.6 GHz. In terms of gain and efficiency, the embroidered vias shorting method, which is the simplest and cheapest method to implement, has slightly lower performance than the silver fabric folded strip and eyelet shorting methods due to its higher resistance. The last two methods can offer a very low-loss shorting however with higher manufacturing cost and complexity. All the details are discussed as the following.

5.2.1 L-slot PIFA antenna

The antenna structure is shown in Fig. 5.1 and Table 5.1 lists the corresponding dimensions. To achieve a low profile and wearable design with triple-band operation, an L-slot PIFA is adopted here since similar design principles have been proved to have multi-band performance [153]. In order to fulfil the wearability requirements without compromising the performance of the antenna, a biocompatible silver-coated nylon RIPSTOP fabric has been selected for the realization of the top patch and ground plane. This conducting fabric has a low sheet resistance of 0.01 $\Omega/square$ which is comparable to good metallic conductors. For the substrate, a thin and highly flexible Cuming Microwave C-Foam PF-4 foam with a thickness of 2.4 mm has been chosen because of its water resistance and low loss ($tan\delta$ = 0.0001). However, due to the low relative permittivity ε_r = 1.06, wearable antenna designs based on this structure are generally larger than circuit board counterparts. Hence shorting methods, as used in PIFA configurations to make these structures more compact, become more significant.

A 50 Ω SMA probe feed is employed for the purpose of testing. Figure 5.2 presents the electric field distribution and 3D radiation pattern at three resonances of the antenna with folded strip shorting wall. It is shown that at the lowest resonance, the antenna mainly radiates through the L-slot. At the middle resonance, it mainly radiates through the fundamental cavity mode from the whole patch but with 45 degree rotation. For the highest frequency resonance, the antenna radiates via a higher order mode of the structure. The radiation patterns at all three resonance frequencies are showing a relatively wide broadside beam, whereas the ground plane provides isolation towards the back where usually the human body is present. The lowest resonance is sensitive to L_1 and W_1 while the middle and the high resonances are more sensitive to L_2 and W_2 due to their radiation mechanism. The antenna has been designed using CST and these principles should be applicable for similar L-shaped slot PIFA designs.

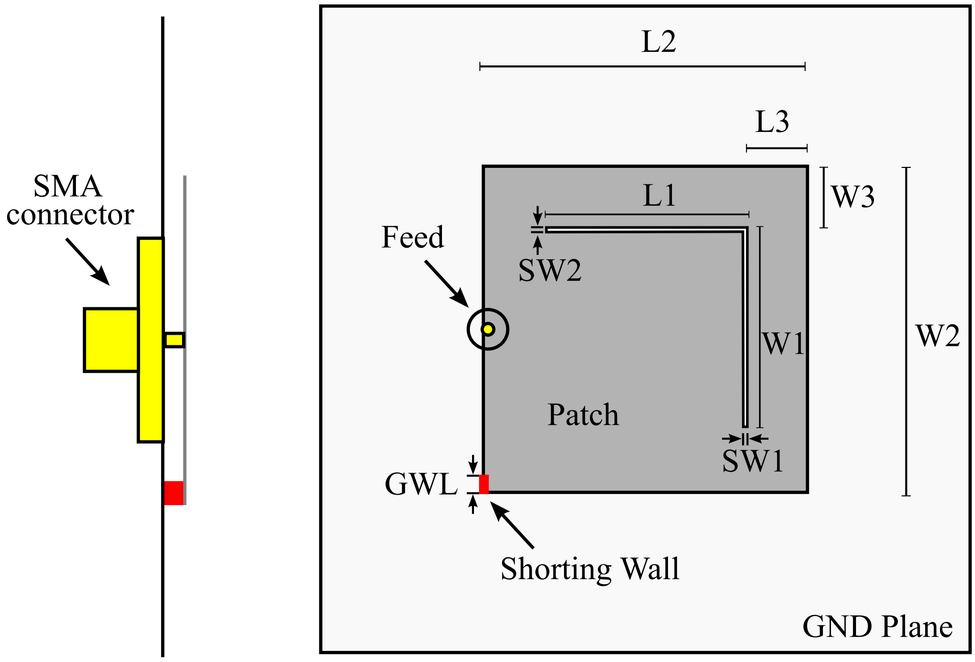

Figure 5.1. L-slot PIFA antenna configuration. Layout of the L-slot PIFA antenna with indication of its design parameters.

Table 5.1. L-slot antenna dimensions. Dimensions of the proposed antenna in (mm)

L_1	L_2	L_3	SW_1	SW_2	W_1	W_2	W_3	GWL
15.0	25.0	4.7	0.3	0.3	15.0	25.0	4.7	1.4

5.2.2 Shorting strategies

The shorting methods for wearable antenna technology should be based on the following practical considerations:

- Easy access to the necessary materials and low cost.
- Easy and inexpensive manufacture methods.
- Acceptable antenna performance.

The three previously mentioned shorting strategies, namely folded textile strip, embroidered vias and a metallic eyelet, are chosen for this antenna design as they fulfill the above criteria. The details are discussed as follows.

1. **Shorting with silver fabric**: The resonant patch and the ground plane can be connected with a thin folded strip of silver fabric [124]. Due to the high conductor

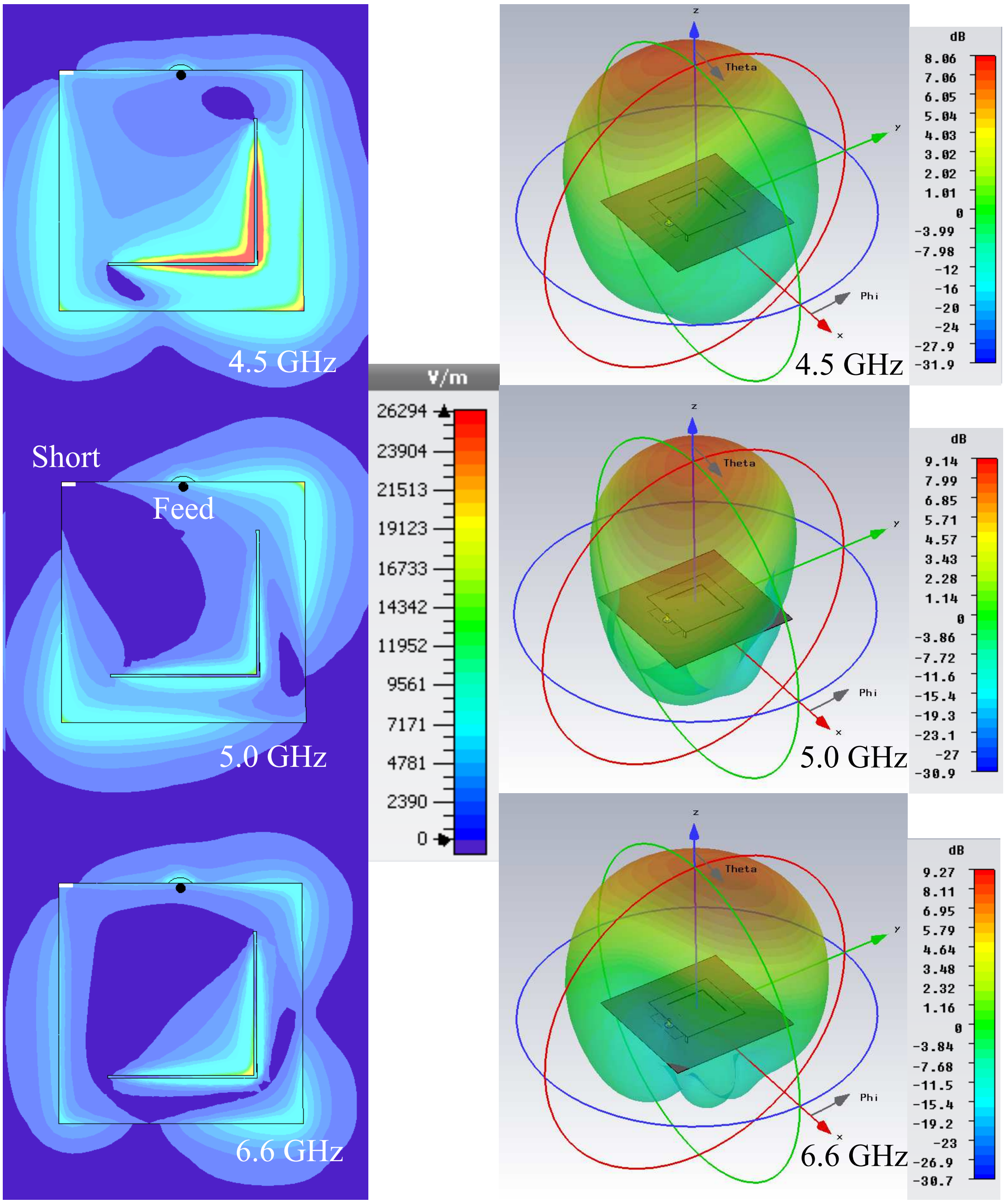

Figure 5.2. E-field distribution and radiation patterns of the proposed antenna. Simulated lectric field distribution and 3D radiation pattern with folded strip shorting wall obtained from CST. The electric field distributions are on the left while the 3D distributions are on the right.

efficiency in this shorting method, a good antenna performance can be expected. The main advantage of this method is indeed that a near-perfect connection between the patch and ground can be formed. The main disadvantage however is that the manufacture method is rather cumbersome, as the ground plane cannot be realized as a single fabric piece. For instance, one possible implementation method is cutting the shorting strip and the top patch as a single piece and then electrically connecting the shorting strip to the ground plane using conductive epoxy or conductive threads.

2. **Shorting with embroidered vias**: A conductive wall can be embroidered with a computerized embroidery machine using silver-coated yarns. The clear advantages of this method for the design at hand are ease and speed of manufacture. However, due to the limited conductivity of the conductive yarn, lower antenna efficiencies can be expected. This technique has been previously employed for a wearable half-mode substrate integrated antenna and resulted in high efficiency [21].

3. **Shorting with eyelets**: Eyelets made from copper can be manually attached to the two fabric layers to create the desired short, similarly to rivets used in PCB manufacture to create vias. This eyelet shorting method has been used in the past in [20]. The required manual labor increases the manufacture cost, but with the added benefit of high efficiency.

The shorting wall configurations for the proposed methods are shown in Fig. 5.3. As a reference, a shorting wall made of Perfect Electrical Conductor (PEC) is included in the study. The top illustration represents the configuration for the folded strip made of silver fabric. The same configuration is used as reference by replacing the strip by PEC. The middle image illustrates the shorting method using embroidered vias. The shorting arrangement based on a copper eyelet can be seen in the bottom configuration. A sheet resistance of $0.01\ \Omega/square$ has been used for the short realized using the first method, according to the silver fabric datasheet. The embroidered vias have been simulated as an equivalent sheet with a sheet resistance of $10\ \Omega/square$, as successfully modelled in [21] for typical embroidered densities. Copper is used as the material for the eyelet utilized in the third strategy. For reference, PEC is used as the material for the short as the fourth shorting method.

5.2.3 Results and discussion

The reflection coefficient $|S_{11}|$, gain, and efficiency of the PIFA with the proposed three shorting strategies are compared to the PEC shorting method to identify the impact of imperfect shorting on the antenna performance. The comparison of the $|S_{11}|$ parameter is shown in Fig. 5.4. Due to the sensitivity of the resonance to the width of the shorting

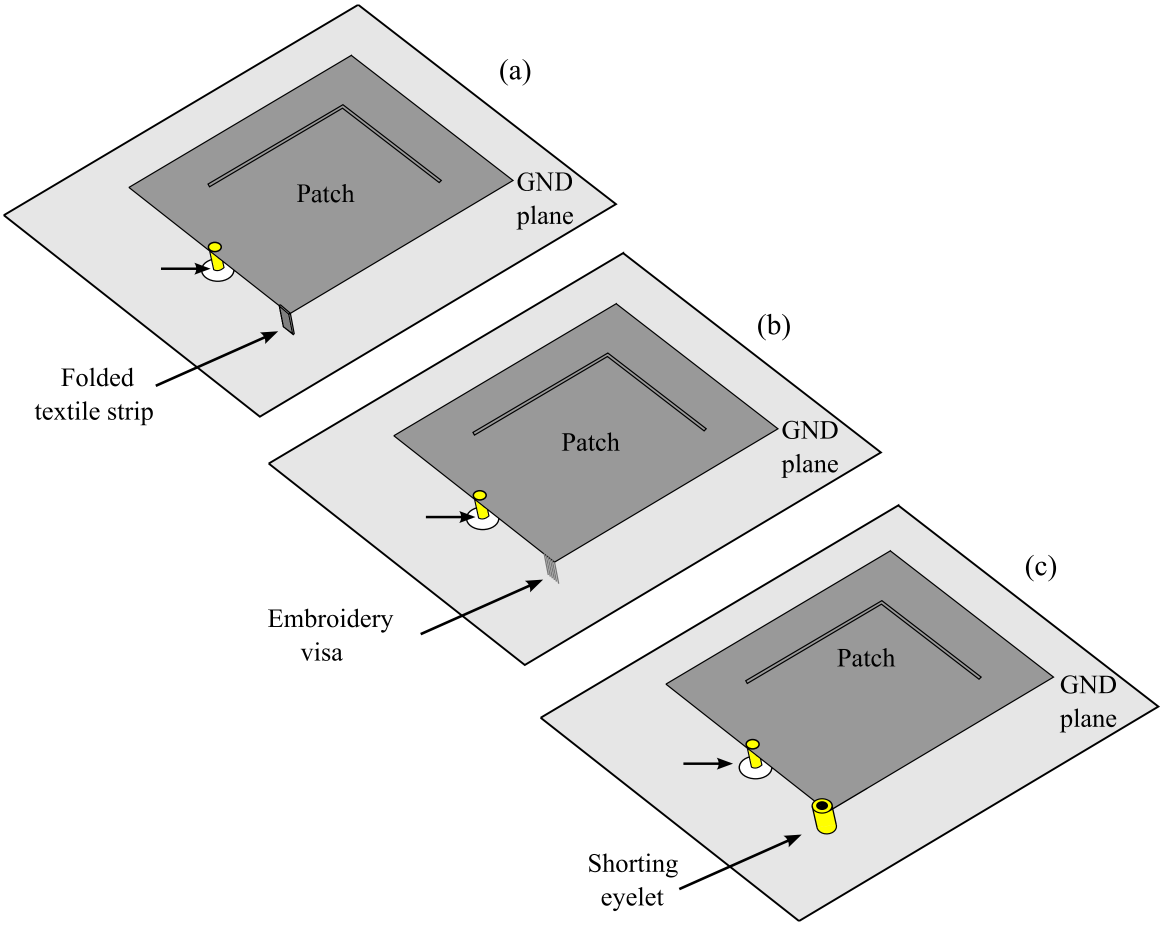

Figure 5.3. Shorting configurations. The configuration in (a) is applied for both shorting walls made out of silver fabric and PEC (reference). The configuration in (b) shows the embroidered vias while the one in (c) is for copper eyelet.

wall in the design, this dimension is chosen to be identical to the eyelet width. As presented in Fig. 5.4, there are no significant differences between the shorting methods at the middle resonance frequency, this is attributed to the very limited current running through the shorting wall. For the lowest and highest frequencies, minor variations can be observed between the curves obtained with different shorting methods.

Table 5.2 shows the maximum gain of the proposed antenna obtained with different shorting methods at its three resonances. As a result of the relative high sheet resistance of the embroidered conductive wall, the gain of the antenna with the embroidered walls is around 2.6 dB below the gain with other shorting methods at 4.5 GHz, and 0.6 dB lower at 6.6 GHz. Furthermore, negligible variations in gain at 5 GHz are attributed to the nearly symmetrical radiation along the diagonal of the patch which causes almost zero current running through the shorting wall.

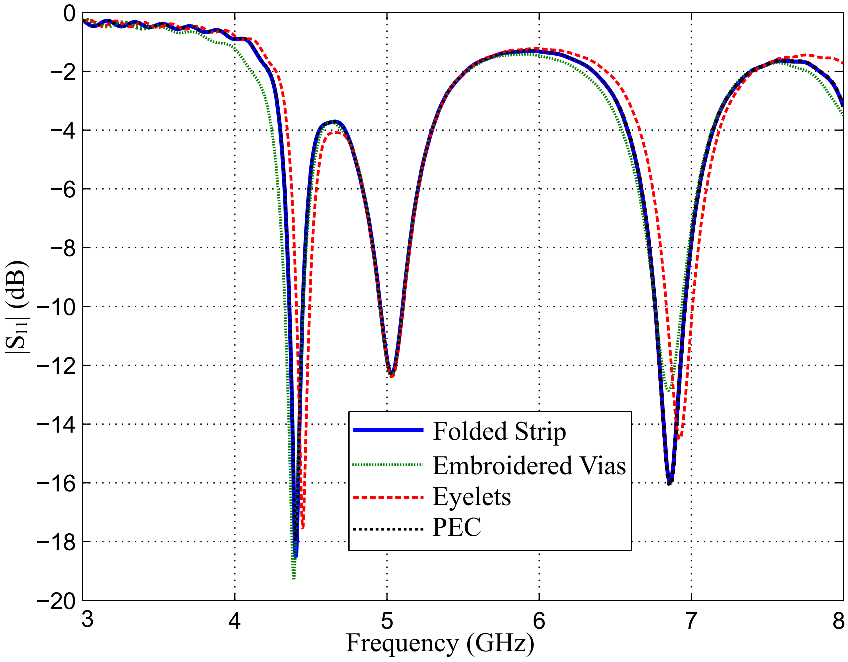

Figure 5.4. Simulated reflection coefficient of the L-slot PIFA antenna. Simulated reflection coefficient $|S_{11}|$ of the proposed L-slot PIFA antenna.

Table 5.2. Antenna gain comparison between shorting strategies. Antenna simulated gain comparison between folded strip, embroidered vias, copper eyelet and PEC.

Resonance Frequency	Antenna Gain (dB)			
	Folded strip	Embroidery vias	Copper eyelet	PEC
4.5 GHz	8.1	5.4	8.0	8.1
5.0 GHz	9.1	9.1	9.1	9.1
6.6 GHz	9.3	8.7	9.1	9.3

Similarly, a comparison of the radiation efficiency between the four shorting methods is presented in Table. 5.3. The results indicate again that the resistance of the shorting section is one of the important factors to be considered during antenna design: the radiation efficiency of the antenna using embroidered vias is around 0.7 and 2.8 dB less than that of the others at 4.5 and 6.6 GHz respectively. This is explained by the relative higher conductor loss in the shorting wall.

5.2.4 Summary

Based on all the simulated results, it has been found that the resonant modes at three operating frequencies of 4.5, 5.0, and 6.6 GHz are affected differently by the shorting

Table 5.3. Antenna radiation efficiency comparison between shorting strategies. Antenna simulated radiation efficiency comparison between folded strip, embroidered vias, copper eyelet and PEC.

Resonance Frequency	Antenna Radiation Efficiency (dB)			
	Folded strip	Embroidery vias	Copper eyelet	PEC
4.5 GHz	-0.3	-3.1	-0.2	-0.3
5.0 GHz	-0.0	-0.1	-0.2	-0.0
6.6 GHz	-0.0	-0.7	-0.2	-0.0

strategies. The fabric folded strip methods and eyelet shorting strategy yield comparable results, with efficiencies higher by 0.6 to 2.6 dB compared to the embroidered vias at the highest and lowest resonance frequencies. These differences are attributed to the relatively high sheet resistance of the embroidered conductive wall. However, in terms of fabrication simplicity, embroidering the vias can be automated and presents the simplest and cheapest method. Performance improvement could be achieved by increasing the conductivity of the conducting yarns, or through use of metallic threads. For the middle frequency, no significant differences are observed between the different shorting methods due to the very limited current running through the shorting wall. This shows that to avoid significant impact on antennas resonances, the positioning for the eyelets shorting should aim for minimal physical disturbance of antenna currents.

5.3 Detachable wearable textile antenna feeding

Generally antennas made from conductive textiles can be garment-integratable and washable thus they can offer convenience and re-usability for wearable applications. The performance of washable antennas such as gain, reflection coefficient and radiation efficiency have been demonstrated in [154, 155], where reliable and acceptable antenna performances have been achieved after several washing cycles. However, the connected electronics are not washable in most scenarios, and therefore low-cost and easy-to-use solutions of detachable connections for garment-integrated antennas are a significant requirement.

A possible solution is utilizing snap-on buttons as detachable RF connectors. Some dedicated snap-on connectors designed for wearable RF applications have been reported in [156]. In contrast to specialized solutions, a cheaper and more convenient

RF connector solution for a 2.4 GHz probe-fed textile patch antenna has been proposed in [126], by taking advantage of commercial snap-on buttons commonly used in clothing. Despite affecting the antenna resonance frequency and return loss, these buttons still exhibit good performance as RF connectors. Further studies investigating the characteristics of these buttons used as RF connectors in coaxial-to-microstrip transitions [157, 158] and for several plaster microstrip antennas [157, 159] have been also reported. The results have demonstrated that the snap-on button is an appropriate connector for applications up to 3 GHz. Additionally, a successful snap-on-button-based transition between a 2.4 GHz planar inverted-F antenna and an electronic circuit board has also been demonstrated [160]. However, all these research works were performed in conjunction with unbalanced antennas and transmission lines.

In the following, the use of a pair of commercial snap-on buttons as detachable RF connectors between a balanced wideband textile dipole antenna and a passive sensor-enabled RFID tag in a wearable elderly activity monitoring system is presented. Antenna measurements and investigations of the system indicate excellent performance of the RF connectors for balanced antennas with operating range from 780 to 1030 MHz. The proposed snap-on button pair connection offers not only a solid mechanical connection and detachability but also shows a minimal impact on RF performance. Moreover, an investigation of the characteristics of the snap-on button coupling arrangement for balanced transmission line transitions demonstrates a stable applicability up to at least 5 GHz.

5.3.1 The wearable electronic system

The considered application is a wearable RFID system with an operating frequency of 923 MHz, aiming at activity monitoring for elderly [32, 161]. It consists of at least one battery-free tag with an antenna, a reader with several antennas and back-end systems. The RFID tag [161] is a passive accelerometer-enabled device with an input impedance of $78 + 16j\ \Omega$, containing a micro-controller unit where a unique identification number is stored. It communicates with a reader through an antenna, where the signal received from the reader is also used as an activating power source. The back-end computer systems collect, analyse and store the data received from the reader and act as a human interface as well. The original tag has a rigid dipole antenna integrated which significantly impairs wearability. In order to improve the system wearabillty and practicality, a textile garment-integrated wideband dipole antenna is introduced as a replacement of the original one. More importantly, snap-on buttons are also introduced as feeding connectors for the textile antenna, which offers reliable detachablility for the tag. The original and the modified configurations of the system are shown in Fig. 5.5. This arrangement with snap-on buttons provides a solution to detach the tag from the textile antenna which can remain integrated with a garment during washing.

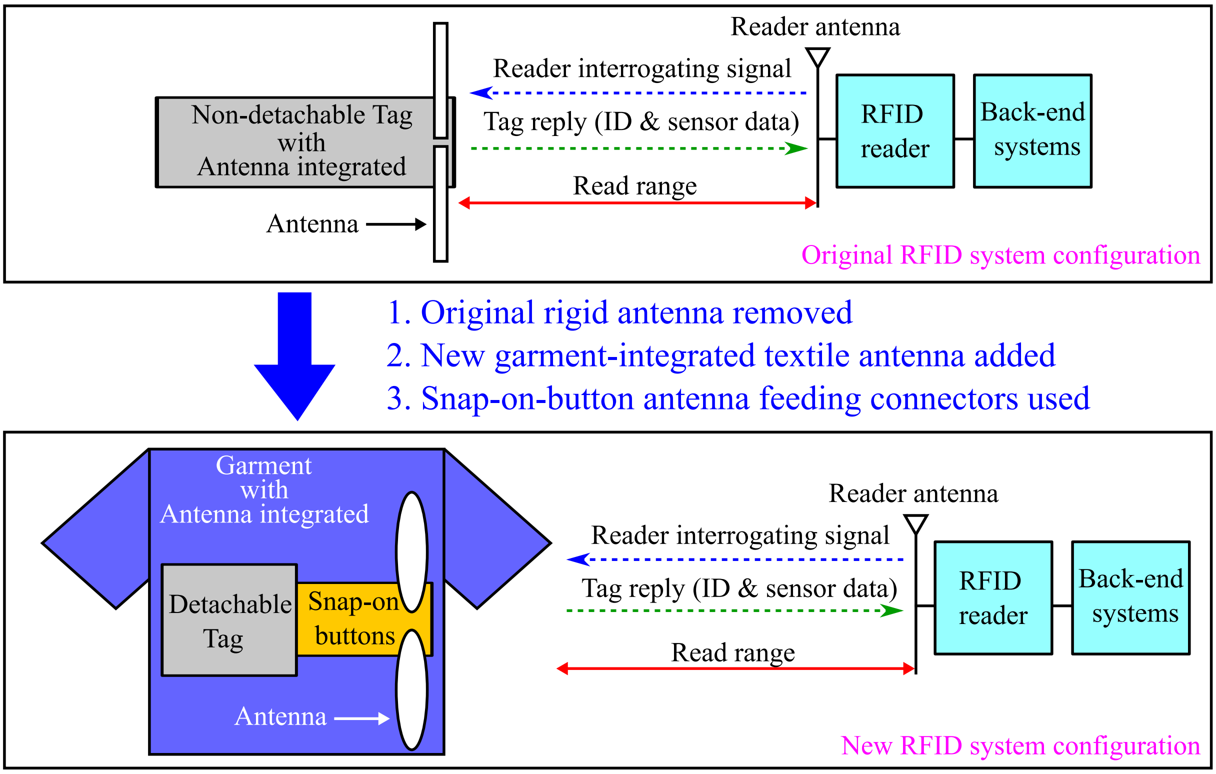

Figure 5.5. The original and the modified RFID system configurations. The original RFID system configuration contains a battery-less tag with a rigid antenna integrated. In the new configuration, a textile garment-integrated antenna replaces the original antenna and a pair of snap-on buttons utilized as connectors is introduced in the antenna feed.

The tag originally comes with a dipole antenna printed on a FR4 substrate [32], as shown in Fig. 5.6. It is noticeable that the original antenna is not appropriate for wearable applications as it is narrowband and not flexible. Thus an alternative wearable wideband antenna has been designed to improve the wearability and robustness to changing electromagnetic environments. The new antenna is a flexible wideband textile dipole antenna with an impedance bandwidth for matching to 78 Ω ($|S_{11}| < -10\,\mathrm{dB}$) ranging from 780 MHz to 1030 MHz. To make the antenna lightweight and flexible, a silver-coated nylon RIPSTOP fabric with a sheet resistance of 0.01 $\Omega/square$ and a thickness of 100 μm has been selected as the conductor. As shown in Fig. 5.6, the

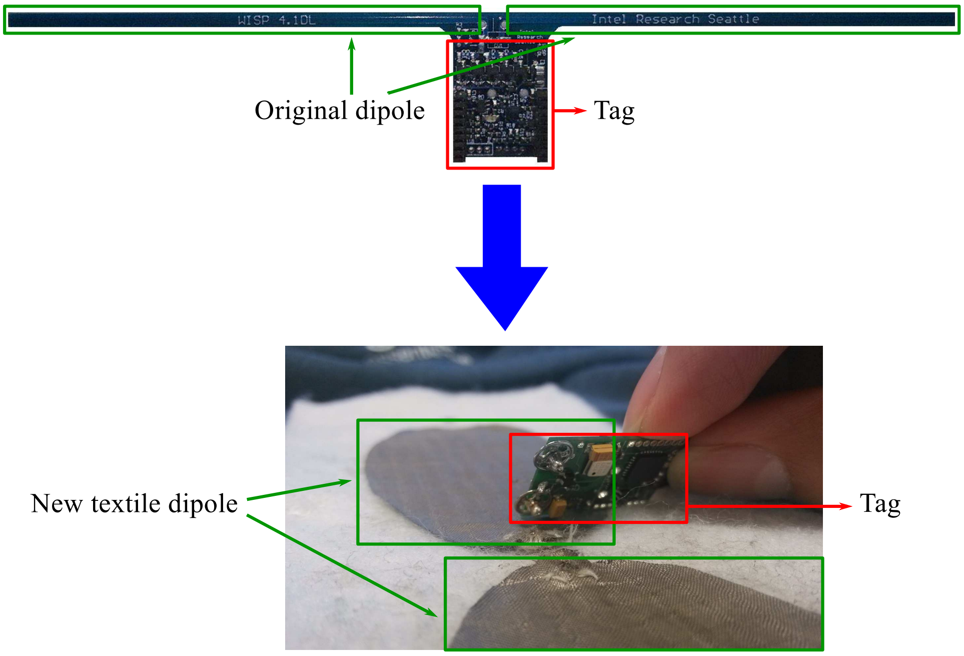

Figure 5.6. The orginal and the new tags. A tag with an original rigid dipole antenna is modified to have a detachable tag and an textile garment-integrated antenna.

new antenna is integrated into a garment and fed by a tag through a pair of snap-on buttons.

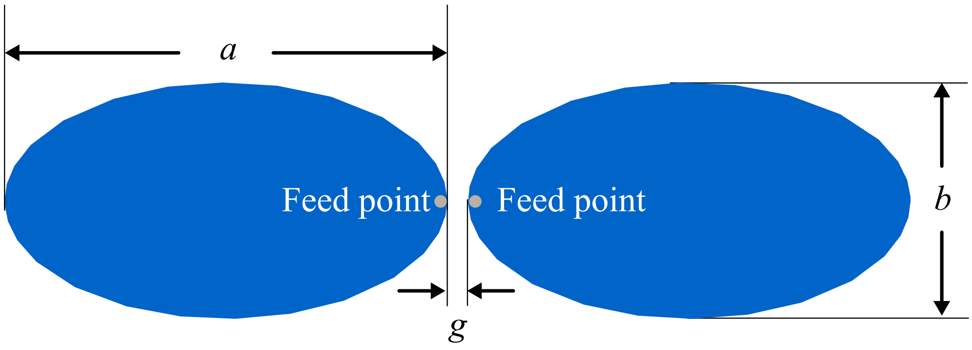

Figure 5.7. The textile dipole configuration. Layout of the textile antenna. The design dimensions are $a = 70$ mm, $b = 40$ mm and $g = 3.5$ mm.

As shown in Fig. 5.7, the antenna is a planar elliptical dipole which has a major axis a = 75 mm and a minor axis b = 40 mm. The elliptical antenna elements offer wideband performances [134] and the ratio of the major and minor axes a/b determines the taper rate of the slots originating from the feed (between the ellipses) and consequently the impedance bandwidth. The critical parameter to control the antenna input impedance is the feed gap size g between the two elliptical elements. An optimal gap of g = 3.5 mm is chosen to set the antenna input impedance at 78 Ω to closely match the tag, as obtained through iterative optimizations in CST. In order to have easy detachability without sacrificing the RF performance, commercial snap-on buttons are employed as the RF connector for this replacement flexible antenna.

5.3.2 Snap-on button connection

The metallic snap-on buttons chosen in the present case are of sewn-on type with appropriate sizes, as shown in Fig. 5.8. Therefore, these buttons can be sewed on the textile antenna using conductive threads to ensure good mechanical and electrical connections. The button dimensions and its 3D model built in CST are shown in Fig. 5.8. The base diameters of 5.5 mm (male) and 6.2 mm (female) give enough real estate for soldering and sewing while the engaged button height of less than 2.7 mm results in a low-profile connection with negligible obstruction to movement. There is a spring embedded in the female button to clip and hold the male button when engaged. This spring mechanism forms solid and reproducible mechanical and electrical connections, as presented as a pair of metallic thin rods in the CST model. A mechanical test involving a spring scale and a fixture to experimentally test the required force to pull a pair of engaged buttons apart indicates that a force of approximately 3 N is needed. This confirms that the mechanical connection is very solid.

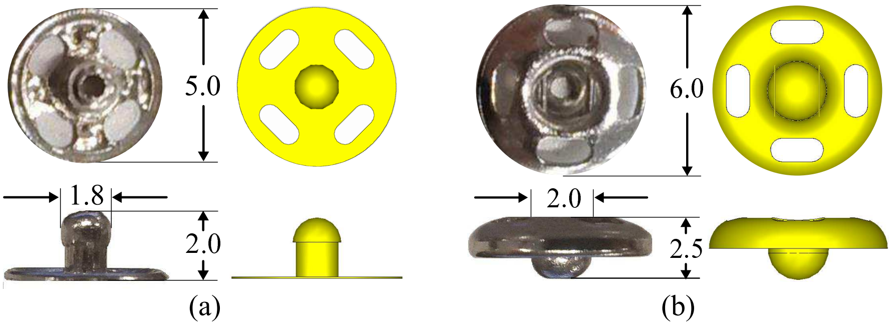

Figure 5.8. The snap-on buttons and their CST model. Dimensions of the used snap-on button in (mm) and its model in simulation: (a) male and (b) female.

To attach to fabrics and textiles, there are four holes on the base of both male and female buttons for sewing propose. As shown in Fig. 5.9a and b, two female buttons are sewed on the textile dipole using conductive threads, while two male buttons are soldered on the tag printed circuit board, one male button being cut to fit the electronics. Consequently the antenna can be easily detached from and reattached to the tag. The

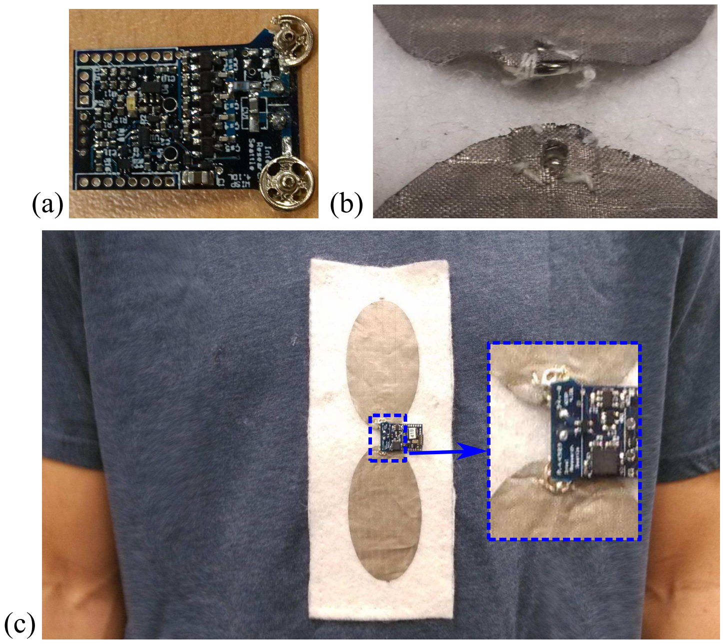

Figure 5.9. The snap-on button feeding arrangement. The snap-on button feeding arrangement: (a) a tag with soldered male snap-on buttons, (b) proposed antenna with sewed female snap-on buttons and (c) a tag with proposed antenna worn on human body.

mechanical compatibility of these buttons with textile materials and most electronics is clear since they can be sewed or soldered on them respectively.

5.3.3 Experimental results

The proposed snap-on buttons have been measured to have excellent mechanical performance, however, as RF connectors, exhibiting satisfactory electrical performance is another crucially necessary requirement. In order to investigate this aspect, two identical textile elliptical antennas have been fabricated and experimentally characterized with different connection methods. The first one employs the balanced paired snap-on buttons feeding arrangement as shown in Fig. 5.9b while the second one adopts a permanent direct contact method realized with conductive epoxy.

For dedicated antenna measurements (i.e. without the tag), a wideband (0.7 - 6 GHz) balun has been adapted from [138, 139] to provide a transition from a 50 Ω microstrip line to 78 Ω balanced coplanar strips. The CST model of the balun and its mode transitions are shown in Fig. 5.10. The balun provides a smooth mode transition from the TEM (transverse electromagnetic) coaxial waveguide mode to the quasi-TEM microstrip line mode then to the quasi-TEM non-planar balanced line mode and finally to

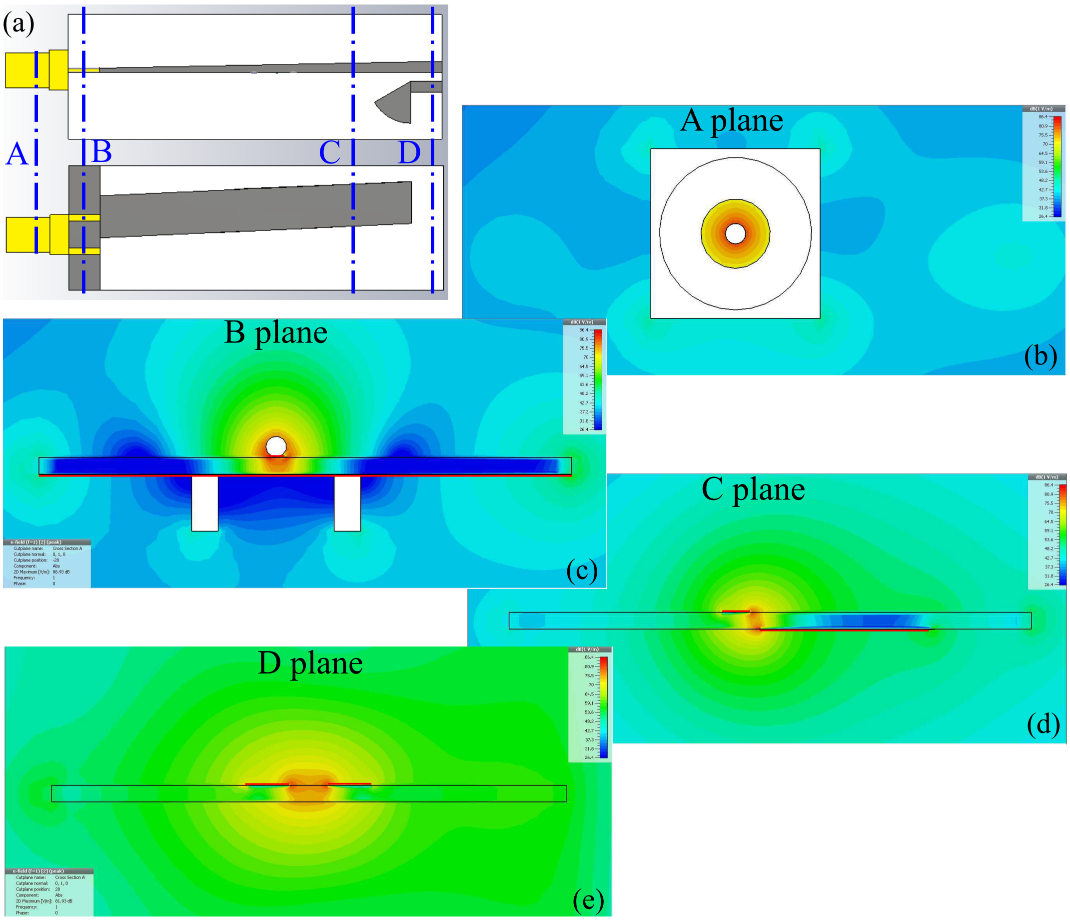

Figure 5.10. 50-Ω microstrip to 78-Ω coplanar strip balun mode transitions. CST model of (a) 50-Ω microstrip to 78-Ω coplanar strips impedance-transformer balun with dotted lines indicating the cross-sectional planes A-D locations, (b) TEM coaxial waveguide mode at plane A, (c) quasi-TEM microstrip line mode at plane B, (d) quasi-TEM non-planar balanced line mode at plane C and (e) quasi-TEM coplanar strip mode at plane D.

the quasi-TEM coplanar strips mode. Its satisfactory RF performance is evidenced in the simulated S-parameters in Fig. 5.11, where the reflection coefficient $|S_{11}|$ remains below -12 dB while the transmission coefficient $|S_{21}|$ is not lower than -1 dB from 0.7 to 6 GHz. For testing the antenna prototype with sewed snap-on buttons, two male snap-on buttons are soldered on the impedance transition balun (as shown in Fig. 5.12a) to feed the antenna. Figure 5.12b shows the balun connected with an antenna prototype.

The simulated and measured reflection coefficient of the two antennas with different realizations of the connection are illustrated in Fig. 5.13. Simulations with and without the 50 to 78 Ω balun are both shown. The slightly lower reflection coefficient observed in the operation band when using the balun is a consequence of small reflections and dielectric losses introduced by the balun. The results from simulation indicate that $|S_{11}|$

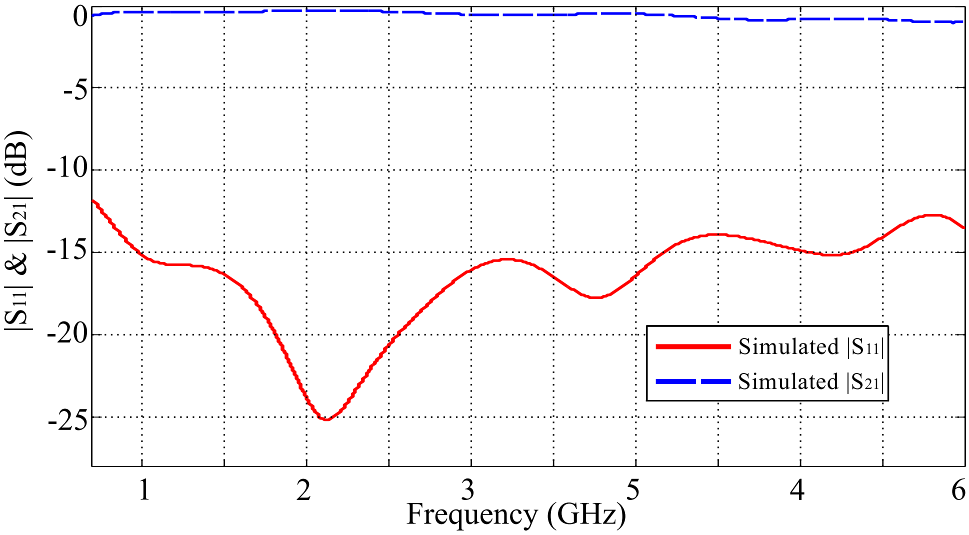

Figure 5.11. Simulated $|S_{11}|$ and $|S_{21}|$ of the balun. Simulated reflection coefficient $|S_{11}|$ and transmission coefficient $|S_{21}|$ of the balun.

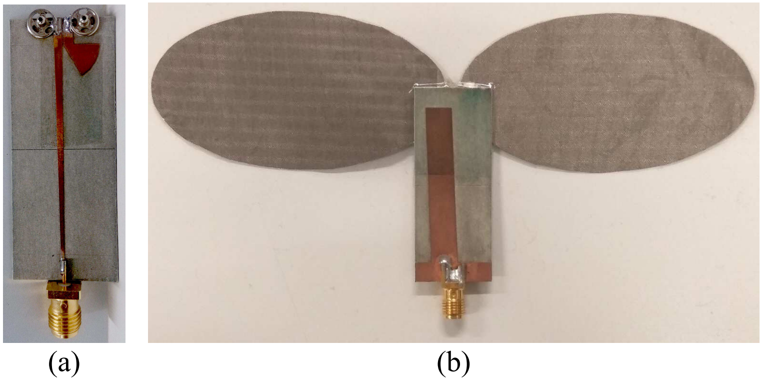
(a) (b)

Figure 5.12. 50-Ω microstrip to 78-Ω coplanar strip balun for antenna measurement. (a) A 50-Ω microstrip to 78-Ω coplanar strips impedance balun with soldered male snap-on buttons and (b) an antenna prototype fed by the balun for testing.

is only slightly affected by the connection with the snap-on button connectors compared to the results with direct connection. In particular, for the simulations without the balun, the resonance frequency increases from 876 to 878 MHz while the impedance bandwidth shifts from 782 - 1038 MHz to 783 - 1042 MHz. The experimental results obtained with the balun are in good agreement and confirm the simulated findings: the measured resonance frequency only has a 9 MHz increment from 867 MHz and the impedance bandwidth moves slightly towards the higher frequency end, namely from 773 - 1007 MHz to 805 - 1012 MHz. Hence, with snap-on buttons, the antenna still maintains its bandwidth and matching to the system.

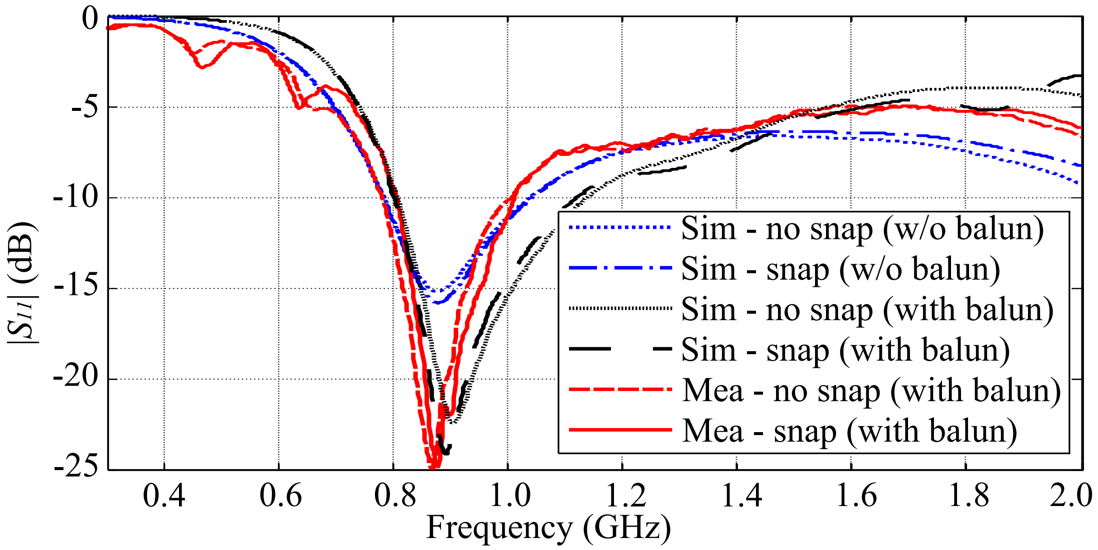

Figure 5.13. Textile dipole antenna simulated and measured $|S_{11}|$. Simulated and measured reflection coefficient $|S_{11}|$ of the proposed antenna. The simulated $|S_{11}|$ parameters for two cases are included: i) the antenna fed with the 50 to 78 Ω balun (with balun); and ii) directly with a 78 Ω port (w/o balun).

A tag attached to a garment-integrated antenna using snap-on buttons and worn by a human subject is shown in Fig. 5.9c. In this configuration, one of the most important parameters of the RFID system is the read range, i.e. the maximum distance from the reader antenna at which the RFID tag is activated (i.e. successfully powered) and communication is successful, as shown in Fig. 5.14. In the present case, as the operational frequency band of the wearable RFID system is generously covered by the antenna impedance bandwidth for both types of connections (direct and snap-on), similar performances are expected. This is validated in the experiments with a female human subject, where identical read ranges, namely 3.0 m, have been obtained for the tag with direct and snap-on connections to the antenna. It is noted that this read range can be further enlarged with appropriate techniques to isolate the dipole radiation from the human body.

The presented simulation results have been obtained for the ideal snap-on button connection configuration, which considers the maximum and flattest contact surface for the components connected. However, the thickness of the materials touching both female and male buttons can influence the gap and consequently the capacitance between male and female connector parts. To investigate how this can affect RF performance, a simulation-based study has been conducted. As demonstrated in Fig. 5.15, the simulated $|S_{11}|$ is not significantly affected when increasing the gap from 10 μm

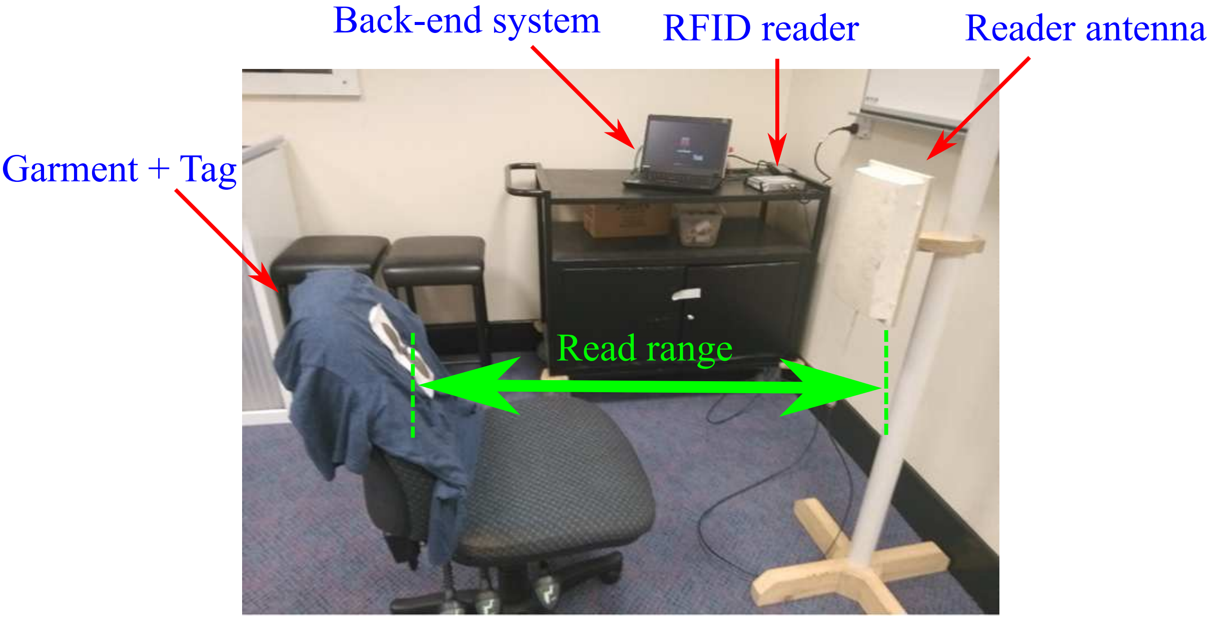

Figure 5.14. Read range of a tag in the RFID system. Tag read range is defined as the maximum distance to the reader antenna for which the tag is activated.

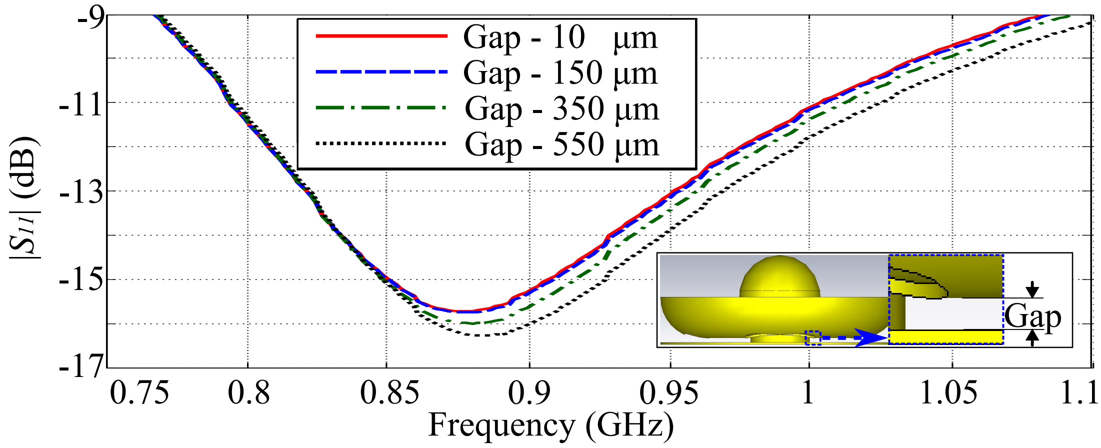

Figure 5.15. Simulated $|S_{11}|$ versus engaged snap-on button gap. Simulated reflection coefficient $|S_{11}|$ of the proposed antenna with different gaps between female and male snap-on buttons.

to 550 μm which is the maximum possible gap obtained via empirical observations of the buttons. This confirms the robustness of the snap-on button connection in the proposed design.

5.3.4 Balanced textile transmission line connector

These snap-on buttons can also utilized as detachable RF connectors for balanced textile transmission lines. To characterize the RF performance of the paired snap-on buttons connections in balanced structures up to 5 GHz, a pair of connected back-to-back 125 Ω (limited by the minimum achievable gap between two trips) coplanar strips were used for testing. For reference, a through coplanar strip line with the same length was used. As shown in Fig. 5.16, both the test and reference structures consist of two baluns and a pair of transmission lines of same length made from silver fabric. The impact on the RF performance from the button connections can be extracted through S-parameters comparison, with time gating used to isolate the impact on the snap-on connections from the parasitic effects of the baluns. Based on these measurements, the resulting transmission coefficients are shown in Fig 5.17. The test structure holds a slightly lower transmission coefficient than the reference, which demonstrates a good RF performance of the proposed paired snap-on button connection, with insertion losses from 0.29 to 0.76 dB up to 5 GHz.

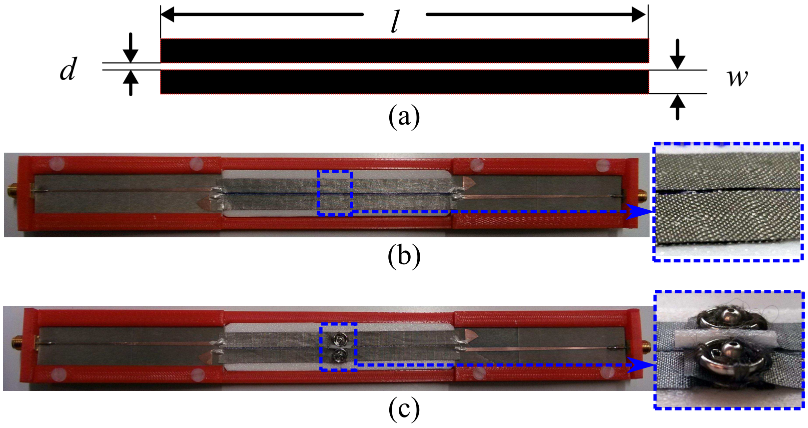

Figure 5.16. Coplanar strips test structure. The realized back-to-back balanced transmission line structure. (a) Dimensions of the coplanar strips, $l = 100$ mm, $d = 0.55$ mm, $w = 6$ mm, (b) Textile through coplanar strips transmission line, (c) Transmission line with snap-on buttons connection.

5.3.5 Summary

A practical and affordable solution using a pair of commercial snap-on buttons as detachable RF connectors has been presented for balanced textile structures. This solution has been applied to connect a wideband elliptical dipole antenna in a 923-MHz wearable RFID system. Two identical antennas have been fabricated using silver fabric, and

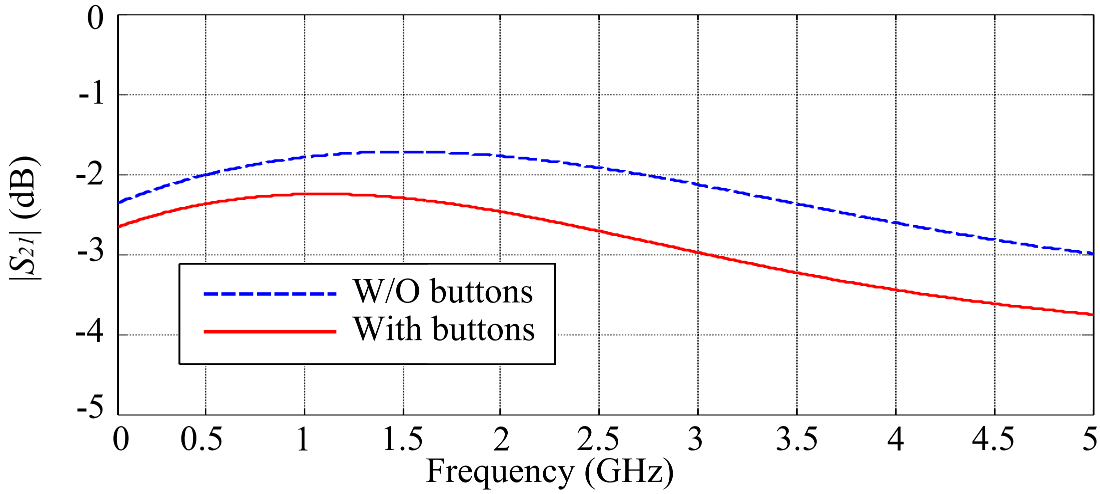

Figure 5.17. Snap-on button insertion loss in coplanar strips structure. Measured transmission coefficient of the reference and investigated back-to-back balanced coplanar strips structures.

experimentally characterized to compare direct contact connection to the proposed balanced snap-on connection. The simulated and measured reflection coefficients indicate that only small variations and an insignificant performance degradation are introduced when using the paired snap-on buttons as RF connectors. This is confirmed by a system test where identical read ranges have been obtained when employing these two types of connections. Further results from a simulation-based study indicate that the gap between engaged female and male buttons has negligible impact on the RF performance. Moreover, measurements on a back-to-back balanced transmission line structure suggest that the button connectors are usable for similar applications at least up to 5 GHz. The utilization of low-cost commercial snap-on buttons offers a practical solution for detachable RF connectors without sacrificing the RF performance in balanced configurations.

5.4 Conclusion

The first part of the chapter has compared three popular shorting strategies namely folded fabric strip, embroidery vias and metallic eyelets, in terms of antenna performance and fabrication complexity/cost. The comparison is based on simulations of an L-slot PIFA antenna using these shorting components with realistic shorting models. It has been found that the antenna resonance modes at three operating frequencies of 4.5, 5.0, and 6.6 GHz are affected differently by the shorting strategies, due to the different current density running in the short. Thus current density in the short should be taken into account for shorting method as well. Because of the relatively high sheet resistance of the embroidered conductive wall, it yields a 0.6 to 2.6 dB lower efficiency at the highest and lowest resonance frequencies compared to the fabric folded strip and eyelet methods. However, the lossier method can be automated using computerized embroidery technology and consequently presents the simplest and cheapest method. In contrast, unless the short can be accommodated outside of the substrate, the high-efficiency fabric folded strip method is usually cumbersome, as the ground plane cannot be realized as a single fabric piece. Similarly, the copper eyelet method offers metallic electrical connection, however with higher fabrication cost and less wearing comfort. For the middle frequency, no significant differences are observed between the different shorting methods due to the very limited current running through the shorting wall. All these results suggest a general guideline in choosing appropriate shorting strategies for textile antenna design in terms of performance and fabrication complexity/cost.

The second part of this chapter has proposed a practical detachable RF connection solution for balanced textile structures based on commercial snap-on buttons. This solution has been applied to connect a wideband textile dipole antenna to an RFID tag in a 923-MHz wearable RFID system. Compared to the performance of a tag directly connected to a textile antenna prototype, the tag using snap-on button connectors only has small variations and an insignificant performance degradation. This is confirmed by the identical read ranges obtained for both tags. Additionally, measurements on a back-to-back balanced transmission line structure suggest that the button connectors are usable for similar applications up to at least 5 GHz. All the findings imply that the utilization of low-cost commercial snap-on buttons offers a practical solution for detachable RF connections without sacrificing the RF performance in balanced textile configurations.

Chapter 6

Wearable Modular Textile Antennas

CONDUCTIVE textiles have been widely utilized as conductors for wearable antennas. This is mainly attributed to their outstanding electrical conductivity and excellent mechanical flexibility. Moreover, commercial snap-on buttons have been proposed as an appropriate RF connection solution for textile antennas, with satisfactory mechanical and electrical performance as well as repeatable detachability. These particular advantages of conductive textiles and snap-on buttons suggest joint applications of those components in wearable antennas, combining flexible conductors with solid connections. In particular, interchangeable antenna designs can neatly exploit these material and connection advantages and consequently promotes system modularity.

In this context, this chapter presents a modular design concept for wearable textile antennas based on conductive fabrics and commercial snap-on buttons, which offers convenient, passive, low-cost, and versatile system modularity. Through manually interchanging and/or rearranging different detachable radiation elements, dedicated antenna functionalities can be fulfilled. This concept is validated by the experimental characterization of various radiation module designs which can provide modularities in resonance frequency, polarization and radiation patterns. Additionally, the idea of utilizing commercial snap-on buttons as detachable shorting vias is also demonstrated in an extended modular design.

6.1 Introduction

In recent years, flexible and wearable antenna designs have received significant attention due to the dramatically increasing demands in various wearable electronic systems [9, 162]. Applications include mobile communications, wireless medical monitoring/diagnosing and military applications [163, 164]. Besides conventional antenna requirements, wearable antennas are expected to be flexible, lightweight, low-cost and garment-integratable [8, 10]. As a result, conductive textiles have been emerging as one of the most promising conducting materials [11, 12]. Many wearable devices made from conductive textiles such as patch antennas [13–15] and arrays [16], ultra-wideband [17,18] and ultra-wideband-notched [19] antennas, as well as antennas based on fundamental mode [20] and half-mode [21, 22] substrate-integrated waveguides have been reported. Moreover, clothing closure accessories have been exploited as support for antenna design. For example, metallic buttons for textiles have been designed as wearable antennas [165, 166], and commercial metallic snap-on buttons also have been proposed as a practical and economical RF connection solution for wearable systems, since they can form detachable RF connection with suitable RF performance [55, 158, 160]. This leads to the idea of making specific radiation elements detachable with snap-on buttons to achieve modular antenna designs, thus enabling passive reconfigurability of the overall system. Although this requires manual operation, passive reconfiguration promotes ease of antenna design [167] and versatile wearable antenna integration since no active components and bias circuits are needed.

Modular antenna designs have been proposed in various wireless communication systems such as mobile phones [168], cellular communication base-stations [169] and avionics systems [170]. They can be categorized into two main groups according to their modular antenna elements, namely identical and different modular antenna elements, which are illustrated in Fig. 6.1a and b respectively. In Fig. 6.1a, an active antenna array comprising of identical sub-array modules [171] is displayed whereas a wireless communication device which can be equipped with different antenna modules [168] is shown in Fig. 6.1b. Typically, identical modular antenna elements are employed as building blocks for antenna array designs [169, 172]. With such modular designs, the array dimensions can be easily reconfigured. On the other hand, modular designs with different antenna modules can be found in systems featuring interchangeable antennas which share one common feed design [168, 170, 173]. These antenna modules are usually of same outline geometry to satisfy the requirements of same fitting and feeding, even if they are serving different functionalities. Such modular antenna designs bring valuable advantages including low manufacturing cost, easy maintenance and most importantly passive system reconfigurability.

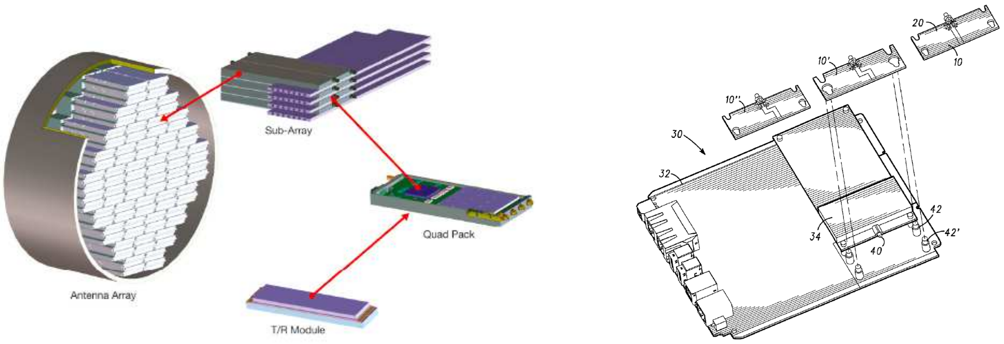

(a) (b)

Figure 6.1. Typical modular antenna designs. (a) An active antenna array design based on modular antenna sub-array, adapted from [171] and (b) an interchangeable and modular antennas in a wireless communications device, adapted from [168].

In the present work, a modular antenna design based on metallized fabric and flexible low-permittivity foam substrate is presented for wearable applications, providing possible system reconfigurabilities for polarization and resonance frequency. Commercial snap-on buttons are employed as RF connectors and mechanical fixtures to enable easy detachability of the modular antenna radiating elements. Various types of antenna functions can be conveniently achieved by interchanging the dedicated patch module or rearranging the configuration of a module by the means of flipping-over, rotating, ground-shorting or folding. To demonstrate the concept, the following five patch modules are discussed in this chapter based on simulated and experimentally validated antenna characteristics:

- A module which can provide interchangeable right hand circular polarization (RHCP) and left hand circular polarization (LHCP) at 5 GHz, through module flipping;
- A module which can provide interchangeability between RHCP, LHCP at 5 GHz and linear polarization (LP) at 4.7 or 5.3 GHz, through simple module rotation and different flap configurations (opened or closed);
- A module which can provide interchangeable resonance frequencies between 2.45- and 5.3-GHz, by operating as a standard $\lambda/2$ patch or a $\lambda/4$ planar inverted-F antenna (PIFA);

- A module which operates at 8 GHz, showing a higher degree of design adaptability with nearly unlimited choices of radiation element geometry;
- A module which can provide interchangeable resonance frequencies between 8, 9 and 10 GHz by patch folding.

Following those demonstrations, an extended design which employs four pairs of snap-on buttons as detachable shorting vias is demonstrated, offering more possibilities and thus versatility in possible module design. It is emphasized that the frequencies of these modules are chosen as representative examples, but the functionality of the principle is not limited to these particular bands. The very good agreement between simulation and experimental results in free-space, worn by a torso phantom and in bending conditions confirm that such passive modular antenna designs can provide a low-cost, easy-maintenance solution to enable versatile system reconfigurabilities for wearable applications.

6.2 The antenna design

The generic antenna configuration is depicted in Fig. 6.2 and the most relevant dimensions are listed in Table 6.1. The antenna configuration is a planar structure and it consists of an interchangeable modular radiating patch dedicated to a specific application and a common base which includes a microstrip proximity coupled feed, a two-layered substrate and five commercial snap-on button connectors. In this chapter, various patch modules with different operating frequency bands such as WLAN 2.4- and 5.3-GHz (IEEE 802.11) bands, or 8 to 10 GHz in the X-band have been chosen as the designed antenna operation frequencies for illustration. But it is emphasized that the concept is not limited to these frequencies.

6.2.1 Antenna materials and structure

To obtain flexibility without sacrificing conductivity, the microstrip feed, the ground plane and the radiating patch elements are made from a silver-coated nylon RIPSTOP fabric (commonly denoted as silver fabric) with a DC sheet resistance of 0.01 $\Omega/square$ and a thickness of approximately 100 μm. The substrate is made of two layers of 1.6-mm-thick highly flexible Cuming Microwave C-Foam PF-4 foams with relative permittivity $\varepsilon_r = 1.06$ and loss tangent $\tan\delta = 0.0001$.

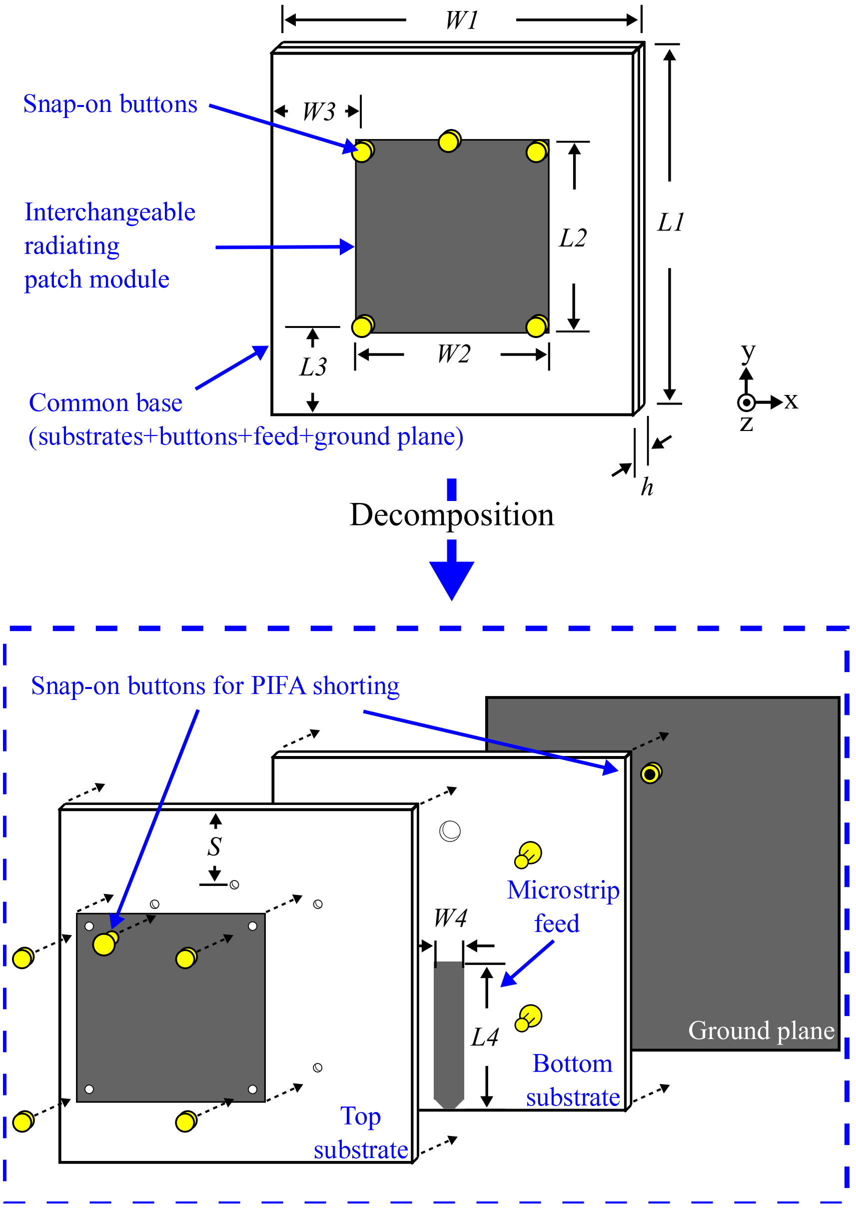

Figure 6.2. The proposed modular antenna configuration. The proposed modular antenna includes a common base and an interchangeable patch module designed for a specific functionality. The common base consists of a ground plane, two layers of substrates, an open-end microstrip proximity-coupled feed and five snap-on buttons. Four snap-on buttons are used as mechanical fixtures for the various patch modules, whereas the fifth optional button is utilized as RF connector to create a short in a PIFA configuration. Various functionalities are fulfilled with dedicated patch modules.

Various patches can be fixed on top of the common base with four pairs of engaged snap-on buttons which provides detachability and consequently interchangeability. For the same reason, a proximity-coupled feed is adopted for the generic design since

Table 6.1. General dimensions of the modular antenna. Dimensions of the common antenna base and the outlined dimensions of the radiating patch modules.

Parameters	W_1	W_2	W_3	W_4	S	L_1	L_2	L_3	L_4	h
Value (mm)	40	19.5	13	6.5	10.5	40	18.5	13.5	15	3.2

the physical separation between feed and radiating element permits a free-standing detachable patch. The two-layer structure serves two functionalities including antenna elements separation and strict immobilization of snap-on buttons. An open-ended microstrip line serving as the antenna feed and four male snap-on buttons serving as the patch fixtures are embedded between the top- and bottom-layer substrate. Note that the top-layer substrate is cut with four holes for the snap-on button male pin to go through. A fifth female snap-on button placed to provide a selective shorting post for a proposed PIFA configuration is sewed onto the ground plane using conductive threads and thus a hole is individually trimmed through both substrate layers to accommodate it.

6.2.2 Snap-on buttons

The snap-on buttons are the key components which mechanically and electrically enable low-cost and practical detachability and interchangeability for the patch modules. The chosen commercial snap-on buttons and their main dimensions are both included in Fig. 6.3. On the one hand, they are selected as mechanical fixtures since their size are appropriate for the patch modules, and more importantly, they offer solid mechanical performance. As discussed in Section 5.2.2, a dedicated test done in [55] indicates that an approximate 3 N force is needed to undo engaged buttons of this type. On the other hand, since these snap-on buttons offer detachable connection with satisfactory RF performance at least up to 5 GHz [55] as discussed in Section 5.2.4, they are also chosen as an RF connector for the PIFA antenna configuration.

6.2.3 Antenna fabrication

To achieve accurate patterning of the geometry, the patch modules and microstrip feed are cut with a laser milling machine (LPKF: Protolaser S). A series of laser-trimmed modular patches in a larger sheet of silver fabric is shown in Fig. 6.4. A dedicated fixture is used to trim holes in the substrates and align the feed line and snap-on buttons

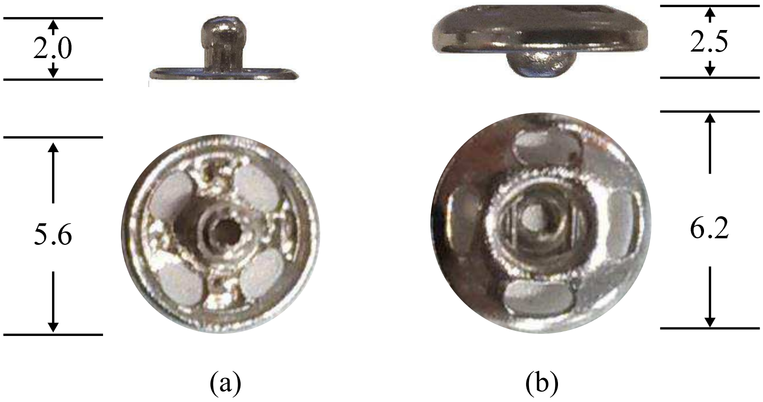

Figure 6.3. The chosen snap-on buttons and their dimensions. Geometries and dimensions (mm) of the commercial snap-on buttons chosen for the button module: (a) male and (b) female snap-on button.

onto the bottom substrate. Machine-washable fabric glue, Wash N Wear Glue White from Helmar®, is applied to attach the ground plane to the substrate, the microstrip feed/buttons to the bottom substrate, the top substrate to the bottom substrate, and the radiation patch to its fabric substrate. As only a very thin layer of the glue is required to form a permanent and solid bond, its influence on the antenna performance is deemed negligible and can be best taken into account as a slight increase in the conductor loss of the metalized textile. Conductive epoxy is adopted to mechanically and electrically connect a SMA connector to the microstrip feed. The conductive epoxy applied is the CW2400 from CircuitWorks® which offers high strength bond and excellent electrical connection with a very low volume resistivity of 0.1 Ω·m.

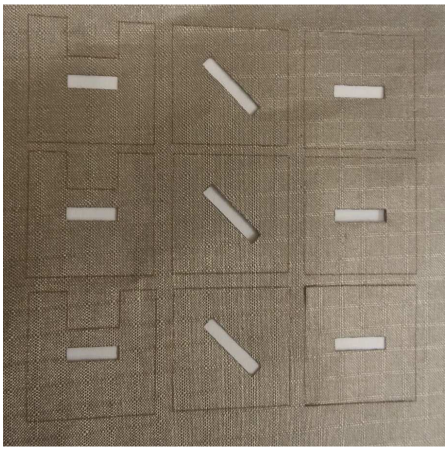

Figure 6.4. Laser-trimmed modular patches. A series of laser-trimmed modular patches in a larger sheet of silver fabric.

6.3 The module design

Since the radiation element is detachable and interchangeable, different patch modules can be designed to serve various functionalities. Moreover, this feature can benefit a low maintenance cost since easy servicing and economical repair can be achieved by direct component replacement.

The alignment and the attaching/detaching repeatability of these patch modules are critical for the antenna performance and thus particular attention is required with regard to the module design. Firstly, the silver fabric is chosen for the module materials as it is conductive, flexible and, more importantly in this case, robust enough to remain undistorted for numerous interchange of modules. Secondly, four positioning holes are created in the modular patches to ensure an accurate module alignment with the male buttons embedded in the top substrate layer. These holes are precisely cut using a laser milling machine. To tightly confine the module alignment with the button fixtures, the hole radius is determined to be 0.7 mm which corresponds to the exact dimension of the neck of the male pin. Very stable alignment and attaching/detaching repeatability have been observed during the measurement campaign for the most-frequently-used modules.

This section shows five typical patch modules which are able to provide various modularities in terms of polarization and resonance frequency.

6.3.1 CP interchangeable module

The first module is based on a single-layer structure and can serve two functionalities individually, namely operating with RHCP or LHCP at 5 GHz. As shown in Fig. 6.5, the module is made of silver fabric and has a diagonal slot in the center which enables RHCP or LHCP depending on its orientation.

Initially, as expected for a rectangular microstrip antenna design on unit permittivity substrate, the patch dimensions are set to be a half of the wavelength at the chosen operating frequency. The patch is then tuned to obtain approximately a 5% higher resonance frequency which will compensate the influence from the diagonal slot introduced later. To achieve circular polarization, the method using a diagonal slot perturbation is selected and initial dimensions of the slot are determined using formula

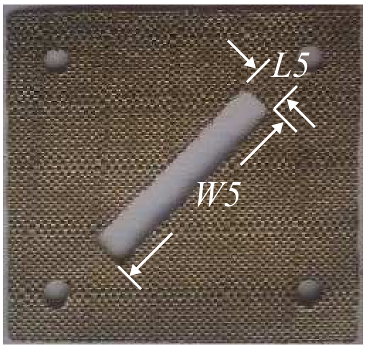

Figure 6.5. CP interchangeable module. A prototype of the 5 GHz LHCP-RHCP interchangeable module and the dimensions: $L_5 = 2\ mm$ and $W_5 = 12\ mm$

(8.20) given in [174]

$$\left|\frac{\triangle A}{A}\right| = \frac{1}{2Q_0}. \tag{6.1}$$

This formula is utilized to find out the initial slot dimensions, where $\triangle A$ is the slot area ($L_5 \times W_5$), A is patch area ($L_2 \times W_2$) and Q_0 is the antenna unloaded quality factor. The value of Q_0 is estimated through the fractional bandwidth ($\triangle f / f_0$) and the voltage standing wave ratio (VSWR) obtained from simulation results using the relationship [175]

$$\frac{\triangle f}{f_0} = \frac{\text{VSWR-1}}{Q_0\sqrt{\text{VSWR}}}. \tag{6.2}$$

Consequently the only unknown $\triangle A$ can be determined accordingly as a starting value. An optimal slot dimension combination which yields a nearly 0-dB axial ratio (AR) is then gained through parameter sweeps in CST. Because of the introduction of the diagonal slot, the resonance frequency is now lower and consequently closer to 5 GHz. Subsequent tuning of L_1 and W_1 is required to achieve a maximum impedance bandwidth and an AR below 1 dB, both centered at 5 GHz. Finally the length of the open microstrip feed is adjusted for best impedance matching. It is worth mentioning that since the microstrip feed line is fixed from this point on, matching techniques for all subsequently designed patch modules will require extra effort. The antenna loaded with the designed patch, as shown in Fig. 6.6a, provides RHCP while in contrast the one shown in Fig. 6.6b provides LHCP. The circular polarization is easily interchangeable by flipping the patch accordingly.

As illustrated in Fig. 6.7, the measured reflection coefficients for the antenna loaded with the circularly polarized modules show a reasonable agreement with the simulated values. The measured $|S_{11}|$ parameter of the antenna yields a -10-dB impedance bandwidth from 4.75 to 5.25 GHz for the LHCP configuration and from 4.80 to 5.35 GHz for

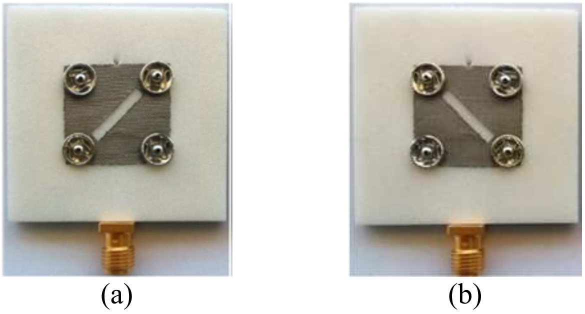

(a) (b)

Figure 6.6. Antenna loaded with the CP interchangeable module. (a) Antenna loaded with circularly polarized patch module in RHCP configuration. (b) Antenna loaded with circularly polarized patch module in LHCP configuration.

the RHCP one, which covers the target center frequency of 5 GHz. The difference is indicative of fabrication tolerances.

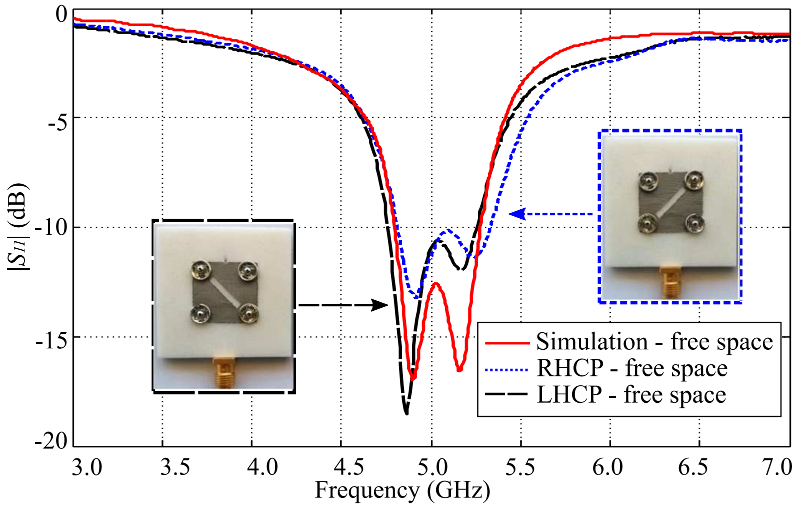

Figure 6.7. $|S_{11}|$ of the antenna with CP interchangeable module. Reflection coefficient comparison of the antenna loaded with the circularly-polarized patch module.

The simulated and measured boresight axial ratios of the antenna in free space are compared in Fig. 6.8 and they exhibit a very good agreement. The 3-dB axial-ratio bandwidth is from 4.95 to 5.08 GHz for the LHCP configuration and from 4.95 to 5.06 GHz for the RHCP one, both centered at approximately 5.01 GHz. The whole 3-dB axial bandwidth (of 2.2%) is covered by the -10-dB impedance bandwidth (of 10%), which indicates that circular polarization is achieved as designed.

The normalized radiation patterns in *xz*-plane (H-plane) and *yz*-plane (E-plane) have been obtained through measurement in an anechoic chamber. The radiation patterns of the LHCP and RHCP antennas in free space are shown in Fig. 6.9. For the LHCP

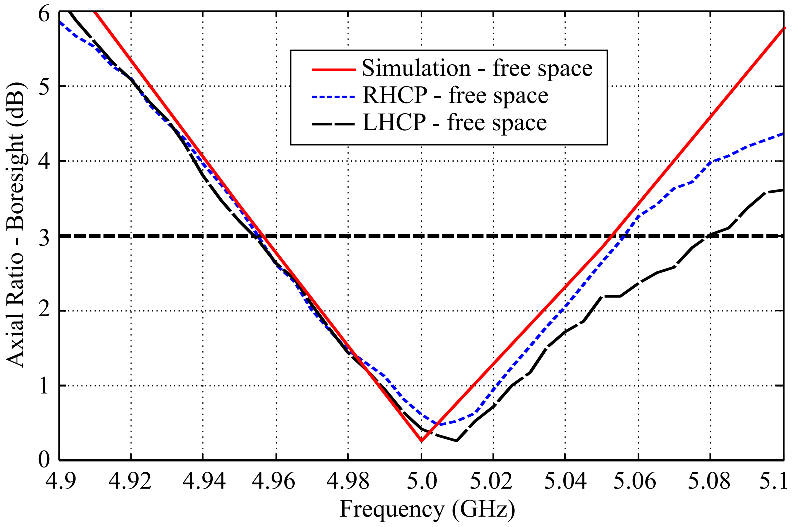

Figure 6.8. Boresight AR of the antenna with CP interchangeable module. Boresight axial ratio of the antenna loaded with circularly-polarized patch module.

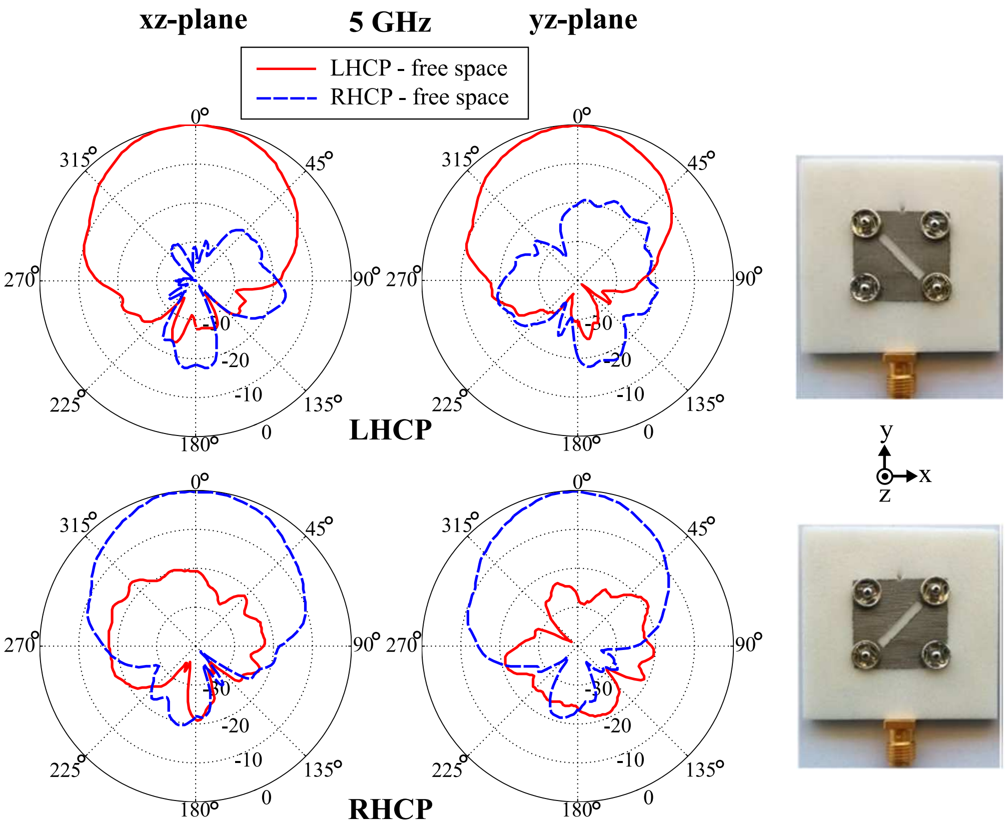

Figure 6.9. Radiation patterns of the antenna with CP interchangeable module. Measured normalized radiation patterns of the antenna loaded with circularly-polarized patch module.

antenna, the desired left-handed polarization (co-polarization) has an around 20-dB power higher level over the unwanted right-handed polarization (cross-polarization).

Due to symmetry, similar radiation patterns are obtained for the RHCP antenna configuration, but with a predominant right-handed polarization rather than the left-handed one. As anticipated for a microstrip patch antenna, all these patterns exhibit a main lobe directed in positive z direction with some small back lobes with amplitude dependent on ground plane size. In addition, a realized gain of 8.0 dBic has been measured for the LHCP antenna and this result is very close to the simulated value of 8.1 dBic.

6.3.2 LP-CP and frequency interchangeable module

The patch proposed in the section is an extended version of the first module just reported above, with extra modularities in LP and variation in resonance frequency. On the one hand, the LP modularity is achieved by introducing a circular patch geometry instead of the original rectangular one, since this allows the antenna to operate at its fundamental TM^z_{110} mode regardless the orientation of the module and its center slot. On the other hand, the slot in the patch is realized by folding a flap rather than trimming the whole slot off, which brings about a closable slot and therefore an interchangeable resonance frequency. The details are discussed as follows.

The proposed module, as shown in Fig. 6.10, is a circular patch with a flap cut in the middle and a sticky tape cover on its top. There are eight holes in the module separated with a 45° angle, which allow the module to have a $\pi/4$ rotation resolution. Additionally the flap can either be folded and put underneath the patch to form an opened slot (Fig 6.10b) or it can fully close the slot (Fig 6.10c). Therefore, a sticky tape cover is introduced to ensure good electrical contact between the flap edges and the module main body. The circular patch module resonates in its fundamental TM^z_{110} mode and hence its radius corresponds approximately to half of the operation wavelength [175]. The slot is introduced to make the antenna circularly polarized but can also be used to obtain two different resonance frequencies (slot closed and opened) in the LP configuration. As a result, to obtain the desired CP performance, the start values of the slot dimensions are obtained based on the method discussed for the first module. Following that, the optimal dimensions are determined based on parametric simulations with CST.

In the configuration for achieving RHCP or LHCP, the module needs to be positioned with the slot opened and aligned with $\phi = 45°$ (Fig 6.11a) or $\phi = 135°$ (Fig 6.11b), respectively. In contrast, to switch to LP (with different resonance frequency), the slot

(a) (b) (c)

Figure 6.10. The LP-CP/frequency interchangeable module. (a) Configuration and dimensions of the proposed patch module: $W_8 = 11.8$ mm, $W_9 = 9.5$ mm, $L_9 = 2.6$ mm and $D = 23.4$ mm. A prototype module realization in (b) opened configuration and (c) closed configuration.

can be closed or opened with either vertical ($\phi = 0^\circ$) or horizontal ($\phi = 90^\circ$) alignment. A lower operational frequency is expected with an opened slot.

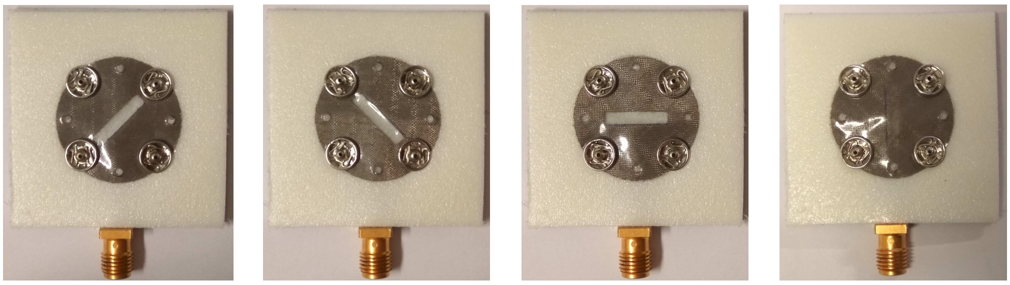

(a) (b) (c) (d)

Figure 6.11. Antenna loaded with the LP-CP/frequency interchangeable module. Antenna loaded with the proposed patch module in different configurations: (a) RHCP configuration, (b) LHCP configuration, (c) LP slot opened configuration and (d) LP slot closed configuration.

The simulated and measured reflection coefficients of the antenna in RHCP mode is shown in Fig 6.12. An excellent agreement between simulation and measurement is observed, with an impedance bandwidth extending approximately from 4.75 to 5.25 GHz (10%). As two orthogonal modes of the circular patch module are needed to excite CP radiation, the two dips in the reflection coefficient as observed in the measurement are suggesting appropriate excitation of orthogonal resonances with frequency offset. To confirm that, the boresight AR has been measured and compared with the simulated result as plotted in Fig 6.13. The measured result has a good consistency with the simulated result, that is, the antenna is circularly polarized within a 3dB AR bandwidth from 4.94 to 5.07 GHz (2.6%). As anticipated, the measured normalized radiation patterns in the xz- and yz- planes also provide further evidence of the RHCP characteristics, as demonstrated in Fig. 6.14, where the co-polar (RHCP) components are at least 20 dB higher that the cross-polar ones (LHCP). By symmetry, the antenna can radiate with LHCP with similar performance when the module is rotated 90° from the RHCP configuration, as shown in Fig 6.11b.

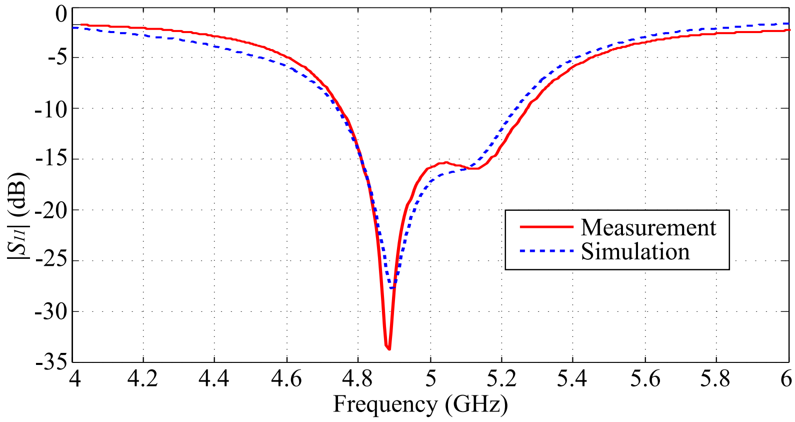

Figure 6.12. $|S_{11}|$ of the RHCP configuration. Simulated and measured $|S_{11}|$ of the antenna in RHCP configuration.

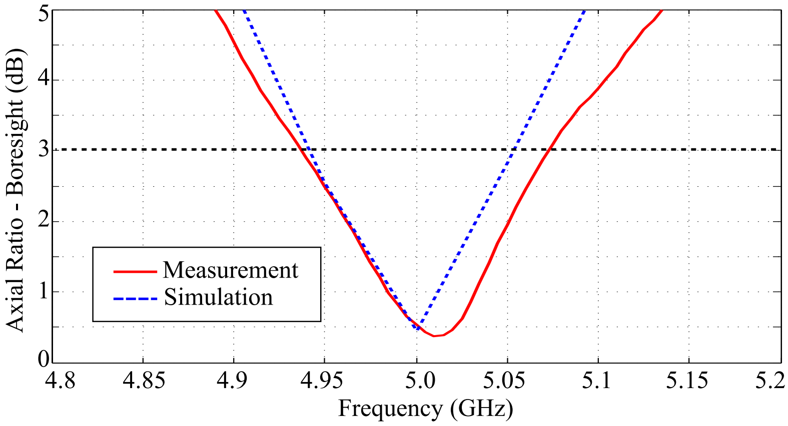

Figure 6.13. AR of of the RHCP configuration. Simulated and measured axial ratio of the antenna in RHCP configuration.

As mentioned, when the module slot is either closed or opened with alignment along the x- or the y- axis, the antenna radiates with linearly polarized waves, as displayed in Fig. 6.11c and d. For these two configurations, the simulated and measured $|S_{11}|$ parameters of the antenna are depicted in Fig. 6.15 where a good agreement is observed. When the slot is fully closed, the antenna resonates at 5.2 GHz with a bandwidth of around 9.5%. For the case that the slot is fully opened and aligned with the x-axis, its center operational frequency is at 4.7 GHz with a 13.5% bandwidth. The measured normalized radiation patterns of these two configurations in the xz- and yz- planes

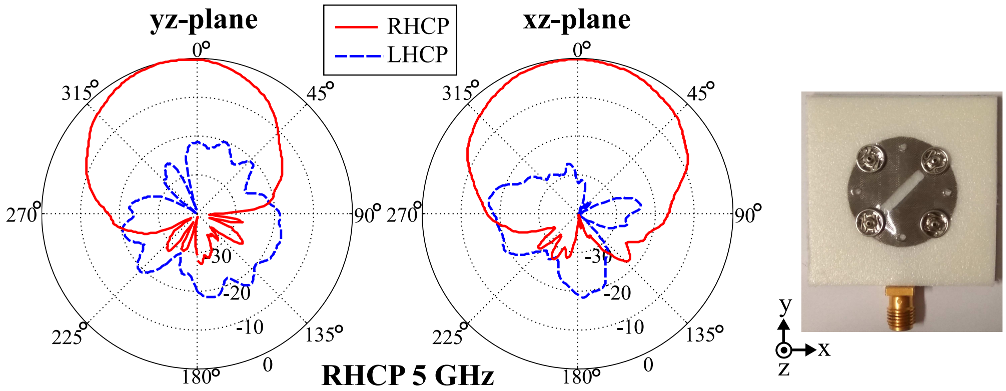

Figure 6.14. Radiation patterns of the RHCP configuration. Measured normalized radiation patterns of the antenna in RHCP configuration in the *yz*- and *xz*-planes at 5 GHz.

are plotted in Fig 6.16. As expected, they are typical half-wavelength patch radiation patterns where the main beam is in the boresight direction. Since a decrease in the resonance frequency is expected with longer slots, further resonance frequencies (e.g. 5 GHz as for the RHCP design) are attainable through introducing slots with appropriate length. This could be even achievable by adding more slices in the flap along its short edges. With the sticky tape cover on the module holding the flap in the slot, a good electrical connection between them can be realized.

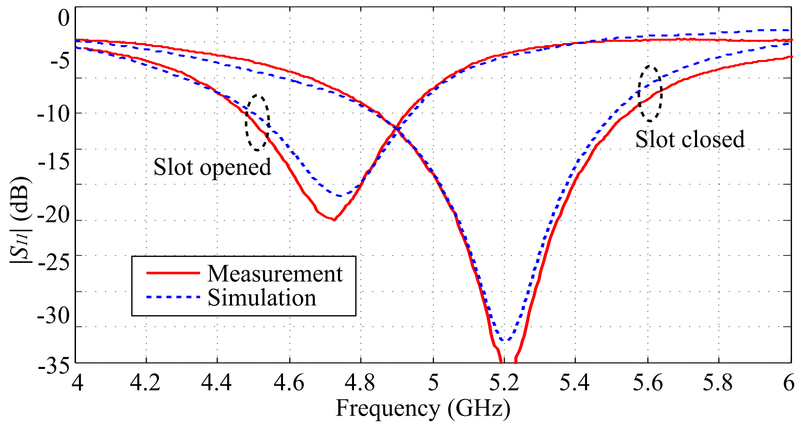

Figure 6.15. $|S_{11}|$ of the LP configurations. Simulated and measured $|S_{11}|$ of the antenna in LP slot closed and LP slot opened configurations.

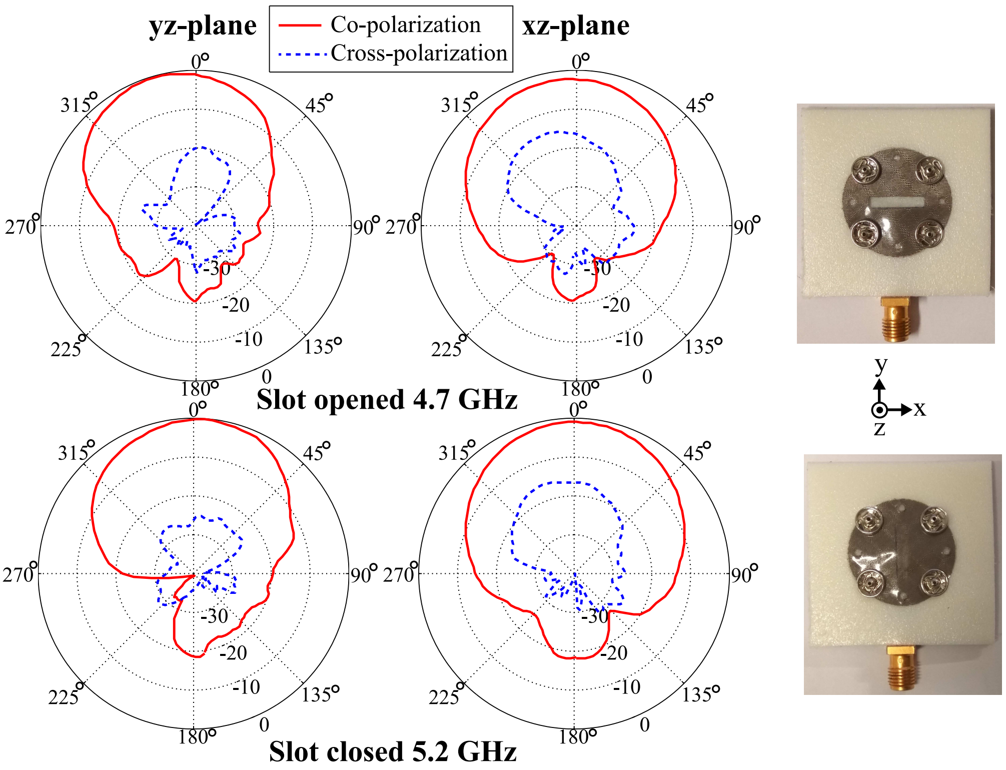

Figure 6.16. Radiation patterns of the LP configuration. Measured normalized radiation patterns of the antenna in LP slot closed and LP slot opened configurations in the yz- and xz-planes at 4.7 and 5.2 GHz, respectively.

6.3.3 $\lambda/2$-patch and $\lambda/4$-PIFA interchangeable module

As illustrated in Fig. 6.2 and Fig. 6.18a, a fifth female snap-on button sewed onto the ground plane can be engaged to a male counterpart to form a patch-to-ground electrical shorting. As a consequence, the antenna operates then as a PIFA antenna (quarter-wavelength patch), as shown in Fig. 6.18a, instead of the standard half-wave microstrip patch configuration as shown in Fig. 6.18b. The two resonance frequencies are generally both inversely proportional to the patch length L_2 and the lower resonance frequency (PIFA) is also additionally dependent on the shorting button's vertical position S. Therefore, S is utilized to tune the lower resonance frequency. Furthermore, transverse slots can be introduced within the patch to individually adjust the higher resonance frequency. Since the resonance frequency tunability is important for obtaining various system reconfigurability, three of this module variations with different transverse slots have been fabricated and tested to verify the prediction. As displayed in Fig. 6.19, a 2-mm wide slot with different length of 6, 10 and 14 mm was introduced in three identical modules respectively.

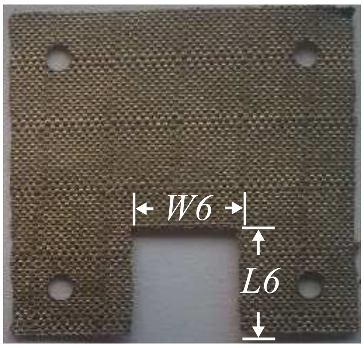

Figure 6.17. The LP frequency interchangeable module. The frequency interchangeable module for quarter-wave and half-wave configurations and its dimensions: $W_6 = 11.8$ mm and $L_6 = 2.6$ mm.

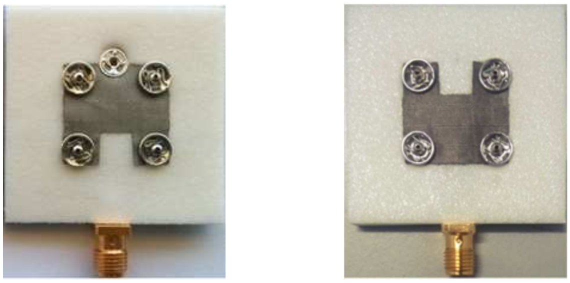

(a) (b)

Figure 6.18. Antenna loaded with the LP module. Antenna loaded with the frequency interchangeable patch module in different configurations: (a) $\lambda/4$ PIFA configuration and (b) standard $\lambda/2$ patch configuration.

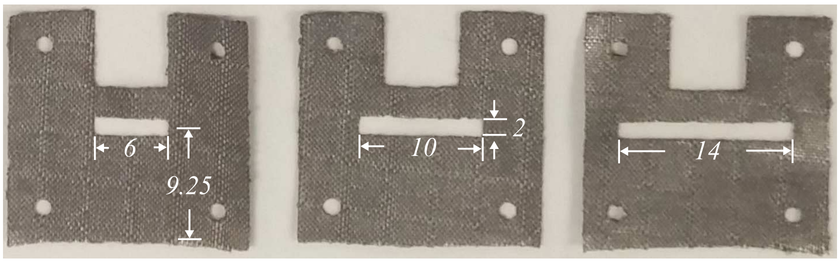

(a) (b) (c)

Figure 6.19. The LP modules with different slots. 5.3 GHz Patch modules with transverse slots of different lengths but with the same width of 2 mm. (a) Patch module with a 6-mm long slot. (b) Patch module with a 10-mm long slot. (c) Patch module with a 14-mm long slot.

As mentioned previously, the microstrip feed has been optimized for the circularly-polarized patch and thus cannot be changed. Therefore, matching technique needs to be applied to the patch modules in this case. To match the antenna in PIFA configuration, a rectangular notch with dimensions $L_6 \times W_6$ is required, as shown in

Fig. 6.17. This notch reduces the capacitance between the patch and the microstrip feed and hence compensates the capacitance decrease in the patch input impedance due to the ground shorting. For the half-wave configuration, a satisfactory matching is achieved by a rotation of the patch module bringing the edge without notch down, and thus leading to a similar input impedance as the circularly polarized module. The antenna in quarter-wave and half-wave configurations are illustrated in Fig. 6.18a and b individually. Switching between two resonance frequencies, 2.45 GHz and 5.3 GHz, is accomplished via a simple rotation of the patch and engaging (or disengaging) the shorting snap-on button.

The measured $|S_{11}|$ parameters of the antenna loaded with linearly polarized patches are largely in accord with simulations, as depicted in Fig. 6.20. The antenna with PIFA configuration has an impedance bandwidth of around 100 MHz centred at 2.45 GHz. The half-wave patch resonates at 5.33 GHz with an impedance bandwidth extending from 5.18 to 5.48 GHz.

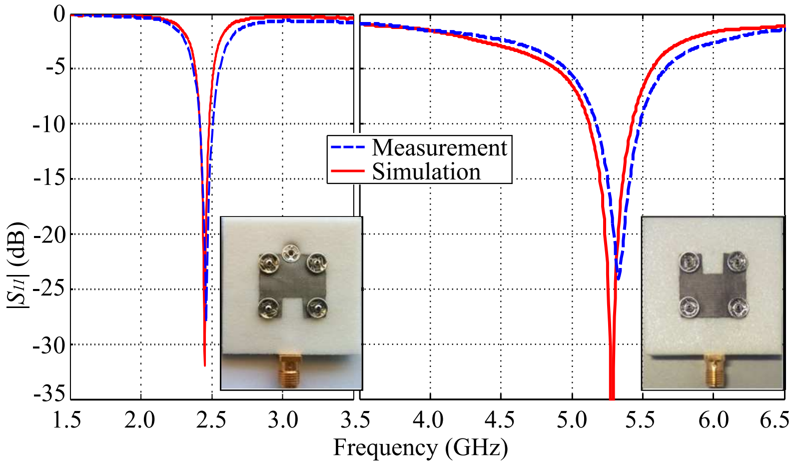

(a) (b)

Figure 6.20. $|S_{11}|$ of the antenna with the LP module. S-parameter comparison of the antenna loaded with the frequency interchangeable patch module. (a) Antenna loaded with the patch module in PIFA configuration (2.45 GHz). (b) Antenna loaded with the patch module in normal configuration (5.3 GHz).

Now considering the half-wave patches with an added transverse slot, their measured and simulated reflection coefficients are displayed in Fig. 6.21, showing reasonable agreement. As expected, the patch with the longest slot (14 mm) yields the lowest resonance frequency at 4.72 GHz while the highest resonance frequency 5.26 GHz is held by the one with the shortest slot (6 mm). The resonance frequency in the middle corresponds to the patch with a slot of length of 10 mm. Theoretically the resonance frequency can be further decreased by extending the slot length or introducing more slots [174].

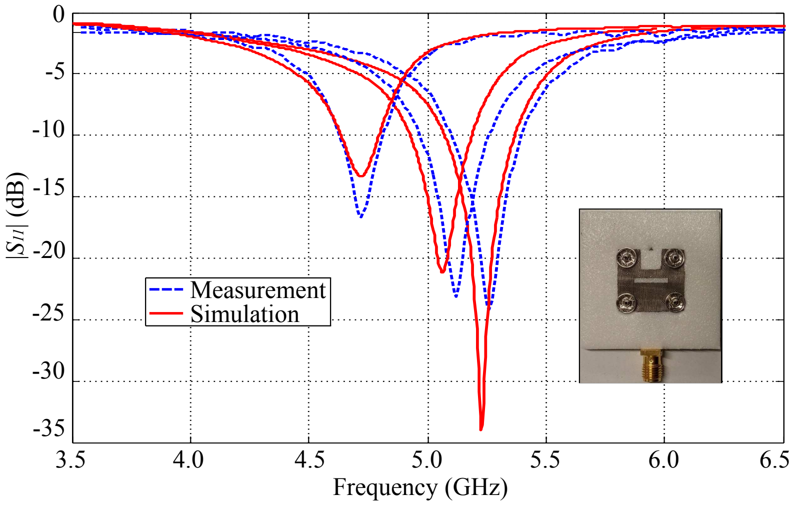

Figure 6.21. **$|S_{11}|$ of the antenna with the slotted LP modules.** S-parameter comparison of the antenna loaded with slotted frequency interchangeable patch modules. The lowest, medium and highest resonance frequencies correspond to the modules with slot length of 14 mm, 10 mm and 6 mm respectively.

The measured normalized radiation patterns are shown in Fig. 6.22. The patterns of the standard half-wave patch are as expected for this type of antenna, whereas the patterns of the quarter-wave patch show a degradation typical for PIFA antennas, with less directivity and increased cross-polarization. The measured antenna gain for the half-wave and quarter-wave patches are 7.8 dBi and 3.1 dBi, respectively. These values are close to the simulated results of 8.3 and 3.5 dBi.

6.3.4 8 GHz module

Compared to the modules discussed before, the present patch module only provides a single functionality but with a higher degree of freedom in terms of module design: An illustrative example is designed for operation at 8 GHz and requires a two-layered structure, as shown in Fig. 6.23a. This last arrangement structure offers more freedom in module design, however at the cost of additional complexity.

This module consists of one layer of non-conductive fabric as a support with the same outline geometry as the other patches and one layer of silver fabric as a radiation element resonating at 8 GHz. This two-layered arrangement provides a more adaptable way for patch module design since the radiating element has more freedom in terms of

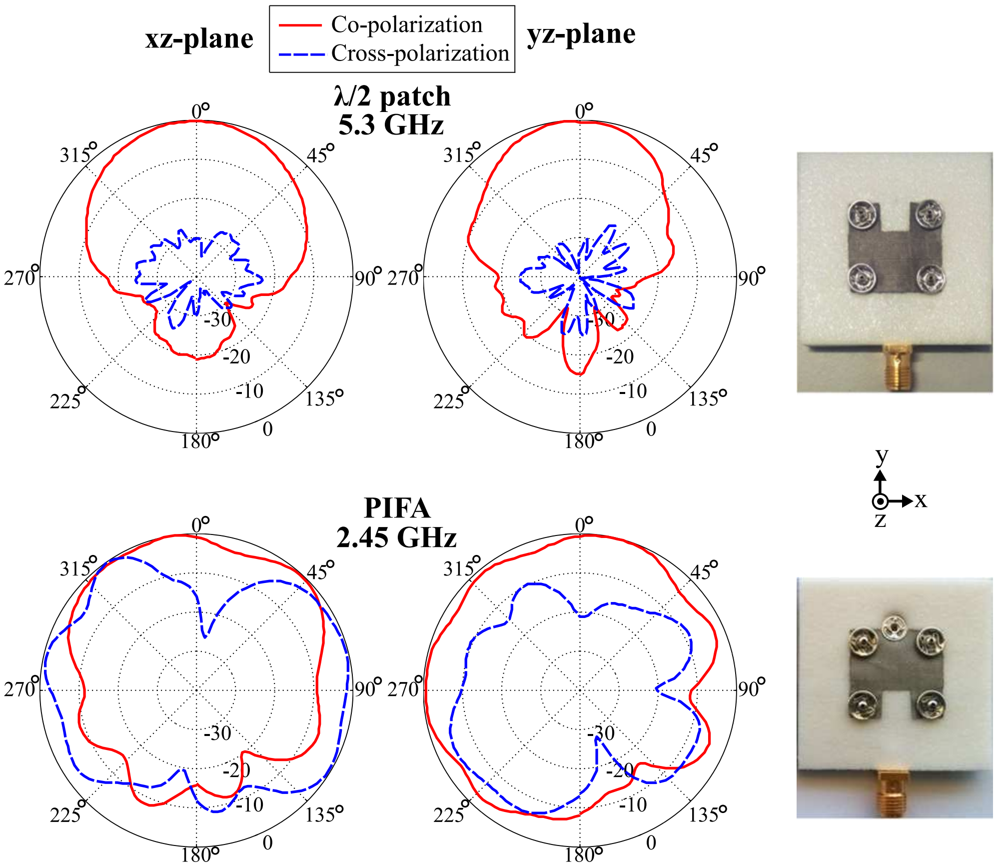

Figure 6.22. Radiation patterns of the antenna with the LP module. Measured radiation patterns of the antenna loaded with linearly-polarized 2.45- and 5.3-GHz patch modules.

size and shape selection, while the non-conductive fabric ensures mechanical fixture. The supporting fabric was chosen as cotton textile commonly used for embroidery. The fabric has a measured thickness of approximately 200 μm, as well as a relative permittivity $\varepsilon_r = 2$ and a loss tangent $\tan\delta = 0.01$ both estimated based on fitted simulation results, which broadly agree with the measured values for cotton textiles in [113,176].

As anticipated, the vertical length L_7 of the radiating element is inversely proportional to the resonance frequency. The bottom of the radiating element is tapered as a triangle to get a satisfactory matching. The antenna loaded with this patch is illustrated in Fig. 6.23b. Owing to the vicinity to the radiating element, coupling to the snap-on buttons should be taken into account in the design. This can be done with simulation tools and complicated current distributions have been observed in simulated results. Moreover, the radiating patch is facing down towards to the substrate to avoid galvanic contact with the two closest female buttons.

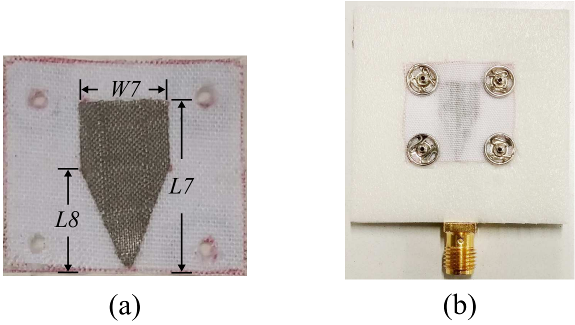

Figure 6.23. The 8-GHz module and its antenna configuration. (a) The 8-GHz module with its dimensions: $W_7 = 7.5$ mm, $L_7 = 15.2$ mm and $L_8 = 9.3$ mm and (b) the antenna loaded with this module.

The measured and simulated reflection coefficients have a good correspondence, as demonstrated in Fig. 6.24. The antenna resonates at 8 GHz with a bandwidth of approximately 500 MHz. The measured normalized radiation patterns are portrayed in Fig 6.25, and as expected, standard half-wave patch radiation patterns are observed, which is confirmed by the simulated electric field distribution of the antenna shown in the inset of Fig. 6.24. The measured antenna gain is approximately 8.9 dBi whereas the simulated one is 9.2 dBi.

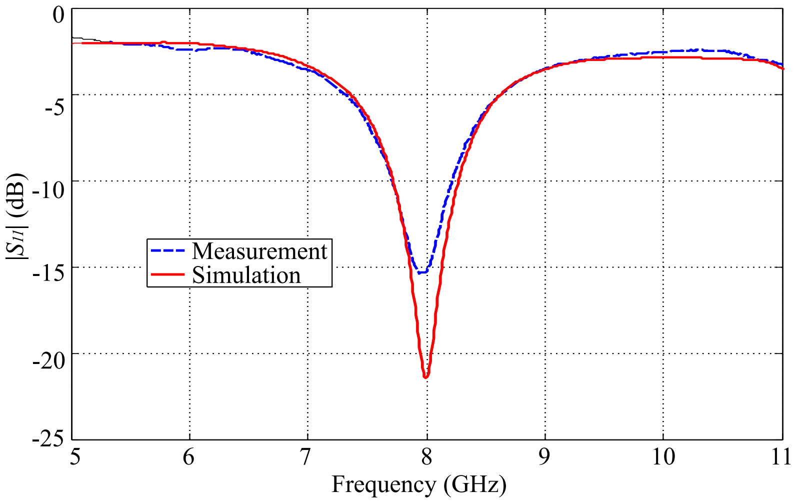

Figure 6.24. $|S_{11}|$ **of the antenna with the 8-GHz module.** Measured and simulated S-parameter comparison of the antenna loaded with 8-GHz patch module.

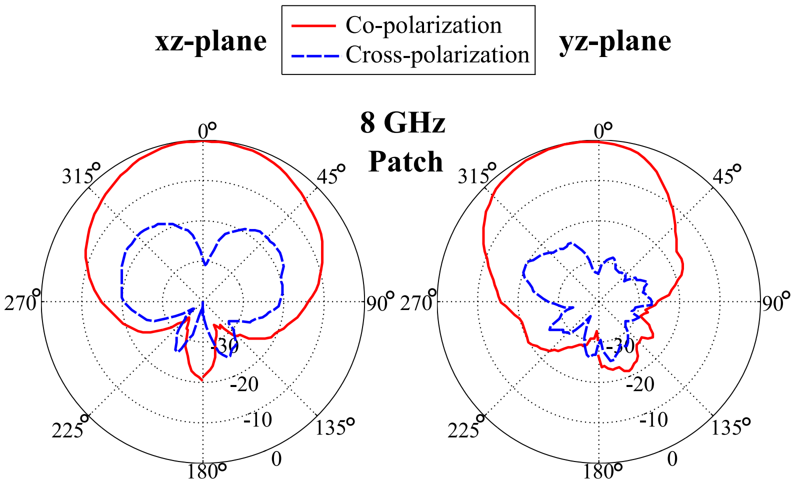

Figure 6.25. Radiation patterns of the antenna with the 8-GHz module. Measured radiation patterns of the antenna loaded with an 8-GHz patch module.

6.3.5 Foldable module

The present module offers a foldable design concept which makes good use of the very unique advantage of conductive textiles, namely mechanical flexibility and resilience. Through a simple folding of the textile radiating element at predetermined lengths denoted by position markers, particular resonance frequencies can be manually interchanged. The mechanical robustness of the conductive fabrics used ensures the durability of the antenna, especially for the proposed patch module which requires numerous foldings.

The geometry and a realization of the proposed patch module are shown in Fig 6.26. It consists of a non-conducting adhesive tape supporting substrate and a silver fabric radiating element. The adhesive tape chosen has a thickness of 100-μm whereas its relative permittivity ε_r and loss tangent $\tan\delta$ are estimated to be 2 and 0.01 according to fitted simulation results, respectively. The vertical length of the radiating patch is in inverse proportion to the resonance frequency. Therefore, folding the radiating patch at particular positions leads to effective antenna length reductions and consequently the desired increases in antenna operational frequencies. The lower section of the radiation patch is tapered as a triangle for matching. The substrate acts as a mechanical support for the radiating element which has its triangle bottom section fixed to the substrate while the rectangular top part is free to move and thus foldable. The two dash lines on the radiation patch upper section shown in Fig 6.26a indicate the respective folding positions for the realized antenna resonance frequencies at 9 and 10 GHz. Hence, together with the unfolded configuration, this antenna module can have three discrete interchangeable resonance frequencies at 8, 9 and 10 GHz. The antenna loaded with the foldable module in these three configurations is demonstrated in Fig. 6.27. The radiating patch is placed in between its substrate and the common base where the tight and secured compression confines the radiation element in both unfolded and folded conditions. This is an important requirement to ensure reproducible antenna performance.

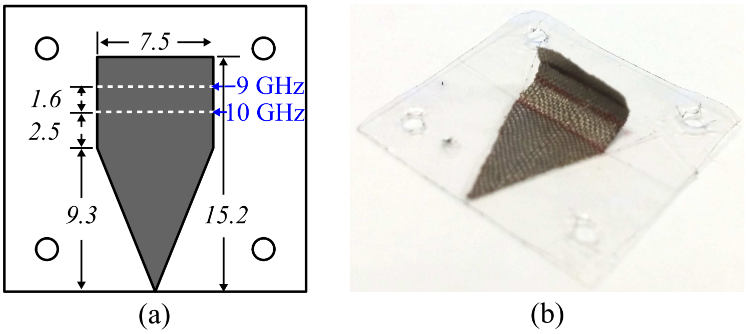

Figure 6.26. The foldable patch module. (a) The configuration and dimensions (mm) of the foldable patch module. The two dash lines indicate the radiation element folding positions for the 9 and 10 GHz configurations. (b) A prototype module realization.

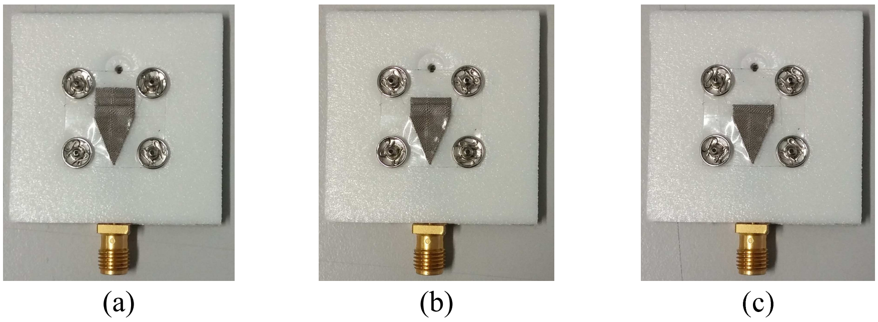

Figure 6.27. Antenna loaded with the foldable module. Antenna realization in the three configurations: (a) 8-GHz unfolded configuration. (b) 9-GHz folded configuration. (c) 10-GHz folded configuration.

It is worth mentioning that the proposed module is not limited to these frequencies and theoretically the antenna can be tuned to any operating frequency between 8 GHz and 12 GHz (X-band). However, options are limited by the practicality of precise folding positions. Nevertheless, overall module usability and operability can be improved by clear and accurate marking of the folding positions on the radiating patch and the substrate accordingly. For this reason, a transparent substrate is preferable as it is easier for visual validations.

In order to verify the performance of the foldable module, a prototype has been fabricated and experimentally characterized, as shown in Fig. 6.26b. Firstly, two pieces of adhesive tape are tailored to the required substrate dimensions, with one of them having a triangle slot of the same dimensions as the radiating element bottom section. Secondly, these two tapes are aligned and attached onto each other (on the adhesive side). A laser-cut silver fabric radiation patch is stuck on it at the precut triangle position. Finally, the folding lines are marked on the patch and the substrate.

The measured and simulated reflection coefficients in the three configurations are plotted in Fig. 6.28. A very good agreement between measurements and simulations is observed. The antenna has resonance frequencies at 8, 9 and 10 GHz whereas the operation ranges are 7.7 - 8.3 GHz (600 MHz), 8.6 - 9.4 GHz (800 MHz) and 9.4 - 11.8 GHz (1400 MHz) for the three configurations, respectively. Based on these results, the X-band frequency spectrum (8 - 12 GHz) can be fully covered by this module design with three appropriate folding positions.

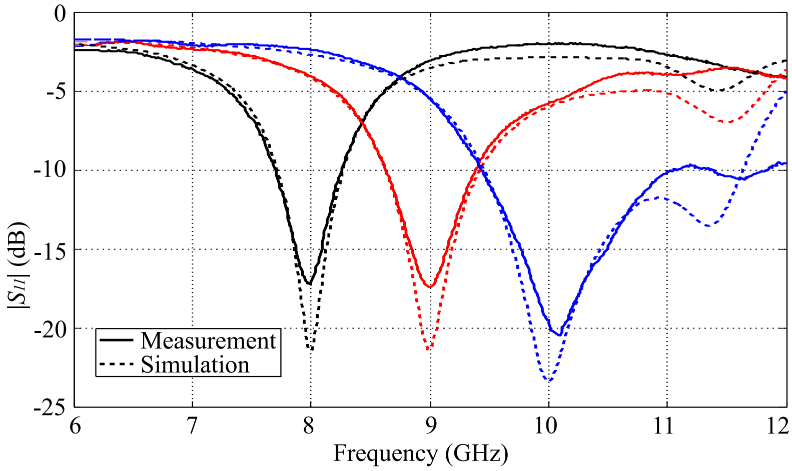

Figure 6.28. $|S_{11}|$ of the antenna with the foldable module. Reflection coefficient comparison of the antenna loaded with the foldable patch module in three different configurations: unfolded 8 GHz, folded 9 GHz and folded 10 GHz.

The xz-plane and yz-plane radiation pattens of the antenna in the three configurations (Fig. 6.27) are shown in Fig. 6.29 and they are normalized to the maximum gain. As expected, these patterns exhibit typical half-wave microstrip patch characteristics. It is noted that the main beam slightly steers away from the +z-axis direction ($\theta = 0°$) toward the +y-axis with increasing antenna resonance frequency. This can be caused by the shortening radiating element electrical length which effectively enlarges the asymmetry introduced by the matching triangle section. The measured maximum gains of the antenna are 9.2, 9.3 and 9.2 dBi for the 8, 9, and 10 GHz configurations respectively, whereas the simulated ones are 9.1, 9.2 and 9.4 dBi accordingly.

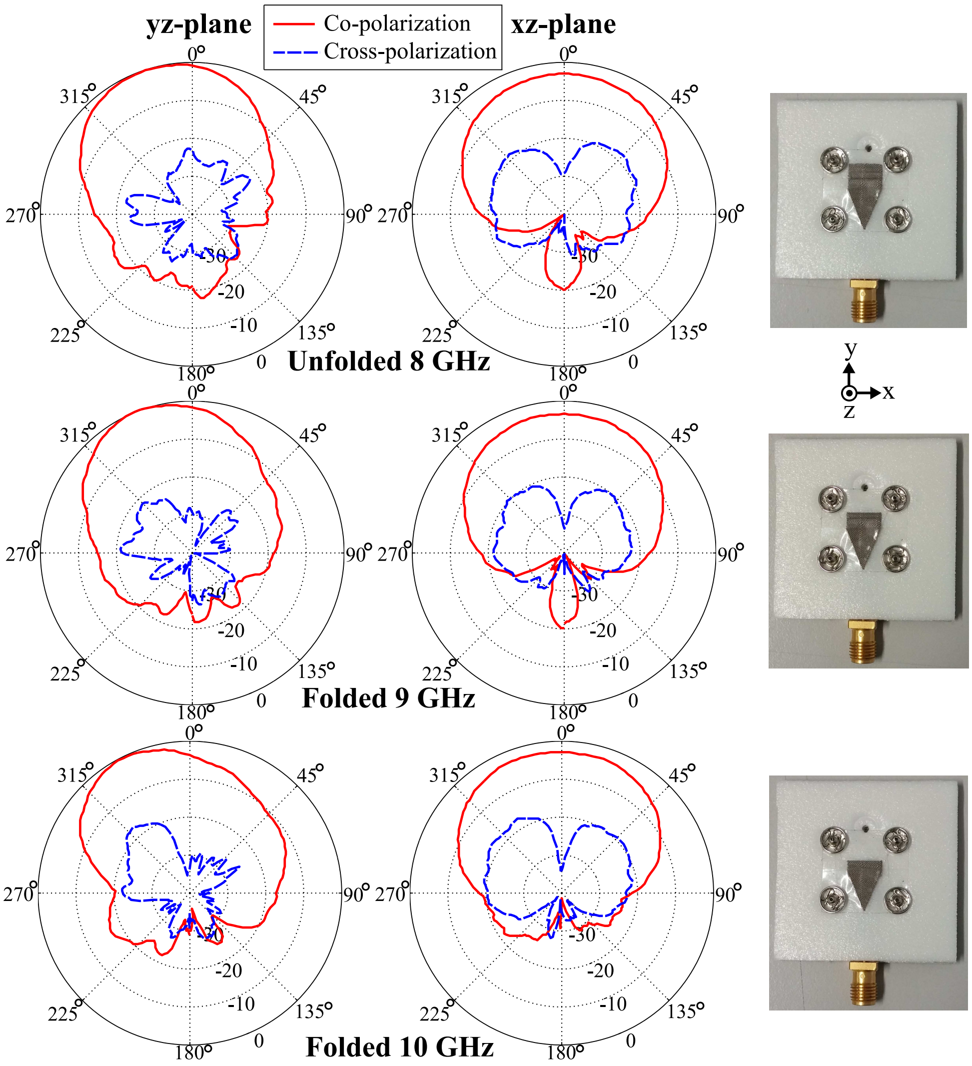

Figure 6.29. Radiation pattens of the antenna with the foldable module. Measured normalized xz- and yz-plane radiation patterns of the antenna loaded with the foldable patch module in three different configurations: unfolded 8 GHz, folded 9 GHz and folded 10 GHz.

6.3.6 Summary on module designs

This section has demonstrated five different patch modules for the proposed modular antenna design, dedicated for various antenna modularity in regard to polarization and resonance frequency. In order to achieve modularity in antenna polarization, as shown in the first two modules, one can alter the current direction and distribution, through changing the orientation of its center slot by the means of flipping or rotating of the module. In terms of resonance frequency modularity, closing/opening/rotating a slot in the module, ground shorting the module and folding the radiating element of the module are the mechanisms utilized for the reported modules in Section 6.3.2, 6.3.3 and 6.3.5, respectively. These mechanisms are also based on controlling the current direction and distribution of the modules. The modules demonstrated in Section 6.3.4 and 6.3.5 show typical two-layer designs which offer more freedom in module design, however at the cost of additional complexity. In summary, these five modules shed a light on some useful and practical strategies and guidelines for designing patch modules.

6.4 Human body and bending impact

As the proposed modular antenna is designed for wearable applications, two critical aspects of wearable antenna designs namely the impact on antenna characteristics due to antenna bending as well as vicinity of a human body, are investigated respectively. An antenna loaded with the LHCP-RHCP module is chosen as the test bed here due to its highly sensitive circular polarized antenna performance. Based on experimental results which will be discussed in the following two sections, the antenna only has insignificant performance degradation under these two impacts.

6.4.1 Human body impact

As wearable antennas are expected to be worn by humans or animals, the impact on antenna characteristics in the vicinity of a human body has been investigated with a torso phantom. The torso (TORSO-OTA-V5.1 from SPEAG) is an anthropomorphically shaped [177] shell phantom which is filled with a broadband tissue simulating gel complying with human target parameters in [178,179] up to 6 GHz. An antenna loaded with the CP interchangeable patch module in the LHCP configuration is chosen in this study. The antenna is attached to the phantom and then measured together in an anechoic chamber, as illustrated in Fig. 6.30.

The measured reflection coefficient and axial ratio for the LHCP antenna placed on the phantom are plotted in Fig. 6.31 and Fig. 6.32, respectively. Insignificant discrepancies

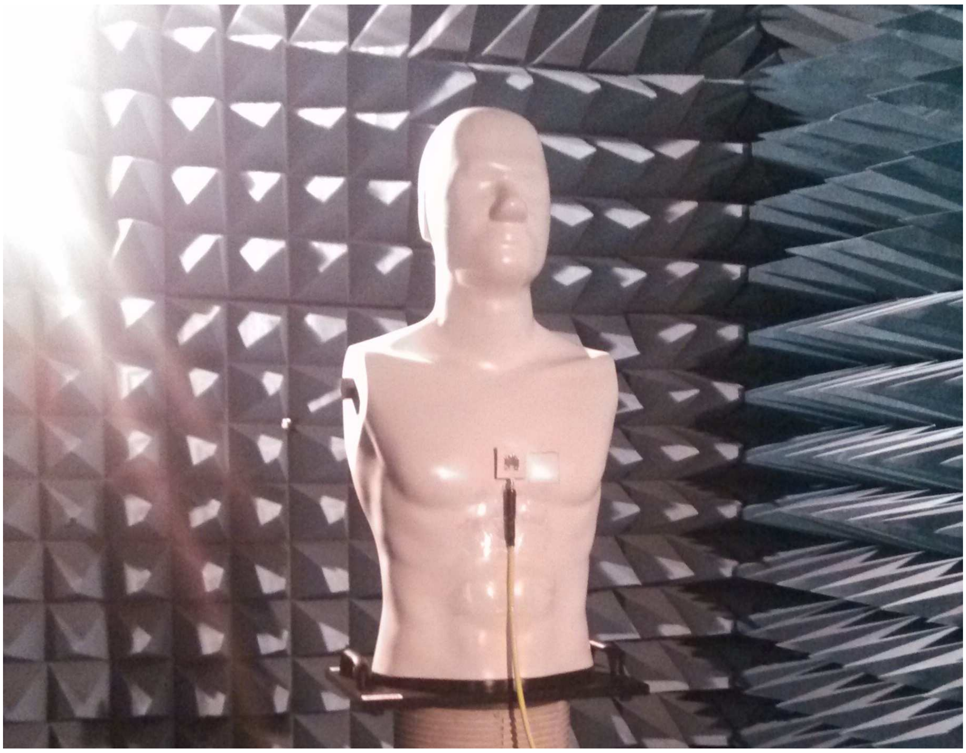

Figure 6.30. An antenna loaded on a torso phantom in an anechoic chamber. An antennas loaded with the LHCP-RHCP module is attached to a torso phantom in an anechoic chamber for testing.

in these comparisons due to the human phantom are observed. In addition, for representation of the radiation characteristics in Fig 6.33, the on-body radiation patterns are normalized to the maximum values in free space, and a slight reduction in LHCP component due to the phantom is observed in both planes. This is confirmed with the simulated and measured realized gain of the antenna shown in Fig. 6.34. In most of the frequency range, there is a reasonable agreement between the antenna realized gain measured in free space and with the phantom. Only a small gain decrement (maximum 0.7 dB) due to the human body is observed in a short frequency range around 5 GHz.

All these results indicate a rather low impact on the antenna performance when worn on the human body. The resilience to degradation when worn on the body is attributed to the isolation effect of the ground plane.

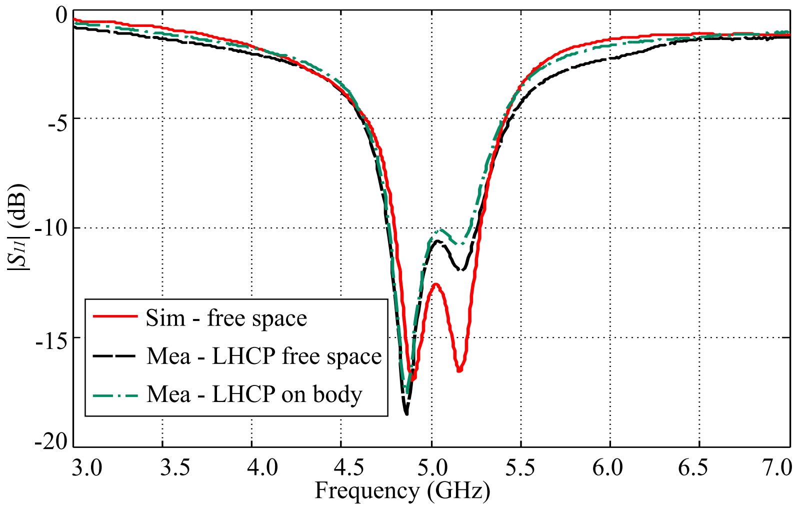

Figure 6.31. $|S_{11}|$ of the LHCP antenna in free space and on a phantom. Reflection coefficient comparison of the antenna loaded with the CP interchangeable module in free space and loaded on a phantom.

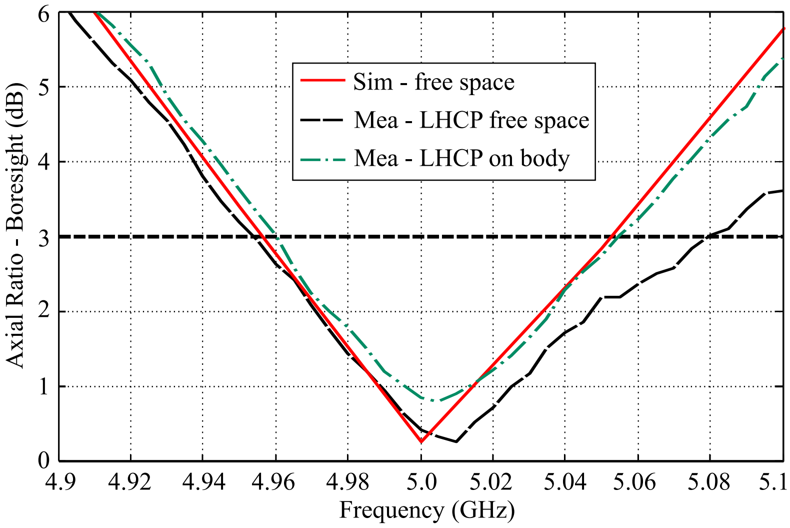

Figure 6.32. AR of the LHCP antenna in free space and on a phantom. Boresight axial ratio of the antenna loaded with the CP interchangeable module in free space and loaded on a phantom.

6.4.2 Bending impact

Another critical aspect of wearable antennas is the influence of bending on their performance. To assess this effect, an investigation of the same antenna under two bending configurations has been carried out. The bending test setup is shown in the inset of Fig. 6.35: namely bending along the y-axis with radius of 30 mm (approximately a forearm radius) and 40 mm (approximately an upper arm radius) respectively. Practically, bending along the x-axis should be avoided since more significant alterations

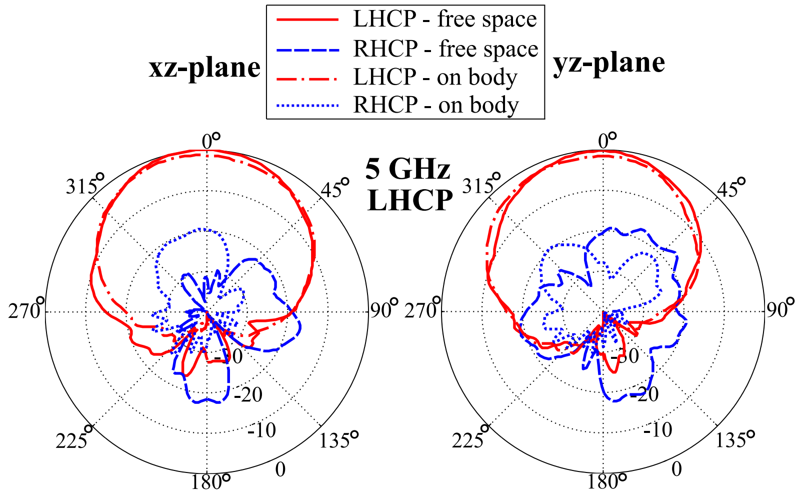

Figure 6.33. Radiation patterns of the LHCP antenna in free space and on a phantom. Measured normalized radiation patterns of the antenna loaded with the CP interchangeable module in free space and loaded on a phantom.

in the effective patch length (L_2) and consequently resonance frequency are anticipated [15, 180]. The measured reflection coefficients of the antenna under unbent and two bent configurations are illustrated in Fig. 6.35. There are no significant variations on the measured $|S_{11}|$ parameters introduced through the antenna bending. This is attributed to the compact size of the antenna leading to minor bending which results in only a small effective antenna length alteration. This result implies that the bending configuration should have a small influence on the impedance bandwidth of both circularly and linearly polarized modules.

In regards to the axial ratio of the bending antenna, the measured results are plotted in Fig. 6.36. According to the measurements, the axial ratio at 5 GHz is less than 3 dB and 5 dB for 40-mm and 30-mm bending radii, respectively. This degradation of the axial ratio bandwidth is not unexpected and can be caused by the changes in the resonance frequencies and the phase differences of both orthogonal modes [180]. A similar phenomenon for a bent circularly polarized textile antenna has been reported in [15]. These findings suggest that the axial ratio of the antenna is still within an acceptable range with a small bending radius (considering an often quoted relaxed tolerance of 6 dB). Therefore, the study indicates that the bending effect should still allow operation of the antenna with slightly degraded axial ratio.

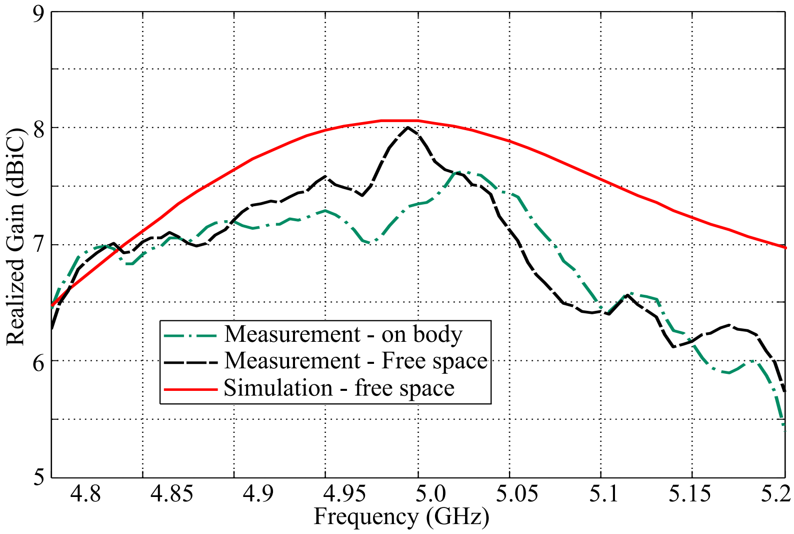

Figure 6.34. Gain of the LHCP antenna in free space and loaded on a phantom. Simulated and measured realized gain of the antenna loaded with the CP interchangeable module in free space and loaded on a phantom.

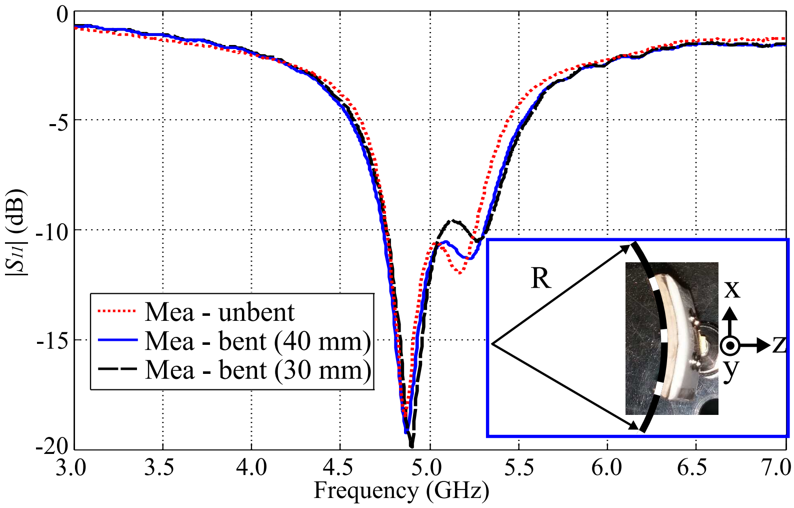

Figure 6.35. $|S_{11}|$ of the LHCP antenna under unbent and bent conditions. Measured reflection coefficients of the antenna under unbent and bent conditions. The inset shows the bending test settings. Two bending radii of the antenna have been determined as R = 30 mm and R = 40 mm respectively. The antenna was bent along the y-axis.

6.5 An extended design with detachable shortings

As mentioned in Chapter 5, an efficient, low-loss and reliable shorting strategy is crucial for designing textile antennas which require ground shorting(s) and/or shorting wall(s). Since commercial metallic snap-on buttons can be employed as detachable

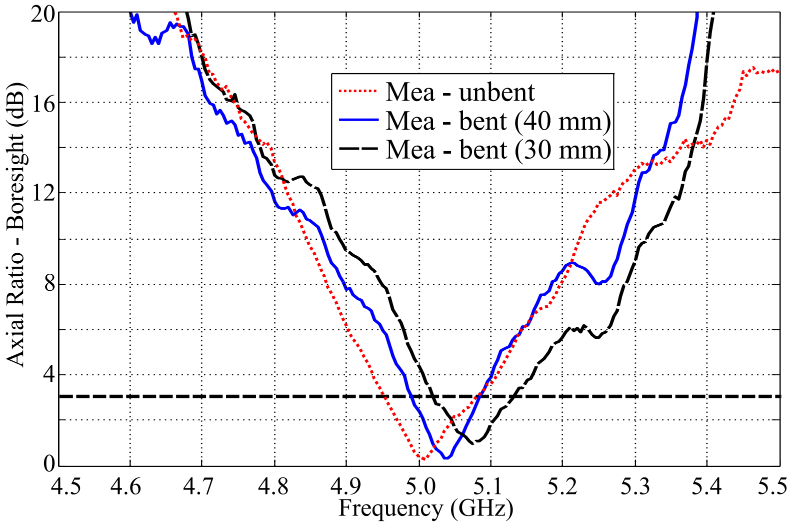

Figure 6.36. AR of the LHCP antenna under unbent and bent conditions. Measured axial ratios of the antenna under unbent and bent conditions.

RF connectors for conductive fabrics with satisfactory mechanical and electrical performance, they are one class of the suitable components for shorting realization for textile antennas. This has been proven in the antenna loaded with the PIFA module, as discussed in Section 6.3.4. The modularity of the present antenna design can be further enhanced when detachable ground shorting(s) based on these snap-on buttons are introduced. To demonstrate this idea in this section, four detachable shortings are integrated into the common feed base of the modular design, which enables a more versatile modularity in antenna pattern characteristics. Then a configuration of this extended design providing interchangeable beam direction is experimentally characterized.

6.5.1 Antenna configuration

The antenna configuration and dimensions are shown in Fig. 6.37. On top of the modular antenna structure as depicted in Fig. 6.2, four additional male snap-on buttons are soldered back to back to the four original male buttons embedded in the middle of the two-layered substrate, to form detachable shortings for the antenna. The two-layer substrate delivers solid and secure positioning for these four shortings. When engaged to female button counterparts, the top four male buttons serve as holders for patch modules whereas the bottom four can be selected to act as engageable shorting vias to the ground plane. By engaging different male button(s) with female one(s), the patch module can be shorted at different corners and thus resonate in different modes.

Therefore modularity in antenna resonance frequency, polarization and beam direction can be achieved on the basis of the common base structure.

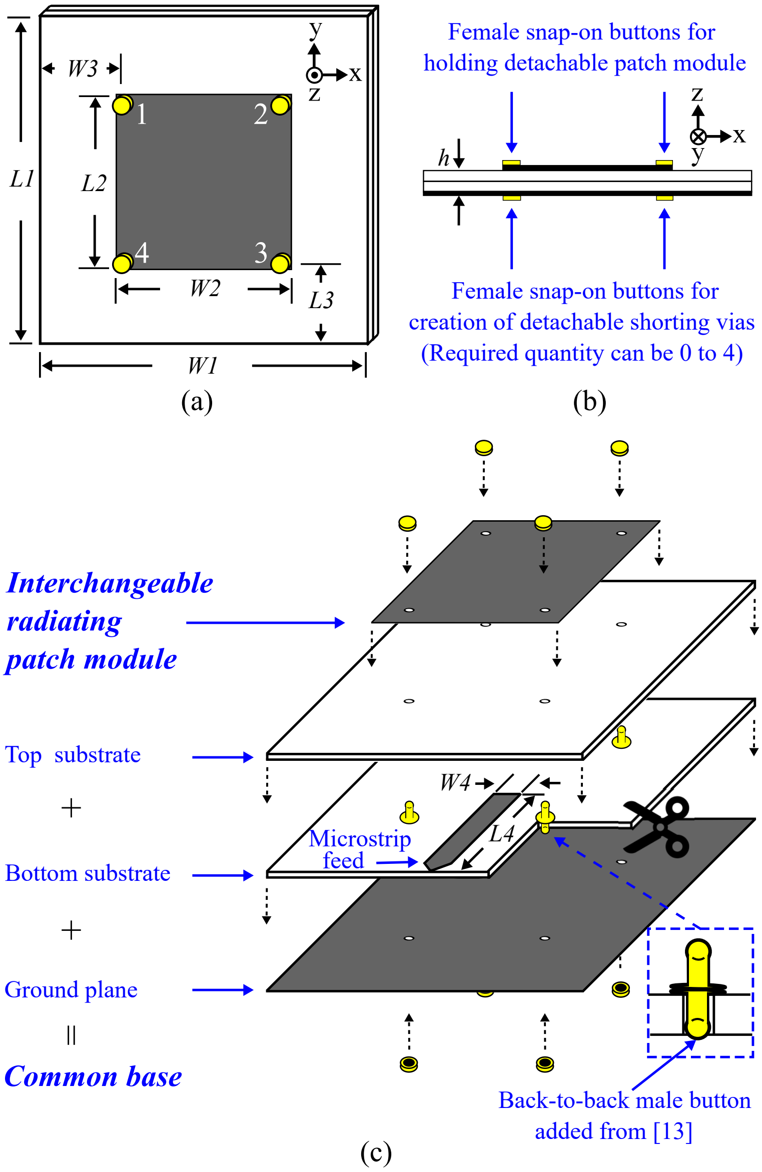

Figure 6.37. Extended design with detachable ground-shortings. Antenna configuration and dimensions. (a) Top view. (b) Side view. (c) Configuration: the antenna consists of an interchangeable radiating patch module and a common base which contains a two-layered substrate, a ground plane, a microstrip feed and snap-on buttons. Shorting vias are created by engaging female buttons on the back of the ground plane.

6.5.2 Configuration with vias

As mentioned, modularity in antenna characteristics can be obtained using various patch modules and different detachable shorting configurations. For instance, the proposed antenna module resonates in the standard half-wave mode with boresight radiation when no shorting vias are engaged. In contrast, when all four vias are engaged, the antenna operates in a planar monopole mode with omnidirectional radiation in the xy-plane [181]. These two configurations can be beneficial for wearable applications where either on-body or off-body communications are desired [182]. However, for brevity, only one particular shorting configuration for the patch module is discussed in this section, namely using shorts at either opposite corners 1 and 3 or 2 and 4 (see Fig. 6.37a. This configuration leads to the radiation pattern being split into two main beams pointing along the diagonal plane in between xz- and yz-planes.

With such shorting vias arrangement as shown in Fig 6.38, the patch module resonates in a mode similar to a magnetic current loop antenna [183], but with electric field nulls at the two shorted corners, and electric field maximas at the two other corners. Based on the equivalence principle, the antenna can be approximately considered as two antiparallel magnetic currents whose highest amplitudes are at the two ungrounded patch corners. As a result, the antenna possesses two main beams pointing away from these unshorted corners. Therefore, through interchanging the location of the shorted corners, the main beam directions can be rotated by 90°. The 3D radiation patterns simulated in CST is depicted in Fig. 6.39, for the configuration with shorts at corners 1 and 3. It clearly illustrates the expected two main beams. The resonance frequency of this particular design is 3.6 GHz which is determined by the length and width of the patch module. It is worth mentioning that for this demonstration the patch dimension was unchanged from Table 6.1, but in principle, the geometry is scalable to achieve other operational frequencies.

6.5.3 Experimental results

To validate the design, a prototype, as shown in Fig 6.40, has been fabricated and experimentally characterized. Two main modifications from the modular design shown in Fig. 6.2 are needed. The first modification was soldering one male snap-on button underneath the original ones individually, with precise back-to-back alignment. The second modification was cutting four through holes in the bottom substrate and the

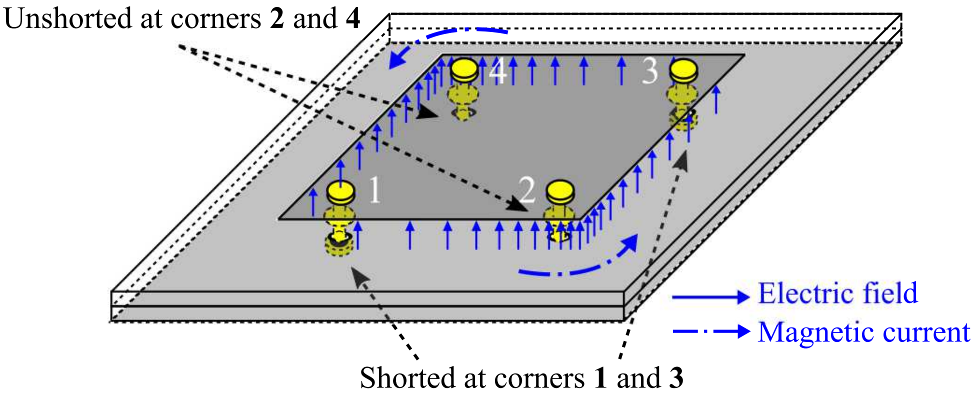

Figure 6.38. Working principle of the proposed configuration. Electric field distribution of the antenna with engaged shorting vias at corners 1 and 3.

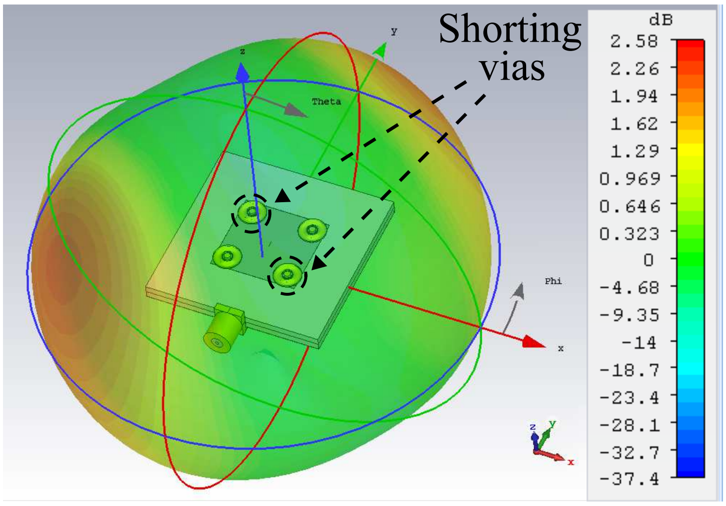

Figure 6.39. Simulated 3D gain pattern of the antenna. The simulated 3D gain pattern of the proposed antenna.

ground plane, to accommodate and provide enough clearance from the added male buttons, respectively. To ensure repeatable electrical connection to the ground plane, the holes trimmed in the ground plane should be smaller than the flat contact area of the female buttons.

The simulated and measured reflection coefficients of the antenna with shorts at corner 1 and 3 are demonstrated in Fig 6.41 and a reasonable agreement is observed. The simulated resonance frequency is 3.6 GHz while the measured value is 3.62 GHz. The small discrepancy can be attributed to the fabrication tolerances.

For the same shorting configuration, the measured antenna radiation patterns at 3.6 GHz in the 45°-plane ($\phi = 45°, 225°$) and 135°-plane ($\phi = 135°, 315°$) in between *xz*- and *yz*- planes are shown in Fig. 6.42. As anticipated, in the 45°-plane, the two main

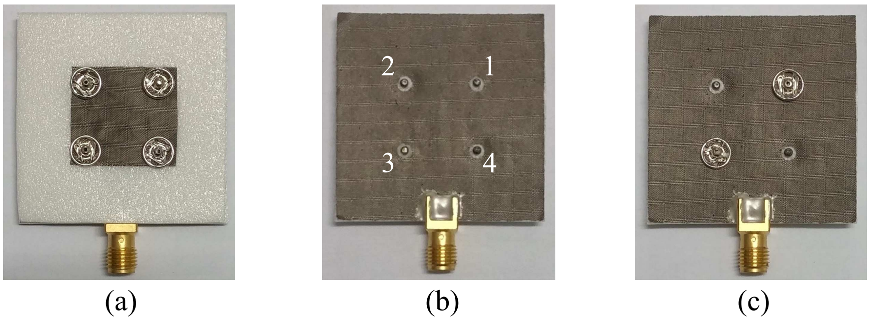

(a) (b) (c)

Figure 6.40. A realization of the proposed antenna. The antenna realization. (a) Top view. (b) Bottom view without female snap-on buttons (no shorts to the ground). (c) Bottom view with engaged female button at corners 1 and 3.

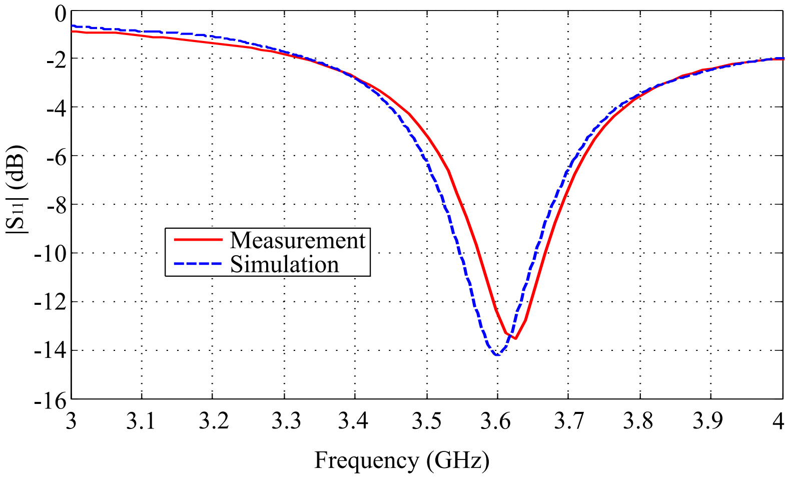

Figure 6.41. $|S_{11}|$ of the antenna with shorts at corner 1 and 3. Measured and simulated $|S_{11}|$ of the antenna with shorts at corner 1 and 3.

beams are pointing away from the ungrounded patch corners. In contrast, the patterns in the 135°-plane are nearly omnidirectional and with a small amplitude, which again agrees with the expectations of Fig 6.39. Because of symmetry, the radiation patterns of the configuration with shorts at corners 2 and 4 should be identical, however, with a 90° anti-clockwise rotation.

6.5.4 Summary of the design

The concept of utilizing commercial snap-on buttons as detachable shorting vias has been implemented together with the modular design. Owing to the utilization of the modularity and the detachability in the shorting vias, the extended antenna design opens more possibilities in designing versatile modularities for providing desired antenna radiation characteristics. The design has been validated through experimental

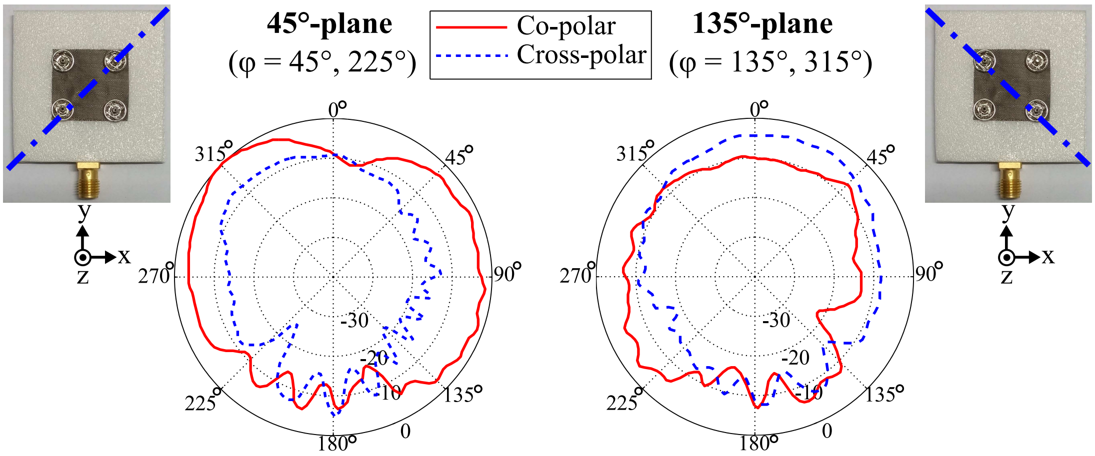

Figure 6.42. Radiation patterns of the antenna with shorts at corner 1 and 3. The measured normalized radiation patterns of the antenna in the 45°- and 135°-plane at 3.6 GHz. The diagonal dotted lines on the antenna indicates the 45°- and 135°-planes. Corners 1 and 3 were shorted in this antenna configuration.

characterization of a dual-beam configuration. The good agreement between simulation and measurement demonstrates the validity of using snap-on buttons as detachable shorting vias. It further suggests a concept where simple manual operations can allow passive reconfiguration of modular textile antenna designs by engaging/disengaging vias.

6.6 Conclusion

In this chapter, a textile modular antenna design for wearable applications has been proposed utilizing commercial snap-on buttons as mechanical and electrical (RF) connectors. Different textile patch modules can be designed to serve various functionalities such as variations in antenna resonance frequency, polarization and possibly beam direction. These modules can be attached to one common proximity-feeding base consisting of ground plane, substrate and open microstrip line. Therefore, this antenna design brings advantages such as low manufacture and maintenance cost, and most importantly, provides a passive way to reconfigure system characteristics for multi-functional wearable systems. Five modules providing interchangeability in linear and circular polarization and resonance bands have been designed, manufactured and experimentally characterized. The measurement results are in very good agreement with simulations. The impact on antenna characteristics due to human body vicinity and small radius bending have also been investigated and the results indicate only an insignificant effect on the reflection coefficient, but some degradations of the circular polarization, which is notoriously sensitive to geometry variation. In addition, the idea of using commercial snap-on buttons to realize detachable shorting vias has been exploited in conjunction with this modular design, resulting in an extended device which can possibly achieve more versatile modularities. All these findings suggest that the reported wearable modular antenna design brings advantages such as low manufacturing and maintenance costs, and most importantly, passive and versatile system characteristics modularities.

Chapter 7

Reconfigurable Wearable Textile Antenna

TEXTILE antennas are well suited for wearable applications, since they can be made flexible, light-weight, electrically and mechanically robust and can be integrated in garments. Additionally, wearable textile antennas should be immune to the impact of bending and interactions with the human body. These two features are the most important and challenging to achieve, but they are paramount to the system reliability. One can exploit frequency-reconfigurable antenna designs to compensate the effect of loading by the human body and the impact of bending. However, very limited research on reconfigurable textile antennas has been reported in the literature, due to the issue associated with the very different physical properties of the rigid and flexible components.

As evolution of the previous chapter on modular textile antenna, this chapter proposes an idea of reconfigurable modules utilizing commercial snap-on buttons in conjunction with integrated varactors and a dedicated bias circuit board. This component can be used to design reconfigurable textile antennas promoting a secure protection for the rigid electronic circuit components combined with a stable and repeatable electrical connection to textiles. A wearable textile patch antenna using a first design of the proposed reconfigurable button module is designed. Preliminarily tests of the concept demonstrate a measured 15.1% frequency tuning range. This suggests that the button module concept is a practical and promising engineering solution for reconfigurable textile antennas.

7.1 Introduction

The interest in wearable electronic systems and their development have dramatically increasing in the last couple of years, both for civil and military applications [2, 112]. As a result, wearable antenna design has become a hot research topic in antenna technology. Since these antennas are flexible, light-weight and electrically and mechanically robust, conventional metallic materials are no longer suitable due to their very limited mechanical resilience. Therefore, novel materials including conductive polymers [5, 85], conductive inks [184], threads [8, 12, 16, 139, 160, 185] and conductive textiles [13–15, 17, 18, 21, 22], have been emerging as the appropriate conductors.

In particular, conductive threads and textiles are two of the most popular conductors for wearable antennas, since they are highly flexible and conductive, light-weight, robust, low-cost and garment-integratable. As a consequence, a wide range of wearable antennas utilizing textile-based materials have been reported in the literature. They range from narrow band [14, 15] to ultra-wideband [18] in terms of operational frequency, from broadside [13, 31, 122] to omni-directional [31] in terms of radiation patterns, and from planar [139, 186] to waveguide-based [21, 22] in terms of antenna structure. Besides these passive antennas, however, only very limited active/reconfigurable textile antennas [127, 187, 188] can be found in the open literature, even if they are highly desirable for wearable applications. This is mainly due to the challenges in achieving reliable textile-to-electronics connections. Reconfigurable antennas can adapt their radiation characteristics such as resonance frequency and radiation patterns, to compensate the detrimental impact on their performance introduced by bending, various environmental conditions like temperature and humidity and interactions with the human body.

A few reconfigurable antennas have been proposed for wearable applications recently, however, they all show limitations on wearability attributed to mechanical inflexibility and/or stability due to the materials and electronic components connection. For example, a radiation pattern reconfigurable monopole/loop antenna realized in FR-4 for a wearable device Fitbit® Flex was proposed by Lee et al. in 2014 [189], as shown in Fig. 7.1. The antenna features a very solid and stable connection between the copper conductors and the electronic components through soldering, however, the inherent mechanical inflexibility of the materials probably restricts the antenna to this Fitbit® device.

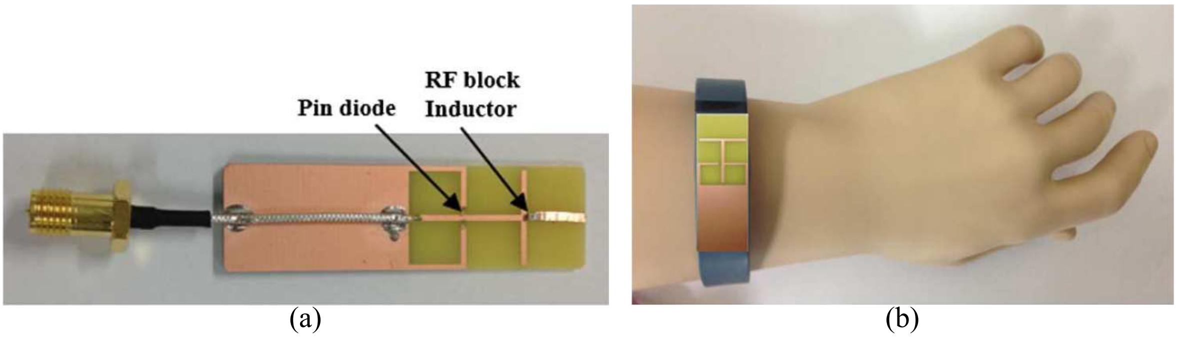

(a) (b)

Figure 7.1. A rigid reconfigurable antenna for a wearable device. (a) A prototype of a radiation pattern reconfigurable monopole/loop antenna realized in FR-4 rigid material, worn by a phantom (b), adapted from [189].

A flexible frequency reconfigurable antenna was reported by Tahir et al. one year later [187], as depicted in Fig. 7.2. This antenna exhibits very good flexibility by using textile substrate and copper tape conductor. However, copper tape is not a very suitable conducting material for wearable devices, as its deformation through external forces is easily irreversible, which will be detrimental for antenna performance and stability. It is believed that another main purpose of using coper tape is its possibility to be soldered, which is necessary to obtain stable connection for the lumped components. If a conductive textile were used instead of the copper tape in this design, the connection between the textile conductors and the lumped components would not be stable, due to their very different physical properties.

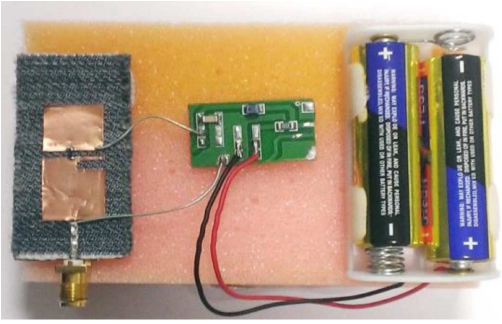

Figure 7.2. A flexible reconfigurable antenna for wearable applications. A prototype of a flexible frequency reconfigurable patch antenna realized in textile and copper tape, adapted from [187].

A radiation pattern reconfigurable textile antenna concept based on metamaterial structure was proposed by Yan recently [188]. The antenna utilizes felt as substrate and conductive textile as conductor and thus features excellent conformability. The pattern reconfigurability between broadside and omni-directional at the 2.4-GHz ISM band was conceptually validated, through testing two prototypes with and without a connection line which simulate the on and off status of a PIN diode, as shown in Fig. 7.3. One can expect that it will be very challenging to securely connect an actual PIN diode between two pieces of fabrics, with reliable and durable performance. Especially when worn by a human subject, the antenna and its lumped components would have high probability to experience external forces which will affect the durability of the connections.

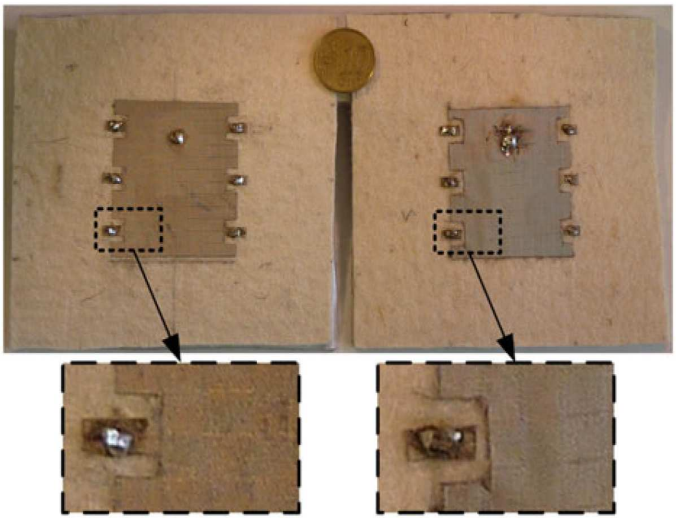

Figure 7.3. A reconfigurable textile antenna concept for wearable applications. Two prototypes of a radiation pattern reconfigurable patch antenna realized in felt and conductive textiles, one with a textile line connected to the vias holes and the other without, adapted from [188].

As discussed in Chapter 5 and 6, commercial snap-on buttons have been proposed as detachable RF connectors for wearable textile antennas [54, 55, 57, 58], since these buttons have excellent compatibility between electronics and textiles and can offer solid mechanical and electrical performance [55]. Based on these advantages of snap-on buttons, they are proposed in this chapter to be exploited in conjunction with integrated varactors and a dedicated bias circuit board to realize reconfigurable button modules for textile antennas. A button module is designed and implemented in a standard textile patch antenna to obtain a frequency tuning range of 15.1%. This validates the proposed concept as a practical and promising engineering solution for reconfigurable textile antennas.

7.2 Reconfigurable button modules

7.2.1 General concept

The general schematic of the proposed reconfigurable button module concept is depicted in Fig. 7.4a, with a diagram of its usage provided in Fig. 7.4b. The button module consists of two parts: first, a dedicated circuitry unit integrated in the middle of the device with a series of lumped components forming a bias circuit; and second, two male snap-on buttons soldered on top and bottom of the circuit unit which act as RF connectors for textiles and can be affixed to their female counterparts. Depending on the antenna design, the bias circuitry may contain DC-blocking capacitor C, active component such as varactor VC and/or PIN diode, RF-blocking resistor R and RF-choke inductor L. The main functionality of the dedicated circuit unit is to provide a compact bias circuitry with robust mechanical protection and soldered connection to the male snap-on buttons. Two female counterpart snap-on buttons are to be engaged with these male buttons to deliver a secure mechanical and electrical connection to the textile materials, as indicated in Fig. 7.4b. It has been proven in Chapter 5 and 6 that these snap-on buttons can offer repeatable solid mechanical connections with satisfactory RF performance for textile materials. Based on this general module structure, button modules with dedicated circuitry unit can be designed for different reconfigurable textile antennas. For instance, one can design a module with a PIN diode instead of the varactor, to achieve a controllable RF switch rather than a tunable capacitor.

7.2.2 The proposed button module

As a proof of this concept, one button module containing a varactor VC, an RF-blocking resistor R and an RF-choke inductor L, is designed and implemented to realize a frequency reconfigurable textile patch antenna for wearable applications. The schematic circuit diagram and a prototype of the designed button module are shown in Fig. 7.5a and b, respectively. By applying different reverse DC bias voltage through the RF-blocking inductor and resistor, the varactor linking two male buttons will have different capacitance accordingly and thus act as a reconfigurable RF circuit for antenna designs.

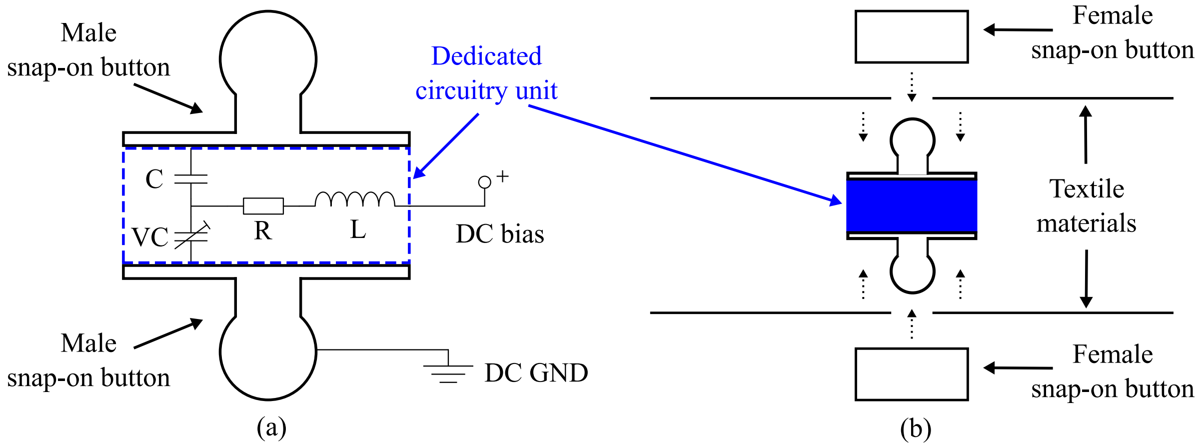

Figure 7.4. General schematic and usage diagrams of the button module concept. (a) General schematic and (b) usage diagrams of the proposed button module concept, where C, VC, R, L are DC-blocking capacitor, varactor, RF-blocking resistor and RF-choke inductor respectively. These components may be loaded on a dedicated circuit unit. The dedicated circuitry unit is soldered with two male snap-on buttons on its top and bottom surfaces for textile connection. The button module is to be engaged with two female snap-on buttons for secure connection with textile materials.

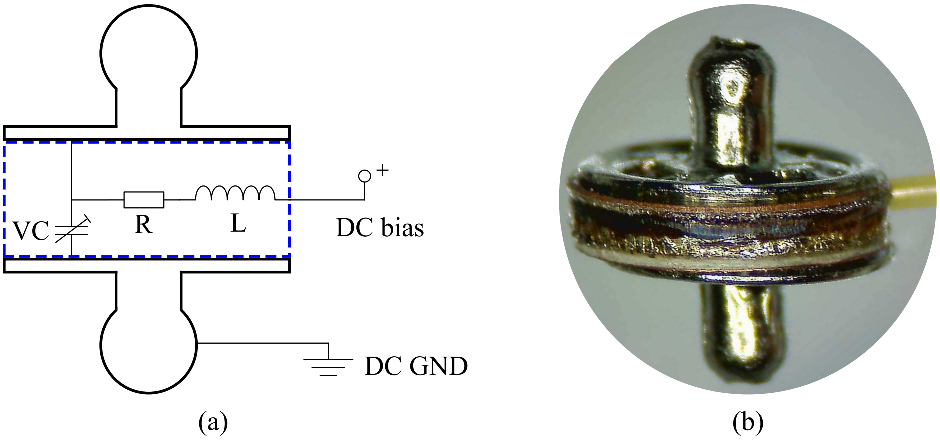

Figure 7.5. Schematic diagram and a prototype of the button module designed. (a) The schematic diagram and (b) a prototype of the proposed button module as a proof of concept, where VC, R and L are varactor, RF-blocking resistor and RF-choke inductor, respectively. Two male snap-on buttons are soldered on the dedicated circuitry unit for textile connection.

Two 3D exploded configuration figures of the circuitry unit are illustrated in Fig. 7.6. The circuitry unit contains a cover and a ring made of copper and a circuit board realized in Rogers RT/Duroid® 6035HTC with a thickness of 254 μm. The cover serves as a mechanical protection and electromagnetic shielding for the bias circuitry whereas the ring provides the required module thickness to fit the design. It is noted that the minimum ring thickness is limited by the highest lumped component thickness. A hole with a width slightly smaller than the DC wire diameter is trimmed in the ring to accommodate the wire and act as a stress relief for the bias contacts. The chosen commercial snap-on buttons are shown in Fig. 7.7, which have appropriate size for the antenna design at microwave frequencies.

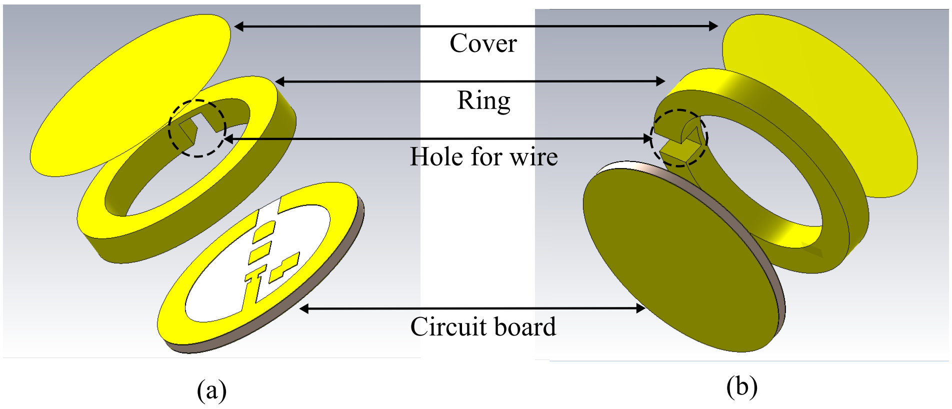

Figure 7.6. The circuitry unit configuration of the proposed button module. (a) Top and (b) bottom 3D exploded views from CST of the circuitry unit of the proposed button module. The circuitry unit consists of a copper cover, a copper ring and a circuit board realized in Rogers RT/Duroid® 6035HTC.

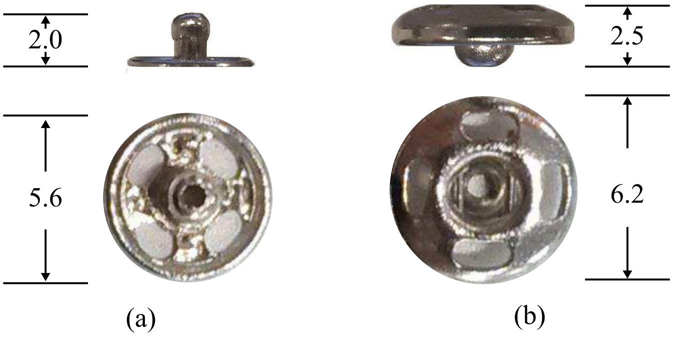

Figure 7.7. The chosen snap-on buttons and their dimensions. Geometries and dimensions (mm) of the commercial snap-on buttons chosen for the button module: (a) male and (b) female snap-on button.

The circuit board geometry and its prototype with lumped components loaded are shown in Fig. 7.8a and b, respectively. The diameter of the circuit board is 5.8 mm which is slightly larger than that of the male button base as depicted in Fig. 7.7a, for ease of fabrication. Surface-mount lumped components are selected due to the very limited space available in the design. As shown in Fig. 7.8a, there is a vias hole in the circuit board to form an electrical connection between the circuit board bottom metal layer and the varactor. The outer circular conductor is used for soldering the ring. A wire used for supplying DC bias voltage will be connected to the inductor.

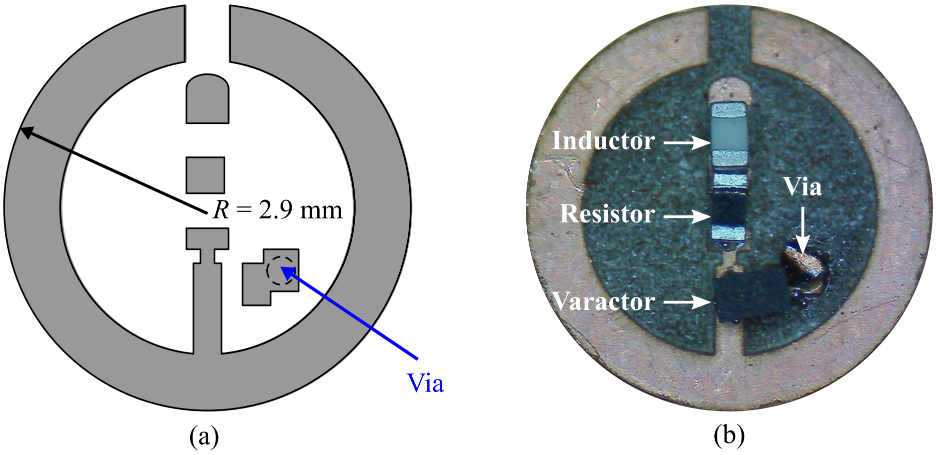

Figure 7.8. Geometry and component-loaded prototype of the circuit board. (a) The geometry and (b) a prototype with lumped components loaded of the circuit board designed for the proposed button module.

The fabrication process of the button module is straightforward. Firstly, lumped components, a pre-made copper ring, a wire and a copper cover are sequentially soldered onto the circuit board. Following that, two male snap-on buttons are soldered to the top and bottom surfaces of the circuitry unit. At this stage, the button module is ready for use. Figure 7.9 shows different phases of the module fabrication process. The status of the module fabrication shown in Fig. 7.9a was just before the bias line wire was about to be soldered to the circuit board. The next picture in Fig. 7.9b illustrates a circuitry unit with one male button soldered on its top while the completed module is shown in Fig. 7.9c. One can observe that the module is very compact and solid. The circuitry is protected between the buttons, and a solid connection to textile is easily realized with the snap-on buttons.

7.3 A frequency-reconfigurable antenna

A frequency reconfigurable textile antenna using the proposed button module is designed to validate the module concept. The chosen design is adapted from the modular antenna design discussed in the previous chapter. It is emphasized that the proposed antenna is only realized for a prompt proof-of-concept validation, and thus the resonance frequency was arbitrarily chosen. More elaborate designs will be the subject of further research work in the near future.

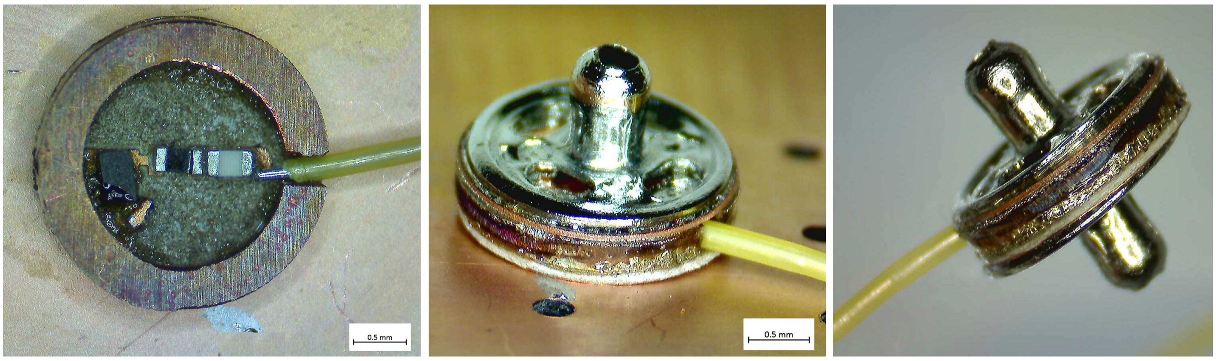

(a) (b) (c)

Figure 7.9. Different phases of the button module fabrication. Different phases of the button module fabrication: (a) The bias wire is ready for soldering onto the circuit board, (b) a male snap-on button is soldered on top of the circuitry unit and (c) the completed button module.

7.3.1 Antenna configuration

The configuration of the antenna is illustrated in Fig. 7.10 while the dimensions are given in Table 7.1. The antenna is a proximity coupled microstrip patch antenna realized in silver fabrics and flexible low-loss foams, similarly as used in the modular antennas presented in the last chapter. The device contains a two-layer substrate which has its bottom backed by a ground plane and a patch attached to its top surface, whereas a 50-Ω open-end microstrip feed line is affixed in between. The center slot is introduced to obtain an extra design freedom for the resonance frequency. The proposed button module is embedded in the substrate located at the patch top edge and connects the patch and the ground plane by engaging with two female counterparts. By adjusting the reverse bias voltage applied to the varactor, the capacitance of the varactor changes and so does the capacitance of the patch edge. As a result, the effective electrical length and therefore the resonance frequency of the patch can be continuously altered accordingly. A similar reconfigurable antenna concept has been proposed in 1983 [190].

Since the patch has no electrical short to other parts of the antenna and hence exhibits a floating voltage potential, the bias circuit does not require the DC-blocking capacitor which is shown in Fig. 7.4. A 1 MΩ resistor, a 100 nF inductor and a Skyworks® SMV1255 varactor are chosen as the components. The varactor can have a maximum reverse bias voltage of 15 V, however, only the capacitance information with reverse voltage from 0 to 8 V is given in the datasheet, namely from 81.21 to 4.26 pF.

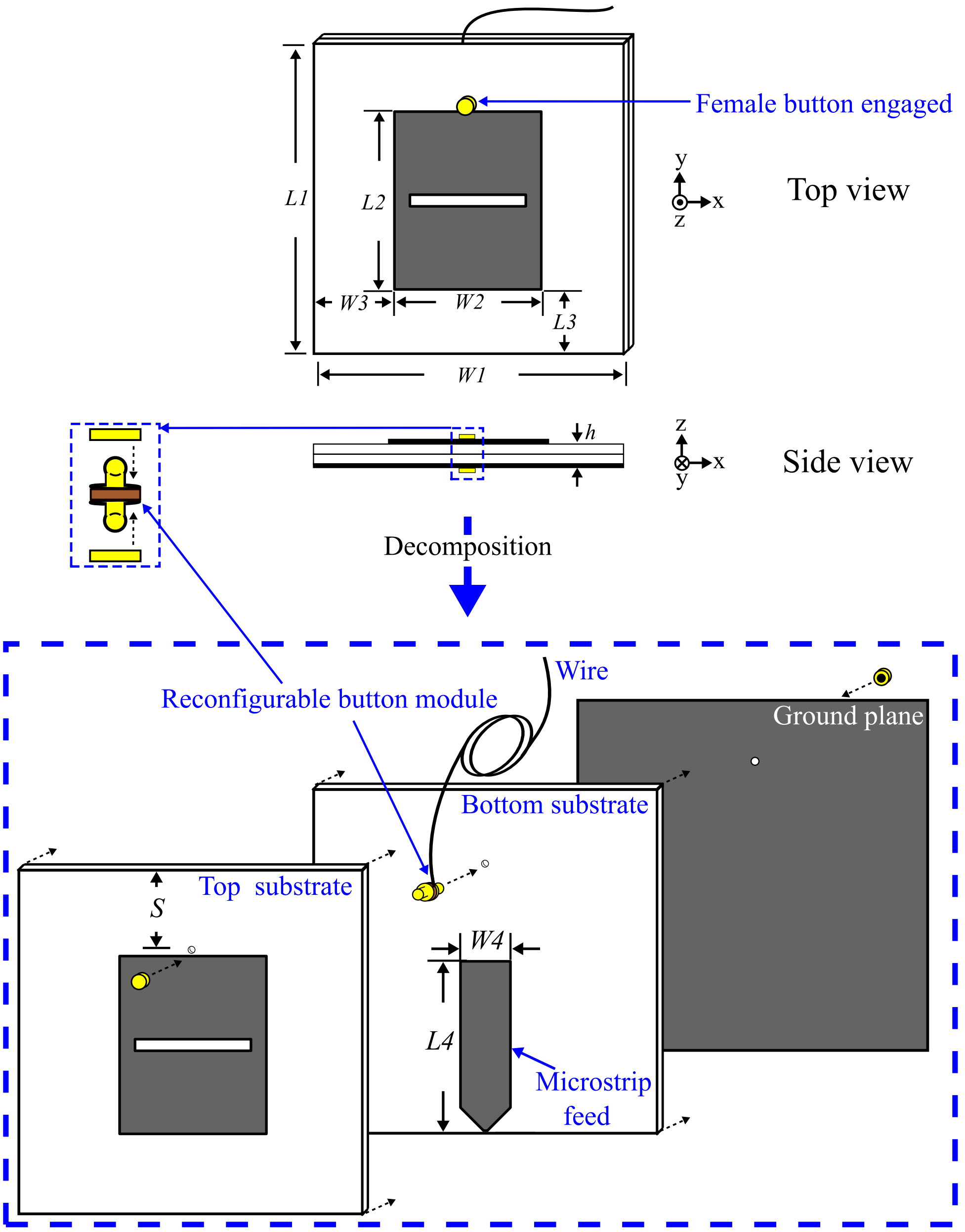

Figure 7.10. The proposed reconfigurable antenna configuration. The proposed antenna consists of a patch, an open-end microstrip proximity coupled feed, a ground plane and a two-layered substrate. The proposed button module is embedded in the substrate located at the patch top edge and connects the patch and the ground plane by engaging with two female buttons. Through applying a variable DC bias voltage to the varactor in the module, the resonance frequency of the antenna can be tuned continuously.

The simulated electric field distributions of the antenna at the lowest and highest resonance frequencies are demonstrated in Fig. 7.11a and b, respectively. These results

Table 7.1. Dimensions of the reconfigurable antenna. Dimensions of the proposed reconfigurable antenna in mm.

Parameters	W_1	W_2	W_3	W_4	S	L_1	L_2	L_3	L_4	h
Value (mm)	45	19	13	6.5	10.3	45	23	11	18	3.2

indicate that the antenna resonates at its TM^z_{010} mode, and that the lowest and highest resonance frequencies at 3.7 and 4.1 GHz correspond to the longest and shortest effective electrical length of the patch, respectively.

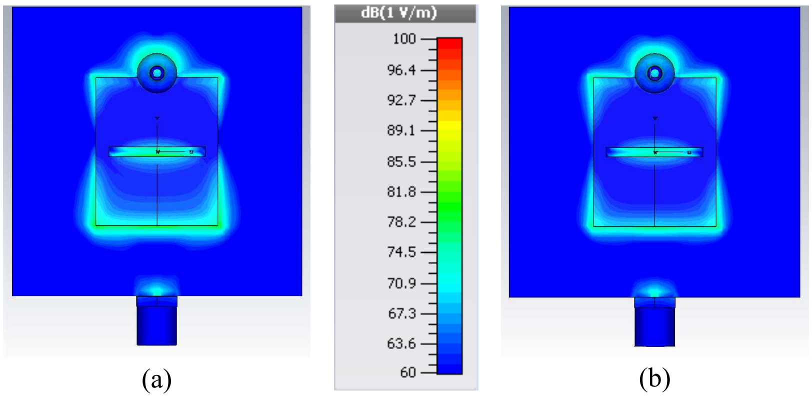

(a) (b)

Figure 7.11. The simulated electric field distributions of the proposed antenna. The simulated electric field distributions of the antenna at (a) the lowest (3.7 GHz) and (b) the highest resonance frequencies (4.1 GHz).

7.3.2 Proof-of-concept experimental results

An antenna prototype has been fabricated and tested, however only in preliminary proof-of-concept measurements due to the very limited time available at the end of the candidature. Figure 7.12 shows the front and back views of the fabricated antenna prototype.

The simulated and measured reflection coefficients with various varactor capacitances are compared in Fig. 7.13. The simulation results are obtained individually from CST with values of 81.21, 13.40, 5.58 and 4.26 pF set for the varactor capacitance. The actual $|S_{11}|$ parameters of the prototype antenna are measured, with the required voltages of 0, 2.5, 4 and 8 V applied for obtaining the corresponding capacitances. The simulation results show that the resonance frequencies varies from 3.72 to 4.15 GHz with the capacitances changed from 81.21 to 4.26 pF, which corresponds a 10.5% frequency tuning

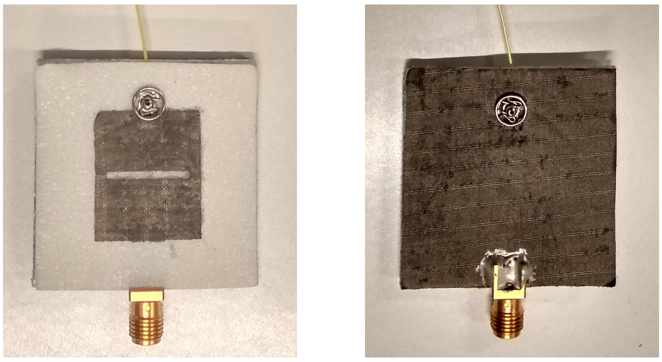

(a) (b)

Figure 7.12. An antenna prototype. (a) The front and (b) the back views of an antenna prototype.

range. In contrast, the measured results exhibit a wider tuning range within the range of voltages applied. The measured reflection coefficient with the maximum applicable reverse voltages of 15 V is plotted in Fig. 7.13 as well, indicating a 15.1% frequency tuning range from 3.77 to 4.38 GHz. The tuning range can be improved by using a varactor with a more appropriate capacitance range with low internal resistance.

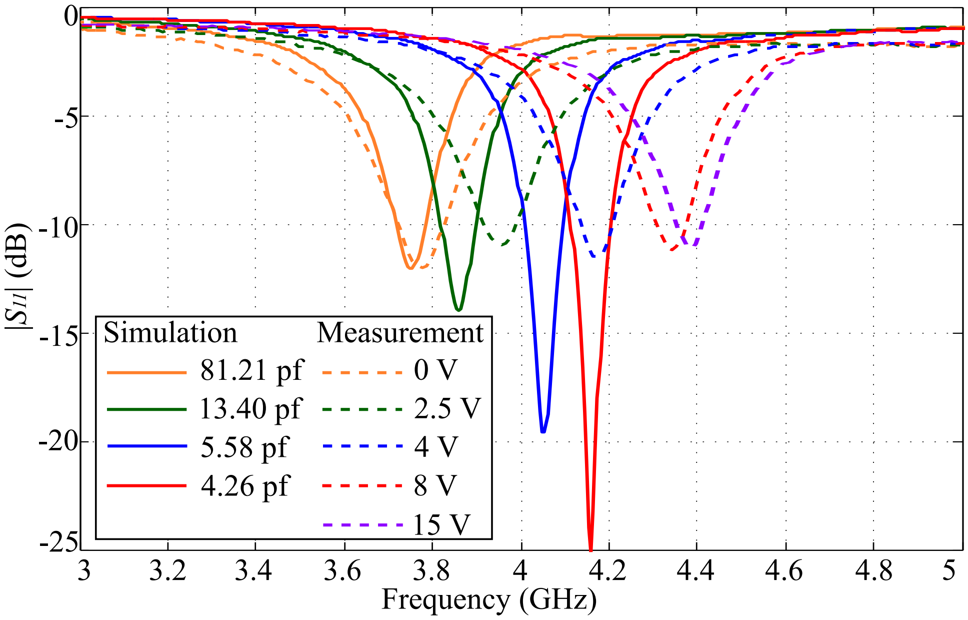

Figure 7.13. Simulated and measured $|S_{11}|$ parameters of the proposed antenna. The simulated and measured reflection coefficients of the proposed antenna. The simulated values are obtained from CST with varactor capacitances set to 81.21, 13.40, 5.58 and 4.26 pf, respectively. Based on information from the varactor datasheet, reverse voltage of 0, 2.5, 4, 8 and 15 V is applied to obtained the measured values.

Since the measured results exhibit a different resonance frequency shift compared to the simulated ones, this implies an effect from fabrication tolerance and/or variation in the button module reactance. In addition, the measured values have a wider shape of the resonance responses and this could be indicative of a higher loss in the antenna prototype which is likely due to the varactor (e.g. there might be an underestimated internal resistance). All these factors need further investigation. Nevertheless, excellent textile-to-module connection and stable antenna performance during the reflection coefficient measurement scheme have been observed. This suggests that the button module concept is a practical and promising engineering solution for reconfigurable textile antenna designs.

7.4 Conclusion

This chapter has presented a reconfigurable button module concept for textile antennas. This component has a compact structure and is built from the combination of commercial snap-on buttons and integrated dedicated active circuitry unit. The attractive advantages of this module concept, towards ”smart” reconfigurable textile antennas, include the secured and solid connection solution for flexible textiles and rigid electronics. This concept can dramatically increase the versatility of the various modules functionality. A frequency reconfigurable antenna based on a dedicated button module has been designed and subjected to a preliminary test. The measured results suggest that this button module concept is a practical and promising engineering solution for reconfigurable textile antennas, although further improvements might be required and will be investigated in future work.

Chapter 8

Wearable Microstrip Antenna Array

MICROSTRIP patch antennas are generally very appropriate for wearable applications, since they are compact, low-profile, and more importantly, electromagnetically isolated from the human body due to the ground plane. Therefore, various microstrip patch antennas and arrays designed for wearable applications have been reported in the literature. In particular, arrays are usually for applications that require high gain antennas and they are expected to be as compact as possible due to the limited real estate of human body.

This chapter presents a novel concept of a compact and high-efficiency series-fed microstrip antenna array for wearable applications. A circular array arrangement delivers a compact structure while the efficient coupling mechanism permits high antenna efficiency. This dual-port array can radiate waves with LHCP or RHCP if one the ports is fed whereas if both ports are excited simultaneously with proper amplitude and phase difference then arbitrary polarization can be achieved. Experimental validations in free space and worn on a torso phantom suggest that this compact array design is highly efficient and has insignificant performance degradation when operating placed on the human body.

8.1 Introduction

Microstrip patch antennas [10, 11, 13, 31, 120–123] and arrays [42, 191] are very commonly utilized for wearable wireless communication systems. This is because they exhibit desired features such as compactness, low profile, low cost and light weight, and more importantly, have excellent electromagnetic isolation from the human body in wearable applications owing to the presence of their ground plane. In particular, microstrip patch arrays are frequently utilized in applications that require high gain antenna(s), since their multiple radiating elements can offer higher gain compared to single antennas, at the cost of larger antenna areas and more complicated feeds.

A typical wearable microstrip patch antenna array designed for integration into a rescue-worker's vest was proposed by Scarpello et al. in 2012 [42]. The antenna array configuration and its hosting vest worn by a human object are shown in Fig. 8.1. The vertically aligned array has four patch elements and each of them is fed by a coaxial cable individually. This feed structure is a straightforward design, however, it requires a set of accessories including four coaxial cables, a cable stretcher and a RF power divider, which makes it cumbersome and thus not conveniently wearable. In contrast, a simpler feeding mechanism is employed in a series-fed textile microstrip array which can be used for wearable applications, as depicted in Fig. 8.2. The array also has four elements which are fed in series by a single microstrip line. Due to this common feeding microstrip line, the feed structure provides a less obtrusive solution compared to the previous one. These two typical array designs illustrate two possible arrangements for feeding microstrip arrays, namely, corporate-feed network in the first design and series-feed network in the other one [192]. Compared with corporate arrangements, series-feed networks have the benefits of simplicity, which can translate into low-loss, low-cost and light-weight feeding structures which are preferable for wearable applications [193].

In terms of coupling mechanisms for series-fed arrays, they can be categorized into direct and aperture couplings [192]. Arrays based on direct coupling include for example cascaded patch arrays [194–197] and comb-line antennas [193, 198–201]. As opposed to aperture coupling [202–204], direct coupling usually requires a simpler coplanar structure rather than a multilayer platform. Proximity coupling is another possible mechanism which also can be implemented in coplanar configuration. Additionally, with no electrical connection between array elements and feed line, this arrangement can lead to a better matching, since impedance variations introduced by the radiating elements

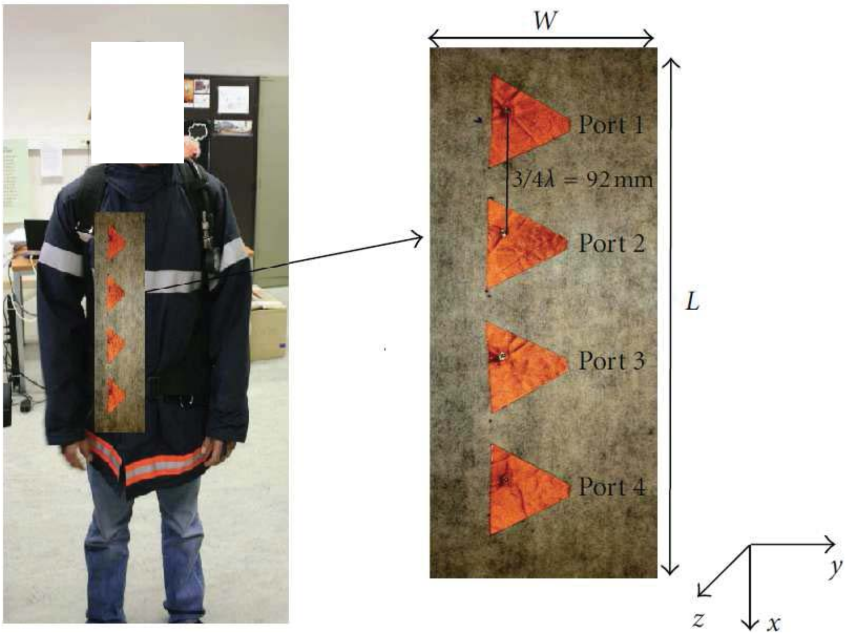

Figure 8.1. A wearable microstrip patch array. A wearable microstrip patch array integrated on a garment worn by a human object, adapted from [42].

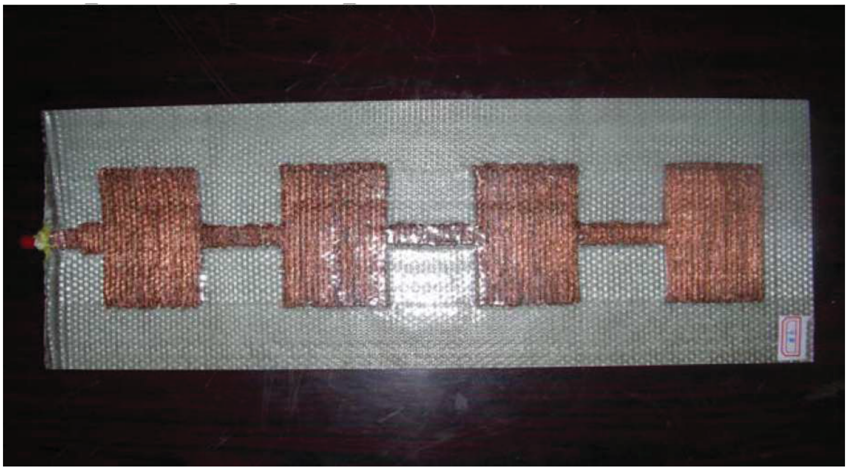

Figure 8.2. A textile microstrip patch array. A microstrip patch array realized in conductive and dielectric textiles, adapted from [191].

on the feed line can be finely controlled and made smaller than in the case of the direct coupling. However, only a few series-fed arrays based on a coplanar proximity coupling mechanism [205,206] have been reported in the literature.

An important design consideration in series-fed arrays is the matched termination required to avoid reflection at the end of the antenna. Additionally, because of the generally weak coupling, a trade-off is required between antenna efficiency (including losses in the termination) and overall size. That is, higher antenna efficiency is achievable at the cost of increasing the number of radiating elements which will result in a larger antenna size [200]. Therefore, designing a high-efficiency antenna with less array elements is a challenging task, which is especially desirable for wearable applications where limited real estate is available. For instance, an 8-GHz linear array in [200] needs to have 12 elements, spaced by a wavelength, to achieve a 60% efficiency. A 10-GHz circular array reported in [202] requires 8 patches to deliver a 75% efficiency without considering the materials losses. Since this array is based on aperture coupling mechanism, the antenna size is not compact due to its multilayer structure even if a circular array arrangement was used. One well-known solution that can address this issue is to increase coupling strength between the feed line and the elements [192].

This chapter demonstrates a concept of compact and highly-efficient circular travelling wave series-fed microstrip patch array, which can be used for, but is not limited to, wearable applications. The patch elements are excited by a microstrip line through coplanar proximity coupling. The dual-port feeding with sufficient inter-port isolation (transmission coefficient $|S_{21}|$ below -15 dB) allows to select the direction of the travelling waves, and consequently the circular polarization handedness of the patches. Simultaneous feeding to both ports with proper amplitude and phase difference can result in radiated waves of arbitrary polarization. Owing to the circular array arrangement and the strong proximity coupling, the antenna exhibits a compact structure and achieves a high antenna efficiency of 90% with 7 patches. Based on reciprocity, the antenna can readily be also utilized for polarimetry applications for which the signal amplitude at each port is proportional to the amplitude of each individual handedness. Measured results of an antenna prototype working at 10 GHz successfully validate the concept both in free space and worn by a torso phantom. It is emphasized that the antenna array can be scaled to other frequency band if necessary, for example the 5.8-GHz ISM band which is widely used for wearable applications. The 10 GHz X band was arbitrarily selected for the design validation.

8.2 Array design

8.2.1 Antenna configuration

The proposed antenna configuration and a realization are shown in Fig. 8.3 while the dimensions are listed in Table 8.1. This 10-GHz two-port array consists of a circular microstrip feed line with tapered terminals and 7 circular patch elements at the top layer, and a ground plane at the bottom layer. The circular array geometry with patch elements lying inside the feed line can miniaturize the antenna size by around 20%, compared to a similar array with its elements outside of the feed line. A 0.79-mm thick Rogers RT/Duroid® 5880 substrate with relative permittivity $\varepsilon_r = 2.2$ and loss tangent $\tan\delta = 0.0009$ is chosen as the antenna material. The feed line and the patches are patterned on the top cladding layer with a laser milling machine whereas the bottom cladding layer acts as the ground plane. All simulations shown in the following were performed with CST.

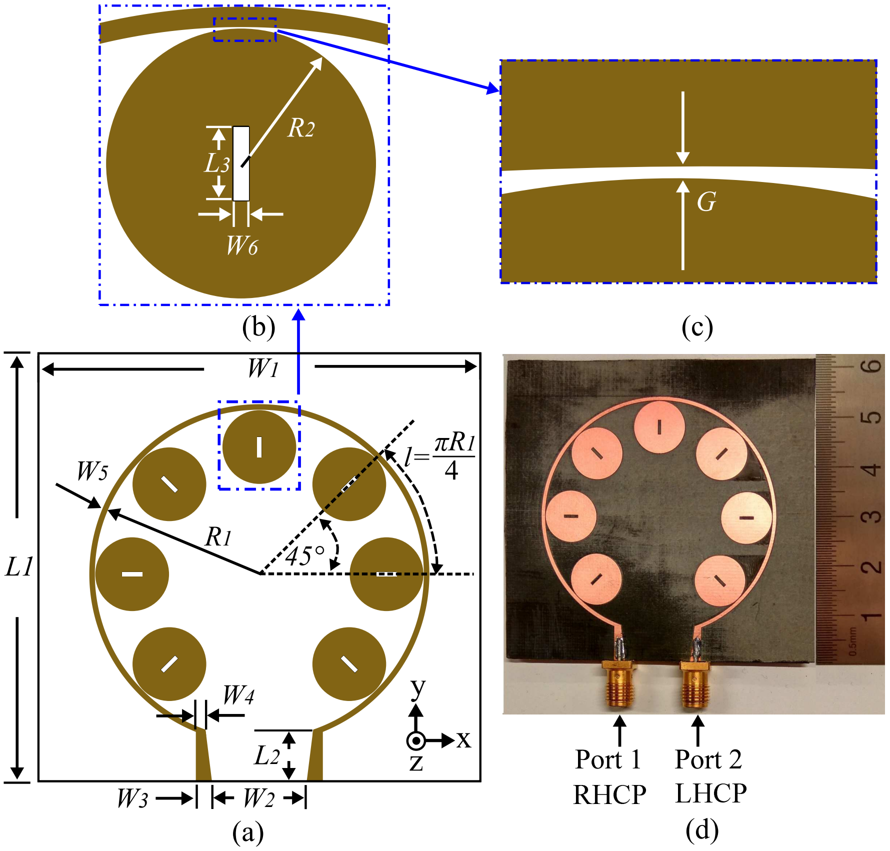

Figure 8.3. The proposed antenna configuration and realization. (a) Overall configuration, (b) patch element geometry, (c) feed-line-to-element gap and (d) a realization of the proposed antenna. The antenna includes a circular two-port microstrip feed, 7 identical circular patches and a ground plane. The circular microstrip feed line has two tapered ends connected to coaxial ports 1 and 2. The patches are aligned along the inner feed line edge with a 45° angular separation, or equivalently $l = \pi R_1/4$.

The individual patches progressively couple and radiate a fraction of energy from the guided wave travelling on the feed line from one port to the other. Provided their equal

Table 8.1. The array dimensions. Dimensions of the proposed antenna array in (mm)

L_1	L_2	L_3	R_1	R_2	G	W_1	W_2	W_3	W_4	W_5	W_6
63.0	7.5	2.9	24.1	5.3	0.06	63.0	9.7	2.3	1.4	0.8	0.6

coupling strength, the absolute radiated power from each patch will decrease over the line length. This can be illustrated by the magnitude of the surface current density **J** on the microstrip line at the closest point to each patch. The surface current density is calculated based on the simulated magnetic field **H** using the following relation

$$\mathbf{J} = \hat{\mathbf{n}} \times \mathbf{H}, \tag{8.1}$$

where $\hat{\mathbf{n}}$ is the unit vector normal to the microstrip line surface. Since the simulated magnetic fields are expressed based on the coordinate system (x, y) shown in Fig. 8.3a, a ration of axes needs to be applied to elements which are not aligned along the principle x and y axes, i.e. for all elements except the top one. This is required in order to find out the component of the current density tangential to the feeding line at the observation point. For instance, for the first element from port 1, a 45° or -45° axes rotation can be implemented to map the original coordinates (x, y) to the new ones $(x'$, $y')$, that is

$$\begin{bmatrix} x' \\ y' \end{bmatrix} = \begin{bmatrix} cos\theta & sin\theta \\ -sin\theta & cos\theta \end{bmatrix} \begin{bmatrix} x \\ y \end{bmatrix}, \tag{8.2}$$

where the rotation angle $\theta = 45°$ or -45° so that the y' or x' components represent the tangential current density, respectively. An illustration of the rotation of $\theta = 45°$ is shown in Fig. 8.4. The calculated magnitude and phase of the current density are shown in Fig. 8.5.

The array can also be interpreted as a periodic leaky-wave antenna, however with resonant perturbations. These elements resonate at the fundamental mode with circular polarization intrinsically generated by the travelling wave excitation. Figure 8.6 shows instantaneous current maps for one of the patches at two different times chosen in phase quadrature, and illustrates that, as the travelling wave propagates clockwise, the antenna resonates in its TM^z_{110} mode with RHCP, as governed by the Lenz's Law. Thus excitation of port 1 at the nominal frequency will result in broadside radiation with RHCP, whereas excitation of port 2 will yield LHCP. The dual-port array is designed to have sufficient port isolation with transmission coefficient $|S_{21}| <$ -15 dB. An initial

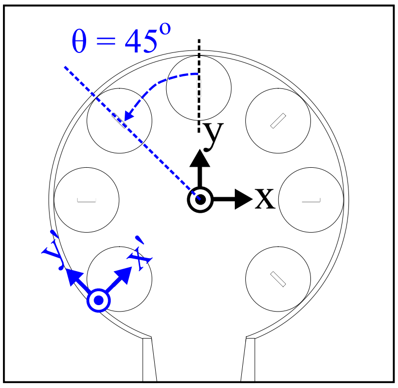

Figure 8.4. A rotation of axes with $\theta = 45^\circ$. A rotation of axes with $\theta = 45^\circ$ is implemented to align the new y' axis to the surface current density component which is tangential at the observation point.

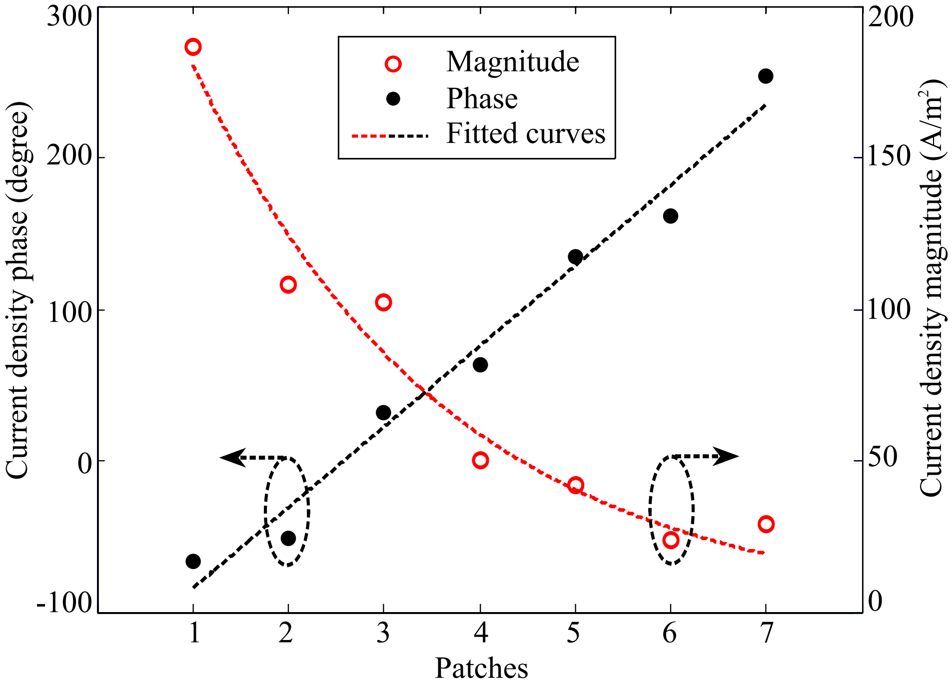

Figure 8.5. Phase and magnitude of the surface current density. Phase and magnitude of the surface current density calculated based on simulated magnetic field on the feed line at the closest points to each patch.

patch radius R_2 can be calculated using a standard equation for circular patches [175]:

$$f_{110} \approx \frac{1.8412}{2\pi R_2 \sqrt{\varepsilon_r}\sqrt{\varepsilon_0 \mu_0}}, \tag{8.3}$$

where f_{110}, ε_r, ε_0 and μ_0 are the TM^z_{110} resonance frequency, relative permittivity of the substrate, free-space permittivity and free-space permeability, respectively. An optimal value can be then obtained through full-wave simulation. A slot is introduced in the middle of the patch to provide an additional degree of freedom for optimization of the circular polarization bandwidth.

The patches need to be in phase to achieve broadside radiation and they are placed along the feed line with a 45° angular rotation determined by the number of elements. To obtain the in-phase condition, the separation between adjacent patches along the microstrip line l is set based on the following rule:

$$l = \lambda_g - \frac{\lambda_g}{8}, \tag{8.4}$$

where λ_g is the guided wavelength on the feeding line. The $\lambda_g/8$ term is included to compensate the $+45°$ phase difference between two neighbouring elements due to their relative orientation. The phase of the surface current density shown in Fig. 8.5 indicates that the phase between subsequent points is reasonably linear as expected. However, a small variation in element phase is observed and this is due to mutual coupling between the closely located patches. Nevertheless, by individually manipulating the gap G between the feed line and the patches (see Fig. 8.3c), a more synchronous polarization state in the array could be achieved at the cost of higher design complexity, however, only with a very marginal improvement in antenna performance. Hence the proposed array is designed with a constant G which makes it a good compromise of simplicity and performance, as discussed in the following.

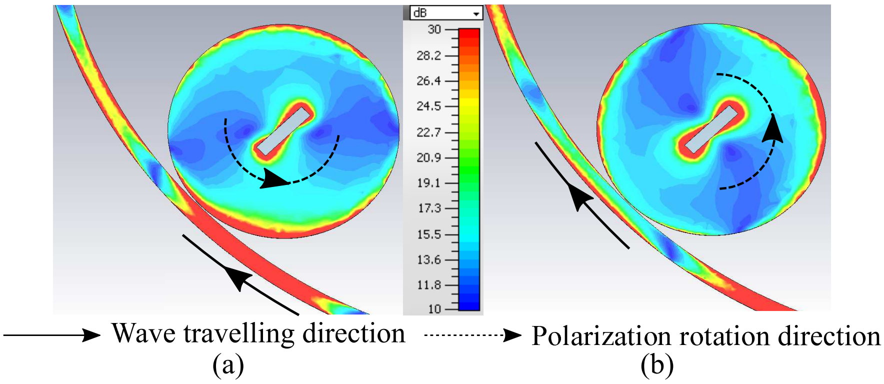

Figure 8.6. Simulated absolute current strength colourmap of one patch. Simulated absolute current strength colourmap for a patch element and part of the feeding line at two different times corresponding to quadrature phases. (a) Phase = 50°. (b) Phase = 140°.

8.2.2 Control of coupling strength

In order to achieve high antenna efficiency and sufficient operational bandwidth with a small number of array elements, a small G is required to enhance the proximity coupling, and thus the rate of energy radiation along the line [192]. To demonstrate that, a parametric study of G associated with antenna efficiency and bandwidth (transmission coefficient $|S_{21}|$ below -15 dB) has been conducted using CST, as shown in Fig. 8.7 and 8.8 respectively. As expected, with a larger G, a lower antenna efficiency and a narrower operational bandwidth is observed. Namely, with G = 0.06, 0.08, 0.12, 0.20 and 0.30 mm, the antenna total efficiency and operational bandwidth (e_{tot}, BW) are (93%, 5.1%), (91.5%, 4.3%), (90.5%, 2.7%), (87.3%, 0%) and (82.5%, 0%), respectively. This is mainly attributed to the fact that the coupling between the line and the elements is reduced, leading to a larger power being transferred to the load.

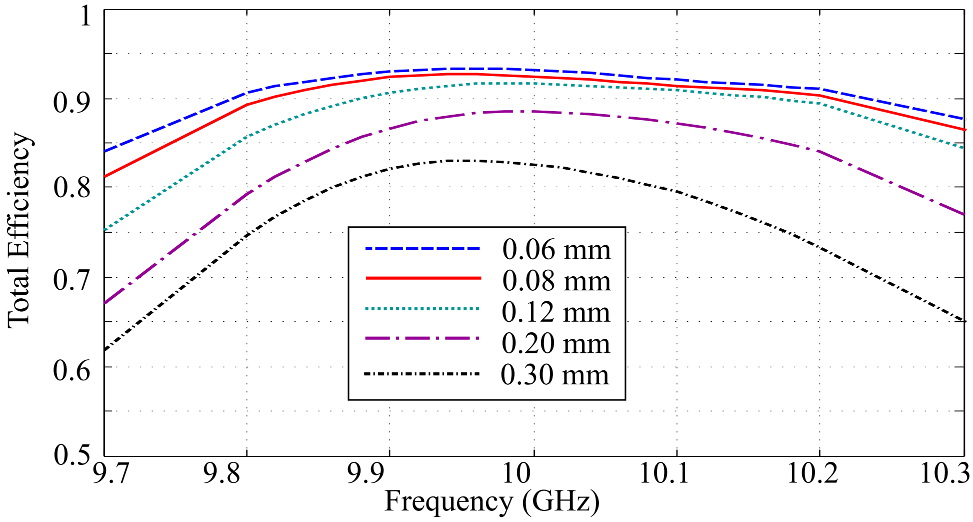

Figure 8.7. Total antenna efficiency comparison over different G. Simulated total antenna efficiencies when $G = 0.30$, 0.20, 0.12, 0.08 and 0.06 mm, respectively.

In principle, the gap could be used to equalize the excitation of the elements. Nevertheless, this increases the complexity of the design for a marginal improvement of performance. In addition, as the antenna is designed to operate in both senses of polarizations, so the gap size has to be pair-wise equal from the feeds. Assuming equal gap size now, the minimum G is practically set by the antenna materials and the fabrication accuracy. A width of 60 μm for G is selected here based on the fabrication limitation of the available laser milling machine (LPKF: Protolaser S). As mentioned, G can be fine-tuned to individually manipulate the element excitation but should be pair-wise equal from the feed to maintain symmetry for the dual feeding design.

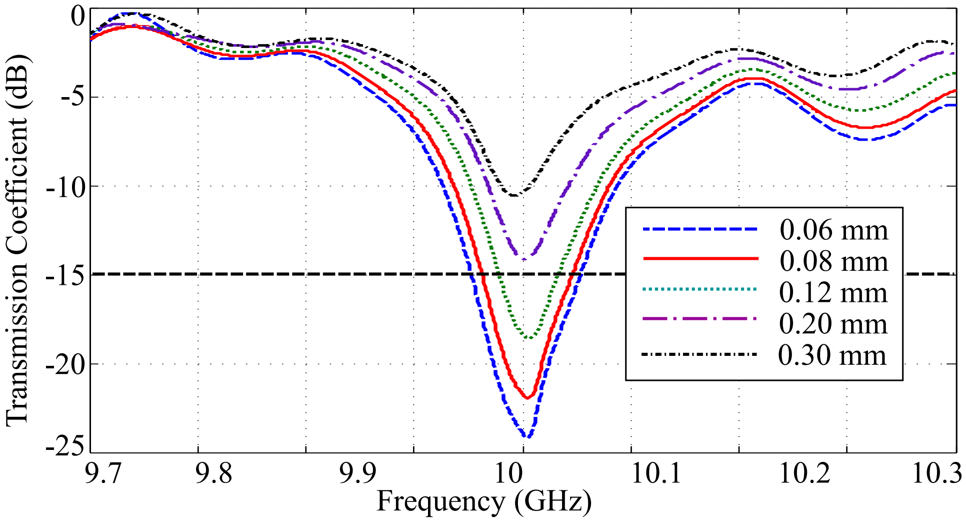

Figure 8.8. Antenna operation bandwidth comparison over different G. Simulated antenna transmission coefficients when $G = 0.30$, 0.20, 0.12, 0.08 and 0.06 mm, respectively. The antenna operation bandwidth is the frequency range that the transmission coefficients are below -15 dB.

In addition, the coupling strength can also be enhanced by narrowing down the feed line width since this will lead to more pronounced fringing field. To demonstrate this feature, simulated power components related to radiation, reflection and transmission for the antenna with feed line width of 0.8 mm and 2.4 mm are plotted in Fig. 8.9, with normalization to the input power. Materials losses are not shown here, because they are small and nearly identical for the two antennas with different line widths (variations $<$ 0.2% of the input power). The results in Fig. 8.9 confirm a stronger coupling for the narrower line width since more power is radiated, and consequently less power is transmitted to the second port. Additionally, the maintained reflection level suggests that the impedance matching is nearly unchanged. A line width of 0.8 mm has been found to be appropriate for the design, since it offers a satisfactory coupling efficiency with an easy-to-match impedance of approximately 93 Ω. The two tapered microstrip lines sections are included at the input ports to minimize reflections due to discontinuities between the 50 Ω coaxial ports and the main feed line.

8.3 Experimental results

8.3.1 Reflection and transmission coefficients

An antenna prototype (Fig. 8.3d) has been fabricated and experimentally characterized to validate the design. As illustrated in Fig. 8.10, the simulated and measured reflection

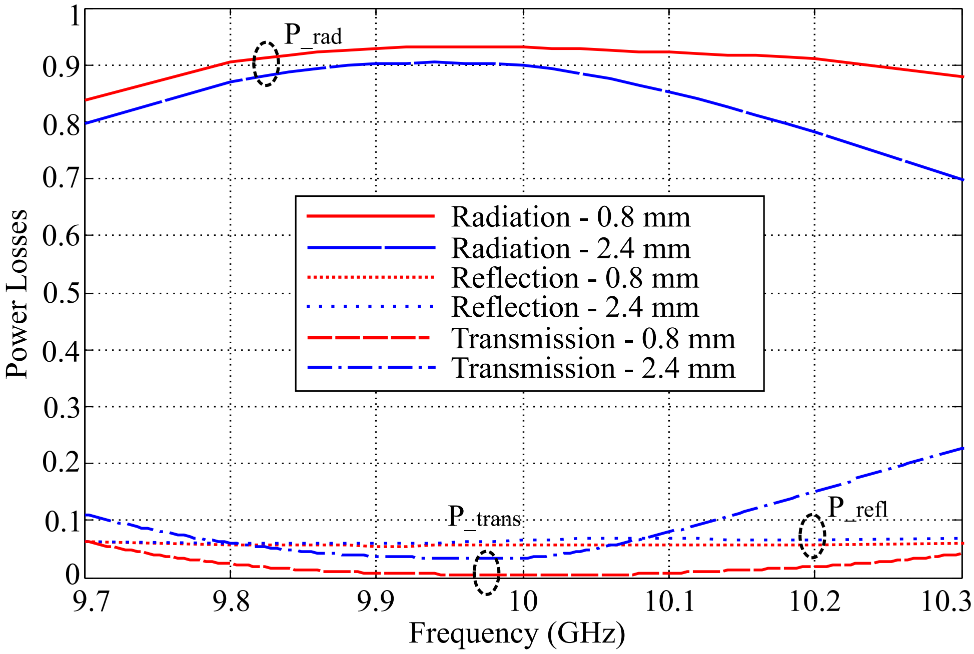

Figure 8.9. Radiated, reflected and transmitted power components comparison. Normalized power components associated with antenna radiation, reflection and transmission as calculated based on simulation, for the antennas having feed line width of 0.8 and 2.4 mm.

and transmission coefficients for the antenna show a good agreement. The antenna operational bandwidth is defined as the band where the measured reflection coefficients ($|S_{11}|$ and $|S_{22}|$) are below -10 dB and the transmission coefficients ($|S_{21}|$ or $|S_{12}|$) are below -15 dB. This bandwidth is shown as the shaded area in Fig. 8.10 and extends from 9.75 to 10.3 GHz (5.5%). Other minima appearing in $|S_{11}|$ at 8.3, 9 and 11 GHz are due to standing waves. Nevertheless, it is clear from the figure that the main limitation arises from the specification on the transmission coefficient. In this bandwidth, there is no more than 5% input power reflected and less than 3.2% input power transmitted to the other port, respectively. This indicates that most of the input power is radiated considering that material losses are low at this frequency. In particular, the specification that $|S_{21}|$ and $|S_{12}| <$ -15 dB implies sufficient port isolation, which makes this antenna suitable for applications in dual-port systems that require both LHCP and RHCP operation. Through reciprocity, the antenna can be used for polarimetric detection as it separates an incident wave in its circular polarization components.

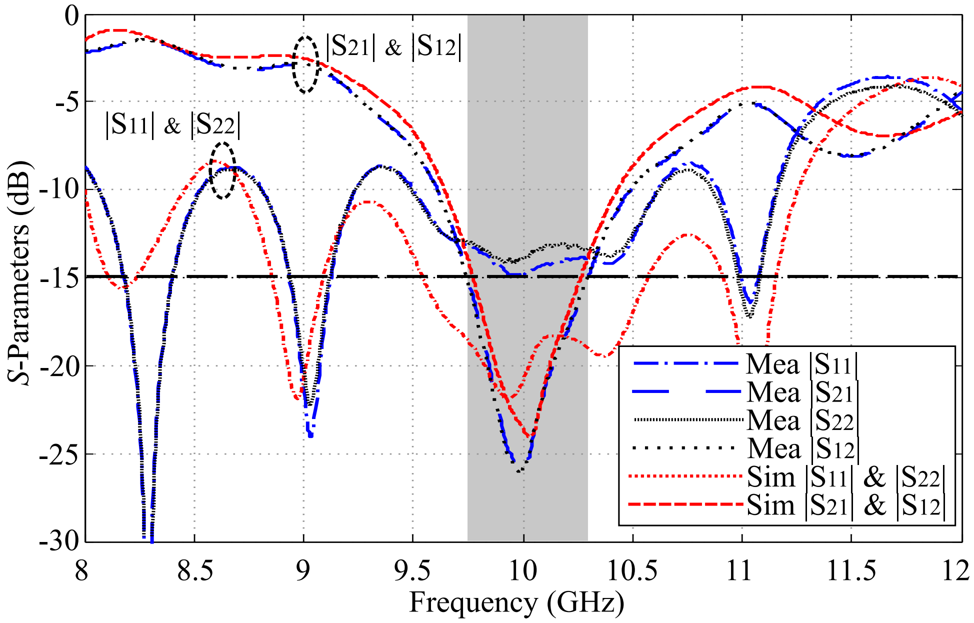

Figure 8.10. Simulated and measured $|S_{11}|$ and $|S_{22}|$ of the array. Simulated and measured reflection coefficients and transmission coefficients of the antenna. The shaded area is the operational bandwidth, defined at $|S_{21}| = |S_{12}| < -15$ dB.

8.3.2 Radiation patterns

The measured and simulated 10 GHz normalized radiation patterns in the *xz*- and *yz*- planes for the antenna fed at one port with the other one terminated are shown in Fig. 8.11. Good consistency between simulation and measurement is attained. The antenna features a 3-dB beamwidth of around 35° and 32° in the *xz*- and *yz*-planes, respectively. This type of radiation patterns is typical for circular arrays whereas fan beam patterns are expected for linear arrays. The side lobe-level is less than -10 dB, acceptable for general applications and can be further improved through manipulation of the individual element amplitude [175]. In the boresight direction, the co-polarized component is approximately 20 dB higher than the cross-polarized one. This confirms satisfactory circular polarization performance. These radiation patterns clearly indicate that one-port feeding at port 1 or port 2 can generate waves of RHCP or LHCP, respectively.

The circular polarization characteristic can also be characterized across the bandwidth by the axial ratio (AR) measurement. As compared in Fig. 8.12, the simulated and measured boresight AR of the antenna with port 2 terminated are consistent. The 3-dB AR bandwidth ranges from 9.66 to 10.66 GHz (10%) which covers the previously

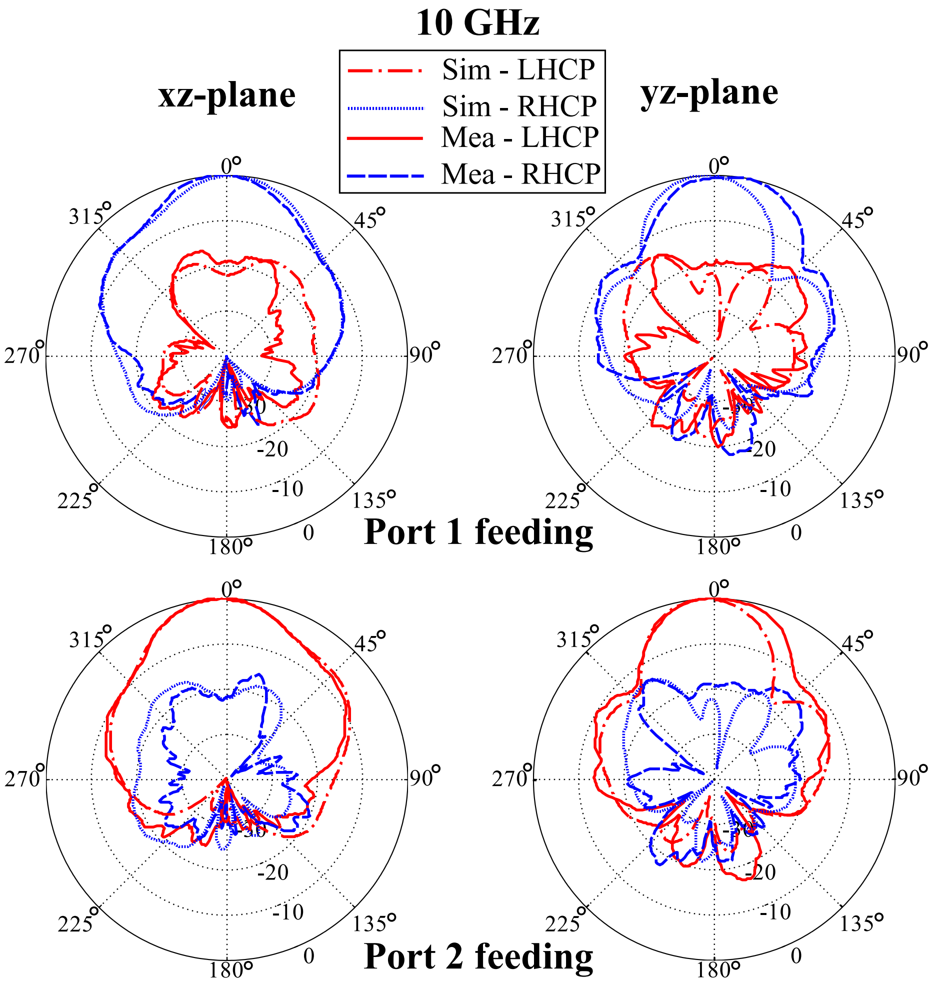

Figure 8.11. Simulated and measured radiation patterns of the array. Simulated and measured 10-GHz normalized radiation patterns in the xz- and yz-planes of the antenna fed at one port with the other one terminated.

defined antenna operational bandwidth (the shaded area in Fig. 8.10) with a nearly 50% margin.

Figure 8.13 plots the simulated and measured 9.8, 10 and 10.2 GHz AR results over θ in the xz-plane with shaded area of 35 degrees (the 3-dB beamwidth). Figure 8.14 shows the ones in yz-plane, with shaded area of 30 degrees (the 3-dB beamwidth). As observed, the simulated 3-dB AR beamwidth are all greater than 35° for these three frequencies (except 9.8 GHz in yz-plane). The measured 9.8, 10 and 10.2 GHz AR in the xz-plane is approximately 45, 25 and 50+ degree, respectively. In the yz-plane, the measured AR beamwidth for 9.8, 10 and 10.2 GHz is around 27, 40 and 32 degree, respectively. The discrepancy can be attributed to the fabrication tolerances and measurement error. The results indicate that the prototype can maintain 3-dB AR over a wide beamwidth of about 30°, overlapping with its 3-dB beamwidth. A very similar axial ratio is obtained when port 1 is terminated.

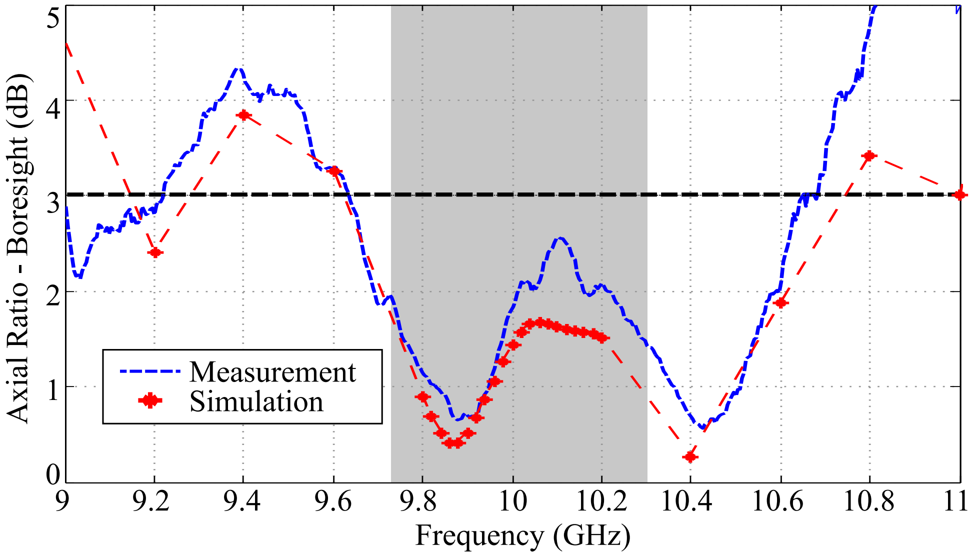

Figure 8.12. Simulated and measured boresight axial ratio. Simulated and measured boresight axial ratio of the antenna with port 2 terminated. The shaded area corresponds to the operational bandwidth defined in Fig. 8.10.

8.3.3 Gain and efficiency

The simulated and measured realized gains of the antenna with port 2 terminated are depicted in Fig. 8.15. A good correspondence between these two results is observed. The measured realized gain is maintained between 11.5 and 13.5 dB within the operational bandwidth and the discrepancy from simulation is most likely due to imperfect measurement. By increasing the number of patches, the array can achieve a higher gain, however, at the cost of an increase in sidelobe level. To obtain the simulated total antenna efficiency e_{tot}, the reflection and transmission coefficients, the power losses due to the antenna metallic (P_m) and dielectric materials (P_d) and the input power at the port (P_{in}) in simulation are used based on the following relation:

$$e_{\text{tot}} = 1 - |S_{11}|^2 - |S_{21}|^2 - L_m - L_d, \tag{8.5}$$

where $L_m = P_m/P_{in}$ and $L_d = P_d/P_{in}$ are the normalized power losses due to metals and dielectrics respectively. As such, the total efficiency accounts for the insertion loss due to the feed line. As illustrated in Fig. 8.15, the simulated total efficiency ranges from 87% to 93% and has an averaged value of 92.3% in the operation bandwidth. Since

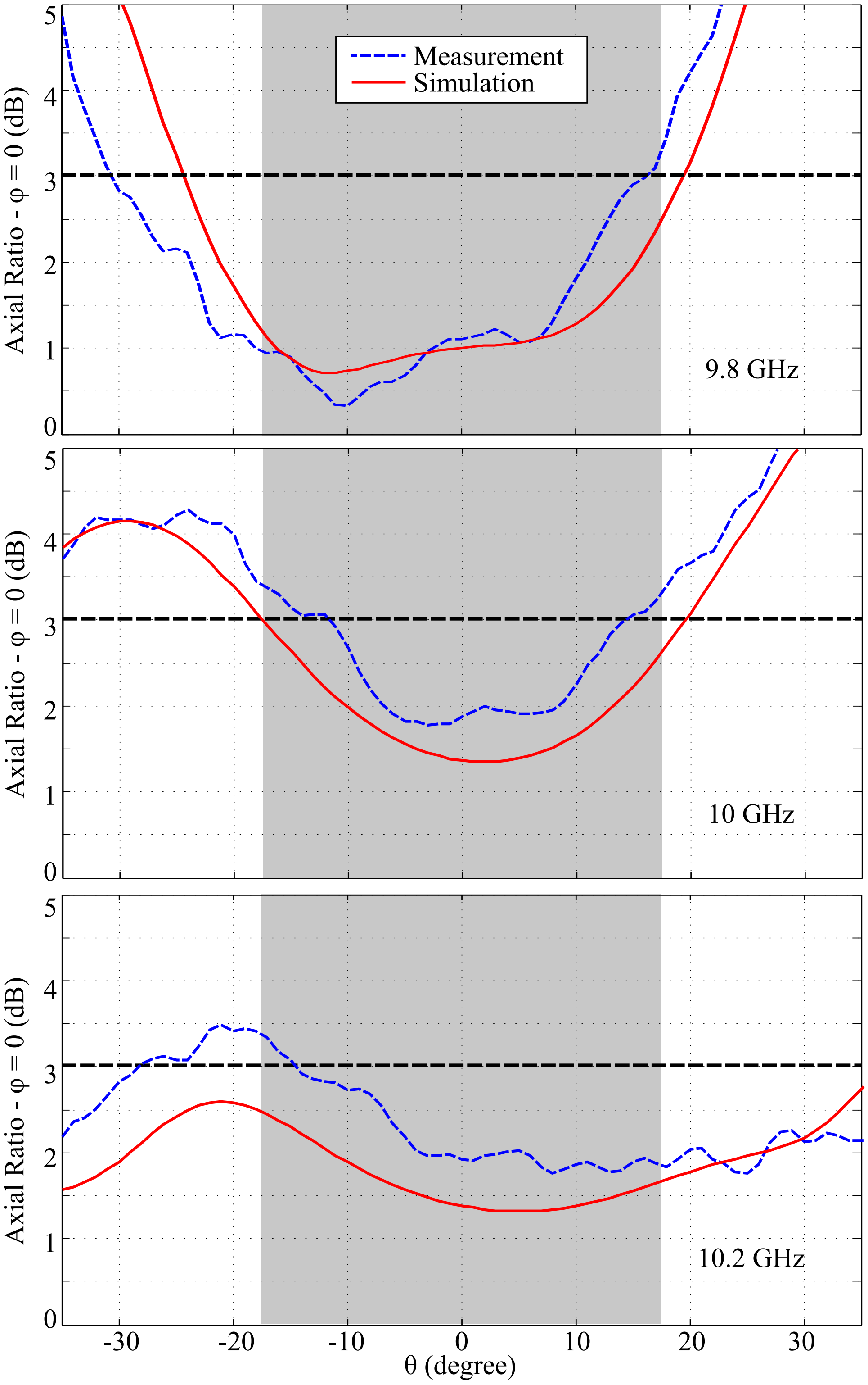

Figure 8.13. Simulated and measured axial ratio over θ in the xz-plane. Simulated and measured axial ratio over θ in the xz-plane, with the antenna port 2 terminated. The shaded area is the 3-dB beamwidth in the considered plane which amounts to 35°, as shown in Fig. 8.11.

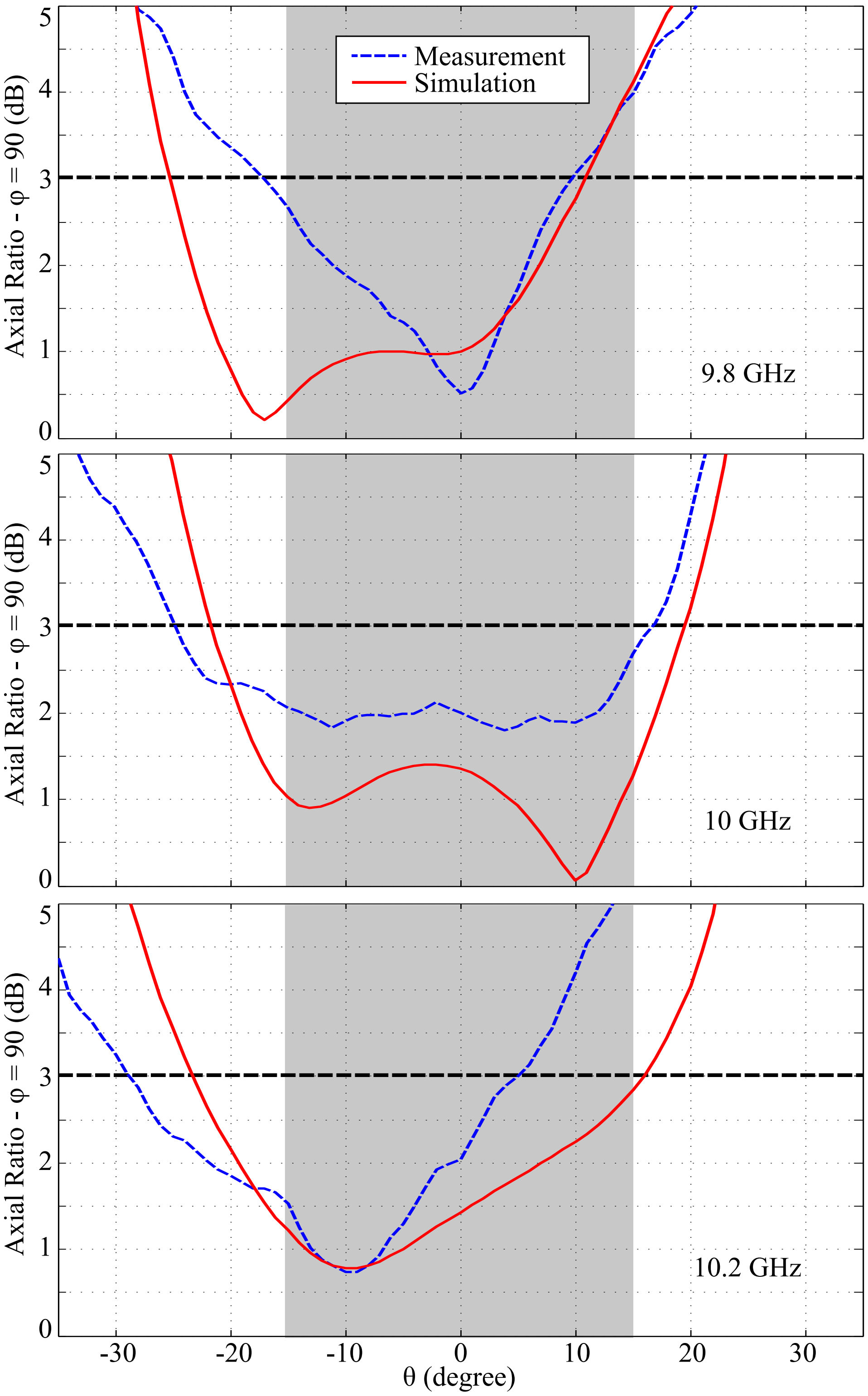

Figure 8.14. Simulated and measured axial ratio over θ in the yz-planes. Simulated and measured axial ratio over θ in the yz-plane, with the antenna port 2 terminated. The shaded area is the 3-dB beamwidth in the considered plane amounts to 30°, as shown in Fig. 8.11.

the measured and simulated S-parameters have only approximately 2.2% discrepancy and both simulated and measured realized gain are very close, the actual total efficiency of the prototype should be around 90%. The high performance is attributed to the efficient feed-line-to-element coupling.

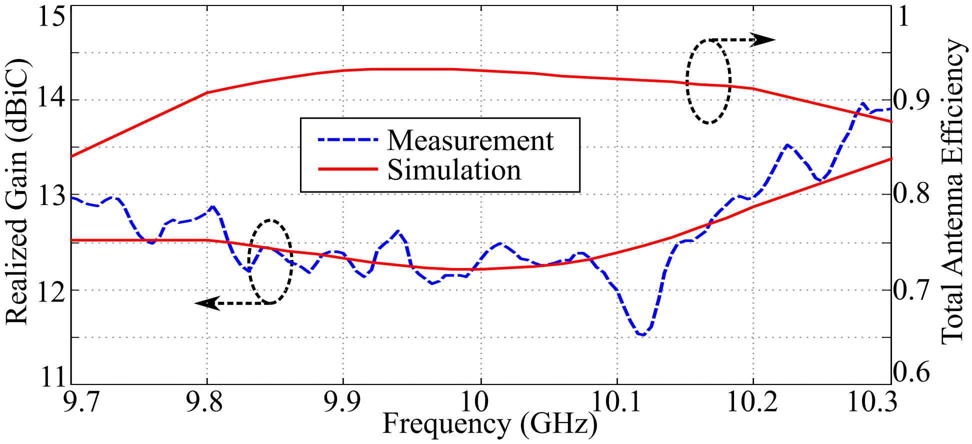

Figure 8.15. Realized gain and total efficiency of the array. Simulated and measured realized gain and simulated total efficiency of the antenna.

8.3.4 Human impact

As the proposed antenna is expected to be used for wearable applications, it is necessary to verify the impact on the antenna performance for operation in the vicinity of a human body. Hence, as shown in Fig. 8.16, an array prototype was attached to a torso phantom and subjected to experimental characterization in regard to S-parameters, AR, radiation patterns and gain.

In the antenna S-parameters measurement, the results in free space and worn by the phantom have nearly no difference. Figure 8.17 shows the measurement of $|S_{22}|$ and $|S_{12}|$ in these two scenarios where only very small variations are observed in the operational bandwidth. As expected, very similar observations are made for the $|S_{11}|$ and $|S_{21}|$ measurements which are not shown for simplicity. This consistent behavior is attributed to the electromagnetic isolation from the human body arising from the antenna ground plane.

The next measurement is the boresight AR and the results are compared in Fig. 8.18. The results for the antenna worn on the torso yield a 0.7 to 1.5 dB higher AR than the ones in free space within the operation band, this small discrepancy is not unexpected

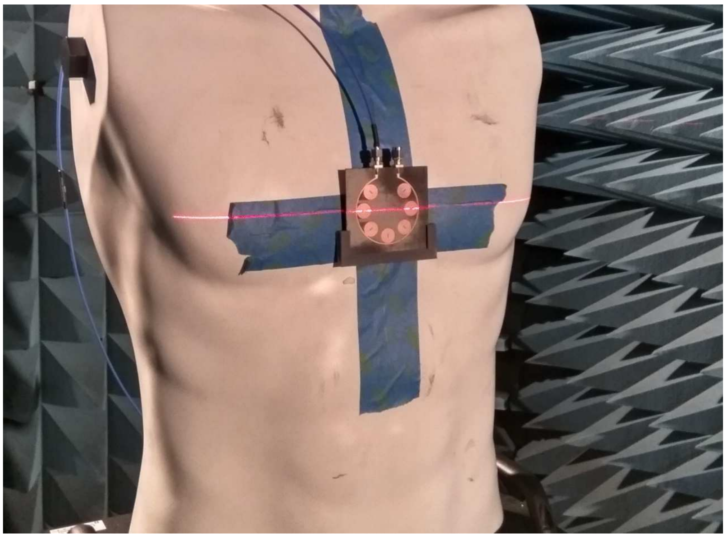

Figure 8.16. An antenna prototype attached to a human phantom for testing. An antenna prototype is attached to a torso phantom for experimental characterization.

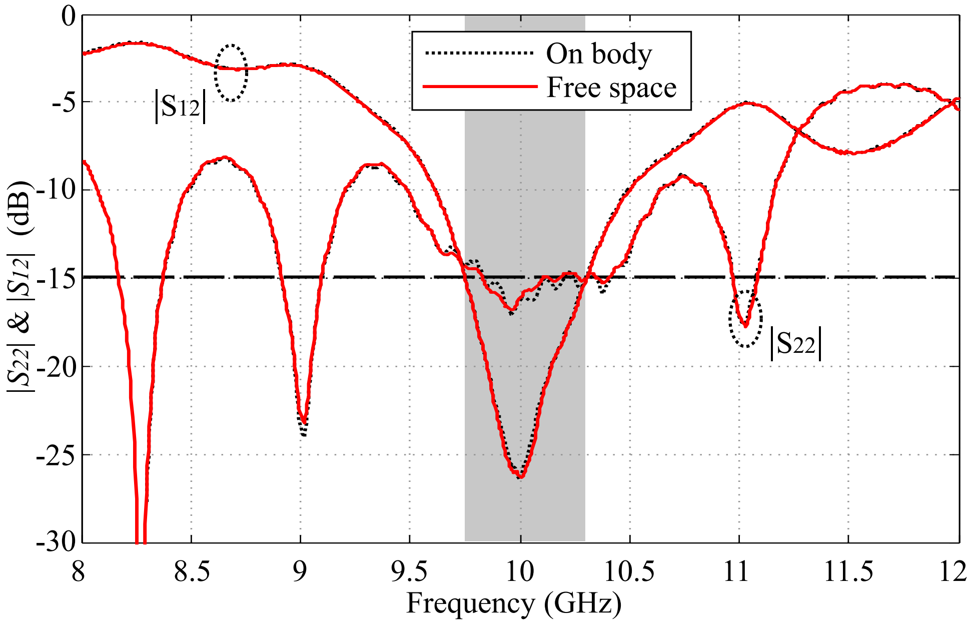

Figure 8.17. $|S_{22}|$ and $|S_{12}|$ of the antenna in free space and loaded on the phantom. Reflection coefficient comparison of the antenna with port 2 terminated in free space and loaded on the phantom.

when a very lossy dielectric, namely the human phantom, is in proximity. Even if the measured AR is slightly over 3-dB in part of operational frequency range, it still can operate satisfactorily in most scenarios.

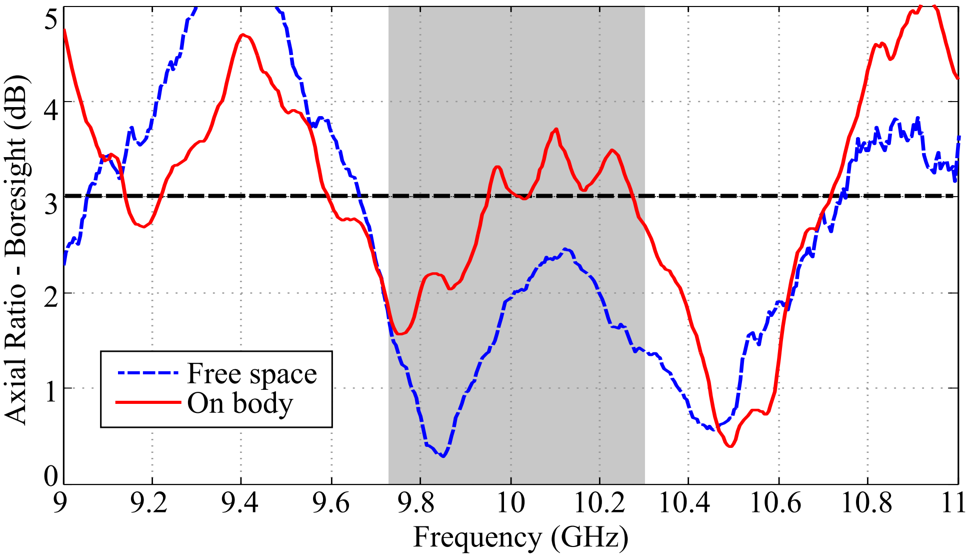

Figure 8.18. Boresight AR of the antenna in free space and loaded on the phantom. Boresight axial ratio of the antenna with port 2 terminated in free space and loaded on the phantom.

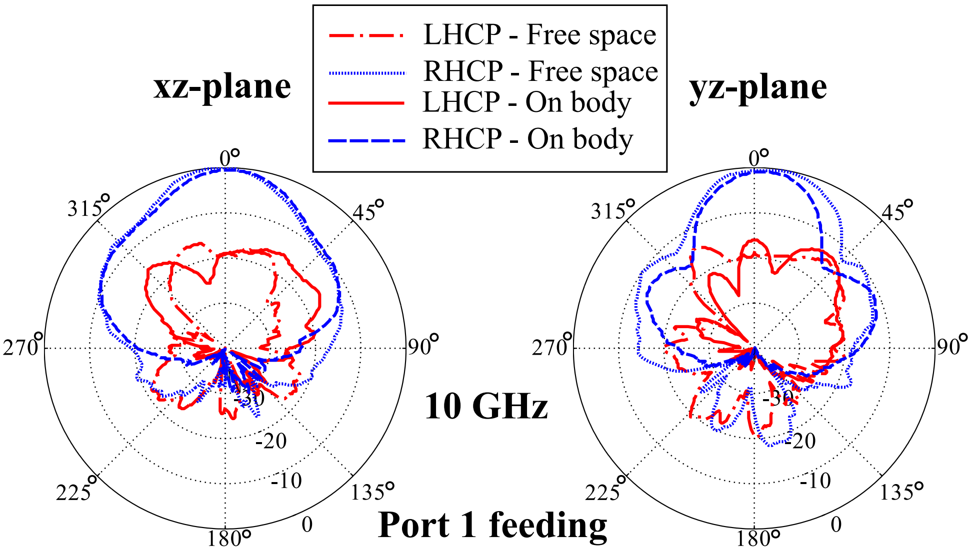

Figure 8.19. Antenna radiation patterns in free space and worn by the phantom. Measured normalized radiation patterns of the antenna with port 2 terminated in free space and loaded on the phantom.

The measured radiation patterns in the *xz*- and *yz*-planes are shown in Fig. 8.19. When compared to the patterns in free space, insignificant impact on the *xz* pattern and a narrower beamwidth in the *yz* plane are observed for the on-body results. This might be due to the different curvatures of the phantom in the vertical and horizontal directions at the antenna loading position. In addition, because of the presence of the phantom, the back radiations of both co- and cross-polarization components in the two planes are reduced significantly in the experiment due to the shadowing from the body.

The simulated and measured realized gain in free space are compared with the one measured with the phantom in Fig. 8.20. From the plot one can observe that the gain variation between the loaded and unloaded cases is not greater than 1 dB, which indicates that the phantom influence on the antenna gain is very limited. Together with the other results discussed above, the antenna performance degradation due to the vicinity of the torso phantom (human body) is not significant, due to the isolation provided by the ground plane.

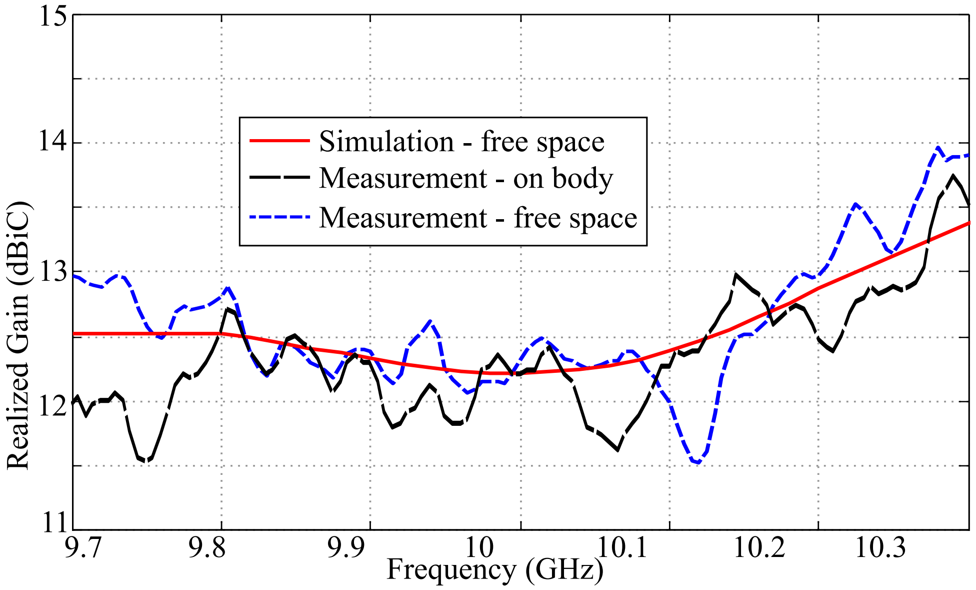

Figure 8.20. Gain of the LHCP antenna in free space and loaded on the phantom. Simulated and measured realized gain of the antenna loaded with the CP interchangeable module in free space and loaded on the phantom.

8.4 Conclusion

A travelling wave series-fed microstrip patch array has been proposed for wearable applications. The two-port array exhibits a compact structure and a high antenna efficiency of around 90% averaged over its operational bandwidth, owing to the circular array configuration and the strong proximity coupling. These are desirable antenna characteristics for wearable antennas. This antenna can be employed as a dual-port antenna to selectively generate RHCP or LHCP waves. With its sufficient port isolation, the antenna can also be used for arbitrarily polarized wave generation or polarimetry applications, through controlling or detecting the relative amplitude and phase of the two orthogonal inputs. An antenna prototype has been fabricated and experimentally characterized with and without a torso phantom. The good agreement between simulation and experimental results has validated the design and confirmed its insignificant degradation in performance due to human body. This novel array design can be used for wearable applications such as positioning and direction finding.

Chapter 9

Wearable Dielectric Resonator Antenna

DIELECTRIC resonator antennas (DRAs) have been extensively investigated since the last three decades, as they are highly promising for wireless communications due to their high radiation efficiency and design versatility. These antennas can be made compact with various shapes and aspect ratios. Additionally, they have wide impedance bandwidth and/or wide beamwidth, and thus they can be attractive antennas for wearable applications where these antenna characteristics are desirable. However, only very limited investigations on wearable applications of DRAs have been reported in the literature, and one of the main barriers is their inherent physical rigidity which significantly reduces the wearability. To resolve this problem, it is proposed to combine the use of flexible dielectric and conductive materials to realize DRAs.

This chapter presents a non-metallic flexible DRA realized with a mixture of PDMS and ceramic powder and proposed for wearable applications. This antenna is excited by a microstrip patch whose conductor is made of graphite paper while its substrate is realized with the ceramic-PDMS mixture. A prototype of the antenna is fabricated and subjected to experimental characterization. The good agreement between simulation and measurement indicates that, this non-metallic flexible antenna exhibits wide impedance bandwidth and broad beamwidth which make it very promising for wearable applications.

9.1 Introduction

Since the first implementation of a cylindrical dielectric resonator antennas (DRA) and its systematic study conducted by Long et al. in 1983 [207], interest in DRAs of various geometries have been steadily increasing due to their attractive antenna characteristics. These features include high radiation efficiency due to the low inherent conductor loss, geometrically flexibility in shape and aspect ratio, relatively wide bandwidth, simple feeding schemes and versatile radiation characteristics by mode selection [208, 209]. Therefore, these antennas are highly promising for a wide variety of wireless communications systems in the microwave and the millimetre-wave regions [210]. In particular, DRAs can be suitable for wearable applications such as RFID-based and wireless body area network (WBAN) systems. This is because these systems generally require very diverse antenna designs in terms of geometry, bandwidth and radiation characteristics, to cater for different body positions and environmental conditions. Especially the design versatility of DRAs in terms of geometry and radiation characteristics open new possibilities for adaption to various body physical and electromagnetic conditions, while their relatively wide bandwidth offers high tolerance to changing conditions. However, only a very limited number of research works on wearable DRAs have been reported in the literature [43–45, 211, 212]. One of the main reasons is believed to be the mechanical inflexibility of these antennas which significantly deteriorates their wearability. Hence this is a primary antenna engineering problem to solve for this particular application.

The very first DRA proposed for wearable applications to the author's knowledge, was from Almpanis et al. who introduced a truncated conical design working from 3 to 5 GHz with a small ground plane [43]. The configuration and a prototype of the antenna are shown in Fig. 9.1a and b respectively. This UWB antenna is based on a inverted truncated annular conical dielectric resonator (DR) which can offer a wide impedance bandwidth and radiate with a omnidirectional pattern. The feeding mechanism was based on a center rod on a small ground plane excited through a SMA connector. Even though the small ground plane was implemented to deliver a better wearability, the rigidity of the antenna materials and the probe-fed feeding configuration probably did not offer a very comfortable wearing experience.

As a result, to improve the wearability, approaches of reducing antenna physical size and making the antenna mechanically flexible were deployed in some recently reported works [44, 45, 212]. For instance, a rectangular stacked DRA design simulated

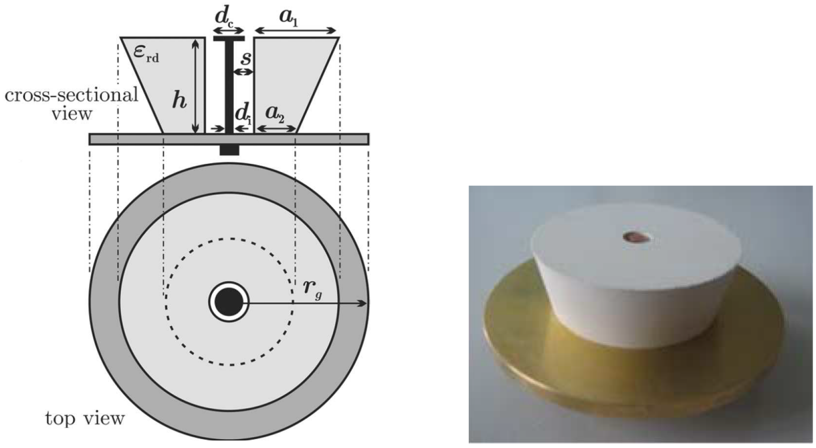

(a) (b)

Figure 9.1. The first DRA proposed for wearable applications. (a) The cross-sectional and top views and (b) a prototype of the first DRA conceptually proposed for wearable applications, adapted from [43].

using CST was proposed by Esselle's team for wearable medical applications [45], as shown in Fig. 9.2. Based on the simulated results reported, this probe-fed antenna can achieve an at least 50% volume reduction via using a copper side wall. The resulting device operates with a wide impedance bandwidth from 4.7 to 9.9 GHz by exploiting a multi-segment/multi-permittivity structure. On the other hand, as shown in Fig. 9.3, three different types of cylindrical DRAs employing textiles as flexible ground plane and/or substrate were proposed by Kishk's team [212], to obtain a higher antenna conformability. These three antennas were designed for the 5.8-GHz ISM band with a footprint of 60 × 60 mm^2 and a height from 12 to 18 mm. For both cases, the antenna flexibility and consequently wearability are still limited, since their DRs are rigid and relatively thick.

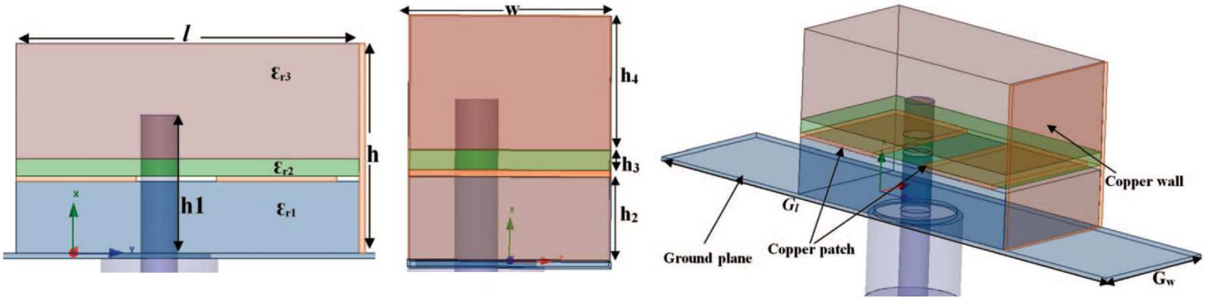

Figure 9.2. A rectangular multilayer DRA proposed for wearable applications. The two side and perspective views of the antenna proposed in [45], adapted from [45].

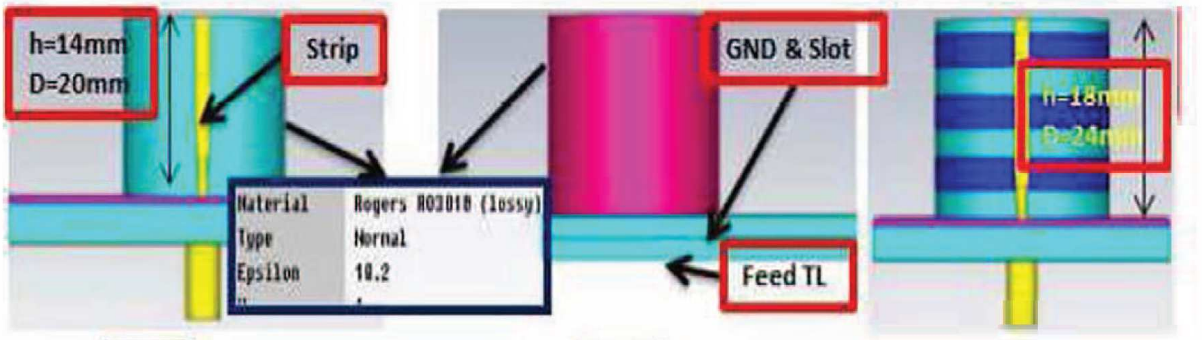

Figure 9.3. Three cylindrical DRAs proposed for wearable applications. The side views of the three DRAs proposed in [212], adapted from [212].

In this chapter, a wideband DRA whose DR and feeding structure are both made mechanically flexible is proposed for wearable applications. The DR is realized in a mixture of polydimethylsiloxane (PDMS) and ceramic powder and thus exhibits an excellent conformability. The feeding configuration is a microstrip patch whose substrate and conductors are made of the ceramic-PDMS mixture and graphite paper respectively. This antenna feed is flexible and excites the DRA from the side rather than the bottom, which makes it more appropriate for wearable applications. Based on this principle, one antenna prototype was realized and subjected to experimental characterization. The good agreement between the simulation and measurement indicates that, the proposed DRA has a wide beamwidth of around 100° in the E-plane and a wide fractional impedance bandwidth of 53%. Combining these features with the presence of a ground plane for isolation, the proposed antenna is expected to be appropriate for wearable applications, although further experimental validation on the flexibility is planned in future work. This is due to the fact that, the antenna ground plane offers a good electromagnetic isolation to the human body whereas the wide impedance bandwidth relaxes the tolerance limit for antenna physical bending.

9.2 DRA design

9.2.1 DRA configuration

The configuration and the CST model of the proposed antenna are shown in Fig. 9.4a and b respectively whereas the antenna final dimensions are listed in Table 9.1. The

Table 9.1. The antenna dimensions. Dimensions of the proposed antenna in (mm).

L_1	L_2	L_3	L_4	W_1	W_2	W_3	W_4	R	h_1	h_2
40.0	11.5	8.5	1.5	40.0	14.0	3.5	2.5	13.0	4.5	2.5

device is comprised of two main components, namely a cylindrical dielectric disk operating as the resonator and a microstrip non-resonant patch working as the feed. Exploiting this feeding arrangement promotes better wearability thanks to the side feed, as well as electromagnetic isolation owing to ground plane configuration. The patch top edge is aligned with the center of the DR to excite its HEM$_{11\delta}$ mode, since in this configuration their field distributions are matched, as depicted in Fig. 9.5. Alternatively, it can be interpreted that the DR fundamental mode is excited by the equivalent magnetic current formed by the electric field distributed between ground plane and patch edge in the antenna center. The simulated electric field distribution confirms that the DR resonates at the HEM$_{11\delta}$ mode at around 5.8 GHz, as shown in Fig. 9.6. At higher frequencies, the mode transforms to a hybrid mode combing the TM$_{01\delta}$ and HEM$_{11\delta}$, as shown in 9.7. As a consequence, these two closely located modes result in a wide impedance bandwidth.

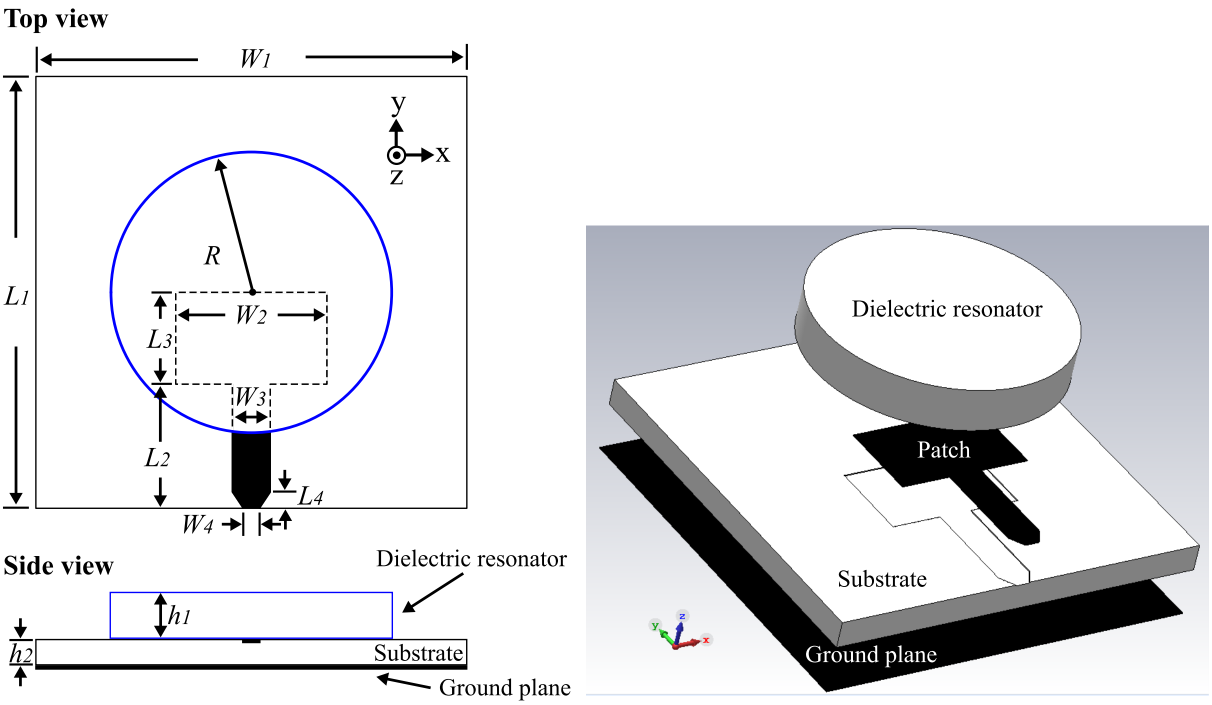

(a) (b)

Figure 9.4. The proposed antenna configuration and 3D model in CST. (a) The top and side views and (b) the 3D exploded model in CST of the proposed wearable DRA.

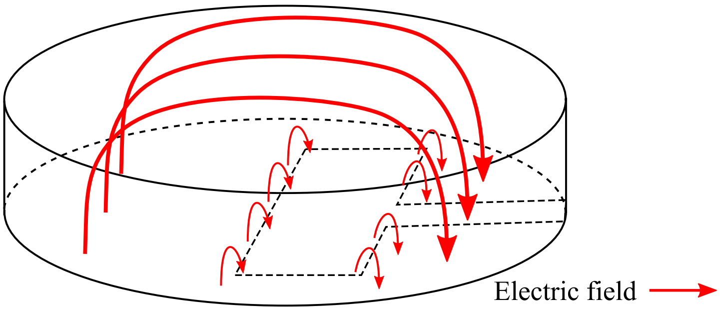

Figure 9.5. HE$_{11\delta}$ mode excitation illustration. The electric field distribution inside the DR illustrating how the HE$_{11\delta}$ mode is excited.

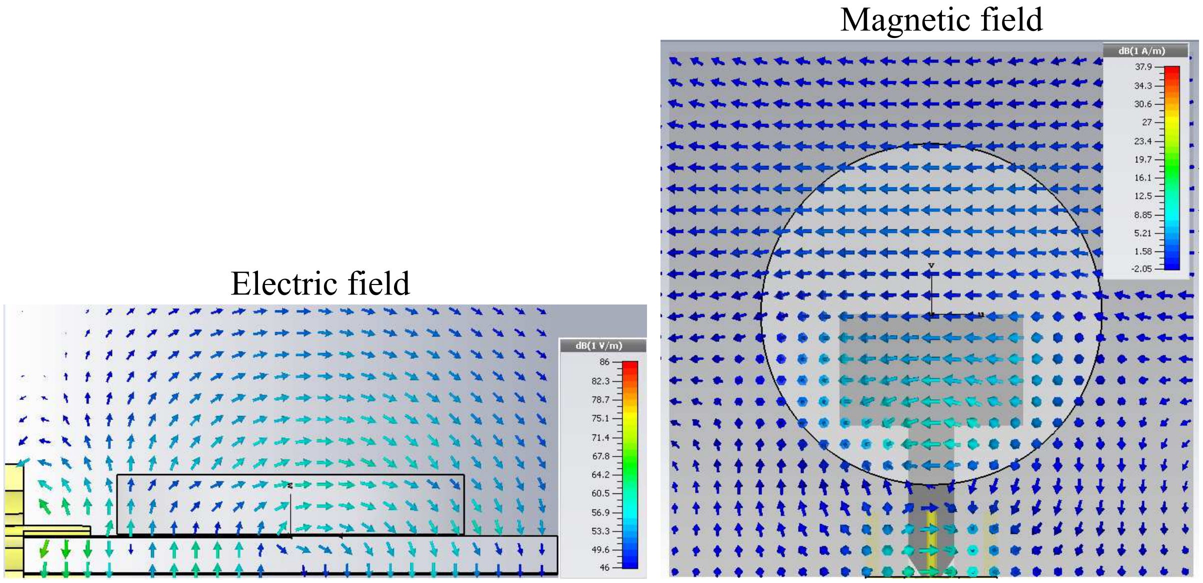

(a) (b)

Figure 9.6. Simulated E- and H-field distributions of the HE$_{11\delta}$ mode. The simulated (a) electric field and (b) magnetic field distribution inside the DR at the HE$_{11\delta}$ mode of 5.8 GHz.

The patch is connected to a 50-Ω microstrip line for feeding. The ground plane not only serves for the patch, but also conventionally acts as an electric wall for the DR which leads to an approximate 50% volume reduction by making its resonance frequency to be half, according to image theory. Therefore, the substrate section that is directly connected to the DR should be considered as part of a multilayer DR structure. The resonance frequency of the fundamental HEM mode $f_{(HEM_{11})}$, radius a, height h and relative permittivity ε_r of the DR have the following closed-form relations obtained through numerical results [208]:

$$f_{(HEM_{11})} = \frac{k_{0a}c}{2\pi a}, \tag{9.1}$$

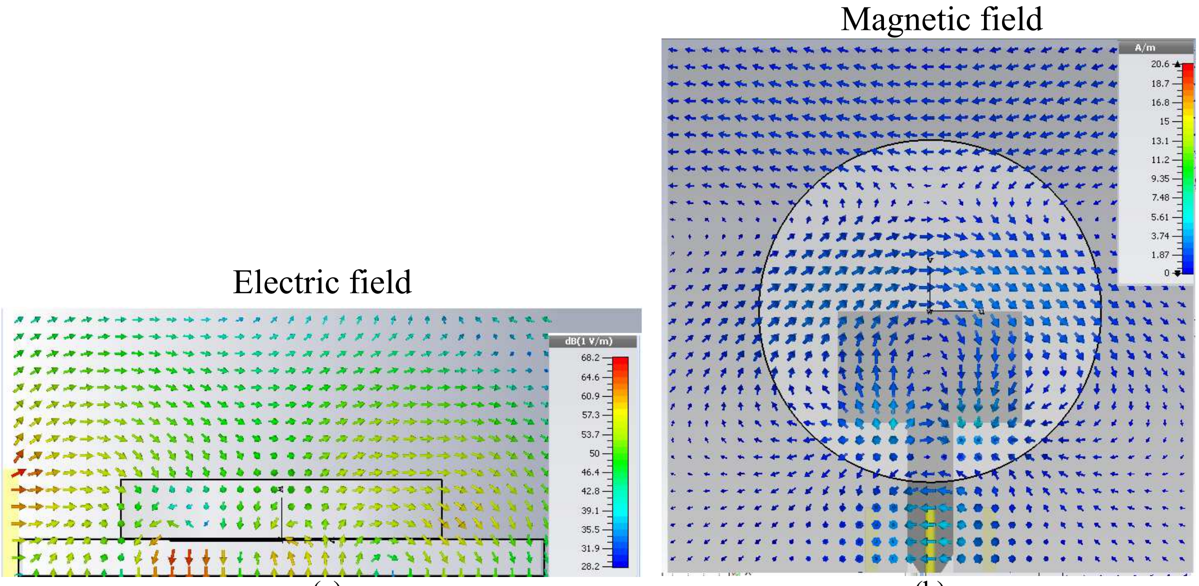

(a) (b)

Figure 9.7. Simulated E- and H-field distributions of the hybrid mode. The simulated (a) electric field and (b) magnetic field distribution inside the DR in the hybrid mode of 8.6 GHz.

$$k_{0a} = \frac{6.324}{\sqrt{\varepsilon_r + 2}}\left[0.27 + 0.36(\frac{a}{2H}) + 0.02(\frac{a}{2H})^2\right] \tag{9.2}$$

where c and k_{0a} are the speed of light and the normalized wavenumber, respectively. The resonance frequency is set here to be the ISM 5.8-GHz band. The exact relative permittivity of the DR is obtained through dedicated measurements on the fabricated material prototypes. Then, based on these expressions, the combination of the height and radius of the DR can be determined according the following principle: the ratio between the DR radius and height should be high to keep a low profile for the antenna, provided the lateral footprint is within a certain range (e.g. maximum 50 mm × 50 mm). At the end, the size of the feeding non-resonant patch is obtained through iterative parametric optimization in CST aiming for a wide and satisfactory impedance bandwidth.

9.2.2 Antenna materials

As this antenna is designed for wearable applications, making the antenna mechanical flexible is one of primary requirements. As a consequence, composites of PDMS and ceramic powder are selected as the materials for the DR and the substrate, since excellent mechanical resilience with a relative permittivity up to 25 can be achieved using these materials, as reported in [213]. The PDMS used was 184 Silicone Elastomer from Sylgard® which has two components Part-A and Part-B while the ceramic powder used was the 90M/ML series from Prosperity Dielectrics Co., Ltd., as shown in Fig. 9.8. The reported relative permittivity ε_r and the loss tangent tanδ of the PDMS are 2.68 and 0.001 respectively at 10 kHz. The ceramic power 90ML has a claimed relative permittivity ε_r of 95. A higher proportion of ceramic powder in the mixture will lead to a higher relative permittivity but also a lower mechanical flexibility. Based on numerous trial-and-error experiments, a weight combination of 20% 90ML and 80% PDMS is believed to be one of the best solutions which provides a relative permittivity of 4 and a loss tangent of 0.046 at 5.8 GHz while maintaining a reasonable flexibility. The DR relative permittivity is relatively low compared to conventional DR, which will lead to a larger antenna size, but in counterpart it promotes a wider impedance bandwidth. The permittivity and loss tangent of the various composite materials samples are measured using a Dielectric Assessment Kit (DAK) from SPEAG.

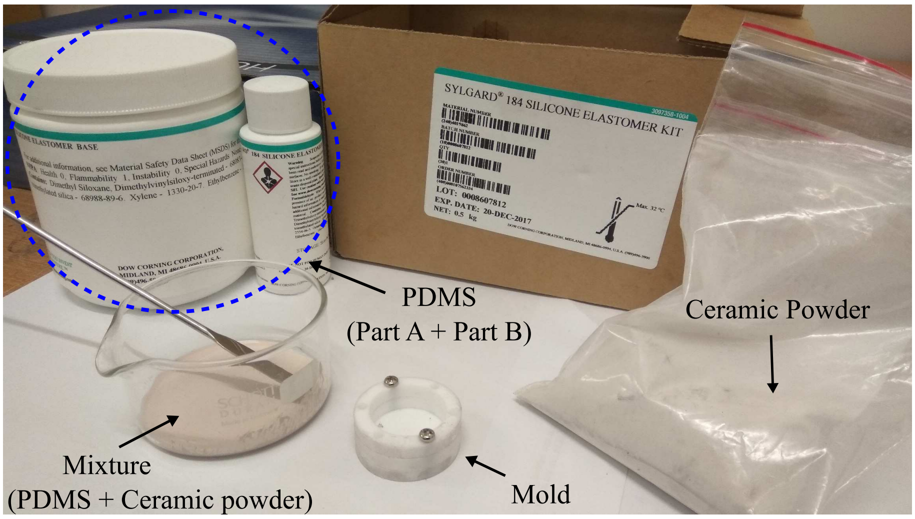

Figure 9.8. The materials and mold for DR fabrication. The ceramic powder, PDMS and a mold required for the DR fabrication.

Due to its low cost, good mechanical flexibility and satisfactory conductivity, commercially available graphite paper is utilized as conductor layer for the patch and the ground plane. The graphite paper has a thickness of 150 μm which is about three times the skin depth at 5.8 GHz (around 57 μm) and a conductivity of 1.33×10^4 S/m. A laser-cut patch and ground plane realized in the graphite paper are shown in Fig. 9.9a and b, respectively. Conductive epoxy CW2400 from CircuitWorks® is employed to glue an SMA connector to the antenna.

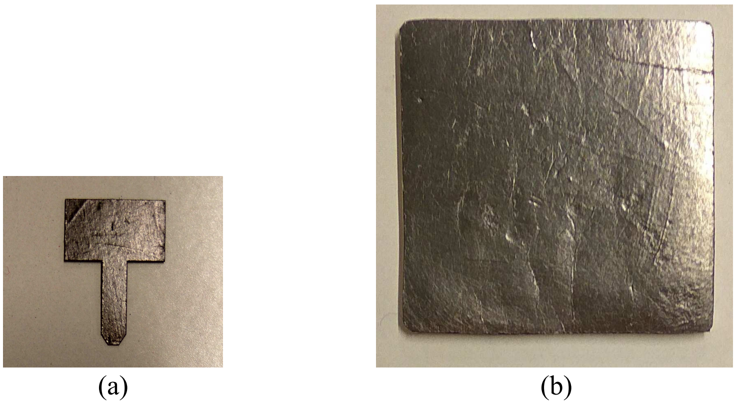
(a) (b)

Figure 9.9. Patch and ground plane made of graphite paper. (a) A patch and (b) a ground plane realized using graphite paper, cut by a laser milling machine.

9.2.3 Antenna fabrication

There are four steps involved for the DR realization. First, well mixed PDMS Part-A and Part-B are mixed in a good stirring with the ceramic powder until they are uniformly distributed in the PDMS. Second, the mixture is placed into a glass chamber with a vacuum pump connected and running until all bubbles are removed from the mixture. This is necessary for the these air bubbles introduced in the stirring step to be eliminated, as they will decrease the permittivity and quality of the DR. Third, the mixture is very gently poured into a mold (see Fig. 9.8) to minimize new bubble production. If deemed necessary, the mixture in the mold can be put into a vacuum chamber again, but only for a very short time frame. The reason is that, due to the higher density of the ceramic powder, it tends to sink in the PDMS and thus creates non-uniformity and uncertainty in the DR permittivity. For the same reason, the last step is placing the mold onto a hotplate with a preset temperature of 150°C, in order to solidify the mixture as rapidly as possible. One flexible DR prototype fabricated is shown in Fig. 9.10.

Figure 9.10. A flexible DR prototype. A DR prototype realized in PDMS and ceramic powder using the mold shown in Fig. 9.8.

Similarly, for the substrate fabrication process, the ceramic-PDMS mixture needs to be prepared following the first two steps mentioned above. The difference is that the material now needs to be combined with the graphite paper patch and the ground plane which have been accurately patterned using a laser milling machine (LPKF: Protolaser S), as shown in Fig. 9.9. Double side adhesive tape is used to accurately affix the patch on the substrate mold based on the desired antenna configuration. The prepared ceramic-PDMS mixture is then very gently poured into the mold and the ground plane is placed on top of it. The whole piece is then put on a preheated hotplate of 150°C for quick drying. When dried, the patch and the ground plane are naturally bonded to the substrate. The final step is to glue the DR on the substrate with PDMS and attach an SMA connector using conductive epoxy. As illustrated in Fig. 9.11, the realized DR, substrate and the whole antenna all exhibit very good mechanical flexibility. Because of its thickness, the antenna inherently has the least conformability.

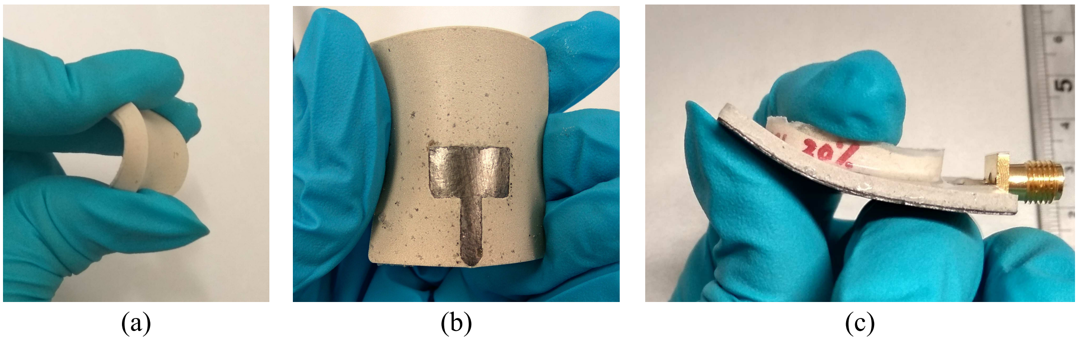
(a) (b) (c)

Figure 9.11. DR, substrate and antenna prototypes under bending condition. Prototypes of (a) a DR, (b) a substrate and (c) an antenna under bending conditions, demonstrating very good mechanical flexibility.

9.3 Experimental results

An antenna prototype, as demonstrated in Fig. 9.12, has been fabricated and experimentally characterized. Good agreement between simulation and measurement validates the design.

The simulated and measured reflection coefficients of the antenna prototype are compared in Fig. 9.13, where a reasonable agreement is observed. The simulated S_{11} shows two resonance at 6 and 8.6 GHz as discussed in Section 9.2.1 and exhibits a good impedance matching ($|S_{11}| <$ -10 dB) from 5.5 to 9.8 GHz, corresponding to an approximate 53% fractional bandwidth. The measured reflection coefficient shows three

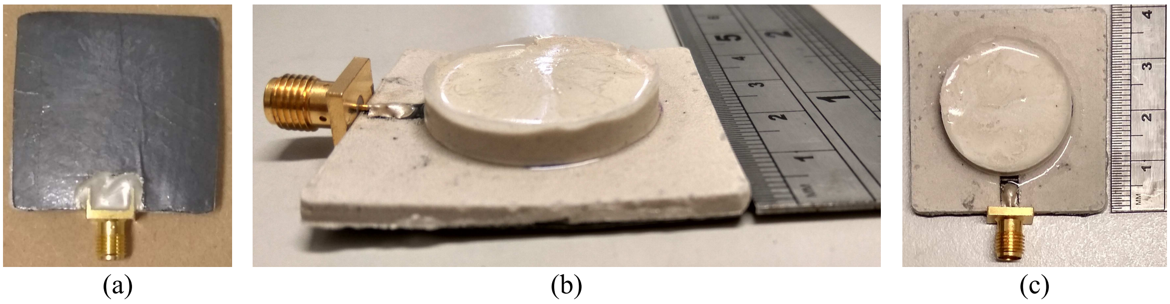
(a) (b) (c)

Figure 9.12. An antenna prototype. (a) A back, (b) a perspective and (c) a top view of the antenna prototype under test.

resonances approximately at 6, 7.3 and 8.8 GHz. The presence of the middle resonance 7 GHz and the frequency shift of the hybrid mode to 8.8 GHz can be due to the fabrication tolerance such as imperfect alignment of the feed which might excite other hybrid modes. In addition, it is noted that a much wider impedance bandwidth extending from 5.5 to 20 GHz was observed during measurement (not shown after 10GHz in Fig. 9.13). This is however attributed to the significant ohmic loss inside the conductors at high frequencies due to skin effect and high roughness of the graphite paper. As a result, the practically usable impedance bandwidth of the prototype remains the same as the simulated one, namely from 5.5 to 9.8 GHz.

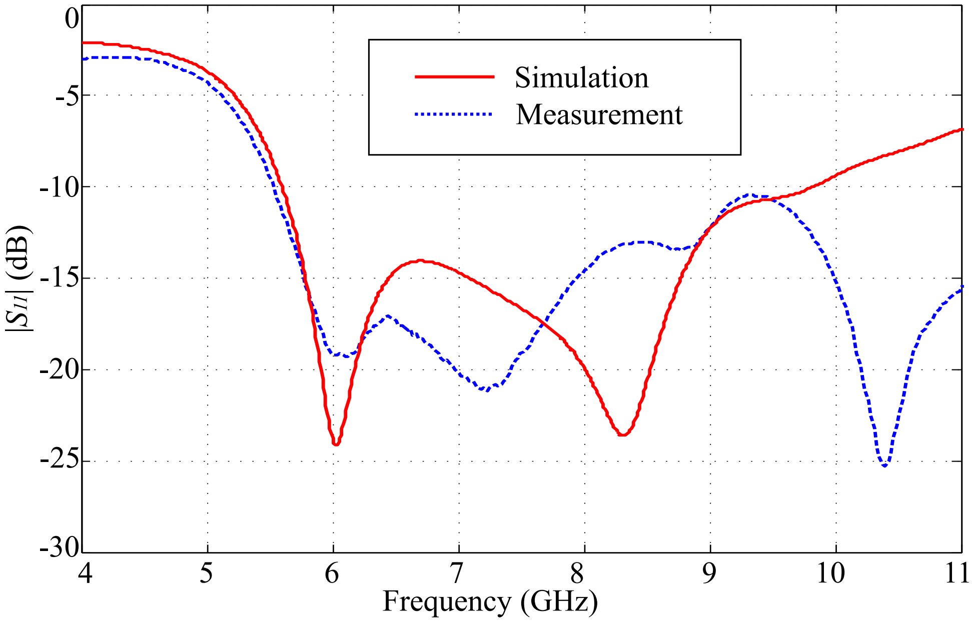

Figure 9.13. Simulated and measured $|S_{11}|$ of the DRA. Simulated and measured reflection coefficients of the proposed flexible DRA.

The simulated and measured radiation patterns at 5.5, 5.8, 6, 7, 8 and 9 GHz in the yz- and xz-plane are shown in Fig. 9.14, and a good agreement is attained. A typical radiation pattern of the fundamental $\mathrm{HEM}_{11\delta}$ mode can be observed for the 5.5, 5.8, 6 and 7 GHz, which correspond to the pattern radiated by a magnetic dipole orientated in the x direction on a finite ground plane. Importantly, such a pattern has a very wide 3-dB beamwidth of around 100° in the yz-plane (E-plane) while the xz-plane has the maximum in the boresight and nulls along the x axis. This is consistent with the magnetic field distribution shown in Fig. 9.6, and proves that the ceramic-PDMS cylinder operates as a DRA despite its low relative permittivity. In the present context, this type of radiation patterns is desired for off-body applications because the very wide beamwidth leads to a very large angular coverage in the y direction. Towards higher frequencies, the main beam starts to become asymmetric and narrower in the yz-plane, due to the hybrid mode introduced by the asymmetric feeding geometry. This kind of more directional pattern is also very practical for off-body communications.

The simulated and measured realized gain are both plotted in Fig. 9.15. A very good consistency is obtained in most of the spectrum and slight discrepancies are likely due to the imperfect measurement. The measured gain from 5.5 to 10 GHz ranges between 3.1 to 7.2 dB, which should be sufficiently high for most wearable applications. The gain has a rising trend which can be explained by the increasing antenna directivity associated with the hybrid mode. In the frequency range beyond 9.5 GHz, the measured antenna gain starts to drop significantly which leads to a reflection coefficient below -10 dB up to 20 GHz. As mentioned, this is due to the ohmic loss in the rough graphite paper and the dielectric loss in the PDMS. The simulated total antenna efficiency is also plotted in Fig. 9.16. As shown in the figure, the simulated total antenna efficiency ranges from 42.8% to 62.5% between 5.5 to 9.8 GHz, with an averaged value of 58.3%. This can be improved by using conductors with higher conductivity and/or dielectric powder with lower loss.

It is emphasized that, the present study is a conceptual preliminary investigation of the proposed flexible DRA structure, and that the impact due to the human body and bending will be considered in future work. However, one can intuitively expect that with its ground plane the antenna should be insensitive to the human host, and that the impact due to bending can be easily compensated by the very wide antenna impedance bandwidth.

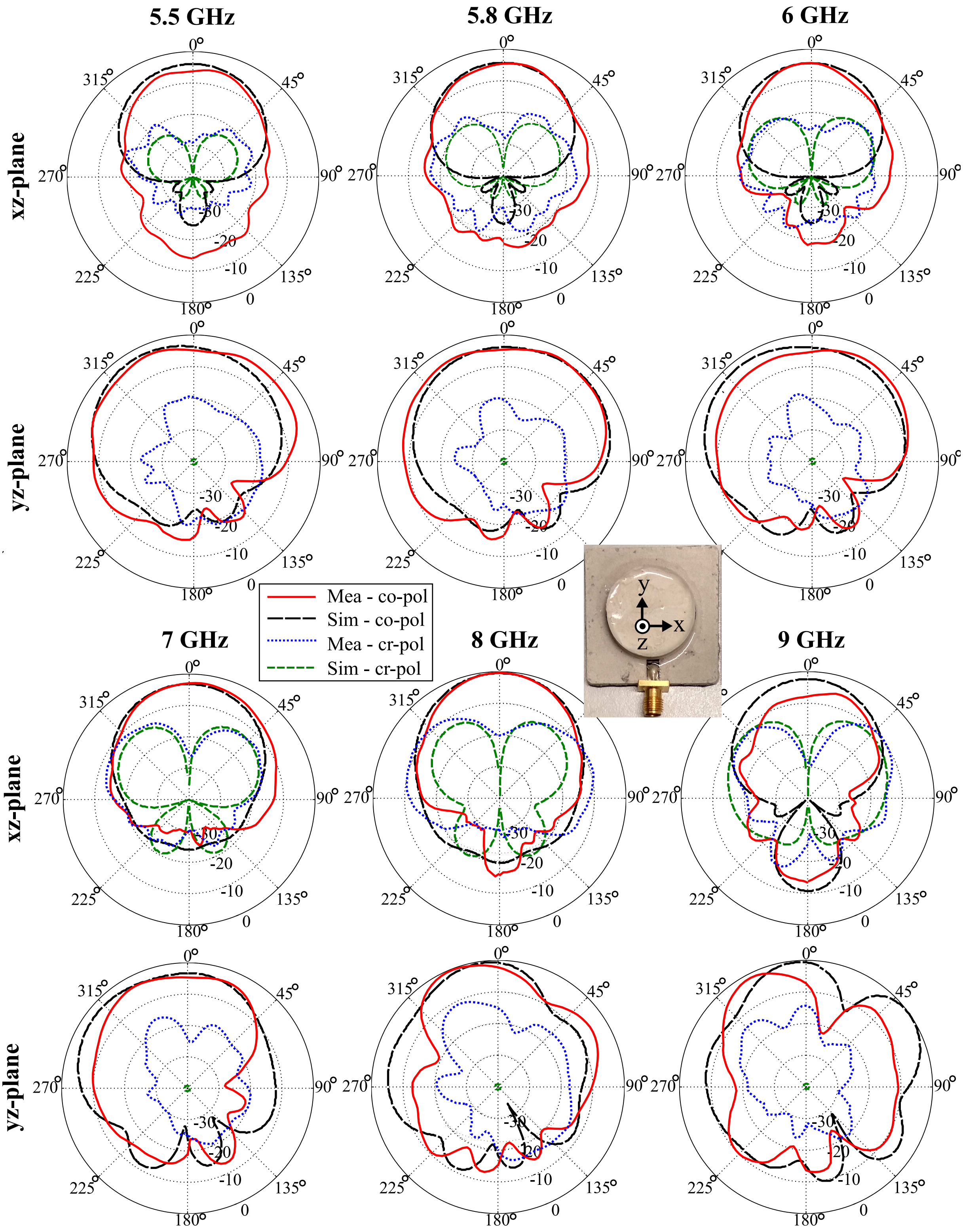

Figure 9.14. Radiation patterns of the proposed antenna. The simulated and measured radiation patterns of the proposed wearable DRA at 5.5, 5.8, 6, 7, 8 and 9 GHz in the xz- and yz-planes.

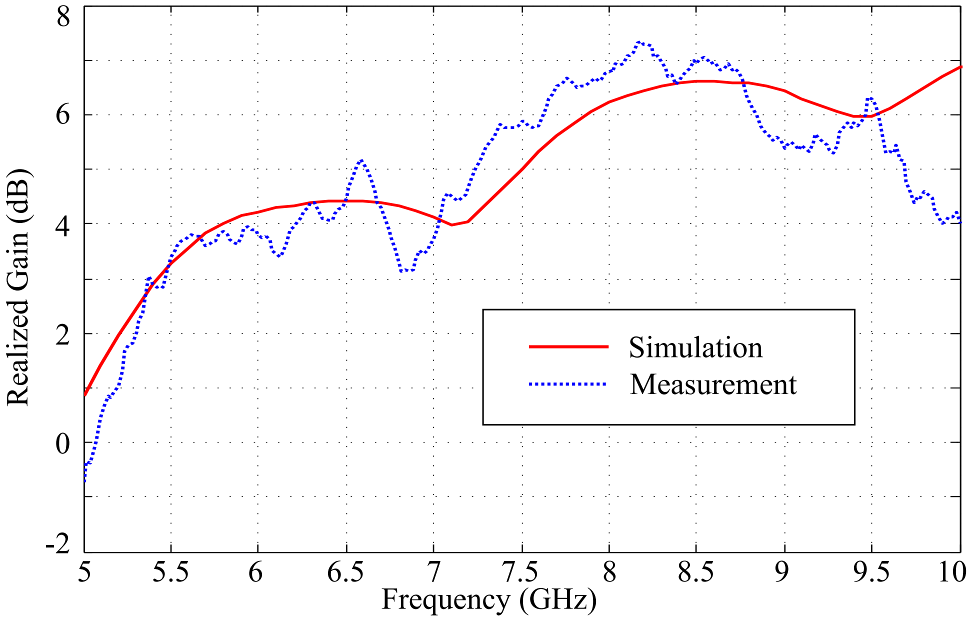

Figure 9.15. Simulated and measured realized gain of the DRA. Simulated and measured realized gain of the antenna.

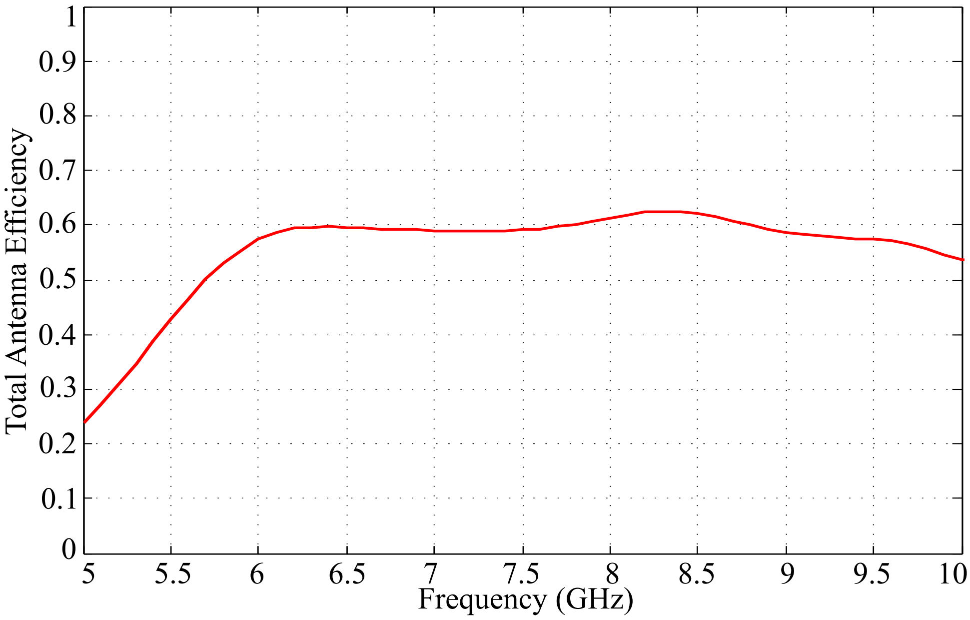

Figure 9.16. Simulated total efficiency of the DRA. Simulated total efficiency of the antenna.

9.4 Conclusion

Mechanical rigidity of conventional DRAs limits their exploitation in wearable applications, although these antennas are conceptually very suitable since they are versatile in design, wideband and highly efficient. Therefore, a flexible and wideband microstrip-fed DRA has been proposed for wearable applications in this chapter. The antenna consists of a DR and a microstrip patch where both are made flexible to improve the wearability. Flexible ceramic-PDMS composites and graphite paper are used as the dielectric and conductive materials for the proposed DRA, to gain mechanical flexibility while attaining satisfactory electrical performance. An antenna prototype has been fabricated and experimentally studied to validate the design. The very good agreement between simulation and measurement indicates that, the proposed antenna concept is viable. The good mechanical conformability, the wide impedance bandwidth ($|S_{11}| <$ -10 dB) of 53% and the large 3-dB beam width of 100° approximately, all make this antenna very promising for wearable applications.

Chapter 10

Conclusion and Outlook

THE research presented in thesis has been described into four major parts mainly associated to flexible, wearable and reconfigurable antennas realized in novel conductive materials. The first part has focused on flexible and high-efficiency antenna designs based on non-metallic conductors, namely conductive polymers and graphene thin films. The second part has placed emphasis on shorting and connection strategies for wearable textile antennas. Following that, the third part has been devoted to modular and reconfigurable wearable textile antennas. And finally, the fourth part has investigated novel antenna structures for wearable applications. This chapter concludes all these four self-contained parts and suggests possible future related work.

10.1 Summary preamble

The research discussed in this thesis is mainly related to flexible, wearable and reconfigurable antennas realized in novel conductive materials such as conductive polymers, graphene and graphite thin films and conductive textiles. The work has been presented in four self-contained sections and they are summarized in this chapter, in terms of the original contributions and results. Additionally, a number of possible future research directions for each of the four sections are also suggested.

10.2 Part I: Flexible and high-efficiency antennas based on non-metallic conductors

This part of the thesis consists of Chapter 3 and 4 which have placed the focus on designing flexible and high-efficiency antennas realized in non-metallic conductors such as conductive polymers and graphene thin films. These two chapters have put the emphasis on appropriate engineering methods to overcome the inherent and process-related limitations of the materials. The engineering approaches include exploitation of non-resonant antenna structure to improve the antenna efficiency, utilization of simple chemical treatment to enhance material conductivity and multilayer laminated structure to increase the effective material thickness. This section summarizes the original contributions and considers the potential future work of this part.

10.2.1 Summary of original contributions

- Based on an efficiency-driven antenna design strategy, a non-resonant UWB antenna operating from 3 to 20 GHz with compact size, high efficiency and exceptional mechanical flexibility has been proposed. The antenna is completely made from polymer consisting of a patterned PEDOT:PSS thin film attached to a transparent sticky tape substrate. The overall dimension is less than a quarter-wavelength at the lowest operation frequency. The device reaches a radiation efficiency of over 85% averaged throughout the frequency band, which is, to the authors', best knowledge, the highest reported value for non-metallic antennas of this type. The realized antenna offers great mechanical flexibility and robustness which indicates its promising potential for possible seamless integration in flexible electronics [5].

- A numerical and experimental study of the impact of bending on the characteristics of a purely polymeric UWB antenna reported in [5] has been conducted. Because the highly flexible polymer antenna is expected to be used under various bending conditions, it is very critical to investigate the possible performance degradations due to bending, including variations in impedance matching and radiation characteristics. The results indicate that, even with considerable bending angles, the antenna still functions well in terms of impedance matching, however, degradation in polarization needs to be taken into account [46].

- A 2.45-GHz dipole antenna realized in methanol-treated conductive polymers PEDOT:PSS has been proposed, featuring excellent mechanical conformability and high efficiency. Through immersing the originally highly conductive PEDOT:PSS thin films in a methanol solution, the treated films have achieved a five-times higher conductivity from approximately 3500 S/m to 18500 S/m. Consequently, a more than 25% antenna efficiency enhancement has been obtained, which has brought the averaged efficiency up to 91.4% of the value of a copper reference antenna with identical geometry [47].

- A flexible 5.8-GHz microstrip-fed slot antenna based on PEDOT:PSS polymer thin film has been designed, fabricated and tested. Due to the use of a highly conductive and flexible PEDOT:PSS film as well as a low-loss flexible polyethylene foam, the antenna exhibits a high efficiency of 82% and fully reversible flexibility. This is a typical engineered multilayer purely polymeric antenna exhibiting reversible mechanical flexibility [49].

- A three-layer laminated thin film structure based on two layers of PEDOT conductors and one layer laminae of SiO_2 in between has been patterned in a strip and tested in a dedicated microstrip line test jig, showing a 5 to 15 dB higher $|S_{21}|$ parameter compared to the single layer PEDOT. These results indicate the laminated structure is promising to overcome the insufficient film thickness problem for some conductive polymers.

- A high-efficiency UWB antenna made of graphene films which are based on binder-free and surfactant-free graphene inks has been proposed. The fabricated antenna yields a high efficiency averaging 79% over the bandwidth from 3.1 to 10.6 GHz, which is, to the authors' best knowledge, the highest reported value for graphene antennas for the microwave region. The combination of high-quality graphene films, efficiency-driven antenna design strategy and appropriate fabrication technique is the key for achieving this outstanding performance [51,52].

10.2.2 Future work

Antenna designs based on conductive polymers

With continuous advances in materials science, it is predictable that the electrical conductivity and the plastic-like mechanical properties of conductive polymers will be improved steadily while other desired characteristics such as biocompatibility and biodegradability will be enhanced as well. As a result, these materials can be utilized for more advanced antenna designs:

- **Reconfigurable and sensing antennas**

  Controlling changes in antenna materials characteristics would be a very promising approach to design antennas with sensibility and/or reconfigurability. These antennas are highly desired for a wide range of applications such as wireless sensor networks. Conducting polymers can have great potential of being such materials, since some of them have sensorial characteristics. For instance, various conductive polymers have intrinsic electrical conductivity due to the conjugated bonds within the polymer molecule, and the mechanism of the charge movement is highly depending on temperature, moisture, light, external excitation such as electrical and mechanical forces [62]. As a result, with changes in these conditions such as light, temperature, humidity and bias voltage, the variation in the electrical conductivity of these polymers can be utilized to design sensing and/or reconfigurable antennas. Since only very limited investigations on these antennas based on conductive polymers [214,215] have been reported in the open literature, this is definitely a promising area to further explore.

- **Implantable and biodegradable antennas**

  On the other hand, on top of their high electrical conductivity and light weight, some conductive polymers can be made biocompatible and biodegradable [216,217]. This unique combination of electrical conductivity, light-weight, biocompatibility and biodegradability opens a door for exploiting these polymers as conductor materials for implantable and/or biodegradable antennas.

Antenna designs based on graphene or its composites

Similarly, a very positive perspective about the development of graphene and its composites is expected, due to the intensive research resources invested globally. Especially as the fabrication and process technologies for graphene will become mature, one can expect that the theoretically and numerically designed graphene antennas can be practically realized and optimized, from microwave to THz and infrared frequency range.

- **Nanoscale and reconfigurable antennas for the THz band**

  As mentioned in Chapter 2, graphene is a very appropriate conductor for antennas dedicated for the THz band, since it supports surface plasmon polariton (SPP) waves in the frequency range [92,94]. In addition, since the graphene resistivity will decrease drastically when a DC bias voltage is applied, reconfigurable antenna characteristics can be fulfilled based on this property. Therefore, development of nanoscale and reconfigurable antennas dedicated for the THz band will continuously be the main focus of the related antenna research. One can expect other important aspects in terms of antenna fabrication and measurement will become another focus at THz frequencies in the very near future.

- **Printable and reconfigurable antennas for the microwave region**

  As discussed in Chapter 4, graphene inks have very attractive properties such as low cost, hight conductivity, easy processability and environmental friendliness, which make them very suitable conductors for inexpensive and corrosion-resistant antennas. Especially, since these graphene inks can be sprayed, inkjet- and screen-printed, even antennas with complicated geometry can be patterned very quickly and accurately on substrates. As a result, printable antennas characterized by convenient and economic fabrication can be one promising future work. On the other hand, similarly to the case mentioned above for the THz band, the changeable resistivity of graphene also can be employed to design reconfigurable antennas in the microwave region. For instance, one can realize a DC-control switch based on graphene layer(s) to design reconfigurable antennas. This will be also another promising aspect worth investigating.

10.3 Part II: Shorting and connection strategies for wearable textile antennas

Chapter 4 represents the second part of the thesis, which has investigated practical shorting and connection strategies for wearable textile antennas, based on textile strips, embroidered vias, metallic eyelets and commercial snap-on buttons. This section concludes the original contributions and suggests potential directions for future work.

10.3.1 Summary of original contributions

- Different practical shorting strategies have been investigated for wearable textile antennas, based on an L-slot planar inverted-F antenna (PIFA). These shorting approaches include a folded strip of silver fabric, embroidered vias and metallic eyelets. The performance of a PIFA antenna realized with these three shorting methods has been compared to an ideal short based on full-wave simulations with realistic shorting models. The results have indicated that the embroidered vias shorting method is the simplest and cheapest method to implement, however, has slightly lower efficiency and gain than the silver fabric folded strip and eyelet shorting methods due to its higher resistance [53].
- Commercial snap-on buttons have been proposed to realize detachable shorting vias for wearable textile antennas. A microstrip patch antenna which utilizes these button shorting vias has been designed, fabricated and experimentally validated. It has been shown that different antenna radiation patterns can be selected, through engaging particular male buttons from the ground plane with female buttons to form shorting vias. This has demonstrated that commercial snap-on buttons can be practically utilized as detachable shorting vias for wearable textile antennas, to obtain passive reconfigurability [54].
- A pair of commercial snap-on buttons has been demonstrated as a detachable RF balanced connection between a garment-integrated textile dipole antenna and a passive sensor-enabled RFID tag and in a wearable wireless system. This connection offers inexpensive, reliable and repeatably detachable RF coupling and feeding connections for balanced textile antennas, as conceptualized in simulations and validated through measurements. Additionally, the RF performance of the proposed snap-on button connection has been characterized in a back-to-back

balanced transmission line structure. The resulting transmission coefficients have indicated the good performance of the snap-on buttons as RF connectors for balanced antennas/transmission lines at least up to 5 GHz with insertion loss better than 0.8 dB [55,56].

10.3.2 Future work

Shorting and connection strategies

Experimental validation for the proposed shorting solutions should be completed to confirm the predictions obtained from the simulated results. Additionally, other metallic accessories for clothing can be worth exploiting as alternative shorting and connection solutions for textile antennas.

- **Experimental validation for different shorting strategies**

  For experimental validation, the simulated L-slot PIFA antenna should be fabricated with different shorting strategies as proposed, namely folded textile strip, embroidered vias using conductive threads, metallic eyelets and snap-on buttons. Evaluations in terms of cost, fabrication difficulty and antenna performance especially the variations in impedance matching and efficiency (especially the variations in impedance matching and efficiency) should be performed. In addition, similar studies should also be conducted for shorting wall realization using these shorting approaches, which requires another antenna test bed. This was not possible in the timeframe of this thesis, but would provide validated characterization of those shorting techniques.

- **Other shorting and connection strategies**

  There are other types of metallic accessories in common use in the clothing industry, for example, buttons and zips. Some of these textile-compatible components might be possibly exploited as alternative shorting and connection methods for wearable textile antennas. For instance, depending on the design, metallic zips can be used as a shorting wall with a manually adjustable length, whereas a metallic button can be adopted as a fastenable electrical connector. Further exploration of this aspect for textile antenna design is interesting and promising.

10.4 Part III: Modular and reconfigurable wearable textile antennas

The third part of this thesis has proposed a modular and a reconfigurable design for wearable textile antennas in Chapter 6 and 7, respectively. The original contributions and future work are summarized in the present section.

10.4.1 Summary of original contributions

- An antenna design concept with interchangeable radiation elements which provide modularity in antenna characteristics for wearable applications has been presented. By utilizing commercial snap-on buttons both as mechanical holding mechanism and for RF connection, a variety of modularly interchangeable microstrip patches have been employed to demonstrate geometry reconfigurabilities in terms of resonance frequency and polarization. Three patches offering interchangeability in circular polarization at 5 GHz, interchangeability in resonance frequencies of 2.4- and 5.3-GHz and operation at 8-GHz have been proposed as typical designs, respectively. The good agreement between simulation and experiment of the fabricated antennas in free space, worn by a torso phantom and in bending conditions, have validated the concept and proven that this type of modular design can offer convenient, passive, low-cost, and versatile system modularities, which can be very beneficial for low-cost wearable applications [57].

- As an extension of the module library for the modular wearable textile antenna concept mentioned above [57], a foldable patch module has been proposed, showing passive discrete resonance frequency modularity at 8, 9 and 10 GHz. Particular resonance frequencies can be passively interchanged, by simply folding the textile radiating element at predetermined lengths denoted by position markers. The results obtained from the prototype-based experimental characterization have indicated that the foldable module functions as expected. This design has emphasised that the reported modular antenna design offers a practical, low-manufacture-cost, low-maintenance-cost, passive and versatile solution to reconfigure system characteristics for multi-functional wearable systems [58].

- A circular patch module with a rectangular flap cut in the middles has been proposed, as another new member of the module library for the modular concept. This module not only has interchangeability between right-handed circular polarization (RHCP), left-handed circular polarization (LHCP) and linear polarization (LP), but also has passive reconfigurability in resonance frequency for LP, through simple module rotation and different flap configurations (opened or closed). This design has confirmed the versatility of the modular concept [59].

- A reconfigurable module consisting of commercial snap-on buttons and a dedicated circuitry unit which can have varactor(s)/PIN diode(s), inductor(s) and capacitor(s) integrated to form an active circuit is proposed for reconfigurable wearable textile antennas. This button module can solve the main challenge in realizing reliable connection between lumped components, circuit board and conductive textiles. The very different physical properties of those flexible and rigid components have been the main obstacle to truly reconfigurable wearable designs. A frequency-reconfigurable PIFA antenna employing this button module has been designed and tested in a preliminary design, and the measured results have validated the concept [60].

10.4.2 Future work

Modular and reconfigurable textile antennas

The modular and the reconfigurable antenna concepts proposed are both based on commercial snap-on buttons. Extending the reconfigurable (active) button module and patch (passive) module libraries as well as combining these two concepts together in antenna design can be two promising directions for the future work.

- **Active and passive module libraries extension**

  More elaborate reconfigurable antenna designs with dedicated active button module(s) should be exploited in the near future. In addition, through identifying commonly used topologies in reconfigurable antenna design, corresponding active button modules (circuitry units) can be also developed accordingly in a similar modular fashion beforehand. This will allow a prompt antenna design for conventional projects. For the same reason, extending the patch modules library for the modular concept is also worth extension.

- **Antenna designs combining these two concepts**

  A very versatile antenna design strategy can be developed by combining the modular and the reconfigurable button module concepts. This is because the design flexibilities obtained from both the passive patch and the active button modules can dramatically increase the versatility in antenna designs. For instance, an antenna may be able to attain frequency reconfigurability in several desired spectrum ranges, by interchanging its patch modules. Therefore, this can be a very promising direction for investigation in the near future.

10.5 Part IV: Novel antenna structures for wearable applications

The last part of the thesis encompasses Chapter 8 and 9 which have proposed novel antenna structures for wearable applications. These antennas include a series-fed dual-circularly-polarized microstrip patch array and a flexible DRA. The original contributions are all summarized in this section, along with the future work.

10.5.1 Summary of original contributions

- A highly efficient series-fed microstrip patch array with a compact size has been proposed for wearable applications. The patch elements are excited by the traveling wave guided by a microstrip line through coplanar proximity coupling. Due to the circular array arrangement and the strong coupling mechanism, the array exhibits a compact size and a high efficiency. A dual-port feeding enables the ability of choosing the direction of the travelling waves, and consequently the sense of circular polarization of the patches. The array can radiate waves of arbitrary polarization when both ports are fed simultaneous with proper amplitude and phase difference. Since the antenna array is very thin and compact while exhibiting a very good isolation from the human object owing to the ground plane, it can be used for wearable applications [61].

- Towards wearable applications, a non-metallic DRA which had its dielectric resonator (DR) and substrate both made mechanically flexible has been designed and subjected to experimentally characterization. The DR of the antenna is realized in a mixture of PDMS and ceramic powder while the microstrip patch feed is based on carbon paper over a substrate made of the ceramic-PDMS mixture. This flexible antenna is promising for wearable applications, because it not only has a ground plane and thus electromagnetic isolation from the human body, but also a wide impedance bandwidth of 53% and a broad beamwidth of nearly 100°.

10.5.2 Future work

Wearable microstrip patch array

The proposed series-fed microstrip patch array concept can be very suitable for wearable applications, because of its simple feeding structure and compact circular arrangement. Actually, the array can be designed in other arrangements depending on applications. For instance, one can deploy a linear array to realize a conformal design to be mounted on a helmet or integrated in a belt. In addition, active lumped circuits can also be introduced in the array to control the coupling strength of each array element and thus steer the main beam. All these advanced antenna designs are desired for wearable applications. Therefore, this can be the promising directions for future research.

Wearable DRA

Towards wearable applications, the proposed DRA has been designed to be fed by a microstrip line while introducing mechanical flexibility to gain comfortable wearing experience. Additionally, the antenna wide impedance bandwidth can compensate most performance degradation due to deformation, and the ground plane provides isolation from the human body. The presented work has demonstrated that DRA designs are a promising path to exploit for wearable applications.

- **Compact dense dielectric patch antenna**

  The first dense dielectric patch antenna was reported by Lai et al. [218] in 2013. This planar antenna is composed of a very thin dielectric disk of a very high permittivity, which operates similarly as a standard half-wave microstrip patch antenna resonating at its TM^{z}_{110} mode. This type of antennas exhibits a compact size and can have a ground plane, which make it very suitable for wearable applications, not to mention their high radiation efficiency and wide beamwidth. Future work can place focus on making these antenna more flexible to improve the wearability.

- **Dielectric resonator antenna as button for clothes**

  DRAs can be designed in various shape and aspect ratio, and hence it is possible to realize them as normal buttons for clothes. This is very beneficial since one can integrate the antenna into a garment without standing out, while the antenna acts as a button simultaneously. In addition, since a fastened button can have a very tight connection to the fabrics underneath, one can utilize a section of the fabrics realized in conductive textiles to form a ground plane for the DRA, which will halve the antenna height. This can be a practical solution for antenna-to-garment integration and is a promising path for future study.

10.6 Concluding statement

The research presented in this thesis has focused on the design, fabrication and system interconnection, for flexible, wearable and reconfigurable antennas based on several promising novel conductive materials. These included conductive polymers, graphene and graphite films and conductive textiles. Since these novel materials have very different characteristics compared to the conventional rigid conductors such as copper, significant efforts have been placed into the material side of antenna engineering principles. One of the main motivations of this thesis was to combine customized antenna technology and material science, and thus create antennas with unconventional characteristics desired for wearable electronic systems. A variety of flexible, wearable and reconfigurable antennas based on the mentioned novel materials have been presented in this thesis, exhibiting promising general characteristics and radiation performance. All these promising achievements have illustrated that the interdisciplinary combination of antenna technology and material science magically explores prospective solutions to present and future antenna design challenges. This might become one of the main directions for antenna development towards next generations of mobile wireless communication systems.

Bibliography

[1] K. Finkenzeller, *RFID Handbook.* Chichester, UK: John Wiley & Sons, Ltd, Jun 2010.

[2] P. S. Hall and Y. Hao, Eds., *Antennas and Propagation for Body-Centric Wireless Communications*, 1st ed. London: Artech House, Incorporated, 2006.

[3] A. Verma, B. Weng, R. Shepherd, C. Fumeaux, V.-T. Truong, G. G. Wallace, and B. D. Bates, "6 GHz microstrip patch antennas with PEDOT and polypyrrole conducting polymers," in *Int. Conf. Electromagn. Adv. Appl.* IEEE, 2010, pp. 329–332.

[4] T. Kaufmann, A. Verma, V.-T. Truong, B. Weng, R. Shepherd, and C. Fumeaux, "Efficiency of a compact elliptical planar ultra-wideband antenna based on conductive polymers," *Int. J. Antennas Propag.*, vol. 2012, pp. 1–11, 2012.

[5] S. J. Chen, T. Kaufmann, R. Shepherd, B. Chivers, B. Weng, A. Minett, and C. Fumeaux, "A compact, highly efficient and flexible polymer ultra-wideband antenna," *IEEE Antennas Wirel. Propag. Lett.*, vol. 14, pp. 1207 – 1210, 2015.

[6] X. Huang, T. Leng, X. Zhang, J. C. Chen, K. H. Chang, A. K. Geim, K. S. Novoselov, and Z. Hu, "Binder-free highly conductive graphene laminate for low cost printed radio frequency applications," *Appl. Phys. Lett.*, vol. 106, no. 20, 2015.

[7] M. Akbari, M. W. A. Khan, M. Hasani, T. Bjorninen, L. Sydanheimo, and L. Ukkonen, "Fabrication and characterization of graphene antenna for low-cost and environmentally friendly RFID tags," *IEEE Antennas Wirel. Propag. Lett.*, vol. 15, no. c, pp. 1569–1572, 2016.

[8] A. Tsolis, W. Whittow, A. Alexandridis, and J. Vardaxoglou, "Embroidery and related manufacturing techniques for wearable antennas: Challenges and opportunities," *Electronics*, vol. 3, no. 2, pp. 314–338, 2014.

[9] I. Locher and G. Tröster, "Fundamental building blocks for circuits on textiles," *IEEE Trans. Adv. Packag.*, vol. 30, no. 3, pp. 541–550, 2007.

[10] K. Koski, A. Vena, L. Sydanheimo, L. Ukkonen, and Y. Rahmat-Samii, "Design and implementation of electro-textile ground planes for wearable UHF RFID patch tag antennas," *IEEE Antennas Wirel. Propag. Lett.*, vol. 12, pp. 964–967, 2013.

[11] C. Hertleer, A. Tronquo, H. Rogier, L. Vallozzi, and L. Van Langenhove, "Aperture-coupled patch antenna for integration into wearable textile systems," *Antennas Wirel. Propag. Lett.*, vol. 6, no. 11, pp. 392–395, 2007.

[12] L. Zhang, Z. Wang, and J. L. Volakis, "Textile antennas and sensors for body-worn applications," *IEEE Antennas Wirel. Propag. Lett.*, vol. 11, pp. 1690–1693, 2012.

[13] C. Hertleer, A. Tronquo, H. Rogier, and L. Van Langenhove, "The use of textile materials to design wearable microstrip patch antennas," *Text. Res. J.*, vol. 78, no. 8, pp. 651–658, 2008.

[14] C. Hertleer, H. Rogier, L. Vallozzi, and L. Van Langenhove, “A textile antenna for off-body communication integrated into protective clothing for firefighters,” *IEEE Trans. Antennas Propag.*, vol. 57, no. 4, pp. 919–925, 2009.

[15] E. K. Kaivanto, M. Berg, E. Salonen, and P. de Maagt, “Wearable circularly polarized antenna for personal satellite communication and navigation,” *IEEE Trans. Antennas Propag.*, vol. 59, no. 12, pp. 4490–4496, 2011.

[16] Z. Wang, L. Zhang, Y. Bayram, and J. L. Volakis, “Embroidered conductive fibers on polymer composite for Conformal antennas,” *IEEE Trans. Antennas Propag.*, vol. 60, no. 9, pp. 4141–4147, 2012.

[17] M. Klemm and G. Tröster, “Textile UWB antennas for wireless body area networks,” *IEEE Trans. Antennas Propag.*, vol. 54, no. 11, pp. 3192–3197, 2006.

[18] P. B. Samal, P. J. Soh, and G. a. E. Vandenbosch, “UWB all-textile antenna with full ground plane for off-body WBAN communications,” *IEEE Trans. Antennas Propag.*, vol. 62, no. 1, pp. 102–108, 2014.

[19] Q. H. Abbasi, M. U. Rehman, X. Yang, A. Alomainy, K. Qaraqe, and E. Serpedin, “Ultrawideband band-notched flexible antenna for wearable applications,” *IEEE Antennas Wirel. Propag. Lett.*, vol. 12, pp. 1606–1609, 2013.

[20] R. Moro, S. Agneessens, H. Rogier, and M. Bozzi, “Wearable textile antenna in substrate integrated waveguide technology,” *Electron. Lett.*, vol. 48, no. 16, pp. 985–987, 2012.

[21] T. Kaufmann and C. Fumeaux, “Wearable textile half-mode substrate-integrated cavity antenna using embroidered vias,” *IEEE Antennas Wirel. Propag. Lett.*, vol. 12, pp. 805–808, 2013.

[22] S. Agneessens and H. Rogier, “Compact half diamond dual-band textile HMSIW on-body antenna,” *IEEE Trans. Antennas Propag.*, vol. 62, no. 5, pp. 2374–2381, 2014.

[23] J. Jung, H. Lee, and Y. Lim, “Broadband flexible comb-shaped monopole antenna,” *IET Microwaves, Antennas Propag.*, vol. 3, no. 2, p. 325, 2009.

[24] H. R. Khaleel, H. M. Al-Rizzo, D. G. Rucker, and S. Mohan, “A compact polyimide-based UWB antenna for flexible electronics,” *IEEE Antennas Wirel. Propag. Lett.*, vol. 11, pp. 564–567, 2012.

[25] G. DeJean, R. Bairavasubramanian, D. Thompson, G. Ponchak, M. Tentzeris, and J. Papapolymerou, “Liquid crystal polymer (LCP): A new organic material for the development of multilayer dual-frequency/dual-polarization flexible antenna arrays,” *Antennas Wirel. Propag. Lett.*, vol. 4, no. 1, pp. 22–5, Dec 2005.

[26] Rushi Vyas, Amin Rida, Swapan Bhattacharya, and M. M. Tentzeris, “Liquid crystal polymer (LCP): The ultimate solution for low-cost RF flexible electronics and antennas,” in *2007 IEEE Antennas Propag. Int. Symp.*, no. 1. IEEE, Jun 2007, pp. 1729–1732.

[27] M. H. Sagor, Q. H. Abbasi, A. Alomainy, and Y. Hao, “Compact and conformal ultra wideband antenna for wearable applications,” *Proc. 5th Eur. Conf. Antennas Propag.*, pp. 2095–2098, 2011.

[28] S. Cheng, A. Rydberg, K. Hjort, and Z. Wu, “Liquid metal stretchable unbalanced loop antenna,” *Appl. Phys. Lett.*, vol. 94, no. 14, p. 144103, Apr 2009.

[29] M. L. Scarpello, D. Kurup, H. Rogier, D. Vande Ginste, F. Axisa, J. Vanfleteren, W. Joseph, L. Martens, and G. Vermeeren, "Design of an implantable slot dipole conformal flexible antenna for biomedical applications," *IEEE Trans. Antennas Propag.*, vol. 59, no. 10, pp. 3556–3564, Oct 2011.

[30] G. J. Hayes, Ju-Hee So, A. Qusba, M. D. Dickey, and G. Lazzi, "Flexible liquid metal alloy (EGaIn) microstrip patch antenna," *IEEE Trans. Antennas Propag.*, vol. 60, no. 5, pp. 2151–2156, May 2012.

[31] R. B. V. B. Simorangkir, Y. Yang, L. Matekovits, and K. P. Esselle, "Dual-band dual-mode textile antenna on PDMS substrate for body-centric communications," *IEEE Antennas Wirel. Propag. Lett.*, vol. 16, no. c, pp. 677–680, 2017.

[32] T. Kaufmann, D. C. Ranasinghe, M. Zhou, and C. Fumeaux, "Wearable quarter-wave folded microstrip antenna for passive UHF RFID applications," *Int. J. Antennas Propag.*, vol. 2013, no. i, pp. 1–11, 2013.

[33] H. Shirakawa, E. J. Louis, A. G. MacDiarmid, C. K. Chiang, and A. J. Heeger, "Synthesis of electrically conducting organic polymers: halogen derivatives of polyacetylene, (CH) x," *J. Chem. Soc. Chem. Commun.*, no. 16, p. 578, 1977.

[34] C. Chiang, C. Fincher, Y. Park, A. Heeger, H. Shirakawa, E. Louis, S. Gau, and A. MacDiarmid, "Electrical conductivity in doped polyacetylene," *Phys. Rev. Lett.*, vol. 39, no. 17, pp. 1098–1101, 1977.

[35] H. Rmili, J.-L. Miane, H. Zangar, and T. Olinga, "Design of microstrip-fed proximity-coupled conducting-polymer patch antenna," *Microw. Opt. Technol. Lett.*, vol. 48, no. 4, pp. 655–660, 2006.

[36] R. Solberg and P. Siemsen, "Development of a conductive polymer, composite, direction-finding antenna," in *IEEE Antennas Propag. Soc. Int. Symp. Dig. Held conjunction with Usn. Natl. Radio Sci. Meet.*, vol. 3. IEEE, 1999, pp. 1966–1969.

[37] P. Pillai, E. Paster, L. Montemayor, C. Benson, and I. Hunter, "Development of soldier conformable antennae using conducting polymers," in *27th Army Sci. Conf.*, 2010, pp. 1–6.

[38] N. Kirsch, N. Vacirca, E. Plowman, T. Kurzweg, A. Fontecchio, and K. Dandekar, "Optically transparent conductive polymer RFID meandering dipole antenna," in *IEEE Int. Conf. RFID*. IEEE, 2009, pp. 278–282.

[39] J. S. Gomez-Diaz and J. Perruisseau-Carrier, "Microwave to thz properties of graphene and potential antenna applications," in *Proc. 2015 Int. Symp. on Antennas and Propagation (ISAP2015)*, Oct 2012, pp. 239–242.

[40] J. Perruisseau-Carrier, "Graphene for antenna applications: Opportunities and challenges from microwaves to thz," in *2012 Loughborough Antennas Propag. Conf.*, Nov 2012, pp. 1–4.

[41] G. Ginestet, N. Brechet, J. Torres, E. Moradi, L. Ukkonen, T. Bjorninen, and J. Virkki, "Embroidered antenna-microchip interconnections and contour antennas in passive UHF RFID Textile tags," *IEEE Antennas Wirel. Propag. Lett.*, vol. 1225, no. c, pp. 1–1, 2016.

[42] M. L. Sarpello, L. Vallozzi, H. Rogier, and D. Vande Ginste, "High-gain textile antenna array system for off-body communication," *International Journal of Antennas and Propagation*, vol. 2012, pp. 1–12, 2012.

[43] G. Almpanis, C. Fumeaux, J. Frohlich, and R. Vahldieck, "A truncated conical dielectric resonator antenna for body-area network applications," *IEEE Antennas Wirel. Propag. Lett.*, vol. 8, pp. 279–282, 2009.

[44] S. H. H. Mashhadi, Z. Wu, and L. Z. Thamae, "Investigation of a wearable broadband textile dielectric resonator antenna," in *2010 Loughbrgh. Antennas Propag. Conf.*, no. November. IEEE, Nov 2010, pp. 349–352.

[45] M. S. Iqbal and K. P. Esselle, "A compact wideband dielectric resonator antenna for on-body applications," in *2014 IEEE MTT-S Int. Microw. Work. Ser. RF Wirel. Technol. Biomed. Healthc. Appl.* IEEE, Dec 2014, pp. 1–3.

[46] S. J. Chen, B. Chivers, R. Shepherd, and C. Fumeaux, "Bending impact on a flexible ultra-wideband conductive polymer antenna," *2015 Int. Conf. Electromagn. Adv. Appl.*, pp. 422–425, 2015.

[47] S. J. Chen, P. Talemi, B. Chivers, R. Shepherd, and C. Fumeaux, "A highly flexible and efficient dipole antenna realized in methanol-treated conductive polymers," *Proc. 2015 Int. Symp. on Antennas and Propagation (ISAP2015)*, pp. 422–425, 2015.

[48] ——, "Purely polymeric antennas with exceptional flexibility and high efficiency," in *2nd Australian Microwave Symposium*, Feb 2016.

[49] S. J. Chen, C. Fumeaux, B. Chivers, and R. Shepherd, "A 5.8-GHz flexible microstrip-fed slot antenna realized in PEDOT:PSS conductive polymer," in *2016 IEEE Int. Symp. Antennas Propag.*, vol. 2015. IEEE, Jun 2016, pp. 1317–1318.

[50] S. J. Chen, P. Talemi, B. Chivers, R. Shepherd, and C. Fumeaux, "Progress in conductive polymer antennas based on free-standing polypyrrole and PEDOT: PSS," in *2016 17th Int. Symp. Antenna Technol. Appl. Electromagn.* IEEE, Jul 2016, pp. 1–4.

[51] T. T. Tung, S. J. Chen, C. Fumeaux, and D. Losic, "Scalable realization of conductive graphene films for high-efficiency microwave antennas," *J. Mater. Chem. C*, vol. 4, no. 45, pp. 10 620–10 624, 2016.

[52] S. J. Chen, T. T. Tung, D. Losic, and C. Fumeaux, "High-efficiency microwave graphene antenna," in *IEEE AP-S Symposium on Antennas and Propagation and USNC-URSI Radio Science Meeting*, Jul 2017.

[53] S. J. Chen, T. Kaufmann, and C. Fumeaux, "Shorting strategies for a wearable L-slot planar inverted-F antenna," in *Int. Work. Antenna Technol. (iWAT)*. IEEE, 2014, pp. 18–21.

[54] S. J. Chen, D. C. Ranasinghe, and C. Fumeaux, "Snap-on buttons as detachable shorting vias for wearable textile antennas," in *2016 Int. Conf. Electromagn. Adv. Appl.* IEEE, Sep 2016, pp. 521–524.

[55] S. J. Chen, C. Fumeaux, D. C. Ranasinghe, and T. Kaufmann, "Paired snap-on buttons connections for balanced antennas in wearable systems," *IEEE Antennas Wirel. Propag. Lett.*, vol. 14, no. X, pp. 1498–1501, 2015.

[56] S. J. Chen, T. Kaufmann, and C. Fumeaux, "Snap-on buttons connections for transmission lines and antennas," in *14th Australian Symposium on Antennas*, Feb 2015.

[57] S. J. Chen, T. Kaufmann, D. C. Ranasinghe, and C. Fumeaux, “A modular textile antenna design using snap-on buttons for wearable applications,” *IEEE Trans. Antennas Propag.*, vol. 64, no. 3, pp. 894–903, 2016.

[58] S. J. Chen, D. C. Ranasinghe, and C. Fumeaux, “A foldable textile patch for modular snap-on-button-based wearable antennas,” in *2016 URSI Int. Symp. Electromagn. Theory*, 2016, pp. 842–845.

[59] ——, “A polarization/frequency interchangeable patch for a modular wearable textile antenna,” in *11th European Conference on Antennas and Propagation*, Mar 2017, pp. 2483–2486.

[60] ——, “A reconfigurable wearable antenna based on snap-on buttons,” in *15th Australian Symposium on Antennas*, Feb 2017.

[61] S. J. Chen, C. Fumeaux, Y. Monnai, and W. Withayachumnankul, “Dual circularly polarized series-fed microstrip patch array with coplanar proximity coupling,” *IEEE Antennas Wirel. Propag. Lett.*, vol. 16, no. X, pp. 1500–1503, 2017.

[62] J. Reboun, A. Hamacek, T. Dzugan, and M. Kroupa, “Sensorial characteristics of conductive polymers,” *2009 32nd Int. Spring Semin. Electron. Technol.*, pp. 1–5, 2009.

[63] M.-Z. Yang, C.-L. Dai, and D.-H. Lu, “Polypyrrole porous micro humidity sensor integrated with a ring oscillator circuit on chip,” *Sensors*, vol. 10, no. 11, pp. 10 095–10 104, 2010.

[64] L. Lin, S. Liu, Q. Zhang, X. Li, M. Ji, H. Deng, and Q. Fu, “Towards tunable sensitivity of electrical property to strain for conductive polymer composites based on thermoplastic elastomer,” *ACS Appl. Mater. Interfaces*, vol. 5, no. 12, pp. 5815–24, 2013.

[65] M. Gerard, A. Chaubey, and B. Malhotra, “Application of conducting polymers to biosensors,” *Biosensors and Bioelectronics*, vol. 17, no. 5, pp. 345 – 359, 2002.

[66] J. Paloheimo, P. Kuivalainen, H. Stubb, E. Vuorimaa, and P. Yli-Lahti, “Molecular field effect transistors using conducting polymer langmuir-blodgett films,” *Applied Physics Letters*, vol. 56, no. 12, pp. 1157–1159, 1990.

[67] G. A. Snook, P. Kao, and A. S. Best, “Conducting-polymer-based supercapacitor devices and electrodes,” *Journal of Power Sources*, vol. 196, no. 1, pp. 1 – 12, 2011.

[68] Y. Liu, B. Weng, J. M. Razal, Q. Xu, C. Zhao, Y. Hou, S. Seyedin, R. Jalili, G. G. Wallace, and J. Chen, “High-performance flexible all-solid-state supercapacitor from large free-standing graphene-PEDOT/PSS films,” *Sci. Rep.*, vol. 5, no. October, p. 17045, Nov 2015.

[69] S. Cichos, J. Haberland, and H. Reichl, “Performance analysis of polymer based antenna-coils for RFID,” in *2nd Int. IEEE Conf. Polym. Adhes. Microelectron. Photonics. POLYTRONIC 02. Conf. Proc.* IEEE, 2002, pp. 120–124.

[70] Y. Wang and X. Jing, “Intrinsically conducting polymers for electromagnetic interference shielding,” *Polymers for Advanced Technologies*, vol. 16, no. 4, pp. 344–351, 2005.

[71] R. L. Haupt, “Reconfigurable patch with switchable conductive edges,” *Microw. Opt. Technol. Lett.*, vol. 51, no. 7, pp. 1757–1760, Jul 2009.

[72] T. Skotheim and J. Reynolds, *Conjugated Polymers: Theory, Synthesis, Properties, and Characterization*, ser. Handbook of Conducting Polymers, Third Edition. CRC Press, 2006.

[73] H. Letheby, "Xxix.-on the production of a blue substance by the electrolysis of sulphate of aniline," *J. Chem. Soc.*, vol. 15, pp. 161–163, 1862.

[74] R. D. Surville, M. Jozefowicz, L. Yu, J. Pepichon, and R. Buvet, "Electrochemical chains using protolytic organic semiconductors," *Electrochimica Acta*, vol. 13, no. 6, pp. 1451 – 1458, 1968.

[75] R. L. Greene, G. B. Street, and L. J. Suter, "Superconductivity in polysulfur nitride $(\mathrm{SN})_X$," *Phys. Rev. Lett.*, vol. 34, pp. 577–579, Mar 1975.

[76] Y. Li, *Organic Optoelectronic Materials*, ser. Lecture Notes in Chemistry, Y. Li, Ed. Cham: Springer International Publishing, 2015, vol. 91.

[77] G. Heywang and F. Jonas, "Poly(alkylenedioxythiophene)snew, very stable conducting polymers," *Adv. Mater.*, vol. 4, no. 2, pp. 116–118, Feb 1992.

[78] U. Lang, E. Müller, N. Naujoks, and J. Dual, "Microscopical Investigations of PEDOT:PSS Thin Films," *Adv. Funct. Mater.*, vol. 19, no. 8, pp. 1215–1220, Apr 2009.

[79] Y. Xia, K. Sun, and J. Ouyang, "Solution-processed metallic conducting polymer films as transparent electrode of optoelectronic devices." *Adv. Mater.*, vol. 24, no. 18, pp. 2436–40, 2012.

[80] R. N. Simons and R. Q. Lee, "Feasibility study of optically transparent microstrip patch antenna," in *IEEE Antennas and Propagation Society International Symposium 1997. Digest*, vol. 4, July 1997, pp. 2100–2103 vol.4.

[81] K. Rao, P. Nikitin, and S. Lam, "Antenna design for UHF RFID tags: a review and a practical application," *IEEE Trans. Antennas Propag.*, vol. 53, no. 12, pp. 3870–3876, Dec 2005.

[82] N. J. Kirsch, N. A. Vacirca, T. P. Kurzweg, A. K. Fontecchio, and K. R. Dandekar, "Performance of transparent conductive polymer antennas in a MIMO ad-hoc network," in *IEEE 6th Int. Conf. Wirel. Mob. Comput. Netw. Commun.* IEEE, 2010, pp. 9–14.

[83] A. Verma, C. Fumeaux, V.-T. Truong, and B. D. Bates, "Effect of film thickness on the radiation efficiency of a 4.5 GHz polypyrrole conducting polymer patch antenna," in *Proc. Asia-Pacific Microw. Conf.*, vol. 14, no. 4, 2010, pp. 95–98.

[84] T. Kaufmann, A. Verma, S. F. Al-Sarawi, V.-T. Truong, and C. Fumeaux, "Comparison of two planar elliptical ultra-wideband PPy conductive polymer antennas," in *IEEE Int. Symp. Antennas Propag.*, vol. 39, no. 17. IEEE, 2012, pp. 1–2.

[85] Z. Hamouda, J.-L. Wojkiewicz, A. Pud, L. Kone, B. Belaabed, S. Bergheul, and T. Lasri, "Dual-band elliptical planar conductive polymer antenna printed on a flexible substrate," *IEEE Trans. Antennas Propag.*, vol. 63, no. 12, pp. 5864–5867, 2015.

[86] A. K. Geim and K. S. Novoselov, "The rise of graphene." *Nat. Mater.*, vol. 6, no. 3, pp. 183–91, Mar. 2007.

[87] F. Bonaccorso, Z. Sun, T. Hasan, and A. C. Ferrari, "Graphene photonics and optoelectronics," *Nat. Photonics*, vol. 4, no. 9, pp. 611–622, Sep 2010.

[88] B. Sensale-Rodriguez, "Graphene-based optoelectronics," *J. Light. Technol.*, vol. 33, no. 5, pp. 1100–1108, Mar 2015.

[89] F. Bonaccorso, L. Colombo, G. Yu, M. Stoller, V. Tozzini, A. C. Ferrari, R. S. Ruoff, and V. Pellegrini, "Graphene, related two-dimensional crystals, and hybrid systems for energy conversion and storage," *Science*, vol. 347, no. 6217, Jan 2015.

[90] T. T. Tung, J. Yoo, F. K. Alotaibi, M. J. Nine, R. Karunagaran, M. Krebsz, G. T. Nguyen, D. N. H. Tran, J.-F. Feller, and D. Losic, "Graphene oxide-assisted liquid phase exfoliation of graphite into graphene for highly conductive film and electromechanical sensors," *ACS Appl. Mater. Interfaces*, vol. 8, no. 25, pp. 16 521–16 532, Jun 2016.

[91] B. Shen, W. Zhai, and W. Zheng, "Ultrathin flexible graphene film: An excellent thermal conducting material with efficient emi shielding," *Adv. Funct. Mater.*, vol. 24, no. 28, pp. 4542–4548, 2014.

[92] M. Dragoman, A. A. Muller, D. Dragoman, F. Coccetti, and R. Plana, "Terahertz antenna based on graphene," *J. Appl. Phys.*, vol. 107, no. 10, p. 104313, May 2010.

[93] K.-Y. Shin, S. Cho, and J. Jang, "Graphene/Polyaniline/Poly(4-styrenesulfonate) hybrid film with uniform surface resistance and its flexible dipole tag antenna application." *Small*, pp. 1–7, 2013.

[94] X.-c. Wang, W.-s. Zhao, J. Hu, and W.-y. Yin, "Reconfigurable terahertz leaky-wave antenna using graphene-based high-impedance surface," *IEEE Trans. Nanotechnol.*, vol. 14, no. 1, pp. 62–69, Jan 2015.

[95] I. Llatser, C. Kremers, D. N. Chigrin, J. M. Jornet, M. C. Lemme, A. Cabellos-Aparicio, and E. Alarcon, "Characterization of graphene-based nano-antennas in the terahertz band," in *2012 6th Eur. Conf. Antennas Propag.* IEEE, Mar 2012, pp. 194–198.

[96] R. Filter, M. Farhat, M. Steglich, R. Alaee, C. Rockstuhl, and F. Lederer, "Tunable graphene antennas for selective enhancement of THz-emission," *Opt. Express*, vol. 21, no. 3, p. 3737, Feb 2013.

[97] Z. Xu, X. Dong, and J. Bornemann, "Design of a reconfigurable MIMO system for THz communications based on graphene antennas," *IEEE Trans. Terahertz Sci. Technol.*, vol. 4, no. 5, pp. 609–617, Sep 2014.

[98] M. Esquius-Morote, J. S. Gomez-Diaz, and J. Perruisseau-Carrier, "Sinusoidally modulated graphene leaky-wave antenna for electronic beamscanning at THz," *IEEE Trans. Terahertz Sci. Technol.*, vol. 4, no. 1, pp. 116–122, Jan 2014.

[99] K. S. Novoselov, V. I. Fal'ko, L. Colombo, P. R. Gellert, M. G. Schwab, and K. Kim, "A roadmap for graphene," *Nature*, vol. 490, no. 7419, pp. 192–200, Oct 2012.

[100] T. Palacios, A. Hsu, and H. Wang, "Applications of graphene devices in RF communications," *IEEE Commun. Mag.*, vol. 48, no. 6, pp. 122–128, Jun 2010.

[101] X. Huang, Z. Yin, S. Wu, X. Qi, Q. He, Q. Zhang, Q. Yan, F. Boey, and H. Zhang, "Graphene-based materials: synthesis, characterization, properties, and applications." *Small*, vol. 7, no. 14, pp. 1876–902, 2011.

[102] Y. Hernandez, V. Nicolosi, M. Lotya, F. Blighe, Z. Sun, S. De, I. T. McGovern, B. Holland, M. Byrne, Y. Gunko, J. Boland, P. Niraj, G. Duesberg, S. Krishnamurti, R. Goodhue, J. Hutchison, V. Scardaci, a. C. Ferrari, and J. N. Coleman, "High yield production of graphene by liquid phase exfoliation of graphite," *Nat. Nanotechnol.*, vol. 3, no. 9, pp. 563–8, 2008.

[103] K. S. K. S. Kim, Y. Zhao, H. Jang, S. Y. Lee, J. M. Kim, K. S. K. S. Kim, J.-H. Ahn, P. Kim, J.-Y. Choi, and B. H. Hong, "Large-scale pattern growth of graphene films for stretchable transparent electrodes." *Nature*, vol. 457, no. 7230, pp. 706–10, 2009.

[104] J. N. Coleman, "Liquid exfoliation of defect-free graphene," *Accounts of Chemical Research*, vol. 46, no. 1, pp. 14–22, 2013, pMID: 22433117.

[105] M. Matsumoto, Y. Saito, C. Park, T. Fukushima, and T. Aida, "Ultrahigh-throughput exfoliation of graphite into pristine 'single-layer' graphene using microwaves and molecularly engineered ionic liquids," *Nat. Chem.*, vol. 7, no. 9, pp. 730–736, 2015.

[106] J. M. Jornet and I. F. Akyildiz, "Graphene-based nano-antennas for electromagnetic nanocommunications in the terahertz band," in *Antennas Propag. EuCAP 2010 Proc. Fourth Eur. Conf.*, 2010, pp. 1–5.

[107] a. Radwan, M. D'Amico, G. Gentili, and V. Verri, "Reconfigurable THz metamaterial antenna based on graphene," in *2015 9th Eur. Conf. Antennas Propagation, EuCAP 2015*, 2015.

[108] K. Nagashio, T. Nishimura, K. Kita, and A. Toriumi, "Mobility variations in mono- and multi-layer graphene films," *Appl. Phys. Express*, vol. 2, p. 025003, Jan 2009.

[109] K.-Y. Shin, J.-Y. Hong, and J. Jang, "Micropatterning of graphene sheets by inkjet printing and its wideband dipole-antenna application," *Adv. Mater.*, vol. 23, no. 18, pp. 2113–2118, May 2011.

[110] P. Kopyt, B. Salski, M. Olszewska-Placha, D. Janczak, M. Sloma, T. Kurkus, M. Jakubowska, and W. Gwarek, "Graphene-based dipole antenna for a UHF RFID tag," *IEEE Trans. Antennas Propag.*, vol. 64, no. 7, pp. 2862–2868, Jul 2016.

[111] T. Dias, *Electronic Textiles: Smart Fabrics and Wearable Technology*, ser. Woodhead Publishing Series in Textiles. Elsevier Science, 2015.

[112] X. Tao, Ed., *Handbook of Smart Textiles*, 1st ed. Hong Kong: Springer, 2015.

[113] R. Salvado, C. Loss, R. Gonçalves, and P. Pinho, "Textile materials for the design of wearable antennas: a survey," *Sensors.*, vol. 12, no. 11, pp. 15 841–57, 2012.

[114] M. Stoppa and A. Chiolerio, "Wearable electronics and smart textiles: A critical review," *Sensors*, vol. 14, no. 7, pp. 11 957–11 992, Jul 2014.

[115] T. Lee. Liquefied aluminium for conductive textiles. [Online]. Available: https://www.tevonews.com

[116] D. Cottet, J. Grzyb, T. Kirstein, and G. Tröster, "Electrical characterization of textile transmission lines," *IEEE Trans. Adv. Packag.*, vol. 26, no. 2, pp. 182–190, 2003.

[117] J. Cho, J. Moon, M. Sung, K. Jeong, and G. Cho, *Human-Computer Interaction. Interaction Platforms and Techniques - Design and Evaluation of Textile-Based Signal Transmission Lines and Keypads for Smart Wear Jayoung*, ser. Lecture Notes in Computer Science, J. A. Jacko, Ed. Berlin, Heidelberg: Springer Berlin Heidelberg, 2007, vol. 4551.

[118] LessEMF. [Online]. Available: https://www.lessemf.com/fabric4.html

[119] J. Vicente and A. A. Moreira, "Electro-textile printed slot antenna over finite EBG structure," in *2010 Int. Work. Antenna Technol.*, no. 1. IEEE, Mar 2010, pp. 1–4.

[120] P. Salonen, Y. Rahmat-Samii, M. Schaffrath, and M. Kivikoski, "Effect of textile materials on wearable antenna performance: a case study of GPS antennas," in *IEEE Antennas Propag. Soc. Symp.* IEEE, 2004, pp. 459–462 Vol.1.

[121] A. Tronquo, H. Rogier, C. Hertleer, and L. Van Langenhove, "Robust planar textile antenna for wireless body LANs operating in 2.45 GHz ISM band," *Electron. Lett.*, vol. 42, no. 3, p. 142, 2006.

[122] I. Locher, M. Klemm, T. Kirstein, and G. Tröster, "Design and characterization of purely textile patch antennas," *IEEE Trans. Adv. Packag.*, vol. 29, no. 4, pp. 777–788, 2006.

[123] A. Paraskevopoulos, A. A. Alexandridis, R. D. Seager, J. C. Vardaxoglou, D. d. S. Fonseca, and W. G. Whittow, "Higher-mode textile patch antenna with embroidered vias for on-body communication," *IET Microwaves, Antennas Propag.*, vol. 10, no. 7, pp. 802–807, May 2016.

[124] P. J. Soh, G. A. E. Vandenbosch, S. L. Ooi, and N. H. M. Rais, "Design of a broadband all-textile slotted PIFA," *IEEE Trans. Antennas Propag.*, vol. 60, no. 1, pp. 379–384, Jan 2012.

[125] L. Vallozzi, P. Van Torre, C. Hertleer, H. Rogier, M. Moeneclaey, and J. Verhaevert, "Wireless communication for firefighters using dual-polarized textile antennas integrated in their garment," *IEEE Trans. Antennas Propag.*, vol. 58, no. 4, pp. 1357–1368, 2010.

[126] I. Belov, M. Chedid, and P. Leisner, "Investigation of snap-on feeding arrangements for a wearable UHF textile patch antenna," in *Ambience Int. Sci. Conf.*, 2008, pp. 84–88.

[127] F. Declercq and H. Rogier, "Active integrated wearable textile antenna with optimized noise characteristics," *IEEE Trans. Antennas Propag.*, vol. 58, no. 9, pp. 3050–3054, 2010.

[128] A. Verma, C. Fumeaux, V.-T. Truong, and B. D. Bates, "A 2 GHz polypyrrole microstrip patch antenna on Plexiglas substrate," in *Asia Pacific Microw. Conf.* IEEE, 2009, pp. 36–39.

[129] U. Bakshi and A. Bakshi, *Antennas And Wave Propagation*. Technical Publications, 2009.

[130] M. Fabretto, K. Zuber, C. Jariego-Moncunill, and P. Murphy, "Measurement protocols for reporting PEDOT thin film conductivity and optical transmission: a critical survey," *Macromol. Chem. Phys.*, vol. 212, no. 19, pp. 2173–2180, 2011.

[131] D. Pozar, *Microwave Engineering, 4th Edition*. Wiley, 2011.

[132] Y. Cho, K. Kim, D. Choi, S. Lee, and S.-O. Park, "A miniature UWB planar monopole antenna with 5-GHz band-rejection filter and the time-domain characteristics," *IEEE Trans. Antennas Propag.*, vol. 54, no. 5, pp. 1453–1460, 2006.

[133] W. Wiesbeck, G. Adamiuk, and C. Sturm, “Basic properties and design principles of uwb antennas,” *Proceedings of the IEEE*, vol. 97, no. 2, pp. 372–385, Feb 2009.

[134] H. Schantz, *The Art And Science Of Ultrawideband Antennas*, 1st ed., ser. The Artech House Antenna and Propagation Library. Artech House, Incorporated, 2005.

[135] F. Boeykens, H. Rogier, and L. Vallozzi, “An efficient technique based on polynomial chaos to model the uncertainty in the resonance frequency of textile antennas due to bending,” *IEEE Trans. Antennas Propag.*, vol. 62, no. 3, pp. 1253–1260, 2014.

[136] D. Alemu, H.-Y. Wei, K.-C. Ho, and C.-W. Chu, “Highly conductive PEDOT:PSS electrode by simple film treatment with methanol for ITO-free polymer solar cells,” *Energy Environ. Sci.*, vol. 5, no. 11, p. 9662, 2012.

[137] R. Po, C. Carbonera, A. Bernardi, F. Tinti, and N. Camaioni, “Polymer- and carbon-based electrodes for polymer solar cells: Toward low-cost, continuous fabrication over large area,” *Sol. Energy Mater. Sol. Cells*, vol. 100, pp. 97–114, 2012.

[138] Y.-h. Suh and K. Chang, “A wideband coplanar stripline to microstrip transition,” *IEEE Microw. Wirel. Components Lett.*, vol. 11, no. 1, pp. 28–29, 2001.

[139] T. Kaufmann, I.-M. Fumeaux, and C. Fumeaux, “Comparison of fabric and embroidered dipole antennas,” in *7th Eur. Conf. Antennas Propag. Comp.*, 2013, pp. 3252–3255.

[140] A. Clogston, “Reduction of skin-effect losses by the use of laminated conductors,” *Proc. IRE*, vol. 39, no. 7, pp. 767–782, 1951.

[141] L. Shafai, S. Latif, and C. Shafai, “Loss reduction in planar circuits and antennas over a ground plane using engineered conductors,” in *7th Eur. Conf. Antennas Propag.*, 2013, pp. 1031–1035.

[142] S. Latif, C. Shafai, and L. Shafai, “Reduction in ohmic loss of small microstrip antennas using multiple copper layers,” in *IEEE Antennas Propag. Soc. Int. Symp.* IEEE, 2006, pp. 1625–1628.

[143] S. I. Latif, L. Shafai, and C. Shafai, “An engineered conductor for gain and efficiency improvement of miniaturized microstrip antennas,” *IEEE Antennas Propag. Mag.*, vol. 55, no. 2, pp. 77–90, 2013.

[144] H. C. Blennemann and R. F. W. Pease, “Novel microstructures for low-distortion chip-to-chip interconnects,” in *Int. Conf. Adv. Interconnect. Packag.*, G. Arjavalingam and J. Pazaris, Eds., vol. 1389, no. 1990, 1991, pp. 215–235.

[145] H. Wheeler, “Transmission-line properties of a strip on a dielectric sheet on a plane,” *IEEE Trans. Microw. Theory Tech.*, vol. 25, no. 8, pp. 631–647, Aug 1977.

[146] T. T. Thanh, H. Ba, L. Truong-Phuoc, J.-M. Nhut, O. Ersen, D. Begin, I. Janowska, D. L. Nguyen, P. Granger, and C. Pham-Huu, “A few-layer graphenegraphene oxide composite containing nanodiamonds as metal-free catalysts,” *J. Mater. Chem. A*, vol. 2, no. 29, p. 11349, 2014.

[147] S. Pang, Y. Hernandez, X. Feng, and K. Müllen, “Graphene as transparent electrode material for organic electronics,” *Adv. Mater.*, vol. 23, no. 25, pp. 2779–2795, 2011.

[148] Q. Zheng, Z. Li, J. Yang, and J.-K. Kim, “Graphene oxide-based transparent conductive films,” *Progress in Materials Science*, vol. 64, pp. 200 – 247, 2014.

[149] H. Schantz, "Introduction to ultra-wideband antennas," in *IEEE Conf. Ultra Wideband Syst. Technol. 2003*, vol. 35741. IEEE, 2003, pp. 1–9.

[150] ——, "A brief history of UWB antennas," *IEEE Aerosp. Electron. Syst. Mag.*, vol. 19, no. 4, pp. 22–26, 2004.

[151] L. Song, A. C. Myers, J. J. Adams, and Y. Zhu, "Stretchable and reversibly deformable radio frequency antennas based on silver nanowires." *ACS Appl. Mater. Interfaces*, vol. 6, no. 6, pp. 4248–53, 2014.

[152] P. Salonen, L. Sydänheimo, M. Keskilammi, and M. Kivikoski, "A small planar inverted-F antenna for wearable applications," in *Dig. Pap. Third Int. Symp. Wearable Comput.* IEEE Comput. Soc, 1999, pp. 95–100.

[153] O. Yurduseven, D. Smith, and M. Elsdon, "UWB meshed solar monopole antenna," *Electron. Lett.*, vol. 49, no. 9, pp. 582–584, 2013.

[154] M. L. Scarpello, I. Kazani, C. Hertleer, H. Rogier, and D. Vande Ginste, "Stability and efficiency of screen-printed wearable and washable antennas," *IEEE Antennas Wirel. Propag. Lett.*, vol. 11, pp. 838–841, 2012.

[155] T. Kellomäki, J. Virkki, S. Merilampi, and L. Ukkonen, "Towards washable wearable antennas: A comparison of coating materials for screen-printed textile-based UHF RFID tags," *Int. J. Antennas Propag.*, vol. 2012, pp. 1–11, 2012.

[156] A. A. Kostrzewski, K. S. Lee, E. Gans, C. A. Winterhalter, and T. P. Jannson, "Innovative wearable snap connector technology for improved networking in electronic garments," in *SPIE 6538, Sensors, Command. Control. Commun. Intell. Technol. Homel. Secur. Homel. Def. VI, 653804*, E. M. Carapezza, Ed., 2007, pp. 653 804–653 804–8.

[157] T. Kellomaki and W. G. Whittow, "Bendable plaster antenna for 2.45 GHz applications," in *Loughbrgh. Antennas Propag. Conf.*, no. November. IEEE, 2009, pp. 453–456.

[158] T. Kellomäki, "Snaps to connect coaxial and microstrip lines in wearable systems," *Int. J. Antennas Propag.*, vol. 2012, pp. 1–10, 2012.

[159] T. Kellomäki, W. G. . Whittow, J. . Heikkinen, and L. Kettunen, "2.4 GHz plaster antennas for health monitoring," in *Antennas Propagation, 2009. EuCAP 2009. 3rd Eur. Conf.*, 2009, pp. 211–215.

[160] B. Ivsic, D. Bonefacic, and J. Bartolic, "Considerations on embroidered textile antennas for wearable applications," *IEEE Antennas Wirel. Propag. Lett.*, vol. 12, pp. 1708–1711, 2013.

[161] D. C. Ranasinghe, R. L. Shinmoto Torres, K. Hill, and R. Visvanathan, "Low cost and batteryless sensor-enabled radio frequency identification tag based approaches to identify patient bed entry and exit posture transitions." *Gait Posture*, vol. 39, no. 1, pp. 118–23, Jan. 2014.

[162] N. H. M. Rais, P. J. Soh, F. Malek, S. Ahmad, N. Hashim, and P. Hall, "A review of wearable antenna," in *Loughborough. Antennas Propag. Conf.*, no. Nov. IEEE, 2009, pp. 225–228.

[163] P. S. Hall and Y. Hao, "Antennas and propagation for body centric communications," in *First Eur. Conf. Antennas Propag.* IEEE, 2006, pp. 1–7.

[164] P. J. Soh, G. A. Vandenbosch, M. Mercuri, and D. M.-P. Schreurs, "Wearable wireless health monitoring: current developments, challenges and future trends," *IEEE Microw. Mag.*, vol. 16, no. 4, pp. 55–70, 2015.

[165] B. Sanz-Izquierdo, F. Huang, and J. Batchelor, "Small size wearable button antenna," *1st Eur. Conf. Antennas Propag.*, vol. 42, no. 12, 2006.

[166] R. Garg, P. Bhartia, I. Bahl, and A. Ittipiboon, "Button antenna on textiles for wireless local area network on body applications," *IET Microwaves, Antennas Propag.*, vol. 4, no. May, pp. 1980–1987, 2010.

[167] K.-L. Wong and Z.-G. Liao, "Passive reconfigurable triple-wideband antenna for LTE tablet computer," *IEEE Trans. Antennas Propag.*, vol. 63, no. 3, pp. 901–908, 2015.

[168] D. J. Gioia, R. G. Uskali, and P. A. Kindinger, "Modular printed antenna," U.S. Patent 20 030 169 205 A1, Sep 11, 2003.

[169] M. Johansson, S. Petersson, and S. Johansson, "Modular high-gain antennas," in *IEEE Antennas Propag. Soc. Int. Symp.*, vol. 1, no. 1. IEEE, 2008, pp. 1–4.

[170] G. Quagliaro, "Modular antenna system," U.S. Patent 6 831 610 B2, Dec 14, 2004.

[171] M. Howard. [Online]. Available: http://www.aerodefensetech.com

[172] C. C. Chen, "Beamforming structure for modular phased array antennas," U.S. Patent 5 162 803, Nov 10, 1992.

[173] M. Lara, M. Mayes, W. Nunnally, T. Holt, and J. Mayes, "Modular interchangeable high power helical antennas," in *IEEE Pulsed Power Conf.* IEEE, 2011, pp. 358–363.

[174] R. Garg, P. Bhartia, I. Bahl, and A. Ittipiboon, *Microstrip Antenna Design Handbook*. Artech House, 2001.

[175] C. Balanis, *Antenna Theory: Analysis and Design*. Wiley, 2005.

[176] C. Hertleer, A. van Laere, H. Rogier, and L. van Langenhove, "Influence of relative humidity on textile antenna performance," *Text. Res. J.*, vol. 80, no. 2, pp. 177–183, 2010.

[177] C. C. Gordon, T. Churchill, C. E. Clauser, B. Bradtmiller, and J. T. McConville, "Anthropometric survey of U.S. army personnel: methods and summary statistics 1988," 1989.

[178] CTIA, "Test plan for wireless device over-the-air performance," 2013.

[179] G. TR25.914, "Measurements of radio performances for UMTS terminals in speech mode."

[180] T. Kellomäki, "Analysis of circular polarization of cylindrically bent microstrip antennas," *Int. J. Antennas Propag.*, vol. 2012, pp. 1–8, 2012.

[181] T. Kaufmann and C. Fumeaux, "Low-profile magnetic loop monopole antenna based on a square substrate-integrated cavity," *Int. J. Antennas Propag.*, vol. 2015, Article ID 694385, 6 pages, 2015.

[182] G. A. Conway and W. G. Scanlon, "Antennas for over-body-surface communication at 2.45 GHz," *IEEE Trans. Antennas Propag.*, vol. 57, no. 4, pp. 844–855, 2009.

[183] N. Nguyen-Trong, L. Hall, and C. Fumeaux, "A frequency- and pattern-reconfigurable center-shorted microstrip antenna," *IEEE Antennas Wirel. Propag. Lett.*, in print, 2016, DOI:10.1109/LAWP.2016.2544943.

[184] J. Matthews and G. Pettitt, "Development of flexible, wearable antennas," *3rd Eur. Conf. Antennas Propag.*, pp. 273–277, 2009.

[185] Y. Ouyang and W. Chappell, "High frequency properties of electro-textiles for wearable antenna applications," *IEEE Trans. Antennas Propag.*, vol. 56, no. 2, pp. 381–389, 2008.

[186] A. Kiourti and J. Volakis, "High-geometrical-accuracy embroidery process for textile antennas with fine details," *IEEE Antennas Wirel. Propag. Lett.*, vol. 14, no. X, pp. 1474 – 1477, 2015.

[187] F. A. Tahir and A. Javed, "A compact dual-band frequency-reconfigurable textile antenna for wearable applications," *Microw. Opt. Technol. Lett.*, vol. 57, no. 10, pp. 2251–2257, Oct 2015.

[188] S. Yan and G. A. E. Vandenbosch, "Radiation pattern-reconfigurable wearable antenna based on metamaterial structure," *IEEE Antennas Wirel. Propag. Lett.*, vol. 15, pp. 1715–1718, 2016.

[189] C. M. Lee and C. W. Jung, "Radiation-pattern-reconfigurable antenna using monopole-loop for Fitbit Flex wristband," *IEEE Antennas Wirel. Propag. Lett.*, vol. 14, pp. 269–272, 2015.

[190] P. Bhartia and I. Bahl, "A frequency agile microstrip antenna," in *1982 Antennas Propag. Soc. Int. Symp.*, vol. 20. Institute of Electrical and Electronics Engineers, 1982, pp. 304–307.

[191] C.-Z. Du, S.-S. Zhong, L. Yao, and Y.-P. Q. Qiu, "Textile microstrip array antenna on three-dimensional orthogonal woven composite," in *Antennas Propag. (EuCAP), 2010 Proc. Fourth Eur. Conf.*, 2010, pp. 4–5.

[192] J. James and P. Hall, *Handbook of Microstrip Antennas*, ser. IEE Electromagnetic Waves Series 28, vol. 2. Peter Peregrinus Ltd., London, United Kingdom, 1989.

[193] D. Pozar and D. Schaubert, "Comparison of three series fed microstrip array geometries," in *Proc. IEEE Antennas Propag. Soc. Int. Symp.* IEEE, 2002, pp. 728–731.

[194] T. Metzler, "Microstrip series arrays," *IEEE Trans. Antennas Propag.*, vol. 29, no. 1, pp. 174–178, Jan 1981.

[195] P. Hallbjörner, I. Skarin, K. From, and A. Rydberg, "Circularly polarized traveling-wave array antenna with novel microstrip patch element," *IEEE Antennas Wirel. Propag. Lett.*, vol. 6, no. 99, pp. 572–574, 2007.

[196] T. Yuan, N. Yuan, and L. W. Li, "A novel series-fed taper antenna array design," *IEEE Antennas Wirel. Propag. Lett.*, vol. 7, pp. 362–365, 2008.

[197] R. Pilard, C. Luxey, P. Brachat, G. Jacquemod, D. Titz, F. Gianesello, F. Ferrero, D. Gloria, and A. Bisognin, "Differential feeding technique for mm-wave series-fed antenna-array," *Electron. Lett.*, vol. 49, no. 15, pp. 918–919, Jul 2013.

[198] H. Moheb, L. Shafai, and M. Barakat, "Design of 24 GHz microstrip travelling wave antenna for radar application," in *IEEE Antennas Propag. Soc. Int. Symp. 1995 Dig.*, vol. 1. IEEE, 1995, pp. 350–353.

[199] K. Sakakibara, S. Sugawa, N. Kikuma, and H. Hirayama, "Millimeter-wave microstrip array antenna with matching-circuit-integrated radiating-elements for travelling-wave excitation," in *Proc. Fourth Eur. Conf. Antennas Propag.*, 2010, pp. 1–5.

[200] T. R. Cameron, A. T. Sutinjo, and M. Okoniewski, "A circularly polarized broadside radiating 'herringbone' array design with the leaky-wave approach," *IEEE Antennas Wirel. Propag. Lett.*, vol. 9, pp. 826–829, 2010.

[201] L. Zhang, W. Zhang, and Y. P. Zhang, "Microstrip grid and comb array antennas," *IEEE Trans. Antennas Propag.*, vol. 59, no. 11, pp. 4077–4084, 2011.

[202] C. Min and C. E. Free, "Analysis of traveling-wave-fed patch arrays," *IEEE Trans. Antennas Propag.*, vol. 57, no. 3, pp. 664–670, 2009.

[203] B. Zivanovic, T. M. Weller, and C. Costas, "Series-fed microstrip antenna arrays and their application to omni-directional antennas," *IEEE Trans. Antennas Propag.*, vol. 60, no. 10, pp. 4954–4959, Oct 2012.

[204] S. Karimkashi and G. Zhang, "A dual-polarized series-fed microstrip antenna array with very high polarization purity for weather measurements," *IEEE Trans. Antennas Propag.*, vol. 61, no. 10, pp. 5315–5319, 2013.

[205] M. Carter and E. Cashen, "Linear arrays for centimetric and millimetric wavelengths," in *Military Microwaves' 80; Proceedings of the Second Conference*, vol. 1, 1981, pp. 315–320.

[206] R. Owens and J. Thraves, "Microstrip antenna with dual polarisation capability," in *Military Microwaves Conf*, 1984, pp. 250–254.

[207] S. Long, M. McAllister, and Liang Shen, "The resonant cylindrical dielectric cavity antenna," *IEEE Trans. Antennas Propag.*, vol. 31, no. 3, pp. 406–412, May 1983.

[208] R. K. Mongia and P. Bhartia, "Dielectric resonator antennasa review and general design relations for resonant frequency and bandwidth," *Int. J. Microw. Millimeter-Wave Comput. Eng.*, vol. 4, no. 3, pp. 230–247, Jul 1994.

[209] A. Petosa and A. Ittipiboon, "Dielectric resonator antennas: A historical review and the current state of the art," *IEEE Antennas Propag. Mag.*, vol. 52, no. 5, pp. 91–116, Oct 2010.

[210] K. Luk and K. Leung, *Dielectric Resonator Antennas*, ser. Antennas S. Research Studies Press, 2003.

[211] A. R. Chandran, N. Timmons, and J. Morrison, "Compact microstrip line fed dielectric resonator based wearable antenna," *2014 IEEE Conf. Antenna Meas. Appl. CAMA 2014*, pp. 1–4, 2014.

[212] M. M. Tahseen and A. A. Kishk, "Textile-based wideband flexible wearable dielectric resonator antennas for WLAN-band," in *2016 17th Int. Symp. Antenna Technol. Appl. Electromagn.* IEEE, Jul 2016, pp. 1–3.

[213] S. Koulouridis, G. Kiziltas, Y. Zhou, D. J. Hansford, and J. L. Volakis, "Polymer-ceramic composites for microwave applications: Fabrication and performance assessment," *IEEE Trans. Microw. Theory Tech.*, vol. 54, no. 12, pp. 4202–4208, Dec 2006.

[214] N. Ehteshami and V. Sathi, “New optically controlled frequency-agile microstrip antenna,” *J. Electron. Mater.*, vol. 42, no. 1, pp. 162–167, 2012.

[215] S. Manzari, C. Occhiuzzi, S. Nawale, A. Catini, C. Di Natale, and G. Marrocco, “Humidity sensing by polymer-loaded UHF RFID antennas,” *IEEE Sens. J.*, vol. 12, no. 9, pp. 2851–2858, Sep 2012.

[216] C. M. Boutry, H. Chandrahalim, P. Streit, M. Schinhammer, A. C. Hanzi, and C. Hierold, “Towards biodegradable wireless implants,” *Philos. Trans. R. Soc. A Math. Phys. Eng. Sci.*, vol. 370, no. 1967, pp. 2418–2432, May 2012.

[217] R. Balint, N. J. Cassidy, and S. H. Cartmell, “Conductive polymers: Towards a smart biomaterial for tissue engineering,” *Acta Biomater.*, vol. 10, no. 6, pp. 2341–2353, Jun 2014.

[218] H. W. Lai, K. M. Luk, and K. W. Leung, “Dense dielectric patch antenna-a new kind of low-profile antenna element for wireless communications,” *IEEE Trans. Antennas Propag.*, vol. 61, no. 8, pp. 4239–4245, 2013.

Biography

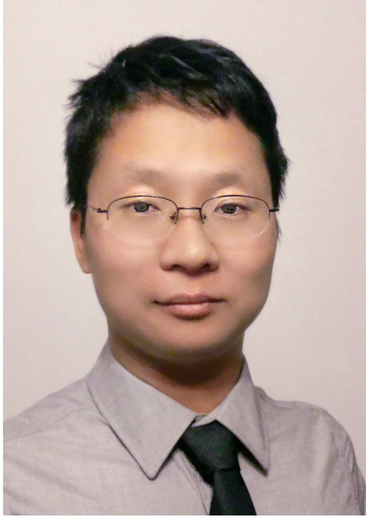

Shengjian Jammy Chen was born in Guangzhou, Guangdong, China. He received his B.Eng. degree from the Faculty of Information Engineering, Guangdong University of Technology, China in 2003, and his M.Eng. degree from the School of Electrical & Electronic Engineering, the University of Adelaide, Australia in 2013. He was awarded the Australian Postgraduate Award in 2013 to pursue his PhD degree in the School of Electrical & Electronic Engineering, the University of Adelaide, under the supervision of Prof. Christophe Fumeaux, Dr Damith Ranasinghe and Dr Thomas Kaufmann. His research interests include wearable and reconfigurable electromagnetic structure development based on novel materials such as conductive polymers, conductive fabrics and graphene, RFID-based wearable applications, and leaky wave antennas.

During his candidature, he received a number of scholarships including the Australian Postgraduate Award (2013) and the Simon Rockliff Scholarship for outstanding postgraduate mentorship from DSTG (2015). Also, He was the recipient of a number of awards including the Young Scientist Best Paper Award at the International Conference on Electromagnetics in Advanced Applications (ICEAA) 2015, the Young Scientist Best Paper Award and Travel Bursary Award at the International Conference on Electromagnetics in Advanced Applications (ICEAA) 2016, and the Honorable Mention at IEEE AP-S Symposium on Antennas and Propagation and USNC-URSI Radio Science Meeting (APS/URSI) 2017.

Shengjian Jammy Chen has served as a reviewer for a number of recognized journals including *IEEE Antenna and Wireless Propagation Letters* and *IEEE Transactions on Microwave Theory and Techniques*. He is a student member of the Institute of Electrical and Electronics Engineers (IEEE) and IEEE Antennas and Propagation Society.

Shengjian Jammy Chen
shengjian.chen@adelaide.edu.au
longz8@hotmail.com